

Gravitational Waves from Eccentric Binary Systems and Globular Clusters

Laura Rhian Pickard

Mullard Space Science Laboratory
Department of Space and Climate Physics
University College London

A thesis submitted to University College London
for the degree of Master of Philosophy

I, Laura Rhian Pickard, confirm that the work presented in this thesis is my own. Where information has been derived from other sources, I confirm that this has been indicated in the thesis.

Abstract

Binary systems have long been expected to be sources of gravitational waves. The nature of the emission from a binary is determined by its orbital parameters, with eccentricity having a particularly notable effect, changing the frequency at which the peak emission occurs, and the range of harmonic numbers it occurs over. Globular clusters, containing many binary systems, are therefore likely to have significant gravitational wave emission.

I calculate the gravitational wave emission from the known eccentric binaries in the galaxy, and use the results to create a luminosity function for the gravitational wave emission from these binaries, which is compared to the x-ray luminosity function. The nature of the gravitational wave emission from a binary system whose parameters are not well known could, by comparison, be used to constrain these. The luminosity function for eccentric high mass X-ray binaries in gravitational waves is shown to be very similar to the X-ray luminosity function.

A monte carlo simulation of many binary systems is used to model a globular cluster. I find that the gravitational wave emission occurs over a wide range of frequencies up to a maximum of order 10^{-3}Hz .

Finally, representative simulations for each globular cluster in the galaxy are used to build up a gravitational wave luminosity function for all the globular clusters in the galaxy.

Contents

List of Figures	7
List of Tables	15
1 The nature and detection of gravitational waves	16
1.1 Introduction	16
1.2 History	16
1.3 The nature of gravitational waves	17
1.4 Sources	19
1.4.1 Binary systems	19
1.4.2 Rotating neutron stars	22
1.4.3 Burst sources	22
1.4.4 Cosmic strings	23
1.4.5 Gravitational wave background	23
1.5 Gravitational wave detection	25
1.5.1 Indirect detection	25
1.5.2 Resonant bars	25
1.5.3 Pulsar timing	26
1.5.4 Doppler tracking	27
1.5.5 Interferometers	28
1.6 Chapter summary	31

<i>CONTENTS</i>	5
2 Gravitational wave emission from an eccentric binary system	32
2.1 Introduction	32
2.2 Previous work	34
2.3 Calculation of gravitational wave emission	36
2.4 Programming considerations	38
2.4.1 General structure of program	38
2.4.2 Treatment of Bessel functions	39
2.5 Output and analysis	40
2.5.1 The $g(n,e)$ graph	40
2.5.2 Realistic output	45
2.6 Calculation of gravitational wave emission in each polarisation	48
2.7 Use of programs	56
2.8 Chapter summary	56
3 Application to known eccentric binaries	58
3.1 Introduction	58
3.2 Input parameters	60
3.3 Low Mass X-ray Binaries	60
3.3.1 Circinus X-1	61
3.3.2 4U 1700+24	63
3.4 High Mass X-ray Binaries	65
3.4.1 2S 1845-024	66
3.4.2 GRO J1008-57	68
3.4.3 XTE J0421+560	70
3.4.4 1A 0535+262	76
3.5 Radio pulsars in binary systems	78
3.5.1 J0514-4002A	79
3.5.2 B1259-63=J1302-6350	81
3.5.3 J1811-1736	83

<i>CONTENTS</i>	6
3.5.4 B1913+16=J1915+1606	83
3.6 Aggregate data for HMXBs and radio pulsars in binary systems	86
3.6.1 Radio pulsar binaries	87
3.6.2 HMXBs	88
3.6.3 Comparison of HMXBs and radio pulsar binaries	89
3.6.4 Gravitational wave luminosity function	90
3.7 Chapter summary	95
4 Many binary systems; globular cluster	97
4.1 Introduction	97
4.2 Extending the program to multiple systems	98
4.2.1 Number of systems	99
4.2.2 Generating statistical distributions	99
4.2.3 Running using a batch file	100
4.2.4 Frequency binning	101
4.3 Results	101
4.3.1 Varying eccentricity	101
4.3.2 Varying eccentricity and orbital period	107
4.3.3 Varying eccentricity, orbital period and stellar masses	118
4.4 Chapter summary	120
5 Globular clusters in the Milky Way	122
5.1 Introduction	122
5.2 Globular Clusters and core collapse	124
5.3 Globular Clusters in the Milky Way	124
5.3.1 Simulated gravitational wave emission	132
5.4 Globular Cluster luminosity function and distance determination	142
5.4.1 Gravitational wave luminosity function	142
5.4.2 Electromagnetic luminosity function	147
5.4.3 Distance determination with gravitational waves	148

5.5 Chapter summary	151
6 Conclusions	153
6.1 Motivation	153
6.2 Summary of the work	154
6.2.1 Eccentric binaries	154
6.2.2 Globular clusters	155
6.2.3 Distance measurement	156
6.3 Closing remarks	157
Acknowledgements	159
Bibliography	207

List of Figures

1.1	The effect of a '+' polarisation gravitational wave on space	19
1.2	Background radiation from the Big Bang.	24
1.3	Diagram of resonant bar detector.	26
1.4	Diagram of Michelson interferometer.	28
2.1	Graph showing $g(n,e)$ versus harmonic number, n , as generated by calculation	41
2.2	Graph of the behaviour of the $g(n,e)$ curve from $n=1$ to $n=6$ and $e=0.05$ to 0.99	42
2.3	Graph of the behaviour of the $g(n,e)$ curve from $n=1$ to $n=6$ at $e=0.85$ and $e=0.9$	43
2.4	Graph of the behaviour of the $g(n,e)$ curve at low harmonic and integer n	44
2.5	Graph of the behaviour of the $g(n,e)$ curve from $n=0.001$ to $n=6$ and $e=0.05$ to 0.99	46
2.6	Graph of the behaviour of the $g(n,e)$ curve from $n=0.001$ to $n=6$ at $e=0.85$ and $e=0.9$	47
2.7	Co-ordinate system used when calculating gravitational wave flux at observer	49
2.8	Gravitational waves in the + polarisation for example system with eccentricity 0.3	52

2.9	Gravitational waves in the \times polarisation for example system with eccentricity 0.3	53
2.10	Gravitational waves in the $+$ polarisation for example system with eccentricity 0.6	54
2.11	Gravitational waves in the \times polarisation for example system with eccentricity 0.6	55
3.1	Calculated gravitational wave emission for Circinus X-1	62
3.2	Calculated gravitational wave signal at Earth from Circinus X-1 . . .	63
3.3	Possible gravitational wave emission for 4U 1700+24	64
3.4	Calculated gravitational wave signal at Earth from 4U1700+24	65
3.5	Possible gravitational wave emission for 2S 1845-024	67
3.6	Calculated gravitational wave signal at Earth from 2S1845-024 if at an angle of 60 degrees	68
3.7	Calculated gravitational wave emission for GRO J1800-57	69
3.8	Calculated gravitational wave signal at Earth from GROJ1008-57 . .	70
3.9	Calculated gravitational wave emission for XTE J0421+560	72
3.10	Calculated gravitational wave emission for XTE J0421+560	73
3.11	Calculated gravitational wave emission for XTE J0421+560	74
3.12	Calculated gravitational wave signal at Earth from XTEJ0421+560 if at an inclination angle of 16 degrees	75
3.13	Calculated gravitational wave signal at Earth from XTEJ0421+560 if at an inclination angle of 38 degrees	75
3.14	Calculated gravitational wave signal at Earth from XTEJ0421+560 if at an inclination angle of 60 degrees	76
3.15	Calculated gravitational wave emission for 1A 0535+262	77
3.16	Calculated gravitational wave emission for J0514-4002A	80
3.17	Calculated gravitational wave signal at Earth from J0514-4002A if at an inclination angle of 60 degrees	81

3.18	Calculated gravitational wave emission for J1302-6350	82
3.19	Calculated gravitational wave signal at Earth from B1259-63	83
3.20	Calculated gravitational wave emission for J1811-1736	84
3.21	Calculated gravitational wave emission for J1915+1606	85
3.22	Calculated gravitational wave signal at Earth from B1913+16	86
3.23	Peak gravitational wave emission frequencies of radio pulsar binaries .	87
3.24	Peak gravitational wave emission frequencies of HMXBs	88
3.25	Peak gravitational wave emission frequencies of HMXBs and radio pulsar binaries	89
3.26	Gravitational wave luminosity function for the systems studied	90
3.27	Gravitational wave luminosity function for the systems studied, log- arithmic scale	91
3.28	Gravitational wave luminosity function for the systems studied, ex- cluding the LMC	92
3.29	Gravitational wave luminosity function for the systems studied, ex- cluding the LMC, logarithmic scale	93
3.30	Gravitational wave luminosity function for the HMXB, excluding the LMC, logarithmic scale	94
4.1	100 000 neutron star and $3 M_{\odot}$ systems, normal distribution of ec- centricities with a mean of 0.1 and range of standard deviations . . .	104
4.2	100 000 neutron star and $3 M_{\odot}$ systems, normal distribution of ec- centricities with a mean of 0.9 and range of standard deviations . . .	105
4.3	100 000 neutron star and $3 M_{\odot}$ systems, normal distribution of ec- centricities with a standard deviation of 0.5 and range of means . . .	106
4.4	100 000 two neutron star systems, normal distribution of eccentricities with a mean of 0.1 and range of standard deviations	107
4.5	10 000 systems with 10 day period, eccentricity distribution mean 0.9, with frequency bin width 10^{-5}Hz	109

4.6	10 000 systems with 10 day period, eccentricity distribution mean 0.9, with frequency bin width 10^{-6}Hz	110
4.7	10 000 systems with 10 day period, eccentricity distribution mean 0.9, with frequency bin width 10^7Hz	111
4.8	Results for 100 000 systems with masses 1.4 and $3 M_{\odot}$ split by orbital period	115
4.9	Results for 100 000 systems with masses 1.4 and $3 M_{\odot}$ split by orbital period	117
4.10	Results for 100 000 systems with varying masses split by orbital period	119
5.1	Results for NGC 7099 using the period distribution of Duquennoy & Mayor (1991)	135
5.2	Results for NGC 7099 using the period distribution of Sigurdsson & Phinney (1995) for a core collapsed cluster	136
5.3	Variation of peak power with number of binaries in a cluster, all clusters take period distribution of Duquennoy & Mayor (1991)	138
5.4	Variation of peak power with number of binaries in a cluster, core collapsed clusters take period distribution of Sigurdsson & Phinney (1995)	139
5.5	Variation of peak frequency with peak power, all clusters take period distribution of Duquennoy & Mayor (1991)	140
5.6	Variation of peak frequency with peak power, core collapsed clusters take period distribution of Sigurdsson & Phinney (1995)	141
5.7	Luminosity function for peak gravitational wave emission of galactic globular clusters, all clusters take period distribution of Duquennoy & Mayor (1991)	143
5.8	Luminosity function for peak gravitational wave emission of galactic globular clusters, core collapsed clusters take period distribution of Sigurdsson & Phinney (1995)	144

5.9	Cumulative luminosity function for peak gravitational wave emission of galactic globular clusters, all clusters take period distribution of Duquennoy & Mayor (1991)	145
5.10	Cumulative luminosity function for peak gravitational wave emission of galactic globular clusters, core collapsed clusters take period distribution of Sigurdsson & Phinney (1995)	146
5.11	Electromagnetic luminosity function of Milky Way globular clusters, reproduced from Rejkuba (2012)	147
6.1	Calculated gravitational wave emission for 4U 1223-624	165
6.2	Calculated gravitational wave emission for 2S 1417-624	166
6.3	Calculated gravitational wave emission for EXO 2030+375	167
6.4	Calculated gravitational wave emission for 1A 0535-668	168
6.5	Calculated gravitational wave emission for SAX J2103.5+4545	169
6.6	Calculated gravitational wave signal at Earth from SAXJ2103.5+4545	170
6.7	Calculated gravitational wave emission for V 0332+53	171
6.8	Calculated gravitational wave emission for GRO J1750-27	172
6.9	Calculated gravitational wave emission for RX J1826.2-1450	174
6.10	Calculated gravitational wave signal at Earth from RXJ1826.2-1450 .	175
6.11	Calculated gravitational wave emission for 4U 0115+634	176
6.12	Calculated gravitational wave signal at Earth from 4U0115+634 . . .	177
6.13	Calculated gravitational wave emission for XTE J1946+274	178
6.14	Calculated gravitational wave signal at Earth from XTEJ1946+274 .	179
6.15	Calculated gravitational wave emission for SAX J0635.2+0533	180
6.16	Calculated gravitational wave signal at Earth from SAXJ0635.2+0533	181
6.17	Calculated gravitational wave emission for 4U 1907+09	182
6.18	Calculated gravitational wave signal at Earth from 4U1907+09 at 47.9 degrees inclination	183

6.19 Calculated gravitational wave signal at Earth from 4U1907+09 at 90 degrees inclination	183
6.20 Calculated gravitational wave emission for 2S 0053+604	184
6.21 Calculated gravitational wave signal at Earth from 2S0053+604 . . .	185
6.22 Calculated gravitational wave emission for 4U 1700-37	186
6.23 Calculated gravitational wave signal at Earth from 4U1700-37	187
6.24 Calculated gravitational wave emission for J0045-7319	188
6.25 Calculated gravitational wave emission for J1823-1115	189
6.26 Calculated gravitational wave signal at Earth from B1820-11	190
6.27 Calculated gravitational wave emission for J1750-37	191
6.28 Calculated gravitational wave emission for J2130+1210C	192
6.29 Calculated gravitational wave emission for J2305+4707	193
6.30 Calculated gravitational wave emission for J1740-3052	194
6.31 Calculated gravitational wave signal at Earth from J1740-3052 . . .	195
6.32 Calculated gravitational wave emission for J2140-2310B	196
6.33 Calculated gravitational wave emission for J1537+1155	197
6.34 Calculated gravitational wave signal at Earth from B1534+12	198
6.39 100 000 neutron star and $3 M_{\odot}$ systems, even distribution of eccen- tricities	198
6.35 Calculated gravitational wave emission for J1518+4904	199
6.36 Calculated gravitational wave signal at Earth from J1518+4904 . . .	200
6.40 100 000 neutron star and $3 M_{\odot}$ systems, normal distribution of ec- centricities, mean 0.1-0.9, left to right top to bottom	200
6.37 Calculated gravitational wave emission for J1804-0735	201
6.38 Calculated gravitational wave signal at Earth from B1802-07	202
6.41 100 000 neutron star and $3 M_{\odot}$ systems, normal distribution of ec- centricities, standard deviations 0.1-0.9, left to right top to bottom .	202
6.42 100 000 two neutron star systems, even distribution of eccentricities .	204

6.43 100 000 two neutron star systems, normal distribution of eccentricities, mean 0.1-0.9, left to right top to bottom	205
6.44 100 000 neutron star and $3 M_{\odot}$ systems, normal distribution of eccentricities, standard deviations 0.1-0.9, left to right top to bottom .	206

List of Tables

4.1	Variation of maximum possible eccentricity with period and stellar size, where m1 is a neutron star of radius $2 \times 10^{-5} R_{\odot}$	102
5.1	Globular cluster parameters	126
5.2	Globular cluster parameters	127
5.3	Globular cluster parameters	128
5.4	Globular cluster parameters	129
5.5	Globular cluster parameters	130

Chapter 1

The nature and detection of gravitational waves

1.1 Introduction

Gravitational waves, for which so far there is only indirect evidence, can be useful for studying many astrophysical phenomena. Instruments to detect gravitational waves directly are operating and there are plans for future detectors. In this chapter I explain the nature of gravitational waves and the history of their discovery, explore the astrophysical sources which may produce gravitational radiation and explain how this occurs, and provide an overview of possible detection methods, including the problems encountered with them.

1.2 History

The existence of gravitational waves is predicted by Einstein's general relativity. Since a change in a gravitational field, such as that caused by a moving massive body, cannot have an instantaneous effect on its surroundings, as in Newtonian gravitation, as the change cannot propagate faster than the speed of light in a vacuum, this means the effect of the change must propagate outwards as a gravitational wave.

Joseph Weber claimed to have detected signals in the 1960s (Weber, 1968) but later analysis showed his results were due to noise and to data processing errors (Levine, 2004). His design for a was an early type of bar detector, which was refined and improved by many groups, leading to the cryogenically cooled resonant bars in use today, as detailed in subsection 1.5.2. Interferometer detectors (subsection 1.5.5) are also in use, but thus far no direct detection method has recorded a gravitational wave signal. This is thought to be largely due to the small nature of any signal and the difficulty removing sources of noise from the data.

The measurements of the orbital decay of the binary pulsar PSR B1913+16 Hulse & Taylor (1975) exactly fit the predictions of decay due to emission of gravitational waves. Orbital decay of a binary system indicates that the system is losing angular momentum. The emission of gravitational waves is a mechanism by which this can occur, and in the case of the binary pulsar, is required in order to account for the rate of orbital decay. Thus this discovery provides evidence for the existence of gravitational waves.

A comparison of the measured period shift to that predicted by theory, extended from the original research with more recent measurements, can be seen in Weisberg & Taylor (2004). This discovery won Hulse and Taylor the 1993 Nobel Prize for Physics and this indirect evidence of gravitational radiation remains the only detection to date.

Attempts to directly detect gravitational waves are ongoing but have encountered many difficulties, not least the very small nature of any measurable signal. This is discussed further in section 1.5.

1.3 The nature of gravitational waves

General relativity models gravity as a distortion of space-time caused by the presence of massive objects. A test mass placed near a massive object experiences a force attracting it towards that object, due to the way space-time curves near the large

mass. When such a mass moves, or the amount of mass present changes suddenly, such as in an explosion, there must therefore be a change in the force a test mass would experience. We expect the effect of this change to propagate outwards through the action of a force carrier, the graviton or gravitational wave. (Pickard, 2008)

Measurement of gravitational waves is important therefore, not only for the potential astrophysical and cosmological discoveries, but also as a test of general relativity.

Gravitational waves are transverse waves which travel at the speed of light in vacuum, as shown in the appendix, which shows that the dispersion equation, describing the wave, is the same for gravitational waves as for electromagnetic waves, meaning their speed must be the same. The waves propagate as a deformation of space-time. Unlike electromagnetic waves, which propagate largely as dipole radiation, gravitational waves are quadrupolar. The dipolar component is zero- while electromagnetism has positive and negative charges, for gravitation the equivalent of charge is mass, which is only positive. This means the dipole component of the wave would cancel out, leaving the quadrupole dominant. This is shown mathematically in the appendix.

The wave oscillates in two spatial dimensions while travelling in the third. The oscillation is orthogonal to the direction of travel. Space-time is stretched in one transverse direction and compressed in the other, then the first direction becomes compressed and the second stretched, and so on. There are two possible polarisations, the ‘+’ polarisation having the directions of stretching and squeezing at 45 degrees to the ‘×’ polarisation. See the appendix for a mathematical explanation of this. The effect of a ‘+’ polarisation gravitational wave is shown in figure 1.1, for a wave travelling towards you out of the picture.

As the wave passes, the time it takes a photon to travel between two points changes. The distance as measured by a co-ordinate system does not change, as the co-ordinate labels move along with space. However light travel time between two points can be used to measure the passage of a gravitational wave. This principle

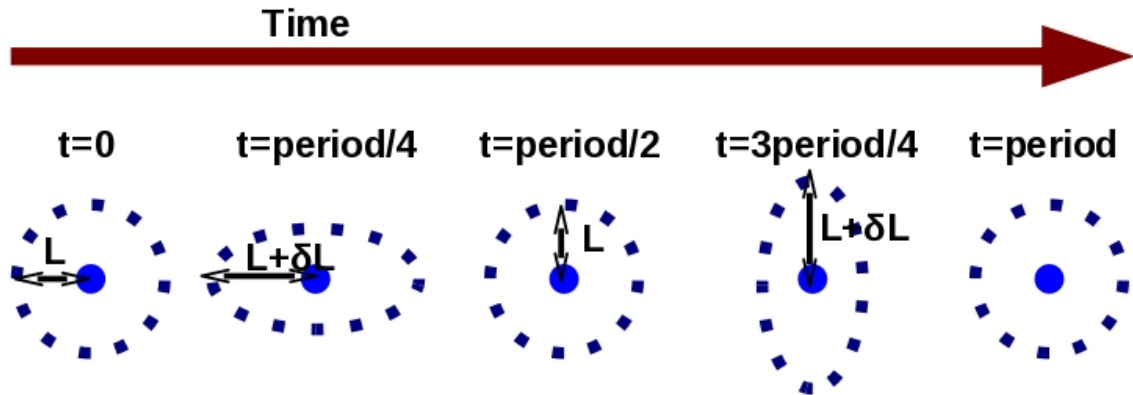


Figure 1.1: The effect of a '+' polarisation gravitational wave on space

has been used to construct interferometric gravitational wave detectors as discussed in subsection 1.5.5.

1.4 Sources

Gravitational waves are expected from any asymmetric, moving mass distribution. This includes clusters of objects and systems involving two or more stars and explosions such as gamma ray bursts. A completely symmetrical moving system, such as a rotating spherical body, would not produce gravitational waves as the mass present at a given point would not be changing. (Pickard, 2008)

We also expect there to be a gravitational radiation background from the big bang, analogous to the cosmic microwave background.

1.4.1 Binary systems

Gravitational wave emission is expected to be detectable from systems involving white dwarfs, neutron stars and black holes. As two stars or black holes orbit each other, they are observed to gradually move closer together. In order to do this, they must be losing energy. This is expected to occur by emission of gravitational waves and is seen as indirect evidence of their existence. A direct measurement of

gravitational waves from such a system would help to constrain parameters such as the masses involved, separation and eccentricity of the binary.

Systems involving white dwarfs or neutron stars are expected to be common and detectable with future equipment. It is speculated that such systems may be so common that they would constitute a noise source when attempting to study other things. A good theoretical description of the signal from such systems, could, therefore, be very useful in allowing their signals to be subtracted and other sources studied.

Eccentricity

If a binary system has an eccentric orbit, this changes the expected gravitational wave emission of the system. A more eccentric, elongated orbit means that the gravitational waves will be emitted across a spectrum of frequencies rather than only at the orbital frequency as would be expected for a perfectly circular system. The emission occurs at harmonics of the frequency expected for a circular system of the same orbital period, i.e. the frequency for a circular system multiplied by integers.

The emission will peak at a higher frequency as eccentricity increases, and the peak power emitted will be greater. This is to be expected since a more elongated orbit means the bodies are moving in a more extreme manner, the orbit having more distant apastron. This is examined in detail in chapters 2 and 3.

X-ray binaries

X-ray binaries, consisting of at least one compact object- a white dwarf, neutron star or black hole- and a binary companion are likely to be good sources of gravitational waves, as they often have high mass bodies in short period orbits.

High mass X-ray binaries consist of a compact object and a giant companion, with X-ray emission from the accretion disk which forms around the compact object

as material transfers over from the companion, as well as from jets if these are present. Eventually these can become compact object-compact object binaries.

Low mass X-ray binaries have a much slower rate of transfer and emit lower energy X-rays, often as bursts or transient sources. Here, the companion star is usually less massive than the compact object. They may form by capture, which would be common in a dense environment such as a globular cluster. Where the compact object is a neutron star, it can accumulate material from the companion until enough has amassed to allow a short burst of nuclear fusion, briefly increasing the output immensely.

Some compact stellar mass black hole binaries may only be detectable by gravitational wave emission as they can be electromagnetically quiet (Amaro-Seoane et al, 2012).

Binary supermassive black holes are thought to have a characteristic signal which may act as a 'standard siren', in analogy to the standard candles of electromagnetic astronomy. If the host galaxy can be identified the redshift can be measured in the usual way. Since a gravitational wave signal would provide a measure of the luminosity distance of the galaxy which is independent of the measured redshift, the relationship between luminosity distance and redshift can be studied. This relationship could allow such measurements to constrain cosmological parameters, most notably the dark energy equation of state. (Arun et al, 2008)

Inspirals and mergers

Mergers, of binary companions or massive objects and captured bodies, are expected to have characteristic gravitational wave signatures.

The merger of two black holes has three phases- the inspiral, as the black holes lose energy and angular momentum by emitting gravitational waves, the merger itself, resulting in a highly distorted remnant black hole, and the ringdown, where the resulting single black hole oscillates and emits gravitational waves as it gradually becomes stable, eventually becoming a stationary Kerr black hole. (Amaro-Seoane

et al, 2012)

When galaxies merge, the supermassive black holes at their centres may form a binary, which can gradually become tighter, due to dynamical friction by stars and gas, until the inspiral is dominated by loss of energy and angular momentum due to gravitational waves. The black holes eventually merge, resulting in a single black hole which oscillates (the 'ringdown' phase) or can escape the galaxy due to gravitational recoil.

Mergers of double white dwarf binaries can lead to type Ia supernovae or result in the creation of a rapidly spinning neutron star.

1.4.2 Rotating neutron stars

While the superfluid core of a neutron star is always axisymmetric, a rotating neutron star can nonetheless have enough asymmetry to cause emission of gravitational radiation (Brady, 1999). The star can be elliptical in shape, meaning that if the axis of rotation is offset from the axisymmetric line through the centre of the star, the star can wobble as the axis of rotation precesses. Similarly if the crust of the star is not uniformly smooth, a bulge to one side provides an asymmetry.

If the neutron star is accreting matter from a companion, it should also gain angular momentum. However in the case of low mass X-ray binaries, the spin frequencies of neutron stars lower than predicted for such a gain. If the star were losing angular momentum through emission of gravitational waves, this might explain the lower than expected spin rate. (Brady, 1999)

Neutron stars can also pulsate, as mentioned in the next section (subsection 1.4.3). (Misner, Thorne and Wheeler).

1.4.3 Burst sources

Events such as supernovae and gamma ray bursts are expected to be associated with bursts of gravitational radiation. Where an asymmetric explosion or collapse takes

place, the change in mass distribution can result in the production of a gravitational wave. The pulsations of a neutron star as it forms and stabilises should also give bursts of gravitational radiation. (Misner, Thorne and Wheeler)

Gamma ray bursts, whether from a collision of two neutron stars or a ‘hypernova’ at the end of a very massive star’s life, are energetic events and detectable by their electromagnetic emission. Positional association of known gamma ray bursts with the gravitational waves detected in a given area should give some indication of the gravitational wave emission from a given event.

We also expect to see gravitational waves as a star falls into a black hole, or as two black holes merge. This could be particularly important in understanding the mergers of supermassive black holes when two galaxies collide.

1.4.4 Cosmic strings

Cosmic strings are hypothetical 1-dimensional topological defects in spacetime. It is possible that cosmic strings formed in the early universe during a phase change associated with symmetry breaking. It is theorised that the strings oscillate and form closed loops, which would decay via gravitational radiation.

The frequency of the gravitational waves emitted from such loop decay would depend on the string ‘tension’ or dimensionless mass per length. Since none have been detected by pulsar timing arrays (see subsection 1.5.3), this gives an upper limit on this parameter. This is discussed in detail in Hogan (2006).

If a signal from a cosmic string should be detected, it would be proof of the existence of a phenomenon which, to date, is only a possibility.

1.4.5 Gravitational wave background

Analogous to the cosmic microwave background, gravitational radiation from the Big Bang is expected to be detectable. Originating from 10^{-22} seconds after the Big Bang, compared to 10^{+12} seconds for the cosmic microwave background, the

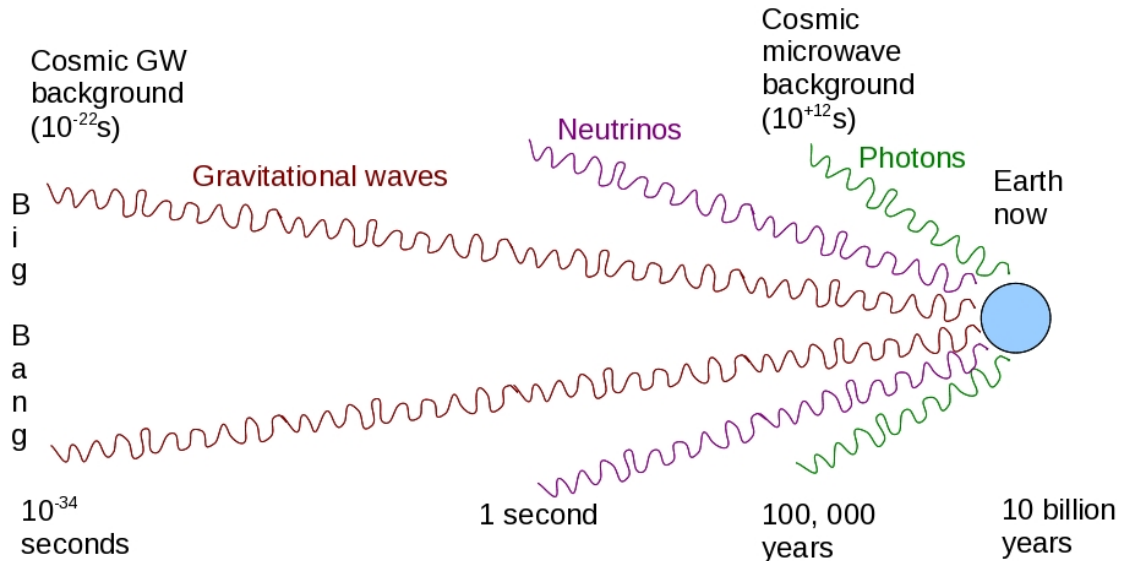


Figure 1.2: Background radiation from the Big Bang.

gravitational wave background is expected to be a great source of information about the early Universe. Gravitation is thought to have decoupled from other forces at the Planck time, 10^{-43} seconds after the Big Bang, which is expected to produce a background of gravitational radiation. However it is thought that relics of the GUT (grand unified theory- all forces apart from gravitation) phase transition at 10^{-22} seconds after the Big Bang might also produce a gravitational wave background. (Brady, 1999)

Figure 1.2 shows the theoretical origin time for gravitational radiation from the Big Bang, compared to neutrinos and electromagnetic radiation. It is clear that gravitational radiation would provide information from much farther back in time than the cosmic microwave background, itself an excellent source of interesting discoveries.

1.5 Gravitational wave detection

Thus far, the only evidence for gravitational wave emission is the indirect detection by orbital decay of a binary pulsar, as described in subsection 1.5.1. There are however numerous facilities working on direct detection, most notably resonant bar detectors (subsection 1.5.2) and laser interferometers (subsection 1.5.5). The existing and proposed detection facilities cover different frequency ranges so would be expected to detect different sources.

1.5.1 Indirect detection

This is the method used by Hulse and Taylor in their groundbreaking discovery (Hulse & Taylor, 1975). Measurements were taken of the time interval between pulses from a binary pulsar arriving at Earth. This allows the orbital period to be deduced. Repeating these measurements over many years gives the change in orbital period- and the rate of orbital decay fitting that predicted for emission of gravitational waves is considered to be an indirect detection of their existence.

1.5.2 Resonant bars

A massive bar is suspended as shown in figure 1.3. As a gravitational wave passes through it, the bar is slightly deformed. If the bar is vibrating at a resonant frequency, the gravitational wave can be detected as a deviation from that resonance. The bar is usually cooled to suppress thermal noise, most operating between 0.1K and 5K. The acoustic signal from the bar can be amplified and measured.

There are numerous such experiments in existence, all with slightly different frequency bands, but most have a peak sensitivity at 1kHz and bandwidth 10-50 Hz. Current detectors include ALLEGRO (USA), ALTAIR (Italy), AURIGA (Italy), EXPLORER (Switzerland), NAUTILUS (Italy) and NIOBE (Australia).

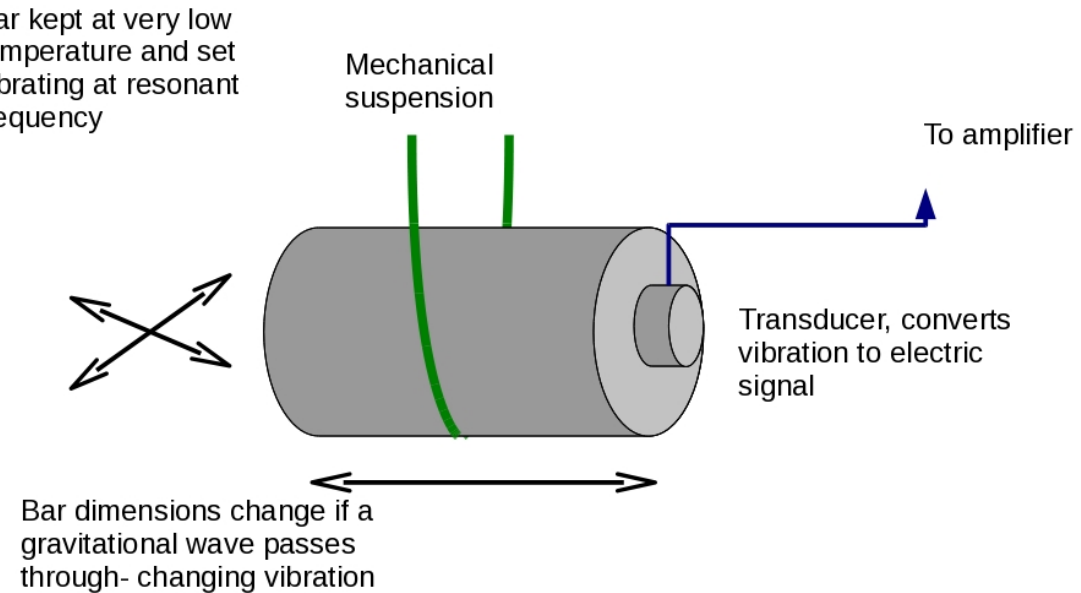


Figure 1.3: Diagram of resonant bar detector.

1.5.3 Pulsar timing

Millisecond pulsars provide very accurate regular signals of pulsed radiation. Models can in some cases predict pulse times of arrival with an accuracy of $< 1\mu\text{s}$ (Hobbs et al, 2010) over years of observation. Millisecond pulsars have very small timing irregularities compared to most pulsars. A pulsar timing array is a set of such pulsars, whose pulse arrival times, taken together, may be used to detect gravitational waves.

A gravitational wave passing by would cause the time of arrival of the pulses to vary slightly. The variation would be small, of the order of 10^{-8} seconds, so arrays of 20-50 pulsars are used. Atmospheric interference is a possible source of error, but monitoring many pulsars means this can be accounted for. (Hobbs et al, 2010)

The observed pulse times of arrival are compared with the models, based on estimates on the pulsar properties from previous timing measurements. The deviations from the model, known as timing residuals, are measured. While a single timing residual may be due to an irregularity in the pulsar spin, if the residuals from many

pulsars are correlated, it is possible that a gravitational wave signal may be seen.

The International Pulsar Timing Array project includes the European Pulsar Timing Array (Lovell Telescope, Westerbork Synthesis Radio Telescope, Effelsberg Telescope and Nançay Radio Telescope), the North American Nanohertz Gravitational Wave Observatory (Arecibo and Green Bank Radio Telescopes) and the Parkes Pulsar Timing Array at the Parkes Telescope in Australia.

A pulsar timing array would be able to measure gravitational waves in the 10^{-6} to 10^{-9} Hz waveband, which includes the expected signal from supermassive black hole binaries formed as galaxies merge. The potential implication of such measurements is discussed in subsection 1.4.1. This waveband is also an area where signals may be seen from cosmic strings if such exist, and the lack of signal so far has been used to constrain the possible properties of cosmic strings, as discussed in subsection 1.4.4. (Hogan, 2006)

The upcoming square kilometre array will allow pulsars to be timed to high precision, of order <100ns. The SKA is expected to detect 14 000 normal pulsars and 6000 millisecond pulsars (Smits et al, 1999). It is hoped that this will allow gravitational wave observation using pulsars to become a working field of astronomy in the near future.

1.5.4 Doppler tracking

The Earth and a distant spacecraft act as test masses. The spacecraft position relative to Earth is monitored using a radio signal sent from a ground station to the spacecraft and coherently returned. The Doppler shift of the signal is measured and continuously monitored.

Should a gravitational wave perturb the path of the signal between spacecraft and ground station, it would cause a brief change in the measured Doppler shift of the signal. The large distances involved, with a signal path of order 1-10AU, would allow detection of sources in the 10^{-3} Hz waveband. (Armstrong, 2008)

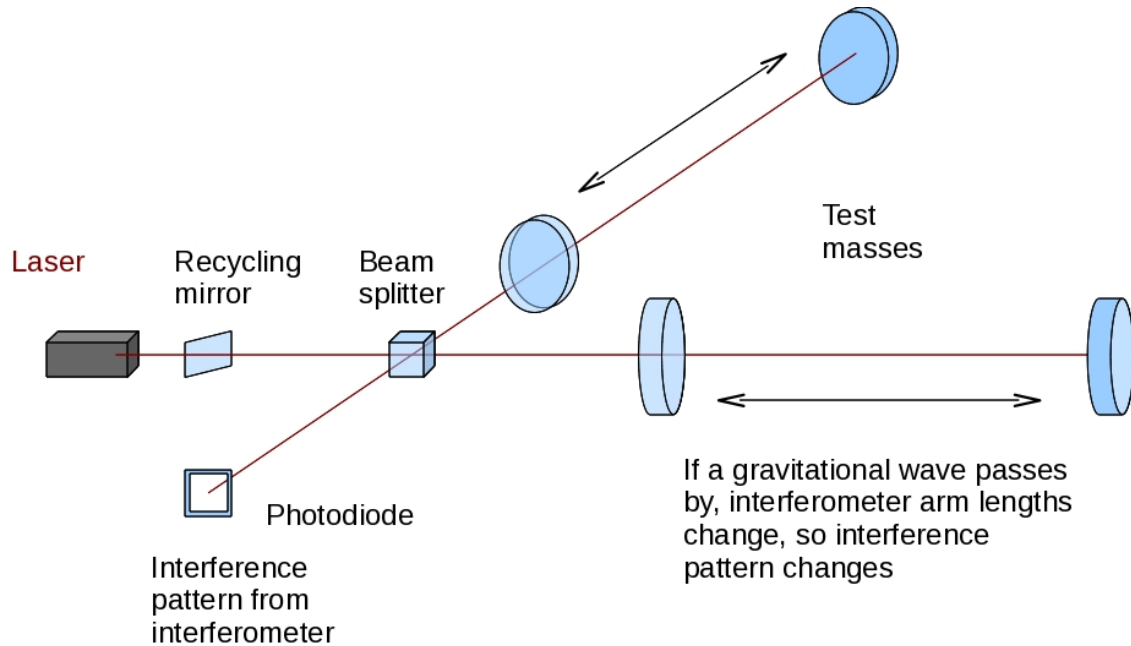


Figure 1.4: Diagram of Michelson interferometer.

1.5.5 Interferometers

In a Michelson interferometer, light from a monochromatic source is split into two beams. These pass along arms at right angles to each other and are reflected back and recombined as shown in figure 1.4.

This gives an interference pattern, dependant on the wavelength of the light and the relative lengths of the arms, which is detected at a photodiode.

When a gravitational wave passes through such a system, one arm will be compressed while the other is stretched. This change in relative arm lengths causes a change in the interference pattern seen at the photodiode.

There are many possible noise sources, including stray cosmic rays impacting the detector, statistical fluctuations in the number of photons meeting the detector and vacuum fluctuations- the creation and annihilation of virtual particles, which may also impact the detector causing noise. Thermal noise is also a problem and ground based detectors must contend with seismic issues as well as expansion and

contraction of the material used to suspend the masses and fluctuations in local gravity.

Ground based interferometry

Ground based interferometers have arms many kilometres in length. Current detectors include LIGO, at two sites in the USA, VIRGO (Italy), GEO600 (Germany), and TAMA3000 (Japan). A possible southern hemisphere interferometer has been suggested. AIGO would be located in Australia.

As a gravitational wave passes through the Earth, these interferometers will each be at a different angle to the wave, so will measure different changes in arm length. Combining measurements should help to accurately determine the source position and the polarisation of the wave.

The LIGO detector should be able to measure a fractional change in arm length of 10^{-21} . The advanced LIGO upgrade is expected to improve sensitivity considerably. Ground based detectors are carefully designed to minimise noise, but are still subject to false signals. Noise sources for LIGO can be seen in Hough (2007)

Gravity gradients are noise caused by fluctuations in local gravity (Johnston, 2002), such as movement of the ground due to seismic effects (Hughes & Thorne, 1998) or moving objects- including people- nearby (Thorne & Winstein, 1999). Internal thermal noise and thermal noise caused by expansion and contraction of the mass suspension is shown, as well as quantum noise which consists of stray cosmic rays and vacuum fluctuations causing false signals at the detector. Some progress has recently been made in minimising vacuum fluctuation noise (The Register, 2011).

These noise sources constrain the frequencies at which the interferometer should be able to detect gravitational waves. LIGO and similar ground based interferometers are most sensitive to frequencies in the 0.1-1kHz range.

Space based interferometry

NASA and ESA had planned to launch a space based gravitational wave detector by 2018. The Laser Interferometer Space Antenna (LISA) would have consisted of three spacecraft flying in formation. Laser beams between each of the spacecraft form ‘arms’ analogous to those in a Michelson interferometer, with laser light from any two spacecraft interfering at the third.

Sadly this project is not going ahead due to financial issues, however it is possible that a similar space based interferometer may be built at some point in the future.

Each laser ‘arm’ was planned to be 5×10^9 m long. LISA was expected to be able to detect changes in arm length of 10^{-11} m. A similar interferometer would detect gravitational waves in the 0.1-100mHz band, so would be expected to see different sources to the ground based detectors.

The three spacecraft would orbit the Sun 20° behind Earth, gradually changing their orientation as they do so. This would allow them to detect gravitational waves from different sources at different points in the orbit and pinpoint their locations.

LISA or a similar interferometer would be an all sky monitor. As the interferometer orbits the Sun, the doppler shift of a source would allow its position to be narrowed down. For a year long observation of a monochromatic source, LISA was expected to have an angular resolution of 10^{-2} to 10^{-4} steradians, with the resolution being better at higher gravitational wave frequencies. (Cutler, 1998; Benacquista, 1999)

Comparison of space and ground based interferometers

LISA mission science office (2007) compares the predicted sensitivities of LISA and Advanced LIGO at different frequencies and shows the classes of sources each would be likely to detect. The difference in frequency range between the two means that both will be required to give a full picture of the gravitational wave universe. There may of course be other, as yet unknown, sources at any frequency. While LISA is

not going ahead, it is possible that any similar future project of the same size might have a similar frequency range.

The New Gravitational wave Observatory, aka e-LISA, an ESA-only project, was proposed in the wake of NASA being unable to continue with LISA. NGO would have three spacecraft, but only two interferometer arms rather than a full triangle, allowing two of the three spacecraft to be smaller and simpler. It was planned to reuse LISA Pathfinder technology.

NGO would have smaller interferometer arm lengths than LISA, of 1×10^9 m km and an expected waveband of 10^{-4} to 1 Hz. (NGO technical & programmatic review report, 2012) While NGO was not selected in 2012, it remains possible that a similar mission may be successful in future.

1.6 Chapter summary

This chapter serves as an introduction to gravitational waves and their astrophysical applications. While thus far only indirectly detected, gravitational waves have the potential to provide insight into many interesting areas of astronomy and answer questions relating to topics as diverse as black hole mergers, measurement of binary systems, gamma ray bursts, the possible existence of cosmic strings and the nature of the universe a fraction of a second after the big bang.

The various different detection methods allow many different frequency bands- and hence many different sources of gravitational waves- to be studied. It is thought that direct detection methods are currently not sensitive enough, since the signals are expected to be extremely small and many noise sources must be accounted for. It is however hoped that future improvements will allow this new and exciting field of astronomy to begin in earnest.

As with any new area of astronomy, perhaps the most interesting things will be those that have not been predicted.

Chapter 2

Gravitational wave emission from an eccentric binary system

2.1 Introduction

In this chapter I describe the construction of a calculation of the gravitational wave emission from a binary system, based largely on the mathematics in Peters & Mathews (1963). This provides a calculation for the power radiated in the n^{th} harmonic of a given binary system, as the power emitted as gravitational radiation for a circular orbit of equal semimajor axis multiplied by an 'enhancement factor' allowing for the very noticeable effect of eccentricity. This factor, which varies with harmonic number and eccentricity, is the key part of the calculation required for the program.

The paper by Peters & Mathews (1963), entitled "Gravitational Radiation from Point Masses in a Keplerian Orbit", derives expressions for the power radiated in gravitational waves from an eccentric binary system. It models a two body Keplerian system, therefore does not include factors like precession that might be seen in a real world system, where other bodies can influence the binary. It also does not include any time evolution of the system. As such, this is suitable for a model of a snapshot in time, as might be seen by a single measurement of a real binary system by an

instrument such as LISA, which, as the formation of spacecraft rotate and they move in orbit around the Sun, would not be expected to be 'pointed' at a single source for a long period of time. Rather, it would observe different sources as it moves around, since as it changes orientation the relative positions of the spacecraft in the formation would be affected by gravitational waves from different directions. Viewing evolution of these systems would require many measurements over many years.

The purpose of my calculation, then, is to calculate the expected gravitational wave emission from a binary system of known orbital parameters, on the basis that, not only can we verify the theory of gravitational wave emission, and by extension general relativity, by checking the measured emission from systems with well known orbital parameters against that predicted by theory, but also we can use gravitational wave measurements to constrain the orbital parameters of less well understood systems. This could lead to better identification of compact objects and black hole candidates, increase our understanding of the interaction between a compact object and main sequence or giant companion, and help us to study what happens when such stars, or pairs of neutron stars collide, black hole mergers or 'swallowing' of stars by black holes. Clear measurements of the orbits of binary systems are vital to these studies, and if we have a good model of the expected gravitational wave emission from a system with any given set of parameters, that can be used to identify the orbital parameters of an otherwise unknown system.

Vital to this is a suitably accurate calculation of Bessel functions of the first kind, for which various were tried before settling on the most accurate when compared to the tables in Abramowitz & Stegun (1968), detailed in subsection 2.4.2.

The calculation outputs a spectrum of power emitted in gravitational waves or simply the 'enhancement factor' (as it is multiplied by a constant for any given system- the power output for an equivalent circular system) versus frequency or harmonic number, requiring as input various orbital parameters and with a user-defined range of frequencies for the output.

The results have been compared to the graphs in the original paper (Peters & Mathews, 1963) and found to match as closely could be expected, remarkably so given that the original curves were likely drawn by hand and hence may not be quite as accurate as a computer generated curve, see figure 2.1.

Generic features of the output are discussed in their relation to real world binary systems in section 2.5 and instructions for use of my program, as applied in chapter 3, are given in section 2.7.

This calculation is used to calculate the expected gravitational wave emission from various known binaries in chapter 3. It is also the basis for the statistical, many systems calculation detailed in chapter 4.

2.2 Previous work

Ultra-compact binaries are expected to be the most numerous sources in the low frequency gravitational wave band (e-LISA Science Case, 2012), with both individual detection- of several thousand systems- and combined contribution to the background being worthy of study. Known, well characterised systems can be used for instrument verification, beyond that, measurements of the gravitational waves can be used to find out more about both the parameters of the systems being studied- and hence the nature, population and evolution of such systems in general (LISA mission science office, 2007).

Nelemans et al (2004) simulate the Galactic population of AM CVn systems, binaries comprising a white dwarf accreting matter from a low mass, helium rich object. They find that the Galaxy should contain 140 000 such systems with periods of \approx 1500s, which are likely to be strong emitters of gravitational radiation. They calculated the optical, X-ray and gravitational wave signals expected and conclude that LISA or a similar detector would be able to detect about 10% of these systems, many thousands of binaries. Of these, about 3% would be expected to also be seen in optical or X-ray bands, allowing independent determination of position, and hence

a more accurate estimate of the systems' orbital parameters.

Many thousands of double white dwarf systems should also be detectable, as mentioned in the LISA science case (LISA mission science office, 2007).

(LISA mission science office, 2007) shows signal amplitude versus frequency for double white dwarfs and neutron star binaries (large symbols) on the left and AM CVn systems with ultra-compact X-ray sources marked (large symbols) on the right. These are compared to the average double white dwarf background (solid line) and LISA sensitivity for an integration time of 1 year with signal to noise ratios of 1 and 5 respectively, the dashed lines.

The gravitational wave background from the extragalactic close binary population is studied in Farmer & Phinney (2003). They characterise systems descended from stars of low to intermediate initial mass and find the gravitational wave background from these systems is dominated by double main sequence binaries for a signal frequency at Earth of $< 10^{-4}$ Hz and by close white dwarf-white dwarf binaries for frequency from 10^{-4} to 10^{-1} Hz. Their models use a thermal distribution of eccentricities. They find that the background may be difficult to subtract, particularly at frequencies of less than 50mHz, as there will be too many double white dwarf pairs contributing to the background to allow it to be resolved, though the major contribution is from nearby binaries. At above 50mHz far fewer double white dwarf binaries contribute to the signal, so it may be easier to subtract the background from such systems in this region.

Benacquista (2006) reviews relativistic binaries in globular clusters. Very short period binaries form as globular clusters evolve, which will be sources of gravitational waves. These binaries can be used to trace the evolution of globular clusters, so a measurement of their gravitational radiation could help us learn more about the nature and evolution of such clusters. This is discussed in more detail in Chapters 4 and 5.

2.3 Calculation of gravitational wave emission

As explained in chapter 1, gravitational waves are emitted due to an asymmetrical movement of mass. In a binary system, the two bodies orbit about their common centre of mass. The more eccentric the orbit, the greater the asymmetry and so the greater the energy emitted in gravitational waves. An elliptical orbit also means the emission will occur at multiples of the orbital frequency since the orbit is elongated, with the peak occurring at higher harmonic number as eccentricity increases.

Peters & Mathews (1963) calculates the predicted gravitational wave emission from an eccentric two body system, using two mathematical methods (inertia tensor and multipole expansion) to reach the same result, and verifying it. I do not reproduce these calculations here, as the paper is available, but simply state the results which are relevant to my research.

The average power $\langle P \rangle$ radiated as gravitational waves by an elliptical binary system can be calculated from the masses, m_1 and m_2 , the separation for an equivalent circular system a and the eccentricity e .

$$\langle P \rangle = \frac{32}{5} \frac{G^4}{c^5} \frac{m_1^2 m_2^2 (m_1 + m_2)}{a^5} f(e) \quad (2.1)$$

$$f(e) = \frac{1 + \left(\frac{73}{24}\right)e^2 + \left(\frac{37}{96}\right)}{(1 - e^2)^{\frac{7}{2}}} \quad (2.2)$$

This is equivalent to the power output for a circular system with otherwise identical parameters multiplied by an eccentricity function, $f(e)$.

The gravitational radiation is emitted not at a single frequency, but across a set of harmonics, whose frequencies depend on the orbital period of the system.

The eccentricity also affects the peak harmonic at which power is radiated. Again from Peters & Mathews (1963) the power in the n^{th} harmonic, $P(n)$ can be calculated as follows, where J_x denotes a Bessel function of the first kind.

$$P(n) = \frac{32}{5} \frac{G^4}{c^5} \frac{m_1^2 m_2^2 (m_1 + m_2)}{a^5} g(n, e) \quad (2.3)$$

$$\begin{aligned}
g(n, e) = & \frac{n^4}{32} \left\{ \left[J_{n-2}(ne) - 2eJ_{n-1}(ne) \right. \right. \\
& + \frac{2}{n} J_n(ne) + 2eJ_{n+1}(ne) - J_{n+2}(ne) \left. \right]^2 \\
& + (1 - e^2) J_{n-2}(ne) - 2J_n(ne) + J_{n+2}(ne)^2 \\
& \left. + \frac{4}{3n^2} J_n(ne)^2 \right\}
\end{aligned} \tag{2.4}$$

These equations form the basis for my calculation, and the graph given in the paper was used to check my results.

It is also noted in the paper that the average power emitted over one orbit in each of the two gravitational wave polarisations can be calculated, thus:

$$\langle P_1 \rangle = \frac{32}{5} \frac{G^4}{c^5} \frac{m_1^2 m_2^2 (m_1 + m_2)}{a^5 (1 - e^2)^{\frac{7}{2}}} \left(\frac{7}{12} + \frac{683}{384} e^2 + \frac{347}{1536} e^4 \right) \tag{2.5}$$

$$\langle P_2 \rangle = \frac{32}{5} \frac{G^4}{c^5} \frac{m_1^2 m_2^2 (m_1 + m_2)}{a^5 (1 - e^2)^{\frac{7}{2}}} \left(\frac{5}{12} + \frac{485}{384} e^2 + \frac{245}{1536} e^4 \right) \tag{2.6}$$

This is not included in the calculation for a single binary system, since its purpose is to give a spectrum of gravitational wave emission across different frequencies rather than merely the total power emitted over an orbit, however it is worth noting that for a given eccentricity e , the ratio of average power over one orbit emitted in one polarisation to average power over one orbit emitted in the other, $\langle P_1 \rangle : \langle P_2 \rangle$ would be a constant, so if a measurement of the average power over one orbit emitted in one polarisation for a binary system is available, the total power can easily be estimated.

The detailed spectrum in each polarisation can also be calculated as described in section 2.6.

For a circular system, with $e=0$, the only emission would be in the $n=2$ harmonic, as for all others the Bessel functions $J_x(0)$ are all zero. But for the $n=2$ harmonic, the terms in $J_{n-2}(0)$ are $J_0(0) = 1$.

2.4 Programming considerations

Equations 2.3 and 2.4 were used as the basis for a program to output power emitted as gravitational waves vs harmonic number or frequency for user input values of the orbital parameters- the masses of both bodies, orbital period and eccentricity. The orbital separation for an equivalent circular system was calculated from the orbital period using Kepler's 3rd law as in equation 2.7. The radii of both stars are also user input variables- these are used to perform a simple check that the eccentricity is realistic. The minimum possible periastron distance is assumed to be the sum of the two radii- i.e. the stars just touching- and used to calculate the maximum possible eccentricity for the system.

$$a = \left(\left(\frac{T}{2\pi} \right)^2 G(m_1 + m_2) \right)^{\frac{1}{3}} \quad (2.7)$$

The study was first implemented in Mathematica for initial testing, then rewritten in Fortran. The main concern was output accuracy, so double precision variables are used throughout and numerous options for Bessel function generation were tested and compared with the tables in Abramowitz & Stegun (1968). The one chosen was accurate to the limits of the output.

2.4.1 General structure of program

The program reads inputs from the screen, calculates the orbital separation and uses the stellar radii to check the input eccentricity is realistic.

Various versions were produced, some outputting power emitted vs harmonic number (n), some power emitted vs frequency. The program allows for non-integer harmonic numbers to be used. Though this is unphysical, so was not used in the final version, it allowed for clearer checking of the mathematical behaviour of the calculation, to ensure all output was as accurate as possible. It also, again for mathematical checking, allowed inspection of the curve at $0 < n < 1$, though for a real system, only $n \geq 1$ is physical as $n = 1$ is the base frequency of the system, the

orbital frequency. For these mathematical tests, results were output every $n/100$. For the final version, modelling real systems, only output at integer n and $n \geq 1$ was required. So the user input of a frequency range was used to calculate how many integer multiples of n fell within that range. The array to hold the output was allocated accordingly, and the calculation done for each integer multiple of n , writing the results to a file which could then be read for graphing.

Doing the calculation involves calling a function which itself then calls various subroutines to calculate the Bessel functions required. The function calculates $g(n, e)$ and multiplies it by the equivalent power for a circular system as in equation 2.3, giving a double precision value for the power emitted in gravitational waves for that system at that harmonic number. This is returned to the main program, which fills an array with frequency (at the given harmonic number) and power columns, before this is output as a file.

2.4.2 Treatment of Bessel functions

For dealing with the Bessel functions, both NAGware and Numerical Recipes functions were considered. Various options were tested including before settling on that which was most accurate compared with the tables in Abramowitz & Stegun (1968). The options were tested by writing a small program that simply outputs tables of Bessel functions as tab separated text files. As well as comparing the numerical output to the tables, these were graphed to check the Bessel functions appeared to be behaving as they should.

The most accurate method I found was a slightly modified version of the bessjy, beschb, and chebev set of functions from the Numerical Recipes book (Press, Teukolsky). I also tried the bessj0 and bessj1 functions of the same book, and the NAGware treatment for Bessel functions of the first kind (Numerical Algorithms Group, NAG library).

I modified it for greater accuracy, using double precision variables, constants and

operations throughout.

2.5 Output and analysis

The program outputs a tab separated file in two columns, which can easily be read to produce a graph. It can output either the power in gravitational waves or simply the eccentricity function $g(n, e)$, equation 2.4 in section 2.3, versus either the harmonic number, n , or the frequency.

In order to check the output was as expected, I ran some tests and compared the sum of the $g(n, e)$ at integer n , as the emission only occurs at integer multiples of the base frequency, to the expected total over all n , which is $f(e)$, equation 2.2 in section 2.3. I tested this at a variety of eccentricities, and, for results from $n = 1$ to a large n , where the graph had visibly tailed off to zero, the sums were correct.

I also attempted to recreate the graph shown in Peters & Mathews (1963). Bearing in mind the difference between a computer generated curve, which does in fact follow the values of $g(n, e)$ for fractional n in order to draw a smooth curve, and the likely hand drawn graph of the 1963 paper, it is clear they give the same results. The original can be seen in Peters & Mathews (1963) and the version generated by the calculation in figure 2.1.

2.5.1 The $g(n, e)$ graph

The graph of $g(n, e)$ versus n can be drawn from any $n > 0$ to any positive n , though only the $n \geq 1$ region can be considered physical as $n = 1$ is the base harmonic of the system, with frequency equivalent to the orbital frequency. Obviously the higher the maximum n , or the greater the resolution required in the graph, the longer the calculation takes to run. For real systems, only integer n are required, but it is worth looking at the graph in more detail in order to check there are no mathematical discontinuities- and for that reason also worth checking the $n < 1$ region. If there were discontinuities, it might have been indicative of a problem with the calculation.

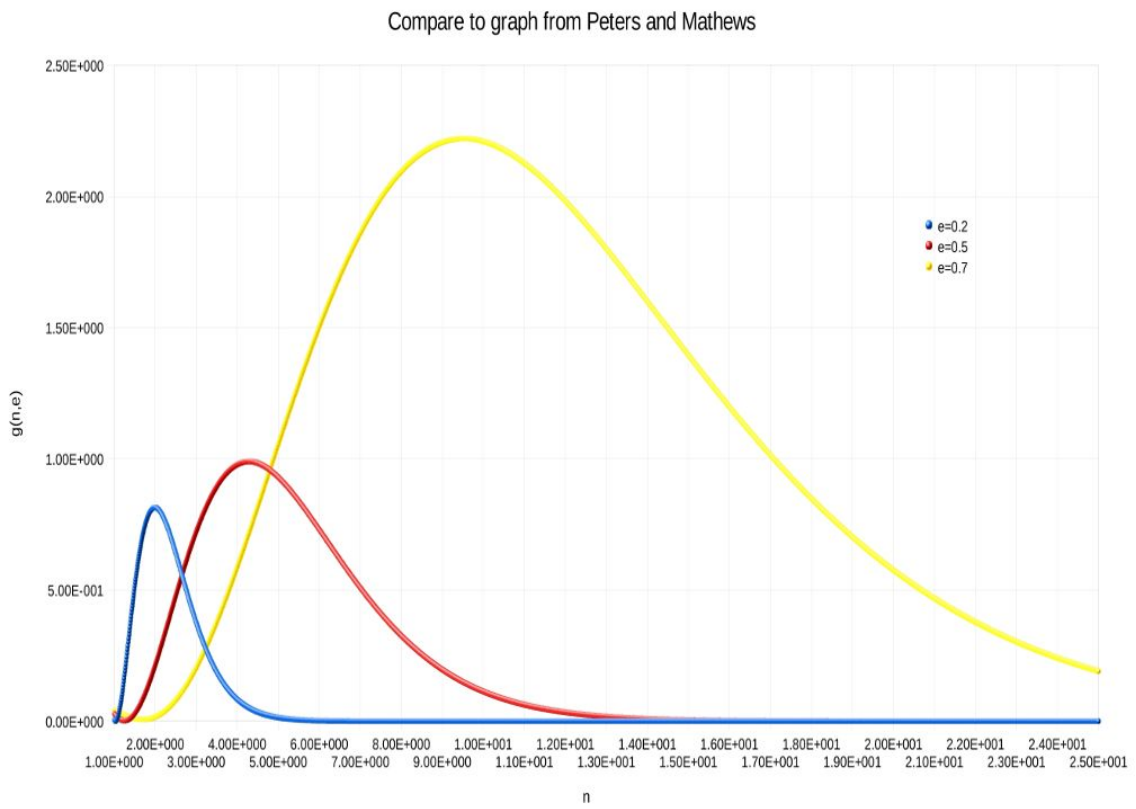


Figure 2.1: Graph showing $g(n,e)$ versus harmonic number, n , as generated by calculation

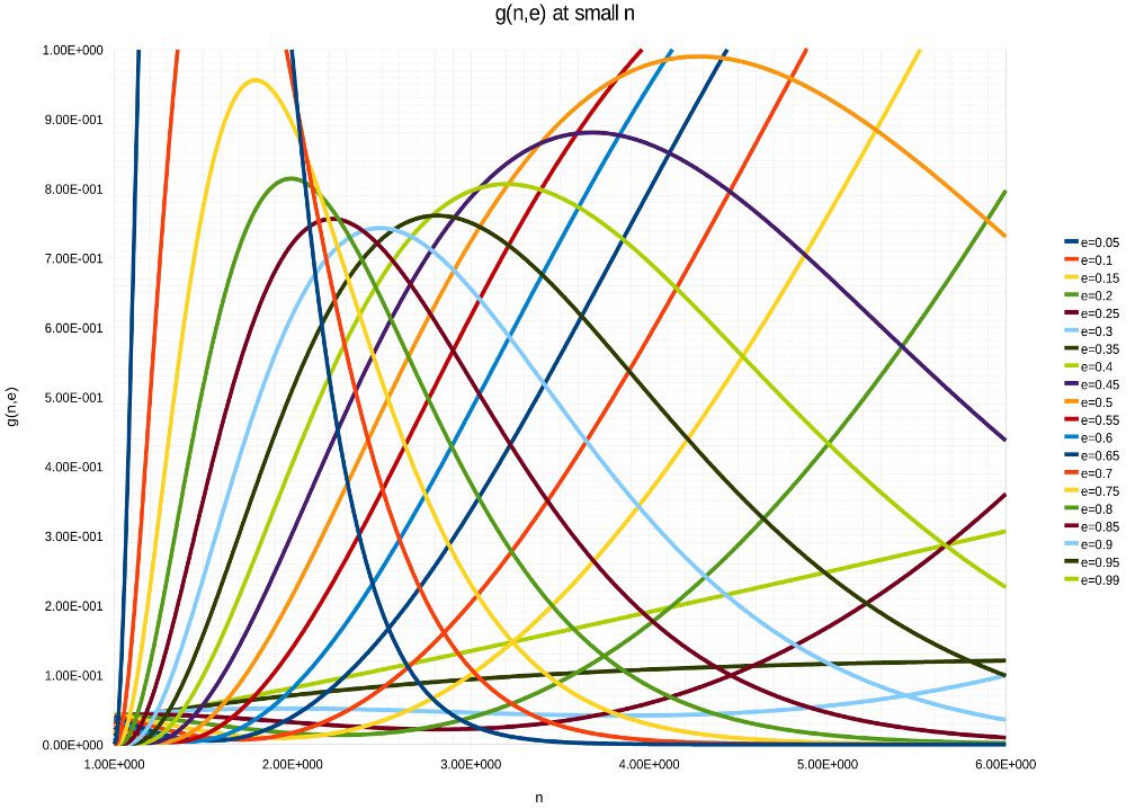


Figure 2.2: Graph of the behaviour of the $g(n,e)$ curve from $n=1$ to $n=6$ and $e=0.05$ to 0.99

While early versions did have these problems, largely due to rounding errors in the Bessel function generation, the final version does not and, as detailed in section 2.4.2, the Bessel function implementation has been checked for accuracy.

The graph, seen in figure 2.2 from $n = 1$ to $n = 6$ for a variety of eccentricities, is a curve which becomes wider- that is to say, the peak moves to a higher harmonic number- as eccentricity increases. As eccentricity tends towards 0, the curve becomes higher and narrower, tending towards a delta function. Increasing eccentricity sees the curve widen, and the peak drop then start to rise once more. At large eccentricities, the higher the eccentricity the higher the peak and higher the harmonic number it occurs at.

This behaviour is consistent with expectation- at higher eccentricity, the bodies

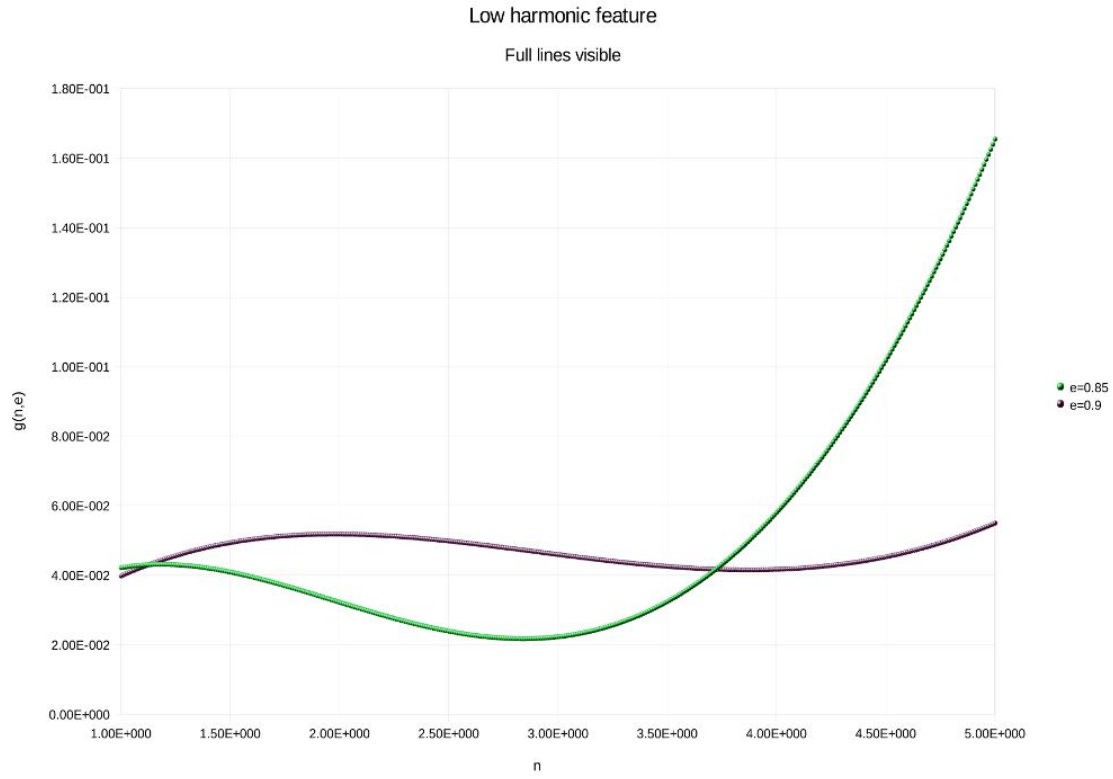


Figure 2.3: Graph of the behaviour of the $g(n,e)$ curve from $n=1$ to $n=6$ at $e=0.85$ and $e=0.9$

move further and faster past each other, giving a wider and more powerful emission of gravitational waves.

The low harmonic feature at $n>1$

It can be seen that at low harmonic number, more noticeable at larger eccentricity, the curves do not stay at zero but rise again towards $n = 1$. At very large eccentricity, the curve rises then falls again towards $n = 1$. This may be more easily seen in figure 2.3.

At larger eccentricity, this feature is noticeable even using only integer values of n , so would be seen in a signal from a real system, as shown in figure 2.4.

These features do follow from the mathematics- and can in fact be seen in the

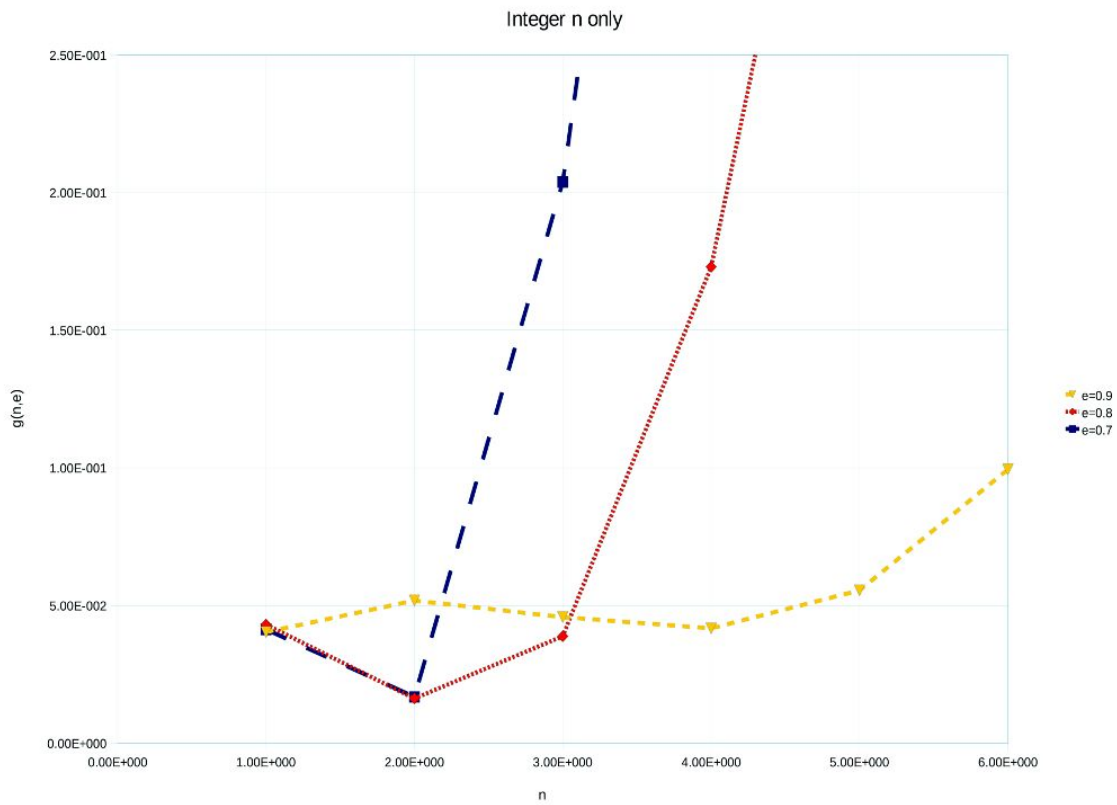


Figure 2.4: Graph of the behaviour of the $g(n,e)$ curve at low harmonic and integer n

original graph from Peters & Mathews (1963) on the higher eccentricity curve. To check this, I looked at the behaviour of the curves in the unphysical, but mathematically plausible $n < 1$ region.

The $n < 1$ region

The $n < 1$ region, while not relevant to measurements of real eccentric binary systems, serves as a check that the calculation functions as it should. Since mathematical solutions are possible in this region, it should be continuous with the curves in the $n \geq 1$ region.

It should be noted that, for a real system, any feature at $n < 1$ would be occurring on a timescale of greater than one orbit, and thus, would not be modelled in a Keplerian two body system such as in this calculation. Thus the visible feature cannot be due to orbital precession or any real value, and is purely a result of the mathematics. In an isolated two body system, with no precession, as modelled here, the signal would be at integer values of n only and there would be no signal below $n = 1$.

The output of the program at $n < 1$ is, as expected, continuous with the output in the realistic $n \geq 1$ region, so acting as confirmation that the small feature at low harmonic number is in fact a real result. This can be seen in figure 2.5 and, more clearly visible, in figure 2.6 which shows only the curves for the $e = 0.85$ and $e = 0.9$ eccentricities.

2.5.2 Realistic output

For a real calculation of the expected signal from an eccentric binary, the calculation has been set to output power emitted as gravitational radiation (in erg/s) versus frequency, calculating a signal and giving a data point at integer multiples n , so integer multiples of the orbital frequency, only. This was used to predict the gravitational wave emission that would be seen from a number of real eccentric binary

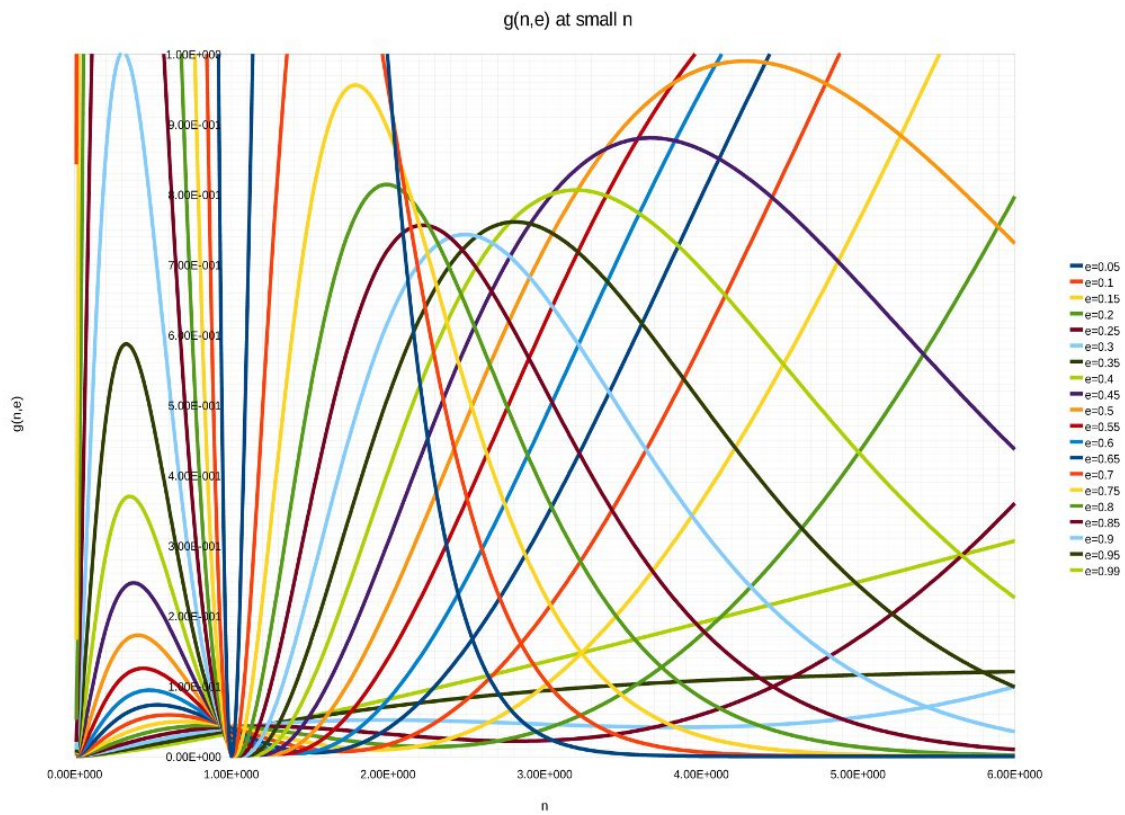


Figure 2.5: Graph of the behaviour of the $g(n,e)$ curve from $n=0.001$ to $n=6$ and $e=0.05$ to 0.99

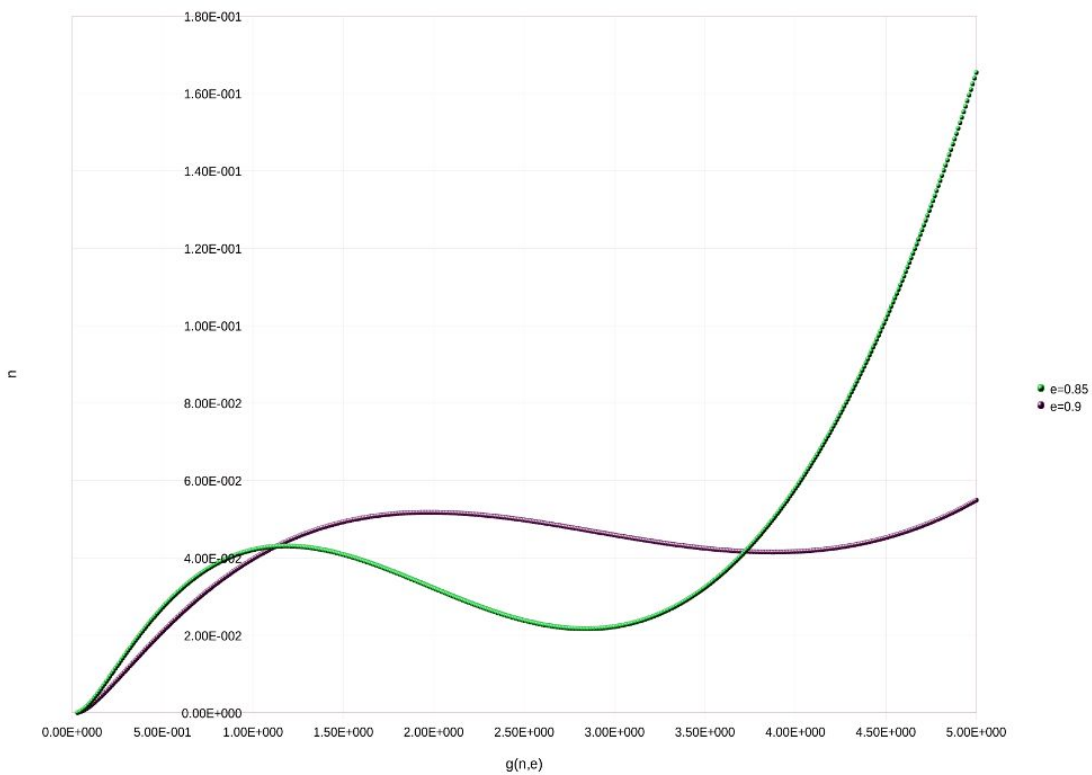


Figure 2.6: Graph of the behaviour of the $g(n,e)$ curve from $n=0.001$ to $n=6$ at $e=0.85$ and $e=0.9$

systems, including high mass X-ray binaries, low mass X-ray binaries and binary systems containing radio pulsars. The results of this study are detailed in chapter 3.

2.6 Calculation of gravitational wave emission in each polarisation

Moreno-Garrido et al (1995) describes a calculation of the gravitational wave emission in each of the 'X' and '+' polarisations from a single system, depending on both the parameters of the system, as in Peters & Mathews (1963), and the position of the system relative to an observer at point P, calculated in terms of distance, R , to the centre of mass of the system and the angles Θ , defined as $\frac{\pi}{2}$ – the angle between the vector \vec{R} and the orbital plane of the system, and Φ , the angle formed by the projection of \vec{R} in the orbital plane and the major axis of the orbital ellipse. This can be seen in figure 2.7, where the X-Y plane is the orbital plane and the X axis is the line of the major axis of the orbit.

Moreno-Garrido et al (1995) calculate the total flux of gravitational waves in each polarisation reaching the observer. They also break down the components of each polarisation, h_x and h_+ , into emission at each harmonic number, allowing a calculation of the spectrum of gravitational waves in each polarisation seen at the observer. Like Peters & Mathews (1963), this involves a Fourier-Bessel expansion.

The modulus squared of each component $(h_x)_n$ and $(h_+)_n$, at a harmonic number n , averaged over an orbit, can be used to calculate the flux of gravitational waves seen by the observer.

Where there is no periastron advance, as is the case with the model of Peters & Mathews (1963) and is suitable for the purposes of this study, looking at a single measurement rather than long term evolution of the system, these components are calculated as follows in Moreno-Garrido et al (1995), which uses $c=G=1$ units. This

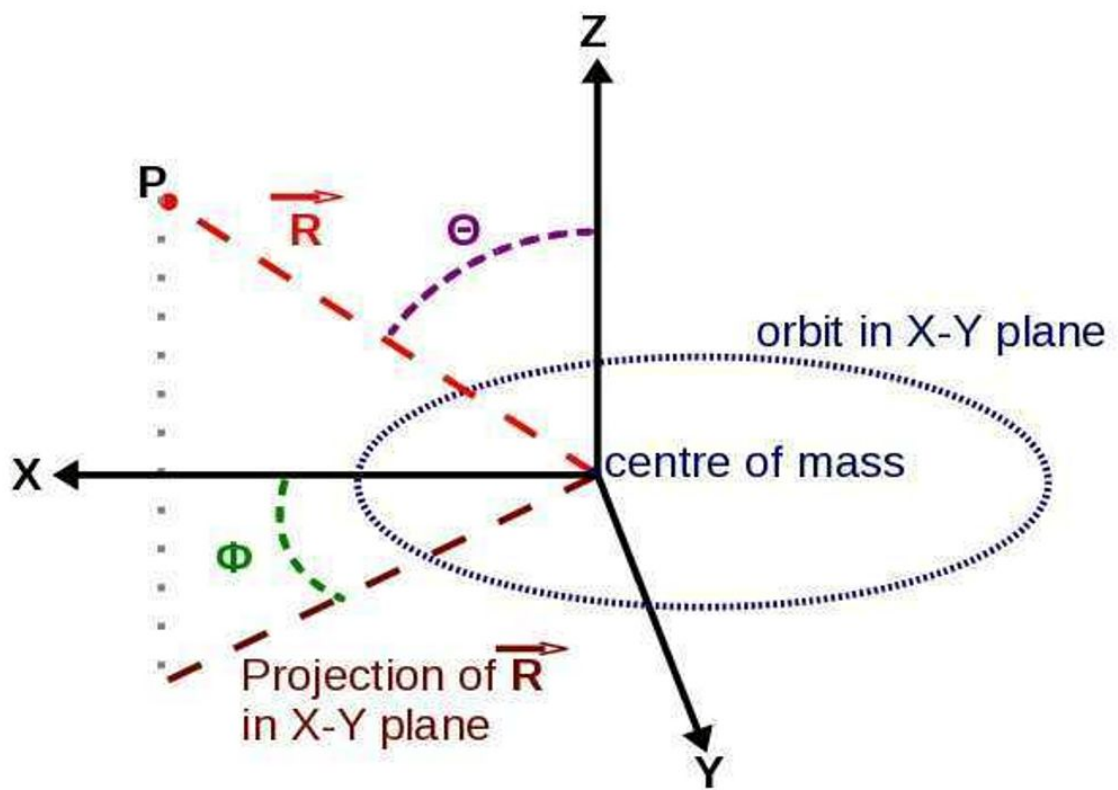


Figure 2.7: Co-ordinate system used when calculating gravitational wave flux at observer

is corrected for in the final calculation.

$$|(h_{\times})_n|^2 = h_0^2 \cos^2 \Theta \left[\left(\frac{C_n}{2} \right)^2 \sin^2 2\Phi + \left(\frac{S_n}{2} \right)^2 \cos^2 2\Phi \right] \quad (2.8)$$

$$\begin{aligned} |(h_+)_n|^2 &= h_0^2 \left\{ \frac{\sin^2 \Theta}{4} A_n \left[\frac{\sin^2 \Theta}{4} A_n + \frac{1}{2} (1 + \cos^2 \Theta) \right. \right. \\ &\quad \left. \left. \times C_n \cos 2\Phi \right] \right\} + \left(\frac{1 + \cos^2 \Theta}{2 \cos \Theta} \right)^2 \left| h_{\times} \left(\Phi + \frac{\pi}{4} \right)_n \right|^2 \end{aligned} \quad (2.9)$$

Note that $h_{\times}(\Phi + \frac{\pi}{4})$ refers to h_{\times} evaluated with Φ replaced by $\Phi + \frac{\pi}{4}$

Where

$$A_n = (1 - e^2) J_n(ne) \quad (2.10)$$

$$C_n = -\frac{(1 - e^2) + (1 - e^2)^2}{e^2} J_n(ne) + \frac{(1 - e^2)^2}{e} 2J'_n(ne) \quad (2.11)$$

$$S_n = -\frac{(1 - e^2)^{\frac{3}{2}}}{e} \frac{2}{n} J'_n(ne) + \frac{(1 - e^2)^{\frac{5}{2}}}{e^2} 2n J_n(ne) \quad (2.12)$$

and

$$h_0 = \frac{2m_1 m_2}{a(1 - e^2)} \frac{2}{R} \quad (2.13)$$

$J'_n(ne)$ was calculated using the recurrence property

$$J'_n(ne) = \frac{n}{2} J_{n-1}(ne) - J_{n+1}(ne) \quad (2.14)$$

Moreno-Garrido et al (1995) use the expression for radiated flux corresponding to a plane wave (Misner, Thorne and Wheeler);

$$T_{0z}^{GW} = \frac{1}{32\pi} \omega^2 (|h_+|^2 + |h_{\times}|^2) \quad (2.15)$$

where

$$\omega = 2\pi n\nu \quad (2.16)$$

is the angular frequency of the system, where $\nu = 1/T$ is the orbital frequency and T is the orbital period

Using dimensional analysis to convert back to cgs units(see the appendix), and putting all this together, it follows that the total flux in gravitational waves at a given harmonic number, F_n , seen by the observer is

$$F_n = \frac{G^3}{c^5} \frac{\pi}{8} n^2 \frac{1}{T^2} (|h_+|^2 + |h_\times|^2) \quad (2.17)$$

And so the flux in each polarisation, at a given harmonic number n , is calculated:

$$F_n = \frac{G^3}{c^5} \frac{\pi}{8} n^2 \frac{1}{T^2} |h_\times|^2 \quad (2.18)$$

$$F_n = \frac{G^3}{c^5} \frac{\pi}{8} n^2 \frac{1}{T^2} |h_+|^2 \quad (2.19)$$

I used these equations in an expansion of my original single system calculation to calculate the possible gravitational wave signal that might be detected at Earth from an eccentric binary system.

The program was run for an example system at 5kpc distance from the observer, with stars of mass $1.4M_\odot$ and $3M_\odot$ and an orbital period of 10 days. The output can be compared to the graphs in the original paper (Moreno-Garrido et al, 1995).

For the example system mentioned, results for an eccentricity of 0.3 are shown in figure 2.8, the flux of gravitational waves in the + polarisation seen at the observer and figure 2.9, the \times polarisation. Results are shown for $\Theta = 0, \frac{\pi}{6}, \frac{\pi}{3}$ and $\frac{\pi}{2}$ and $\Phi = 0, \frac{\pi}{4}$ and $\frac{\pi}{2}$, so the effect of both can be seen.

Similarly, results for the example system with eccentricity set to 0.6 are shown in figure 2.10 for the + polarisation and figure 2.11 for the \times polarisation.

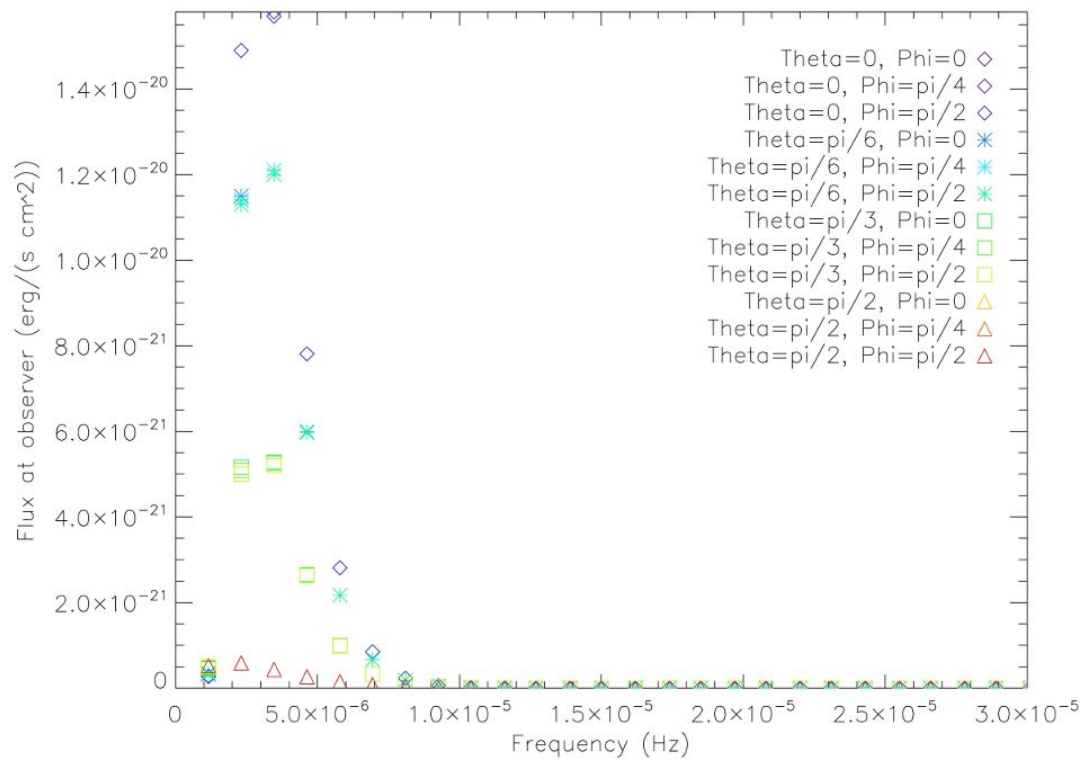


Figure 2.8: Gravitational waves in the + polarisation for example system with eccentricity 0.3

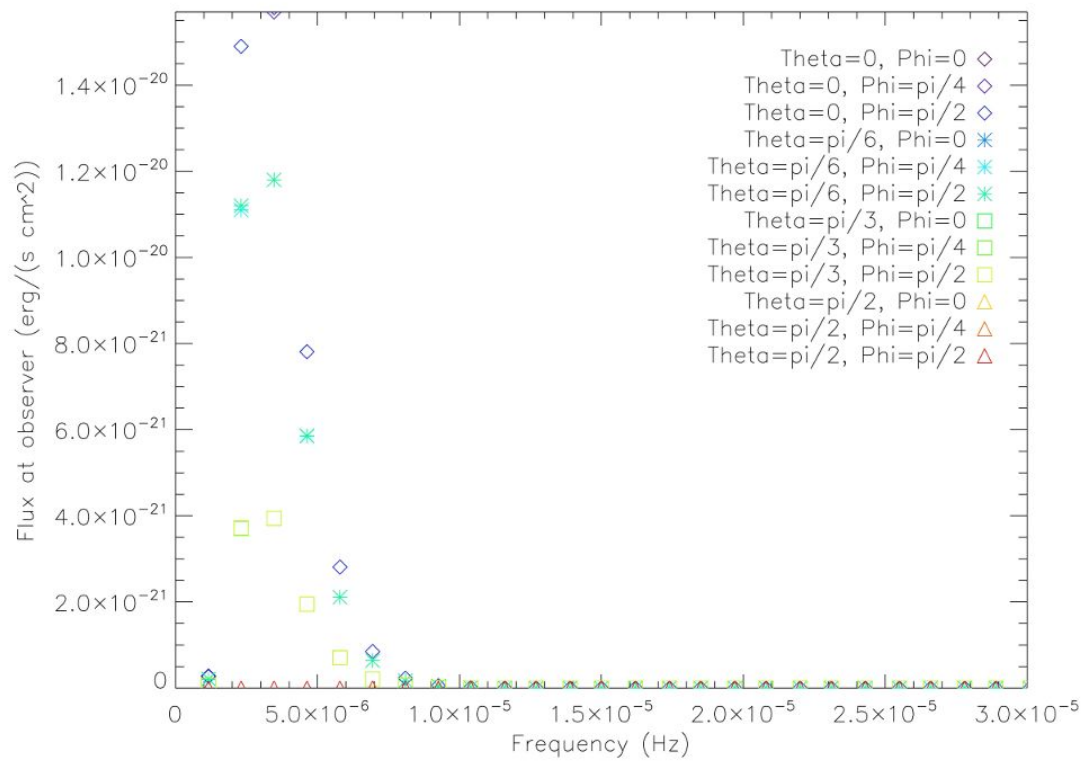


Figure 2.9: Gravitational waves in the \times polarisation for example system with eccentricity 0.3

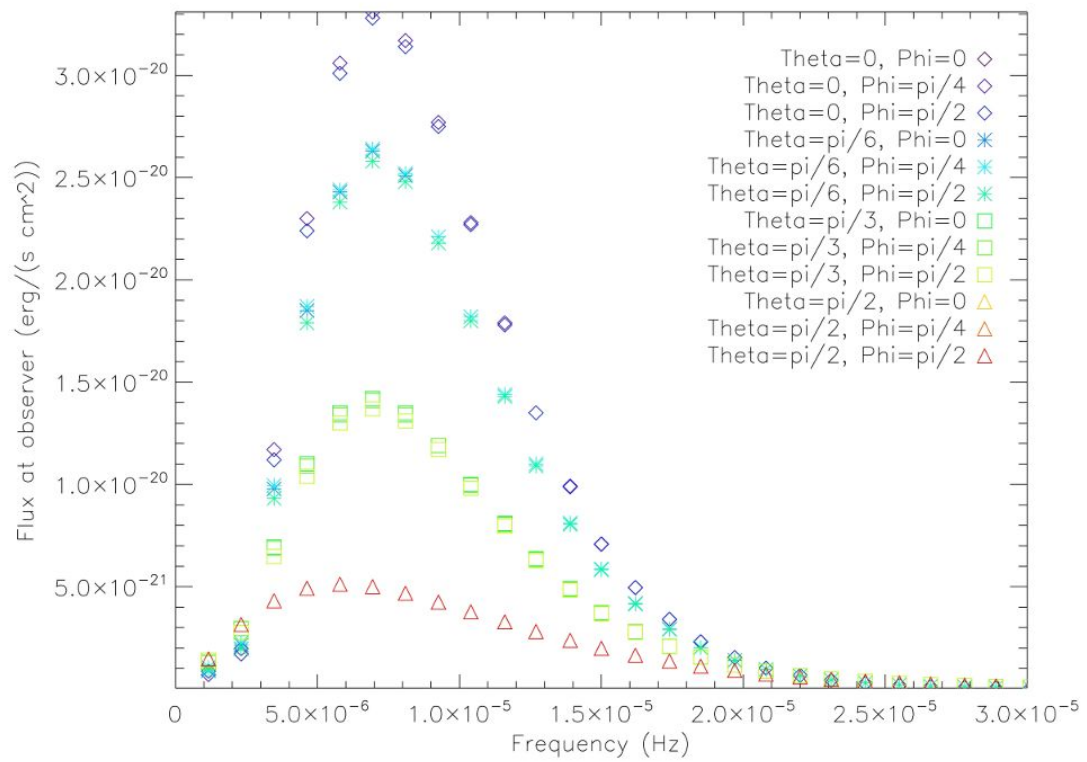


Figure 2.10: Gravitational waves in the + polarisation for example system with eccentricity 0.6

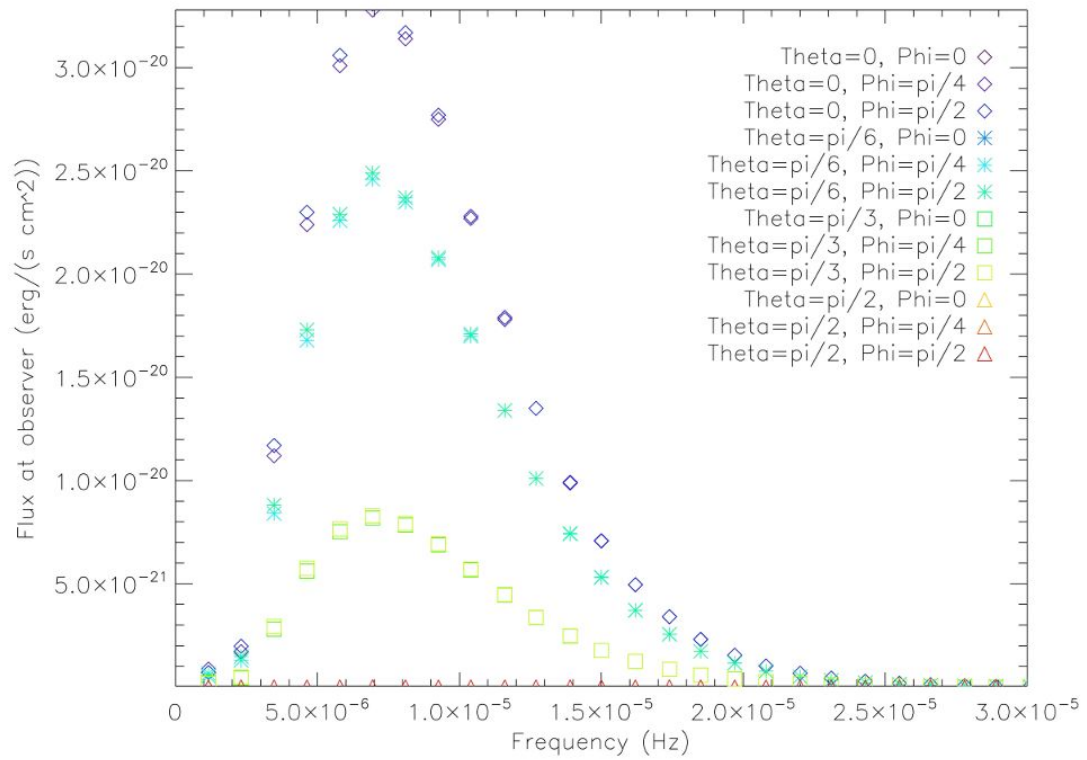


Figure 2.11: Gravitational waves in the \times polarisation for example system with eccentricity 0.6

2.7 Use of programs

To use the programs, the user must enter, when prompted, the masses of the two bodies, orbital period and eccentricity. The radii of the two bodies are also requested. This allows the program to check that the eccentricity entered is feasible but does not contribute further to the calculation. Orbital separation is calculated from the orbital period using Kepler's third law.

For the polarisation program, the user must also enter the distance to the system and inclination (Θ). Φ is not likely to be known for a real system, so the program will output results for $\Phi = 0, \frac{\pi}{4}, \frac{\pi}{2}, \frac{3\pi}{4}, \pi, \frac{5\pi}{4}, \frac{3\pi}{2}, \frac{7\pi}{4}, 2\pi$, with the equivalence of the first and last outputs being a quick check that all is working as it should. These outputs could all then be compared to a measured gravitational wave signal from a real system, in order to determine the likely value of Φ .

The user must also enter the maximum and minimum frequencies for the output. The program then calculates which integer multiples of the orbital frequency fall in this range, adjusts the output array accordingly, runs the calculation for these and outputs the results as a tab-separated text file with the extension .dat. This file can be read into a variety of programs for graphing purposes. In order to ensure the lowest possible signal, $n = 1$, is registered, it is recommended to set the minimum at 0Hz, unless of course the program is used to show the results that would be seen with an instrument with known bandwidth, in which case the maximum and minimum should be set accordingly.

2.8 Chapter summary

This calculation allows modelling of the expected power output as gravitational waves from an eccentric binary system, based on the mathematical description for a Keplerian two body system in Peters & Mathews (1963). It is implemented in Fortran and uses a modified form of some of the functions from Press (Teukolsky)

to calculate the necessary Bessel functions. A calculation of the flux of gravitational waves in each of the $|h_+|$ and $|h_\times|$ polarisations across different frequencies that would be seen by an observer at a known distance is also presented.

Should it become possible to take a real, direct measurement of the gravitational waves emitted from a binary system, as was planned with the LISA mission, these calculations could be used to check whether real measurements of well characterised systems agree with that predicted by the theory. Potentially more interesting is the possibility of using real measurements, compared to the results of these calculations, as a way to constrain the parameters of systems which are not yet well characterised, possibly leading to, for example, identification of the nature of the compact object in an X-ray binary or better measurements of a system where the bodies near collision. This is discussed further in chapter 3.

The calculation can be used as a basis for modelling the overall signal from a large number of binary systems, such as may be found in globular clusters. This is investigated further in chapter 4.

Chapter 3

Application to known eccentric binaries

3.1 Introduction

In this chapter I apply the model of chapter 2 to a number of known eccentric binary systems. Their likely gravitational wave emission is calculated and displayed in graphical form. This demonstrates how, with gravitational wave data, we could better constrain the parameters of such systems, as well as showing how the characteristic emission profile varies with factors such as the period of a system and the masses of the bodies therein.

The effect of eccentricity on the results is, as expected, particularly strong, showing the clear increase in total emission power and shift to higher frequencies as eccentricity is increased. Thus, if a source can be clearly identified by LISA or a similar project- for many of these systems lie within the expected LISA band, or close to it- it should be possible to use the signal to estimate the eccentricity of the system.

The effect of orbital period is also very pronounced, a shorter period producing, as expected, a much higher frequency signal. Short period binary systems are

more likely to lie within LISA's detection range than equivalent systems with longer periods.

I have applied the calculation to 18 high mass X-ray binaries, 14 radio pulsar binaries and two examples of low mass X-ray binaries. The peak predicted emission of the HMXBs studied lies within a narrower band than the radio pulsar binaries, and more radio pulsar binaries are likely to be detectable by LISA than HMXBs within these samples. This may or may not be representative of real populations, as the study sample has been very much constrained by the data available, and should not be considered a general prediction on the relative likelihood of detecting X-ray binaries versus radio pulsar binaries. The samples are by necessity small, restricted to those binaries with some measurements of eccentricity, and work best considered purely as predictions for the gravitational wave output for the individual systems considered, however if this caveat is borne in mind, the combined data can yield some interesting results.

I have used the combined data for all the systems studied to construct gravitational wave luminosity functions for radio pulsar binaries and high mass X-ray binaries in the Galaxy. The resulting luminosity functions are then compared to the X-ray luminosity function for high mass X-ray binaries. These should be read while remembering the small sample size, however the numerous lower eccentricity X-ray binaries are not likely to contribute significantly to the gravitational wave luminosity function, as peak power emission increases substantially with eccentricity. The combined gravitational wave luminosity function of all the binaries studied shows clear contributions from both the radio pulsar binaries and the high mass X-ray binaries.

It should however be noted that this is not the total emission for the Galaxy. Many obscured and non-accreting systems will also be emitting gravitational waves, and the known sample may not be representative of these. This chapter examines the emission from systems with known properties, and there will be many others whose orbital parameters are not known even if the systems themselves are detectable.

Results from this chapter were presented as a lecture at the BritGrav 12 conference (Pickard, 2012).

3.2 Input parameters

To use the model of chapter 2 to simulate the calculated gravitational wave emission of a binary system, I need to know the masses of both stars, the orbital period and the eccentricity of the system. I have therefore only chosen sources where these parameters are known at least within a given range.

For the purpose of the calculation, which includes calculating the maximum possible eccentricity of the system based on constraining the minimum periastron distance by the physical size of the bodies, where no estimate has been found in the literature, the radius of a main sequence or giant star is calculated based on the classic mass-radius formula for a main sequence star, equation 3.1. This affects only the maximum possible eccentricity of the system as calculated and has no bearing on the results for any given eccentricity. The maximum possible eccentricity is calculated as a check to ensure the input eccentricity is physically realistic, but does not affect the output.

$$R = M^{0.8} \quad (3.1)$$

Where R is the radius in units of solar radii, and M is the mass in units of solar masses.

3.3 Low Mass X-ray Binaries

A search of the catalogue of low mass X-ray binaries of Liu et al (2007) using the Vizier interface shows only one system with a listed eccentricity, 4U 1700+24, which has an eccentricity of 0.26. It seems likely that there are other LMXBs with known eccentricities as the well known Circinus X-1 system, which I used as a first example

when developing the calculation, is listed in the catalogue but its eccentricity is not mentioned. For the purpose of showing LMXB case studies of the calculation, results for both Circinus X-1 and 4U 1700+24 are detailed below.

3.3.1 Circinus X-1

Properties

Discovered in 1969 by an Aerobee 150 rocket-mounted experiment and reported in 1971 in The Astrophysical Journal (Margon et al, 1971), Circinus X-1 is a well known X-ray binary(Jones et al, 1973). It consists of a neutron star and a main sequence star thought to be of 3 to $5M_{\odot}$ in size (Stewart et al, 1991). It has a period measured at 16.6 days and the eccentricity is thought to be between 0.7 and 0.9, making it one of the most eccentric binary systems known.

Calculations of gravitational wave emission profiles

The neutron star is assumed to have a canonical mass of $1.4M_{\odot}$ and a radius of $2 \times 10^{-5}R_{\odot}$. The radius of the main sequence star is calculated as in equation 3.1 in section 3.2. I calculate the gravitational wave emission as in chapter 2, for all nine possible combinations of main sequence star mass of 3, 4, and 5 solar masses and eccentricity of 0.7, 0.8 and 0.9 (Murdin et al, 1980). This is an excellent example of the way gravitational wave emission can change depending on the mass, and particularly the eccentricity, of a system. Figure 3.1 shows the results, with eccentricity of 0.7 plotted in asterixes, 0.8 in triangles and 0.9 in diamonds. Main sequence star masses of 3, 4, and $5 M_{\odot}$ are shown in blue, green and red respectively.

Circinus X-1 is thought to be almost edge-on in inclination (Iaria et al, 2005) and located at a distance of 4.1 (Iaria et al, 2005)or 5.5 (Case & Bhattacharya, 1998) kpc. So the possible signal that could be detected at Earth, in each polarisation, can be measured as shown in figure 3.2.

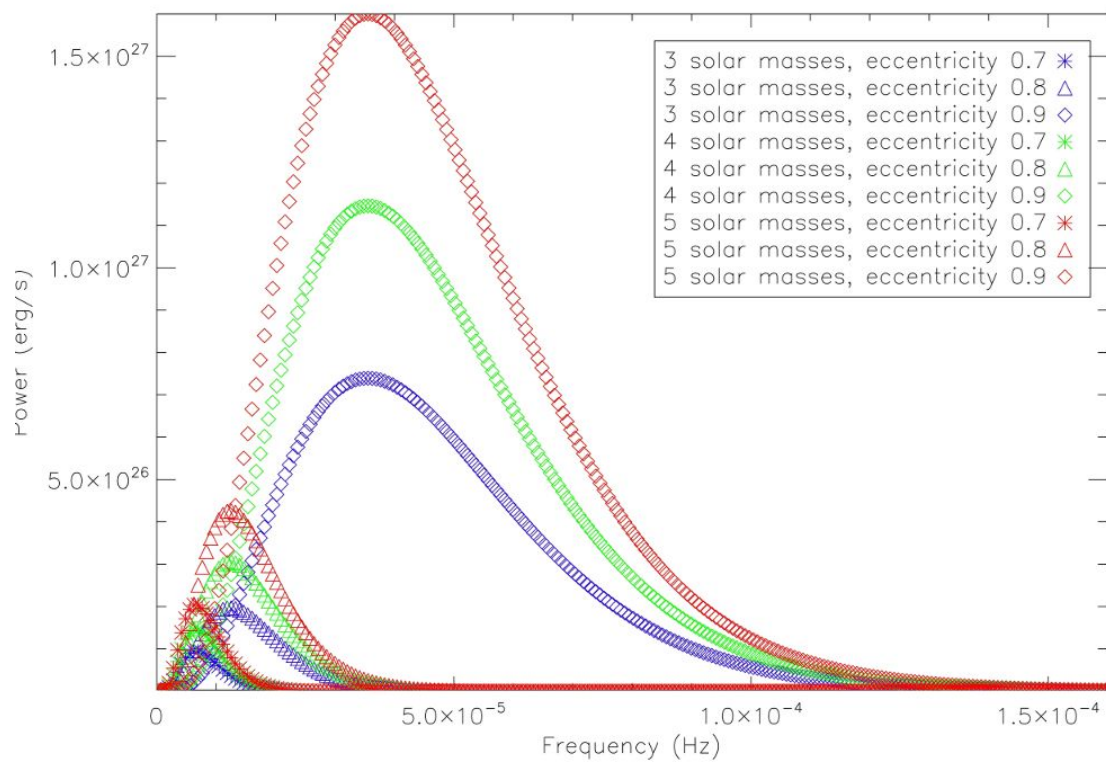


Figure 3.1: Calculated gravitational wave emission for Circinus X-1

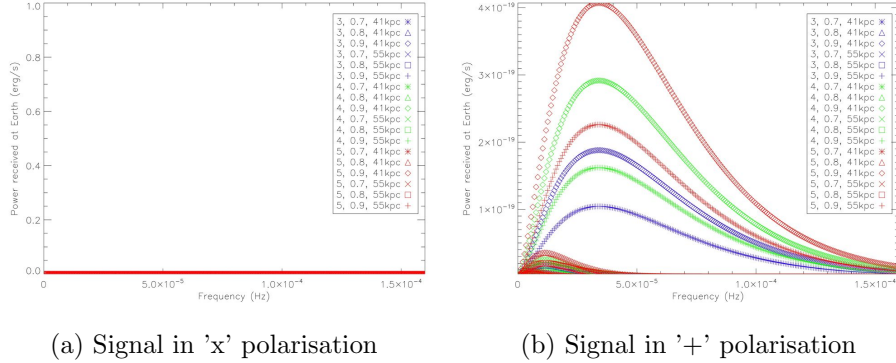


Figure 3.2: Calculated gravitational wave signal at Earth from Circinus X-1

3.3.2 4U 1700+24

This low mass X-ray binary is thought to involve a compact object and an M2 III star (Liu et al, 2007). The compact object is assumed to be a $1.4M_{\odot}$ neutron star, the M2 III star is thought to be of size $60\text{--}70R_{\odot}$ (Masetti et al, 2002) and the mass estimated as $1.3M_{\odot}$ (Masetti et al, 2002). The system has a period of 404 ± 3 days (Galloway et al, 2002) and eccentricity 0.26 ± 0.15 (Galloway et al, 2002).

This is a good example of how the gravitational wave output is affected by eccentricity of the system and by orbital period. Figure 3.3 plots the emission for eccentricity of 0.11, 0.26 and 0.41 in blue, green and red respectively, with an orbital period of 401 days represented by asterixes, 404 days by triangles and 407 days by diamonds.

4U 1700+24 has possible inclination angles of 67 degrees (Abubekerov, 2004) or ≤ 2 degrees (Galloway et al, 2002) and is thought to be at a distance of 0.4kpc from Earth. So the possible signals that could be detected at Earth, in each polarisation could be as shown in figure 3.4. A measurement could clarify which of these possibilities, if either, is correct.

It is easy to see how the possible emission changes with each of these factors- and, therefore, how a measurement of the gravitational wave emission from this system would allow us to narrow down the parameters of its orbit. The large range of

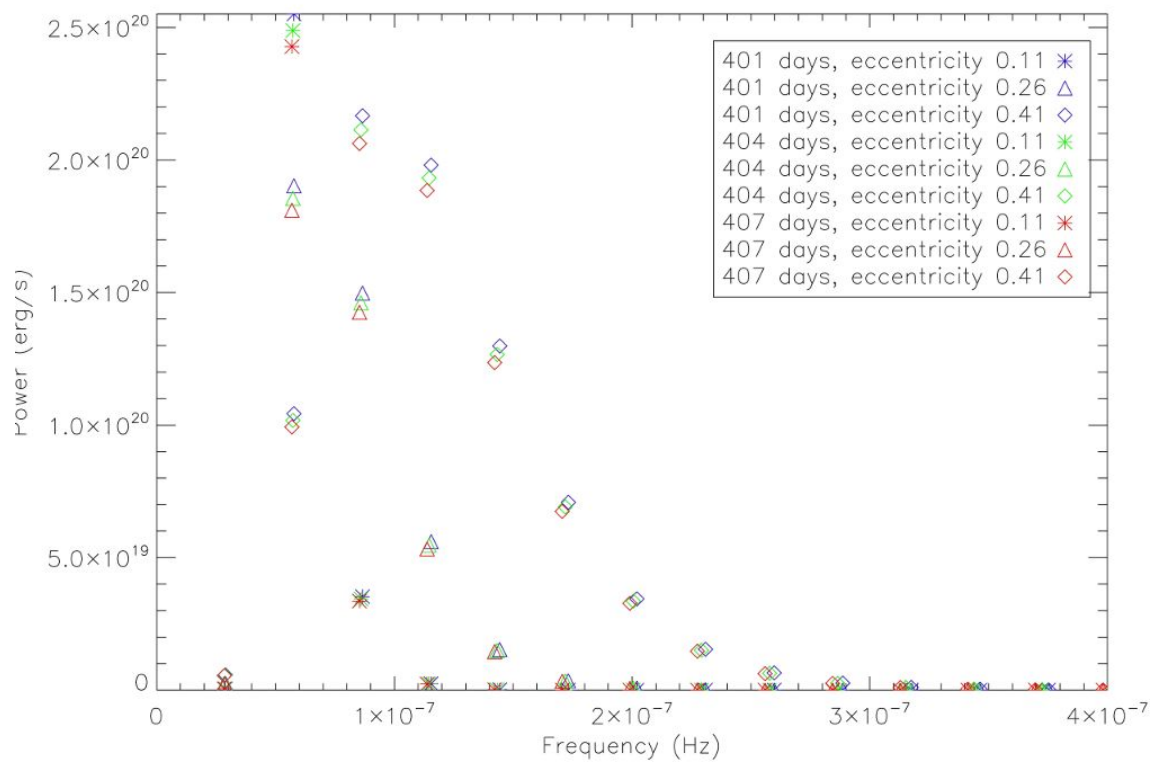


Figure 3.3: Possible gravitational wave emission for 4U 1700+24

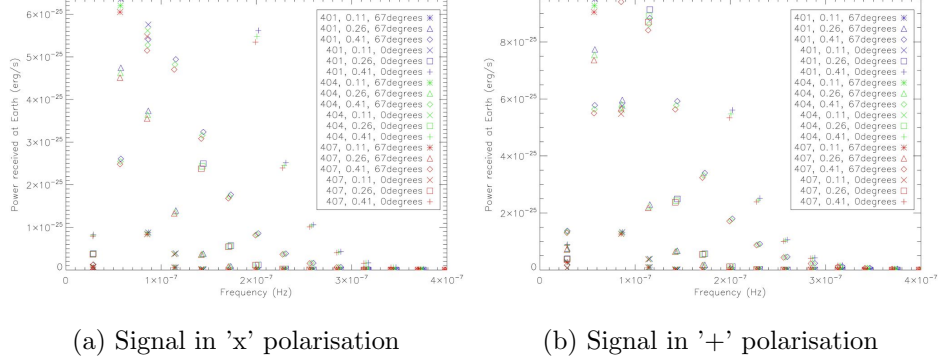


Figure 3.4: Calculated gravitational wave signal at Earth from 4U1700+24

possible eccentricities, varying by ± 0.15 , is a clear real world example of the general effect of eccentricity on the predicted gravitational wave emission as discussed in the previous chapter. The positions of the points on the graph follow the same shape as the curves given by the mathematical output of the calculation as shown in the previous chapter.

3.4 High Mass X-ray Binaries

In contrast to the LMXB catalogue mentioned in section 3.3, the two catalogues for high mass X-ray binaries, in our Galaxy (Liu et al, 2006) and in the Magellanic Clouds (Liu et al, 2005) respectively, provide a wealth of systems with listed estimates of their eccentricity.

Many HMXBs are Be binary systems, where a compact object, usually assumed to be a neutron star, is in a wide orbit in a binary with a more massive star, with orbital period in a range of 16 - 400 days (Coe, 2000), often of moderate, sometimes high, eccentricity.

Studying the gravitational wave output of HMXBs could potentially yield very interesting results. We could use the extra constraint provided by gravitational wave measurement to determine the nature of the compact object or provide good

estimates of the masses of the binary components, which could lead to a better understanding of how such binaries form and evolve.

I chose to study only those binaries with an estimated eccentricity of greater than 0.2, since, as shown for the LMXB Circinus X-1 in section 3.3.1 and in the preceding chapter for the general case, the larger the eccentricity the greater an effect it has on the measurement, making the systems more likely to show up in LISA measurements both by giving a higher peak emission and shifting the position of the peak to a higher frequency. So these more eccentric systems should be easier to both detect and analyze using LISA. For an eccentricity of 0.2 or smaller, as shown for the generic case in the previous chapter, only 5 or fewer discrete signals (with each signal being at an integer multiple of the base frequency of the system) can be seen and all lie at relatively low frequencies, meaning these would be far more difficult to detect and characterise.

Estimates of the masses and radii of the components of each system were garnered from the literature where possible, and where possible estimated by reference to Vacca et al (2000) and Weidner & Vink (2010), giving a range of values for running the calculation.

The results for the four most eccentric binaries are detailed in this chapter, demonstrating the most important facets of the results. Similar information for the rest can be found in the appendix, with overall data at the end of this section.

3.4.1 2S 1845-024

This HMXB, also known as GRO J1849-03 and GS 1843-02, is an X-ray pulsar/Be binary, with a period of 241 days and eccentricity 0.88 (Liu et al, 2006). The compact object is assumed to be a canonical neutron star of $1.4M_{\odot}$. The Be star is thought to have a mass of at least $9M_{\odot}$ (Finger et al, 1999).

The expected gravitational wave output for this binary is shown in figure 3.5, which gives the output for a Be star of mass $9M_{\odot}$, the expected lower limit, and a

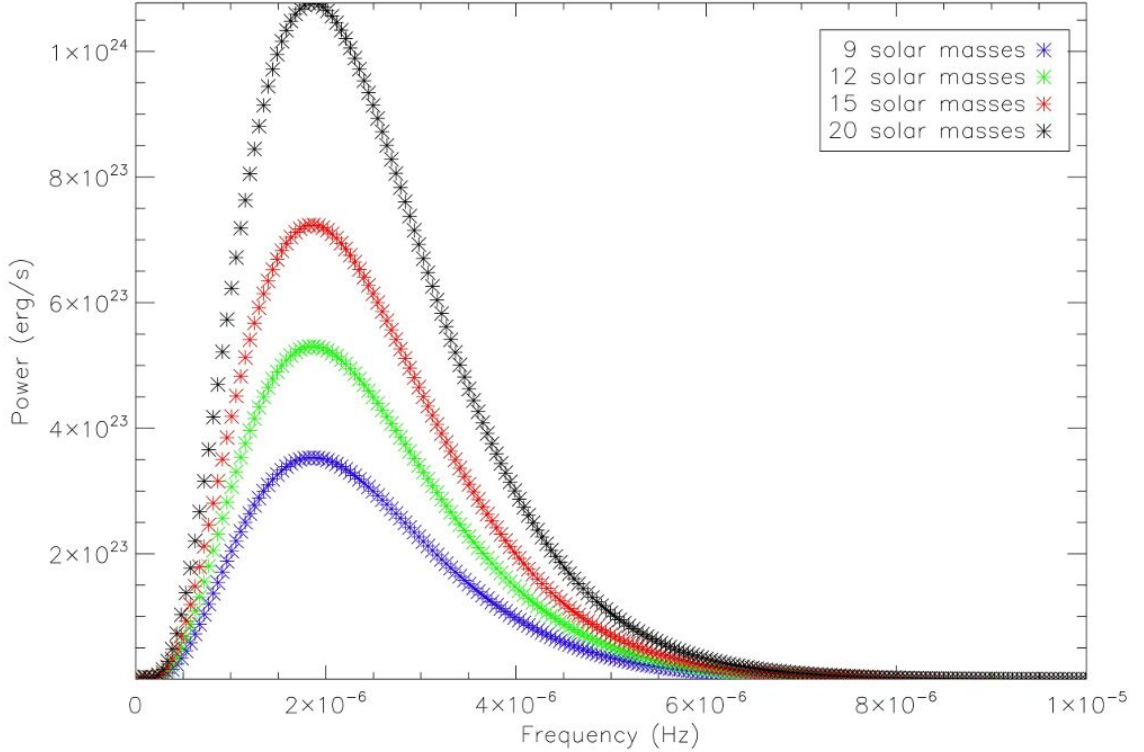


Figure 3.5: Possible gravitational wave emission for 2S 1845-024

range of higher values. Masses of 9, 12, 15 and 20 M_{\odot} are shown in blue, green, red and black respectively. A measurement of the gravitational waves from this system would enable us to constrain the mass far more precisely than our current knowledge allows, by comparison to predictions such as this.

This is the most eccentric of the HMXB systems listed in Liu et al (2006), however it should be noted that even this system peaks at a frequency likely to fall below the LISA range. It however has a relatively long orbital period and, as the next example shows, a shorter orbital period also shifts the peak to a higher frequency.

The system is thought to be 10kpc from Earth (Liu et al, 2006) but the angle of inclination is not known. Finger et al (1999) use an angle of 60 degrees, if this is the case the signal at Earth in each polarisation would be as in figure 3.6.

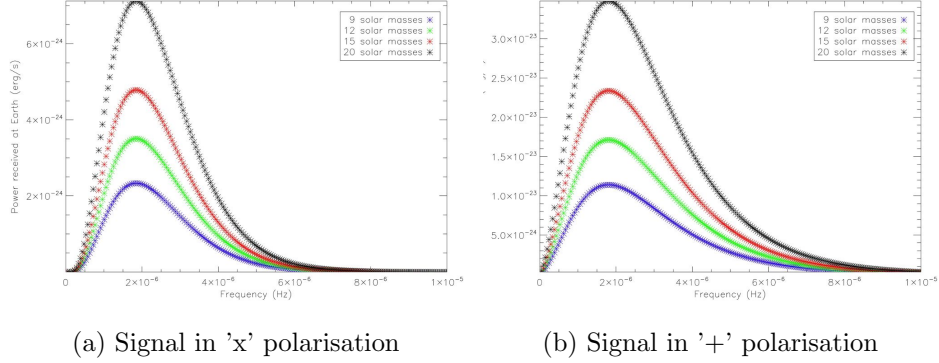


Figure 3.6: Calculated gravitational wave signal at Earth from 2S1845-024 if at an angle of 60 degrees

3.4.2 GRO J1008-57

This binary system has a period estimated at 247.8 days according to Coe et al (2007), based on BATSE data, which is in good agreement with (Naik et al, 2010) the Levine & Corbet (2006) detection of a 248.9 day periodicity in the X-ray curve seen by the RXTE All-sky Monitor over 10 years. This disagrees with the catalogue (Liu et al, 2006), likely due to more recent data, which quotes the result of 135 days from Shrader et al (1999).

It has an eccentricity of 0.66 (Liu et al, 2006). The compact object is assumed to be a $1.4M_{\odot}$ neutron star and the mass of the other star is thought to be in the range 3 to $8M_{\odot}$ (Finger et al, 1994)

Figure 3.7 shows the expected gravitational wave output over a range of masses and for both 247.8 and 135 day periods. Results for a period of 237.8 days are plotted as circles, and 135 days as squares. Masses of 3, 5, and $8 M_{\odot}$ are shown in blue, red and green respectively.

A gravitational wave signal from a binary such as this should make identifying the true period of the system much easier. Gravitational waves are only output at integer multiples of the base frequency of a system, so the frequencies at which the signals occur should allow determination of the period of a binary. The greater

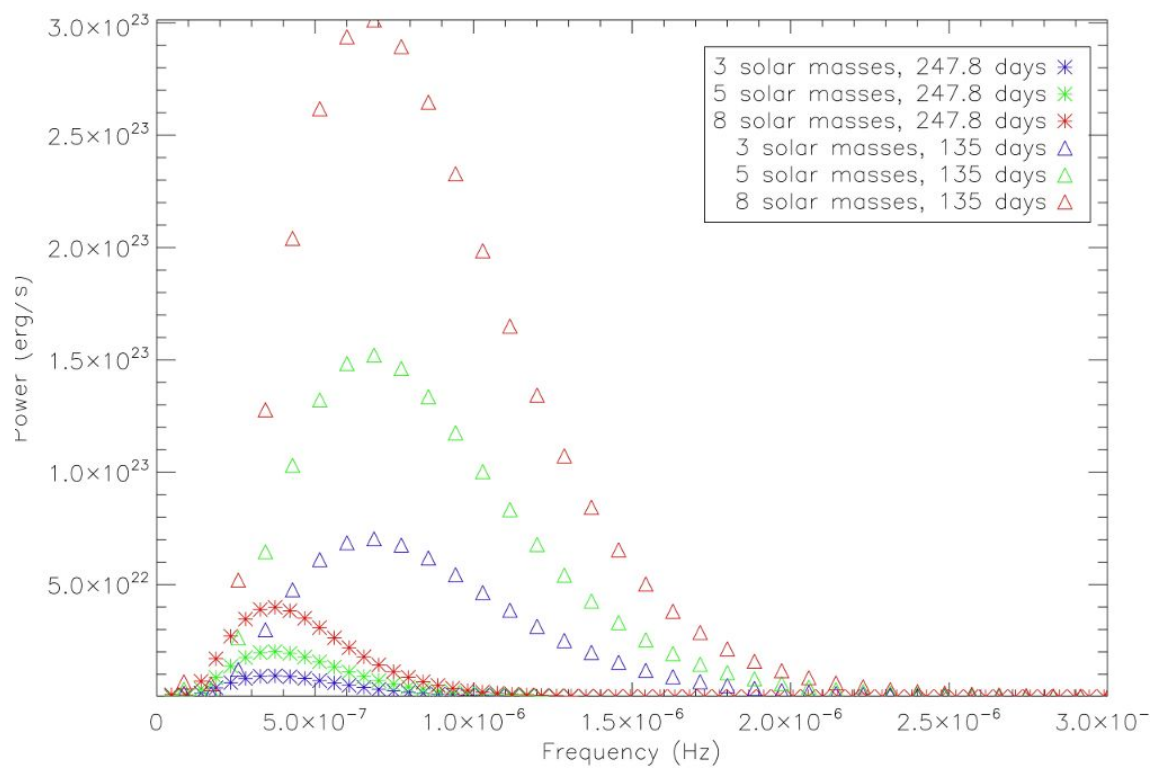


Figure 3.7: Calculated gravitational wave emission for GRO J1800-57

the eccentricity, the larger the number of harmonics clearly emitted so it may be easier to determine the orbital period for very eccentric systems. It can clearly be seen that a shorter period- and hence a faster moving system- emits more powerful gravitational waves than stars of the same mass in an orbit of the same eccentricity but a longer period.

The shorter period also results in a shift of the peak to higher frequencies, similar to that seen when eccentricity is increased. So short period systems with lower eccentricities may be detectable in a similar frequency range to long period systems with high eccentricities. As period, and stellar separation, decrease, orbits tend to become less eccentric, so this result is interesting for study of close binaries.

Coe et al (2007) suggests an inclination angle of 36 degrees. The system is at a distance of 5kpc (Liu et al, 2006). This gives a possible signal at Earth, in each polarisation as in figure 3.8.

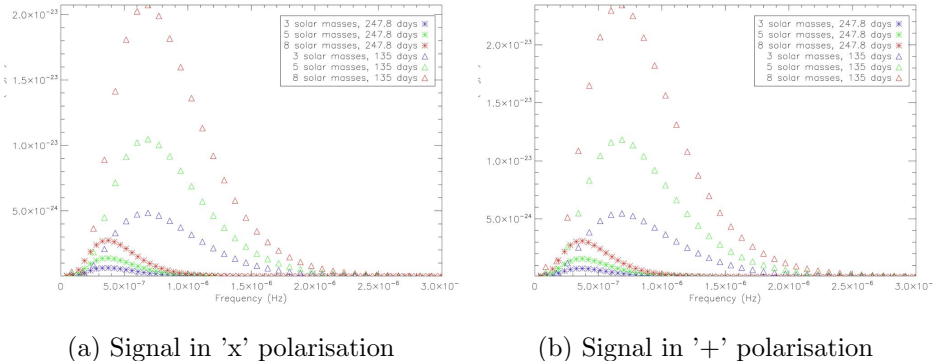


Figure 3.8: Calculated gravitational wave signal at Earth from GROJ1008-57

3.4.3 XTE J0421+560

This X-ray source is thought to have an optical counterpart in CI Cam (Belloni et al, 1999). It has been suggested that this is a supergiant Be system, of spectral type B4 III-V, with a lower limit on the supergiant star mass of $12M_{\odot}$ by Barsukova et al (2005). The mass was estimated at $20M_{\odot}$ by Belloni et al (1999), which is consistent

with this. It has a relatively short period of 19.41 days (Barsukova et al, 2005) and eccentricity 0.62 (Barsukova et al, 2005).

The compact object has been speculated to be a white dwarf (Barsukova et al, 2005) with a mass at least 25 times smaller than the supergiant. It has also been estimated to be a neutron star or black hole (Belloni et al, 1999).

Belloni et al (1999) suggests that the peak X-ray emission is too high to be caused by either accretion onto a white dwarf or thermonuclear burning at a white dwarf surface, and states that the optical spectrum is inconsistent with a nova and the X-ray spectrum harder than one might expect. So they conclude the compact object is either a neutron star or black hole, with X-ray emission during outbursts obscured by shielding- the optical luminosity was seen to be greater by "a factor of ten or more". They conclude we see only x-rays scattered by surrounding material, and that the presence of radio emission suggests a neutron star with a high magnetic field is unlikely, so suggest the compact object to be a neutron star or black hole, and appear to favour a black hole with their conclusions due to the strength of the radio outbursts.

Barsukova et al (2005) disagree, pointing out in a short Astronomers' Telegram notice (number 416) that, according to their calculations based on observations over 7 years following the outburst of 1998, the mass function is $12M_{\odot}$, which gives a lower limit for the mass of the giant star, and that no motion has been noted in a spectral line (He I) likely to be from that star, which leads them to state "the fast moving HeII emitting object should have at least 25 times smaller mass than the primary star" and conclude that the compact object is likely to be a white dwarf surrounded by an accretion disk.

A measurement of the gravitational wave emission from the system could serve to answer the question of which it is, as it provides another way to estimate object masses.

The program was run for the lower limit of $12M_{\odot}$ and the estimated $20M_{\odot}$ supergiant with a white dwarf of mass 25 times smaller than the supergiant ($0.48M_{\odot}$) and

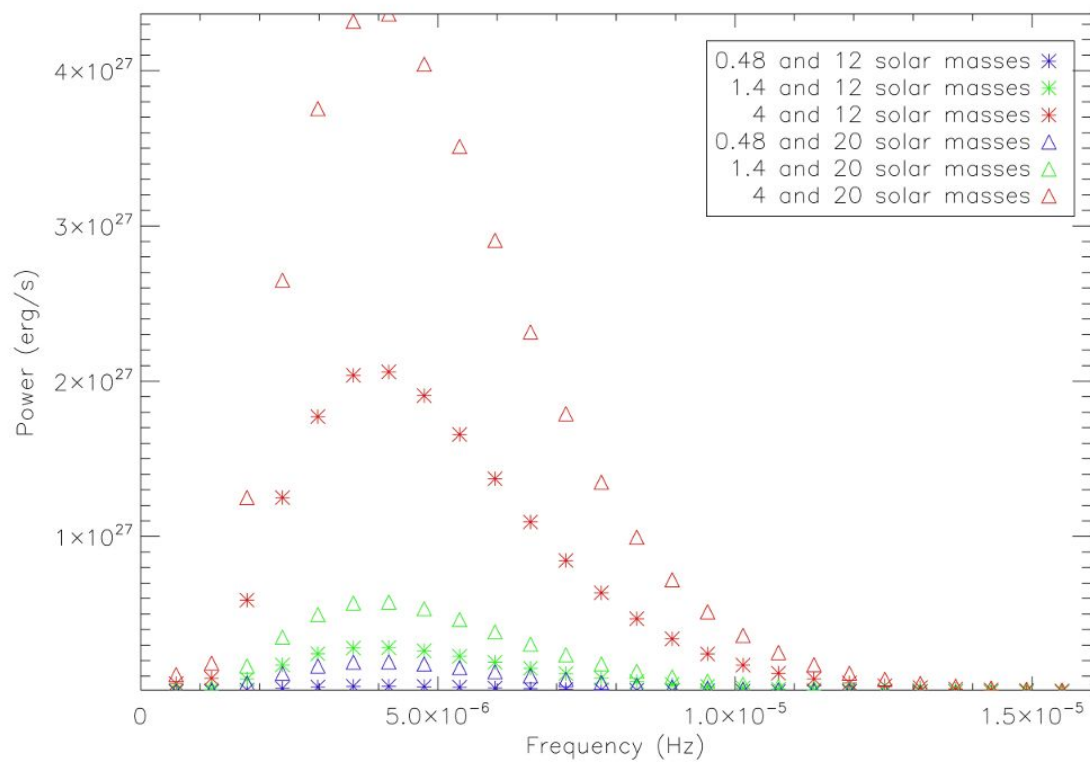


Figure 3.9: Calculated gravitational wave emission for XTE J0421+560

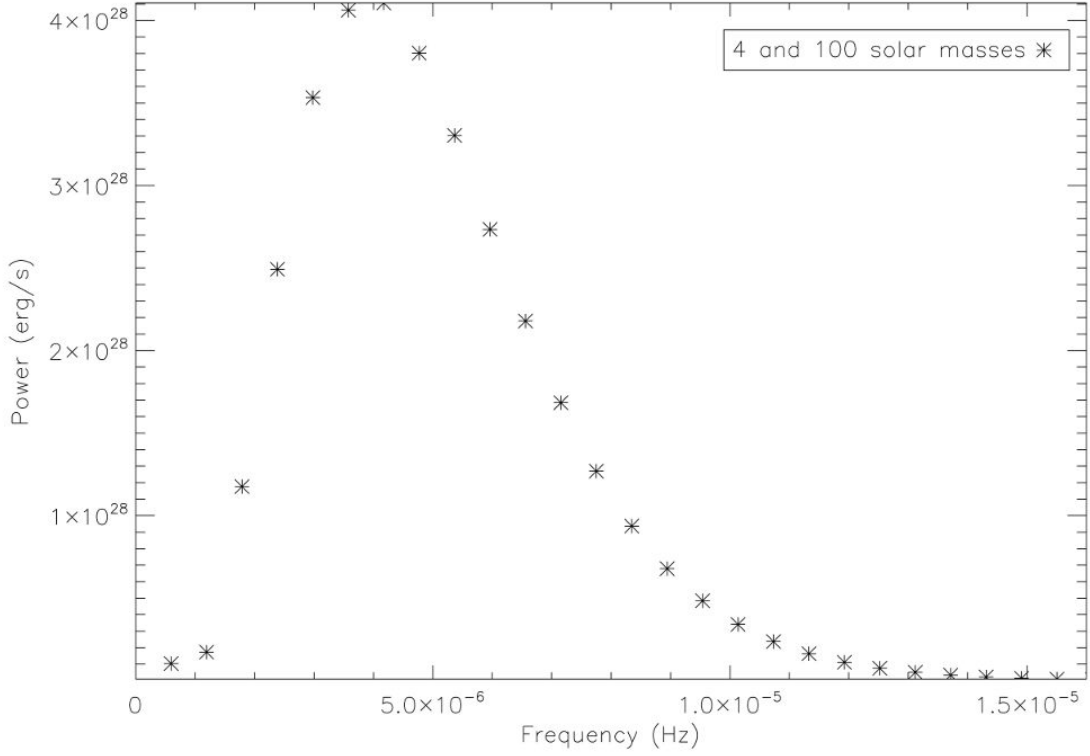


Figure 3.10: Calculated gravitational wave emission for XTE J0421+560

$0.8M_{\odot}$ respectively) and a $1.4M_{\odot}$ neutron star. No possible mass for a black hole, which Belloni et al (1999) considers likely due to the radio emission of the source, has been speculated upon, a $4M_{\odot}$ compact object is included in the results for comparison. These results are shown in figure 3.9. The minimum, $12M_{\odot}$ is plotted with circles and the estimation of $20M_{\odot}$ with squares. The white dwarf possibility is shown in blue, neutron star in green and $4M_{\odot}$ compact object, representing the possibility of the compact object being a black hole, in red.

It should be noted that if the suggestion of Barsukova et al (2005) that the compact object must have a mass 25 times smaller than the supergiant is correct, a compact object of $4M_{\odot}$ would require a $100M_{\odot}$ supergiant, far in excess of the estimated $20M_{\odot}$. This is also included in the results, shown in figure 3.10 as is a $35M_{\odot}$ supergiant with a (25 times smaller) $1.4M_{\odot}$ neutron star in figure 3.11.

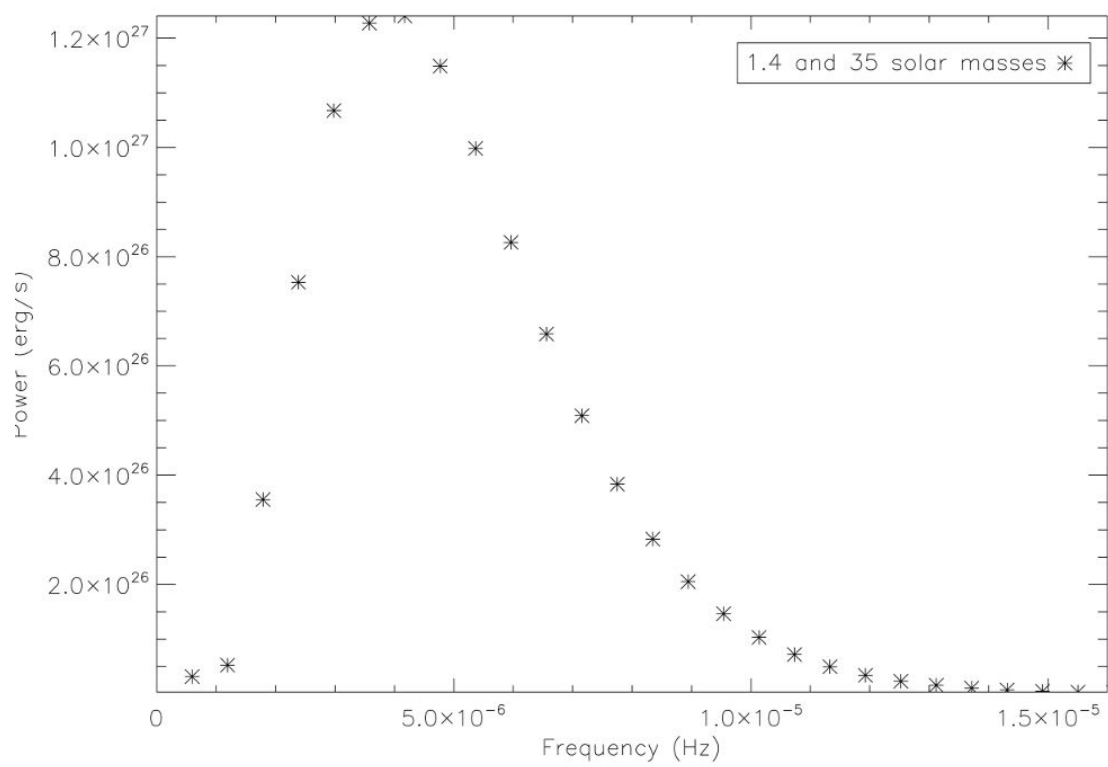


Figure 3.11: Calculated gravitational wave emission for XTE J0421+560

Barsukova et al (2005) also suggest that an inclination angle of ≥ 38 degrees would indicate that the compact object is a white dwarf. The system is thought to be at a distance of 1-5kpc from Earth (Liu et al, 2006). Possible signals at Earth in each polarisation, for inclination angles of 16, 38 and 60 degrees, are shown in figures 3.12, 3.13 and 3.14 respectively. This shows the difference between the signal at the 38 degree limit and the examples on either side of it. A distance of 3kpc is used.

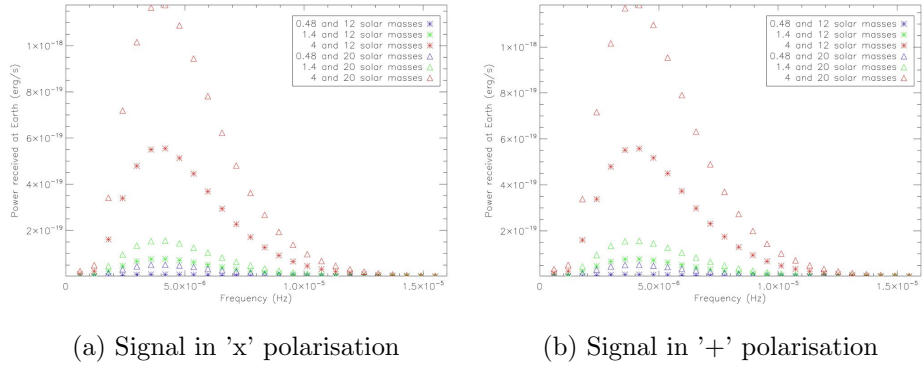


Figure 3.12: Calculated gravitational wave signal at Earth from XTEJ0421+560 if at an inclination angle of 16 degrees

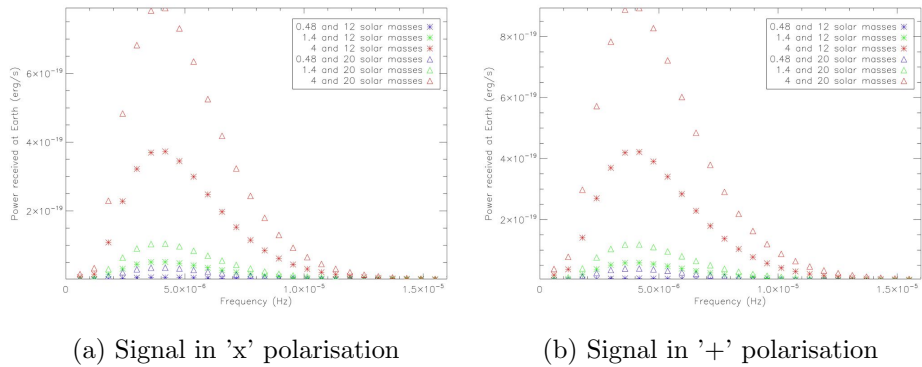


Figure 3.13: Calculated gravitational wave signal at Earth from XTEJ0421+560 if at an inclination angle of 38 degrees

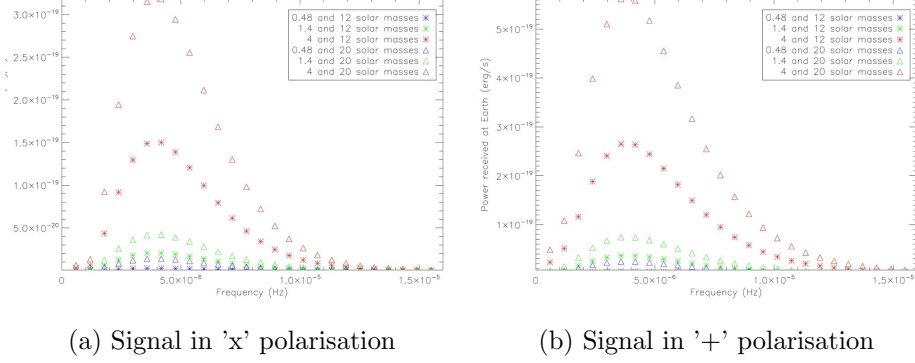


Figure 3.14: Calculated gravitational wave signal at Earth from XTEJ0421+560 if at an inclination angle of 60 degrees

Clearly, in order to determine the angle of inclination, the peak power must be measured. The ratio of peak power in each polarisation may allow the angle to be determined despite the uncertainty in distance to the system, which would also affect the peak size.

3.4.4 1A 0535+262

This binary has a period of 111 days (Reynolds & Miller, 2010) and eccentricity 0.47 (Finger et al, 1996). The optical counterpart to the X-ray source is thought to be HDE 245770 (Giangrande et al, 1980). Giangrande et al (1980) identifies this as an O9.7 IIIe star, whereas Steele et al (1998) suggests it may be of type B0 IIIe. The system is thought to lie 1.4-11.1kpc away (Liu et al, 2006) but its angle of inclination is unknown.

The compact object is assumed to be a $1.4M_{\odot}$ neutron star, with the other star being of type O9.7-B0 IIIe. Giangrande et al (1980) suggests the larger star has a mass of $15M_{\odot}$ and radius $14R_{\odot}$. In addition, the mass and radius limits for the spectral type can be estimated by the method of Vacca et al (2000). Based on this, a B0 III star could have a mass ranging from $22.7M_{\odot}$ (spectral) to $27.4M_{\odot}$ (evolutionary) and the radius is thought to be $14.7R_{\odot}$. Type O9.5 III, the nearest listed to

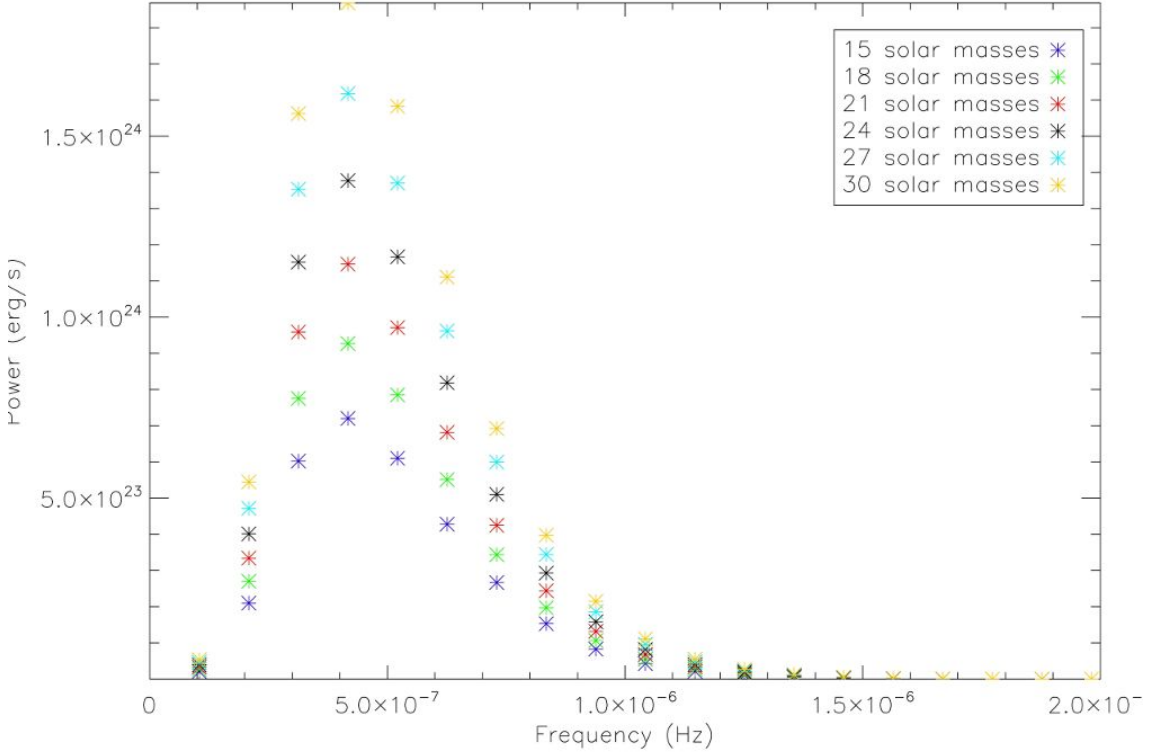


Figure 3.15: Calculated gravitational wave emission for 1A 0535+262

O9.7 III, has a mass range of $24.1M_{\odot}$ (spectral) to $29.9M_{\odot}$ (evolutionary) and again a radius of $14.7R_{\odot}$. The graphs in Weidner & Vink (2010) allow an estimation of mass of an O9.5 III star (the highest limit of the graph) as approximately $19.95M_{\odot}$ to $29.51M_{\odot}$. So the estimate of Giangrande et al (1980) is not consistent with the masses suggested by Vacca et al (2000), however the lower limit apparent at O9.5 III using the results of Weidner & Vink (2010) suggest it may be consistent with that approach if it were extended to type B stars.

The predicted gravitational wave spectra for a range of masses from the suggested $15M_{\odot}$ of Giangrande et al (1980) to a maximum of $30M_{\odot}$, which, being the maximum estimated by Vacca et al (2000) for an O9.5 III star, should be beyond the possible maximum for this system, have been calculated and are shown in figure 3.15. Masses of $15M_{\odot}$, $18M_{\odot}$, $21M_{\odot}$, $24M_{\odot}$, $27M_{\odot}$ and $30M_{\odot}$ are shown in blue, green, red,

black, turquoise and yellow respectively. This system is an example of how masses estimated by spectral type could be narrowed down by use of gravitational wave measurements. More accurate measurements of the masses of stars of different spectral types could help to determine which of the methods for estimating mass by spectral type are the most likely to be correct.

3.5 Radio pulsars in binary systems

The list of pulsars in binary systems in Johnston (2005), which refers largely to radio pulsars, provides another source of binary systems to which the calculation can be applied. These can then be compared to the data for HMXBs, to see if there are any clear distinguishing factors between the two populations and which LISA is most likely to detect. Again, only those with an eccentricity >0.2 are included.

The positions of the radio pulsars were compared to the HMXB (Liu et al, 2006) and LMXB (Liu et al, 2007) catalogues to ensure no systems were listed twice. None had HMXB or LMXB in the catalogues at the exact positions of the radio pulsars.

Radio pulsar binary J0514-4002A is located at 05h14m06.7s (Johnston, 2005), $-40^{\circ}02'50''$, the nearest LMXB is 4U 0513-40 at 05h14m06.410s, $-40^{\circ}02'38.22''$ (Liu et al, 2007), however, this is listed as having no radio emission so is unlikely to be the same source.

Radio pulsar binary J1750-37 is located at 17h50m, -37° (Johnston, 2005), the nearest LMXB is 4U 1746-37 at 17h50m12.728s, $-37^{\circ}03'06.53''$ (Liu et al, 2007), which is also listed as having no radio emission, so is not likely to involve a radio pulsar. LMXB 4U 1746-37 has an orbital period of 5.16 hours, which, compared to the orbital period of J1750-37, 17.3 days, means the two are not the same system.

Radio pulsar binary B2127+11C= J2130+1210C is located at 21h30m01.205s, $+12^{\circ}10'38.2''$ (Johnston, 2005). LMXBs 4U 2129+12 and CXO J212958.1+121002 both came up in the search, at 21h29m58.310, $+12\text{deg}10'02.90$ and 21h29m58.060s, $+12\text{deg}10'02.60$ respectively (Liu et al, 2007). 4U 2129+12 is listed as having radio

emission, however the orbital period of 17.1 hours is significantly greater than that of B2127+11C, which is 0.34 days, equivalent to 8.16 hours. So this is unlikely to be the same system. CXO J212958.1+121002 has no mention of radio emission and a period of 0.376 hours.

None of the other radio pulsar binaries studied had LMXB or HMXB sources nearby, so it seems none of the radio pulsar binaries studied are also HMXBs or LMXBs present in the catalogues Liu et al (2006) and Liu et al (2007).

Three examples are presented below. Results for all the other radio pulsars studied are shown in the appendix.

3.5.1 J0514-4002A

This binary has an eccentricity of 0.89 (Freire et al, 2004). The orbital period is 18.79 days (Freire et al, 2004). For the purposes of this study, the pulsar is assumed to be a $1.4M_{\odot}$ neutron star. The mass of the other star is thought to be $1.1M_{\odot}$ (Freire et al, 2004).

This is the most eccentric orbit of any known binary pulsar as of the time the list I refer to was compiled (Johnston, 2005).

The results for this system are shown in figure 3.16.

It can be clearly seen that, with a short period and high eccentricity, this system is a good candidate for detection in the LISA band, better than most of the X-ray binaries. The results show a predicted peak emission of 7.97×10^{25} erg/s at a frequency of 2.71×10^{-5} . This compares to an average HMXB peak frequency of 2.35×10^{-6} Hz and a highest peak frequency, from the systems studied, of 8.90×10^{-6} Hz. For the LMXB Circinus X-1, if it should have an eccentricity of 0.8 or lower, the peak would occur at a lower frequency (though higher power) than J0514-4002A. Only for the possible eccentricity of 0.9 does the prediction for Circinus X-1 come in at a higher frequency than J0514-4002A, and hence have a better chance of detection by a LISA-like detector. Note that the two are not in competition, a LISA-type detector

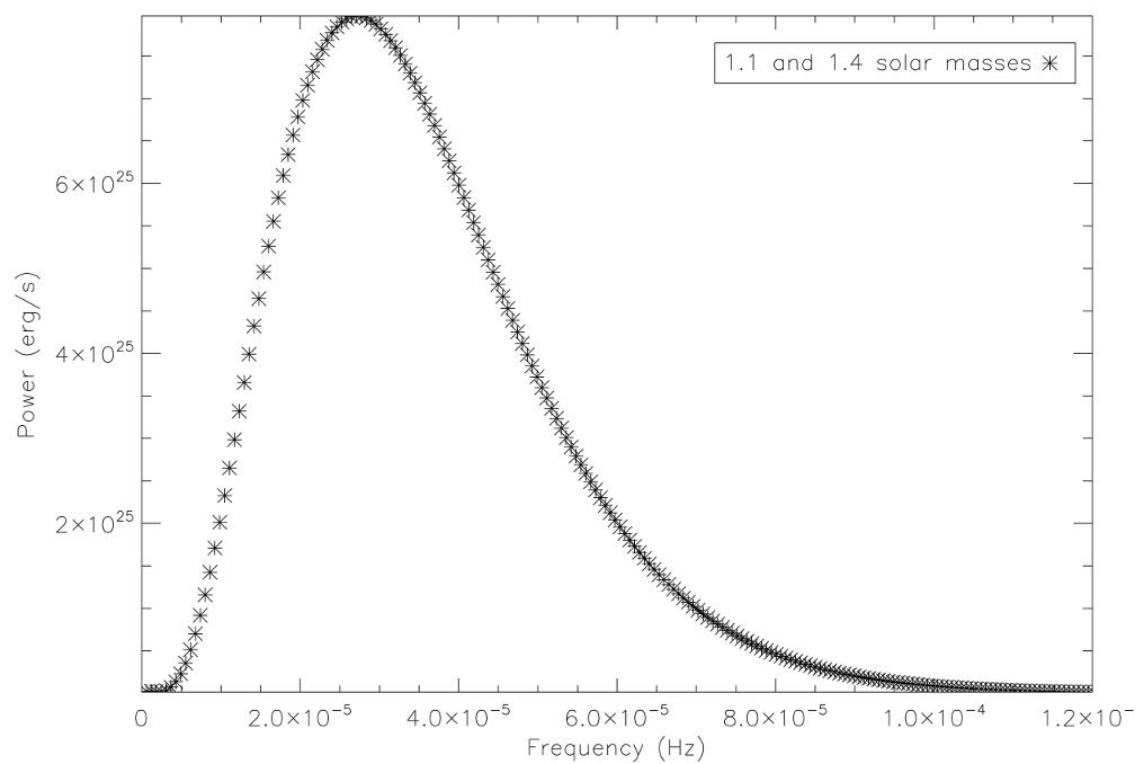


Figure 3.16: Calculated gravitational wave emission for J0514-4002A

may well detect both, but mentioned purely for comparison.

The possible signal at Earth, in each polarisation, is shown in figure 3.17. The system is 12.09 kpc away (Johnston, 2005) and Freire et al (2004) suggest an orbital inclination of 60 degrees is the median of the possible inclinations, so this is used.

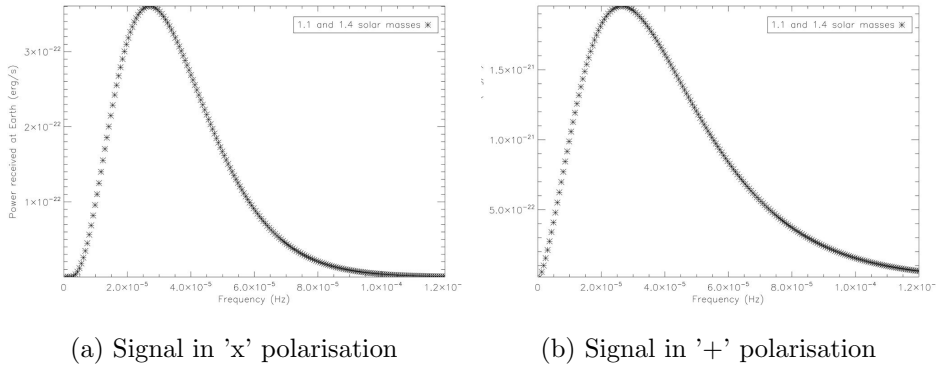


Figure 3.17: Calculated gravitational wave signal at Earth from J0514-4002A if at an inclination angle of 60 degrees

3.5.2 B1259-63=J1302-6350

The eccentricity of this binary system is thought to be 0.87 (Wang et al, 2004) and the orbital period 1236.72 days (Wang et al, 2004), which is the longest orbital period of any known binary radio pulsar according to Johnston (2005). Like many of the listed pulsars in binary systems, some of the information for this system comes from Australia Telescope National Facility Pulsar Group (2004), who have published a catalogue (Manchester et al, 2005) and maintain it on their website, listed in the bibliography. The pulsar is assumed to be a $1.4M_{\odot}$ neutron star, the other star has a mass of $10M_{\odot}$ and radius $6R_{\odot}$ (Wang et al, 2004).

Results for this system are shown in figure 3.18.

The system is at a distance of 4.6kpc (Johnston, 2005) and angle of 36 degrees (Wang et al, 2004). The expected signal at Earth in each polarisation is shown in figure 3.19.

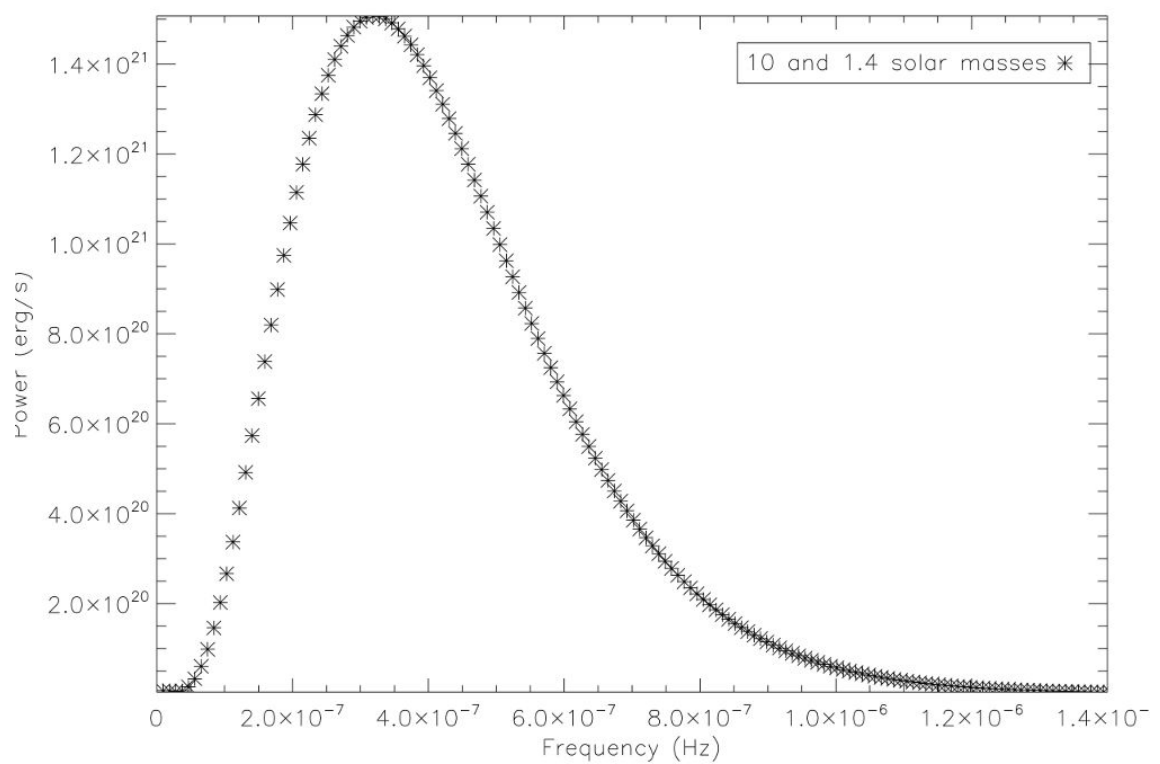


Figure 3.18: Calculated gravitational wave emission for J1302-6350

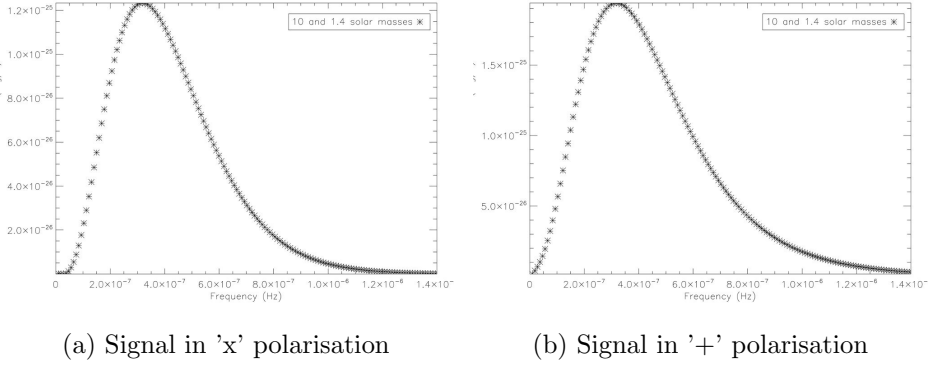


Figure 3.19: Calculated gravitational wave signal at Earth from B1259-63

3.5.3 J1811-1736

This binary has a listed eccentricity of 0.83 (Corongiu et al, 2007). The orbital period is given as 18.78 days (Corongiu et al, 2007). The total mass of the system is thought to be $2.57 \pm 0.10 M_{\odot}$. The distance is thought to be 5.83 kpc (Johnston, 2005) but the inclination is unknown.

It has been proposed that this is a double neutron star system (Corongiu et al, 2007). Corongiu et al (2007) suggests that the smallest possible companion mass, based on their measurements, is $0.93 M_{\odot}$, but if neither star has less mass than the smallest neutron star then measured, $1.17 M_{\odot}$, both must lie in the range $1.17 M_{\odot}$ to $1.5 M_{\odot}$.

The calculation was run for neutron star pairs of $0.93 M_{\odot}$ and $1.64 M_{\odot}$, $1.17 M_{\odot}$ and $1.4 M_{\odot}$, $1.35 M_{\odot}$ and $1.22 M_{\odot}$ and two $1.285 M_{\odot}$ neutron stars, for which the results are given in figure 3.20, plotted in blue, green, red and black respectively.

3.5.4 B1913+16=J1915+1606

This system, known as the Hulse-Taylor binary pulsar, is the system whose measured orbital decay was famously shown to be in accordance with the predictions of general relativity, by gravitational wave emission, leading to Hulse and Taylor being jointly awarded the 1993 Nobel Prize in Physics. This indirect evidence for gravitational

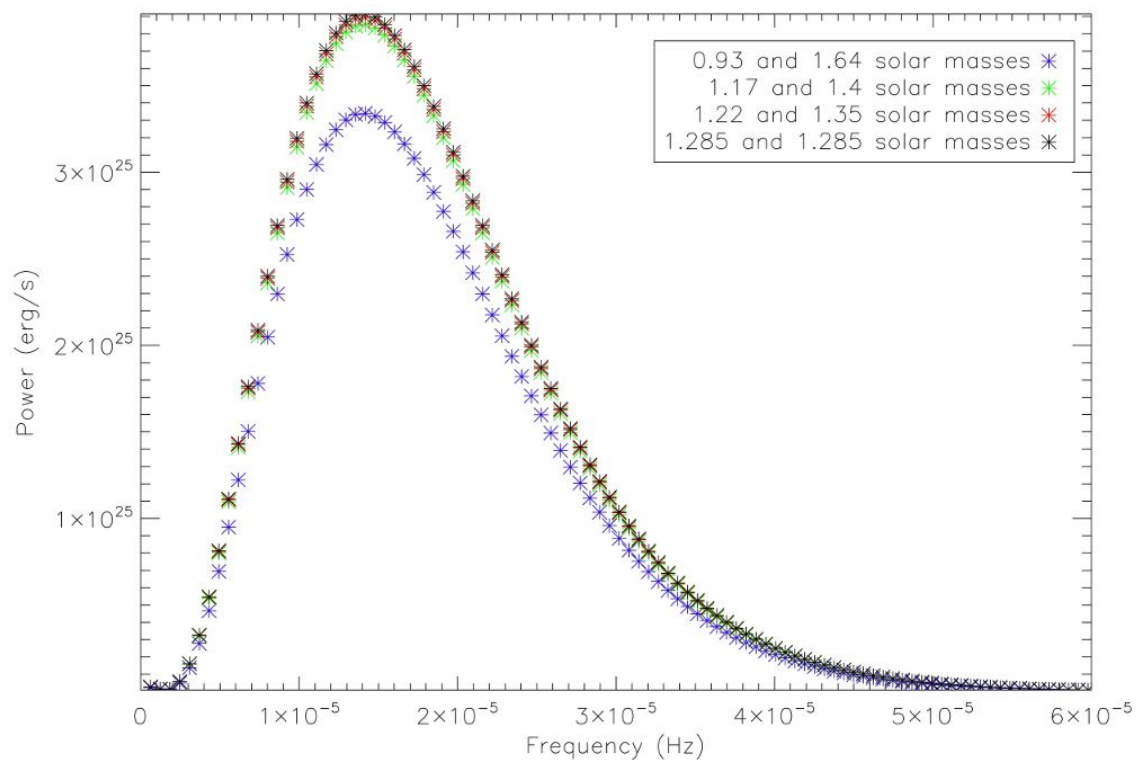


Figure 3.20: Calculated gravitational wave emission for J1811-1736

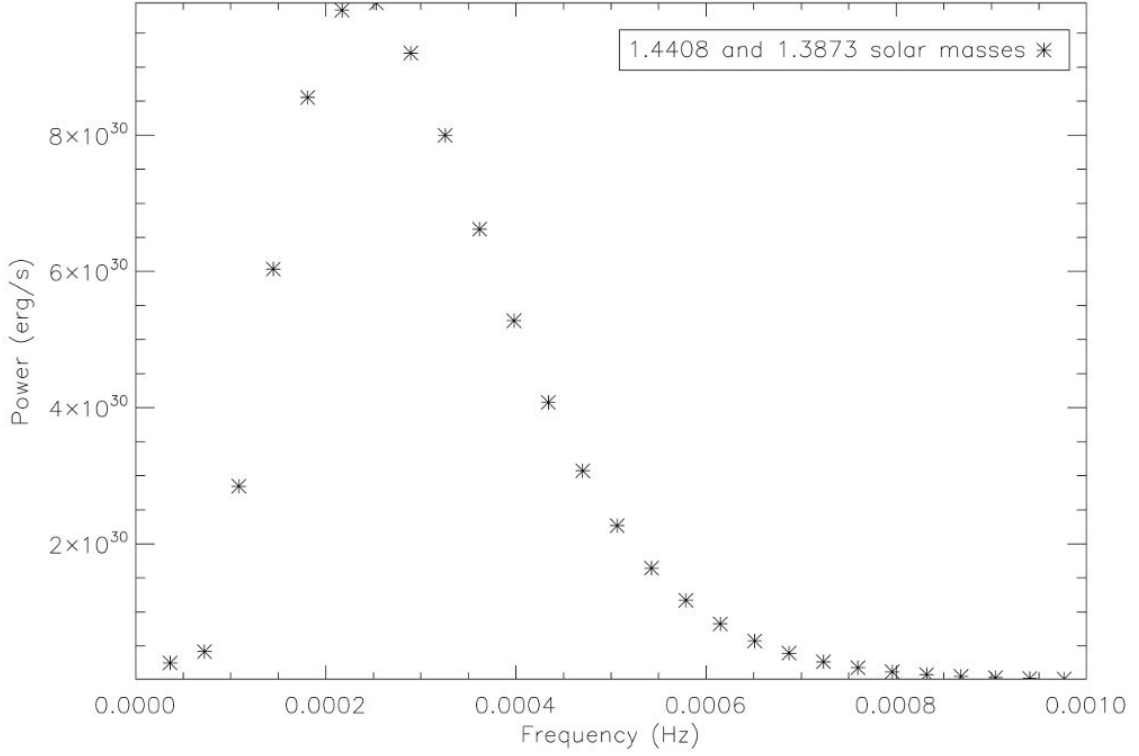


Figure 3.21: Calculated gravitational wave emission for J1915+1606

waves is still the best indication that gravitational radiation as predicted by general relativity should exist, with huge implications for expanding our knowledge of the universe if direct detection can, as is hoped, be achieved.

The measurements of the system in Weisberg & Taylor (2003) give a mass for the pulsar of $1.4408 \pm 0.0003 M_{\odot}$ and the companion of $1.3873 \pm 0.0003 M_{\odot}$. The system has an eccentricity of 0.62 (Hulse & Taylor, 1975), and orbital period 0.32 days (Hulse & Taylor, 1975).

Due to its very short orbital period, the shortest of the systems considered here, combined with fairly high eccentricity, this system is one of the best candidates for detection by a LISA-band detector as the peak predicted gravitational wave emission, as shown in figure 3.21, of 9.94×10^{30} erg/s occurs at 2.53×10^{-4} Hz which is well within the expected LISA frequency band, unlike many of the binaries studied

here which either fall on the edge of said frequency band or are likely to be at too low a frequency.

The system is at thought to be at an inclination of 47.2 degrees (Taylor et al, 1992) or the opposite, 132.8 degrees (Kramer, 1998). It is 7.05kpc distant (Johnston, 2005). The expected signal at Earth, in each polarisation, for an angle of 47.2 degrees is shown in figure 3.22.

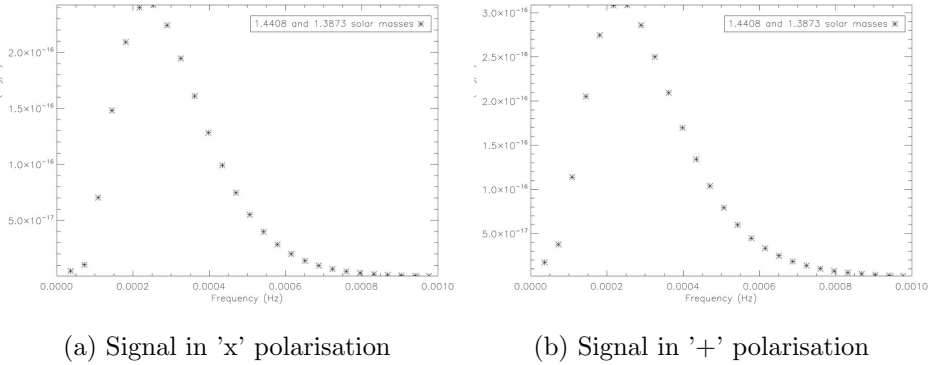


Figure 3.22: Calculated gravitational wave signal at Earth from B1913+16

3.6 Aggregate data for HMXBs and radio pulsars in binary systems

In 3.3, 3.4 and 3.5, graphs showing the predicted gravitational wave emission for two low mass X-ray binaries, four high mass X-ray binaries and four radio pulsars binary systems can be seen. These examples demonstrate the sort of results that can be seen from the calculation and clearly show the importance of a binary system's eccentricity and orbital period in determining the frequency at which gravitational wave emission occurs, as well as the effect of the masses of the component bodies on the power emitted in gravitational waves.

In total, 2 LMXBs, 18 HMXBs and 14 radio pulsar binaries were studied. For ease of reading, detailed results for the remaining HMXB and radio pulsar binary

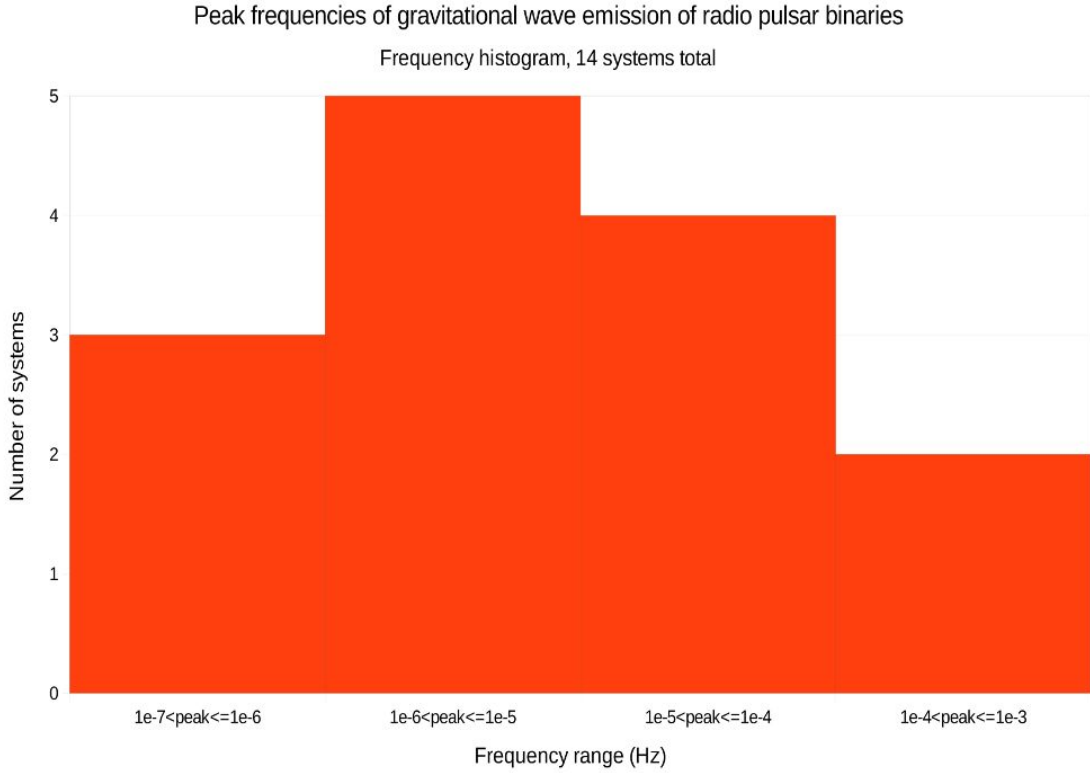


Figure 3.23: Peak gravitational wave emission frequencies of radio pulsar binaries

systems are presented in the appendix. Here, I present overall data for the HMXB and radio pulsar binary samples, bearing in mind the caveat that these were chosen for study simply by being the only available examples with estimated eccentricities of greater than 0.2 (the reason for this cutoff is explained in 3.4), and may not necessarily be a representative sample of the general population of these systems.

3.6.1 Radio pulsar binaries

The 14 radio pulsar binaries studied have possible peak gravitational wave emission frequencies ranging from 3.01×10^{-7} Hz to 3.06×10^{-4} Hz, with a mean of 5.42×10^{-5} Hz.

Sorting into powers of ten, this gives a frequency histogram as in figure 3.23

Depending on the masses of the bodies, the possible peak power ranges from 6.57×10^{20} erg/s to 9.94×10^{30} erg/s, with a mean of 8.80×10^{29} erg/s.

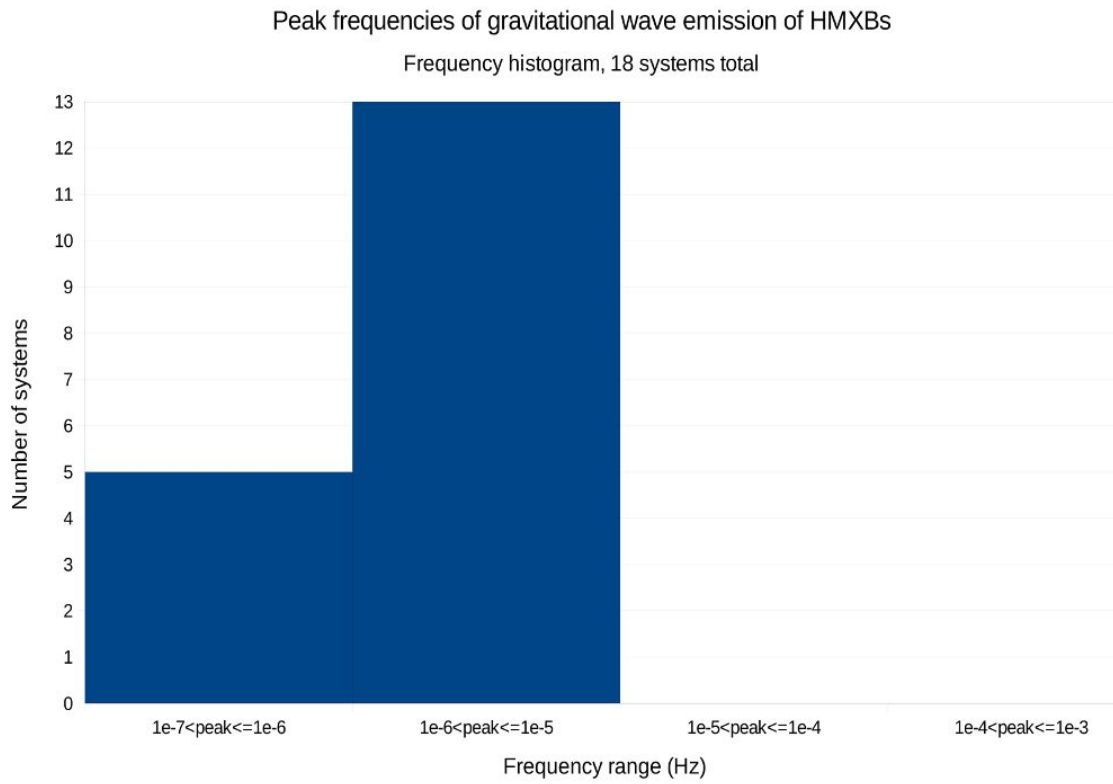


Figure 3.24: Peak gravitational wave emission frequencies of HMXBs

3.6.2 HMXBs

The 18 HMXBs studies have possible peak gravitational wave emission frequencies ranging from 1.14×10^{-7} Hz to 8.90×10^{-6} Hz, a much narrower range than the radio pulsars, as you can see in figure 3.24

The mean peak gravitational wave emission frequency for this sample of HMXBs is 2.35×10^{-6} Hz.

Depending on the masses of the bodies, the possible peak power ranges from 9.28×10^{21} erg/s to 1.99×10^{30} erg/s. The mean is 1.75×10^{29} erg/s.

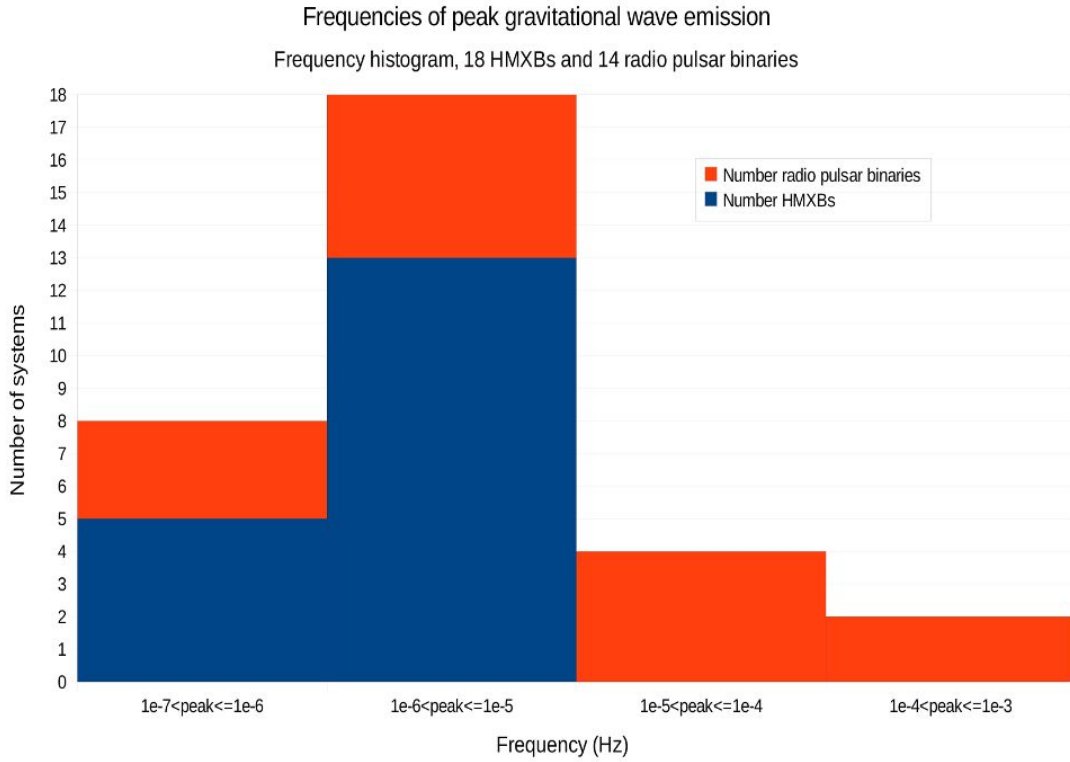


Figure 3.25: Peak gravitational wave emission frequencies of HMXBs and radio pulsar binaries

3.6.3 Comparison of HMXBs and radio pulsar binaries

While only limited conclusions can be drawn from such a sample, at least for these systems, it seems that the peak gravitational wave emission frequencies vary more for the radio pulsar binaries studied than for the HMXBs. The peak power varies slightly more, but not by much.

Of the systems studied, those most likely to be detected by LISA are radio pulsar binaries, since those with peaks at higher frequencies, of order 10^{-4} Hz, are well within the likely LISA sensitivity band, but those of order 10^{-5} fall in a region of decreasing detector sensitivity, and systems with peak frequencies of order 10^{-6} or less are likely to fall outside the LISA band. A comparison of the radio pulsar binaries and HMXB peak frequencies is shown in figure 3.25.

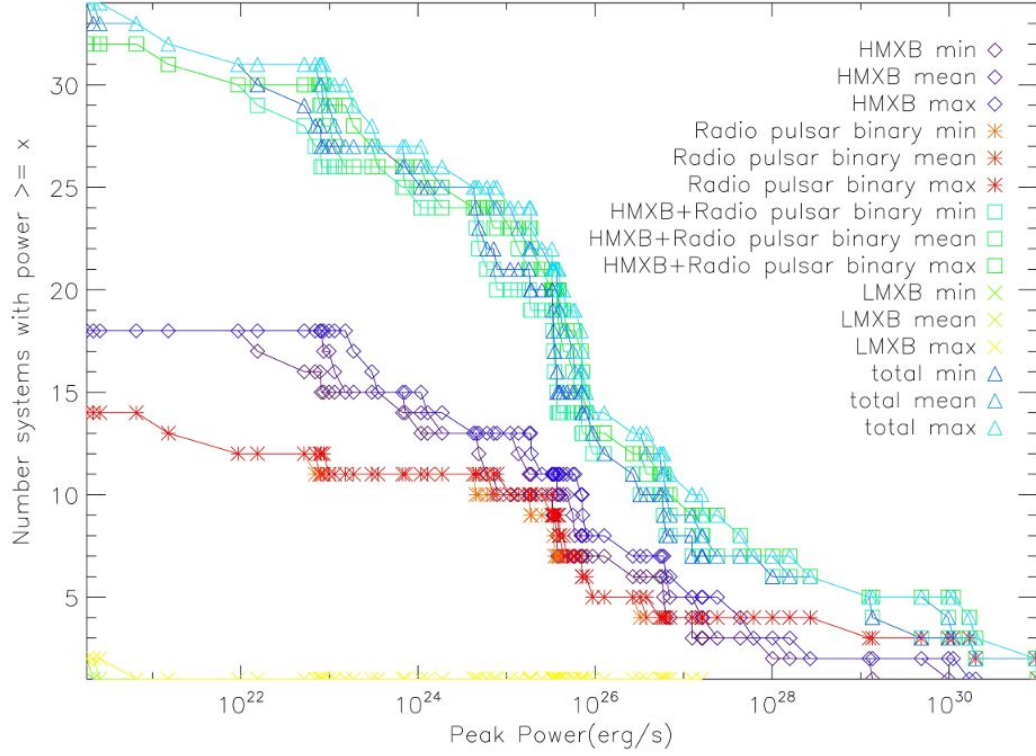


Figure 3.26: Gravitational wave luminosity function for the systems studied

3.6.4 Gravitational wave luminosity function

The cumulative gravitational wave luminosity function of all the binaries studied, figure 3.26, uses the calculation of the power emitted by each system in gravitational waves. Since for many systems there are a range of possible peak powers, depending where the orbital parameters actually lie within the likely ranges studied, for each group- low mass X-ray binaries, high-mass X-ray binaries and radio pulsar binaries- three lines are plotted, corresponding to the minimum, mean and maximum possible values. Totals for all the systems are also shown. Since only two LMXBs were studied, the sum of the HMXBs and radio pulsar binaries only may be a more useful reference point.

The same results are shown with a logarithmic scale for the y axis (number of systems with peak power at or above that shown on the x axis), in figure 3.27.

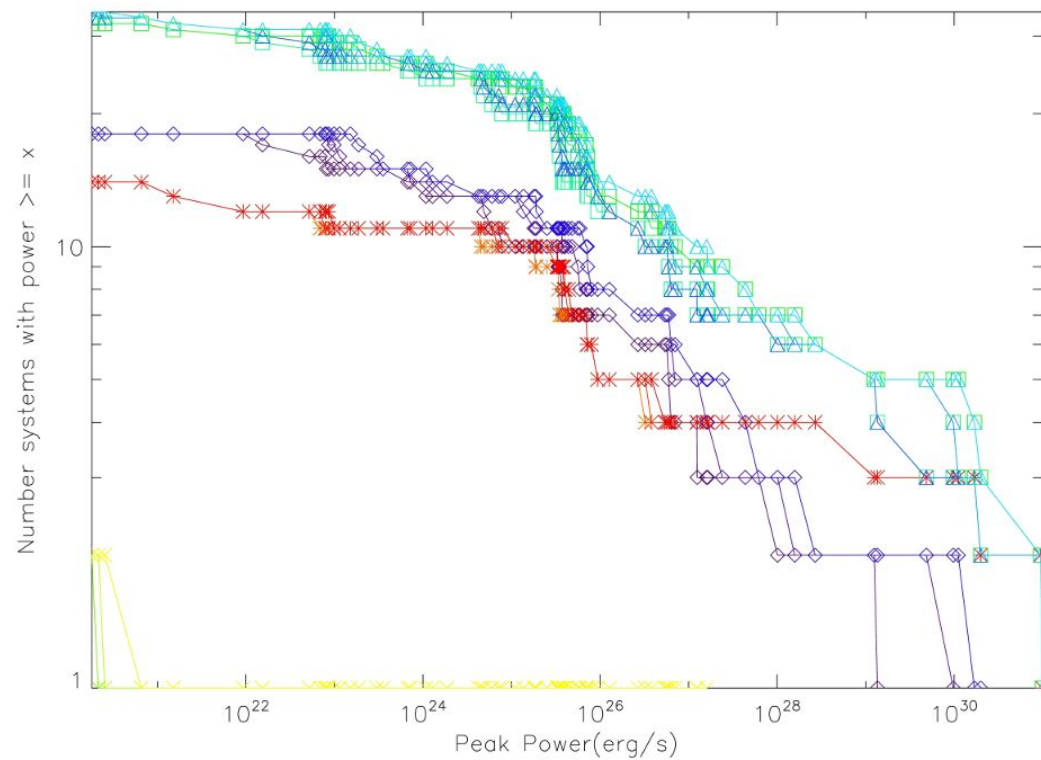


Figure 3.27: Gravitational wave luminosity function for the systems studied, logarithmic scale

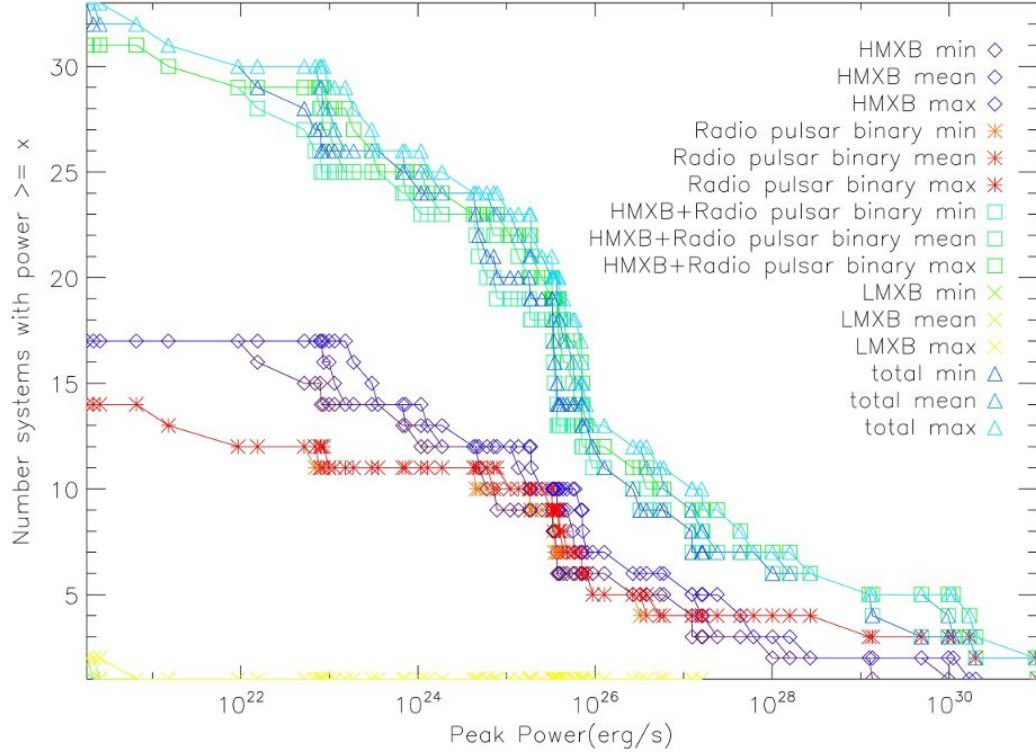


Figure 3.28: Gravitational wave luminosity function for the systems studied, excluding the LMC

The sample studied includes one HMXB located in the Large Magellanic Cloud, HMXB 1A 0535-668. So the gravitational wave luminosity function for the Milky Way must exclude this, as shown in figure 3.28 and on a logarithmic scale in figure 3.29.

The peak power emitted in gravitational waves ranges from 10^{20} to 10^{31} erg/s, with relatively few high power systems. Note that this covers only the peak power emitted rather than the total.

The gravitational wave luminosity function for the Milky Way, figure 3.29, can be compared to the X-ray luminosity function. If the X-ray luminosity function of a galaxy could be related to the gravitational wave luminosity function, it could perhaps allow the stochastic gravitational wave emission from binary systems in

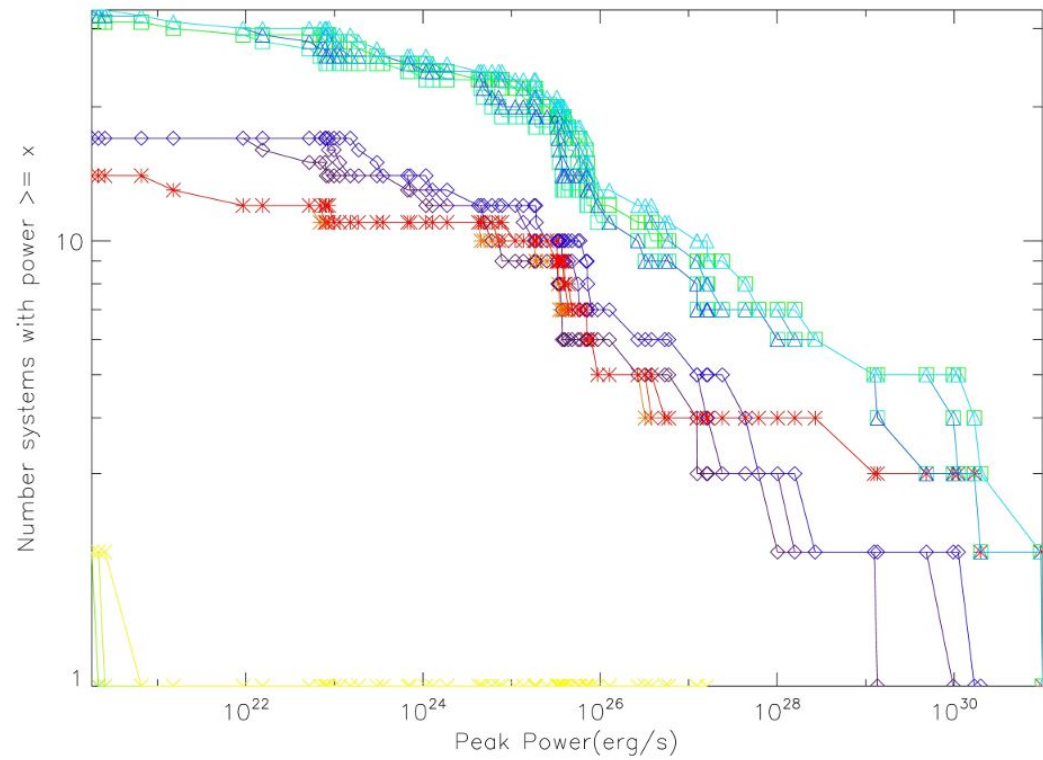


Figure 3.29: Gravitational wave luminosity function for the systems studied, excluding the LMC, logarithmic scale

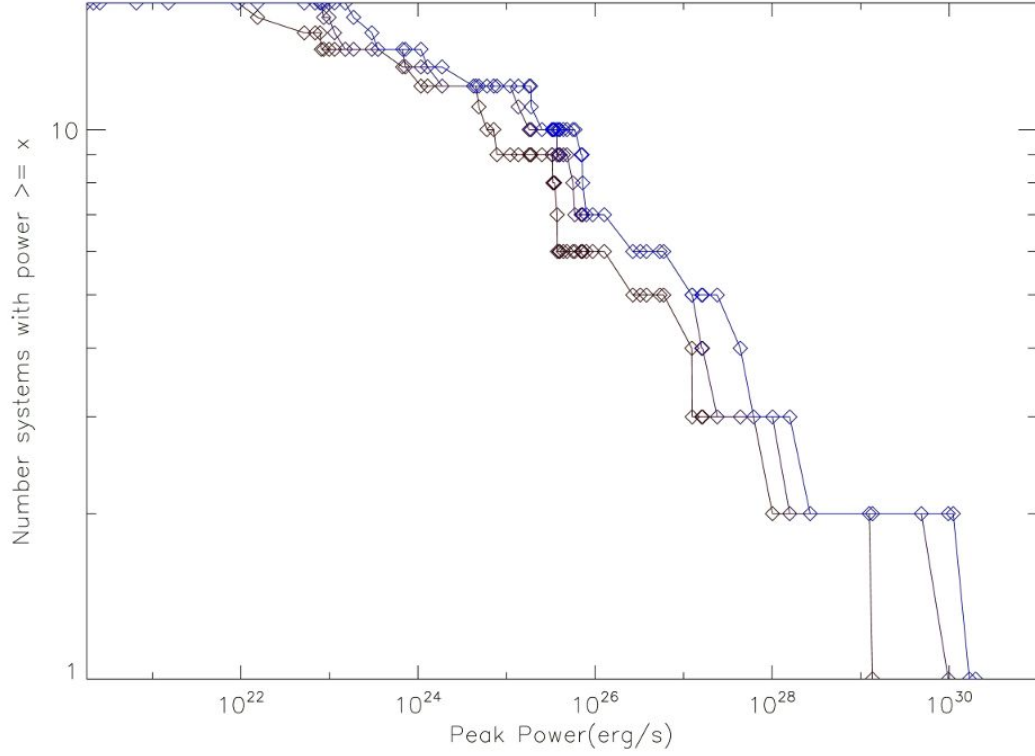


Figure 3.30: Gravitational wave luminosity function for the HMXB, excluding the LMC, logarithmic scale

that galaxy to be estimated, and thus subtracted from measurements where the intention is to study other sources.

The X-ray luminosity function for HMXBs in the Milky Way can be seen in Grimm et al (2003). The essential shape of the luminosity function is very similar to that of the HMXB curve, shown in figure 3.30.

However, it can clearly be seen that the overall gravitational wave luminosity function for the Milky Way binaries studied, figure 3.29, has a different shape due to the contribution from the radio pulsar binaries. As noted in section 3.5, none of the radio pulsar binaries studied correspond to known HMXBs or LMXBs. This suggests the overall gravitational wave luminosity function may have significant contributions from non X-ray binaries.

The sample used represents systems of known orbital parameters, and as such may not be indicative of the overall population. Furthermore, X-ray binaries and radio pulsar binaries are far from the only such sources of gravitational waves, and the results must therefore be viewed in terms of these limitations.

3.7 Chapter summary

This chapter demonstrates the application of the calculation to known eccentric binary systems, and provides results for two low mass X-ray binaries, eighteen high mass X-ray binaries and fourteen radio pulsar binaries. Detailed results can be seen in the appendix.

The systems shown in this chapter demonstrate clearly the effects of orbital period, eccentricity and stellar masses on the gravitational wave output of a system. It can be seen that systems with shorter periods and higher eccentricities have relatively higher frequency peak gravitational wave emission, and so are more likely to be detectable by a LISA-like instrument. The power emitted in gravitational waves varies with both these factors and the masses of the bodies, being higher for higher masses and following the general pattern of variation of $g(n,e)$ with eccentricity detailed in the previous chapter.

Collectively, the data shows that, for this sample, peak gravitational wave emission frequencies vary more for radio pulsar binaries than high mass X-ray binaries. The majority of systems, in both cases, fall outside the likely LISA waveband, though some radio pulsar binaries may be detectable at the lower frequency limit of the LISA waveband.

It is possible that the X-ray luminosity function of a galaxy may, through relation to the gravitational wave luminosity function, be used to predict the gravitational wave background at least in X-ray binaries, which might allow such to be removed from data in order to study other gravitational wave sources. However there are notable differences between the X-ray and gravitational wave luminosity functions

for high mass X-ray binaries in the Milky Way. More importantly, binary systems which are not known X-ray sources, such as the radio pulsar binaries studied, clearly contribute to the overall gravitational wave luminosity function for the Milky Way and would need to be allowed for when attempting to estimate the gravitational wave background in other galaxies. The sample used here should not be considered representative of the overall gravitational wave emission for the Galaxy.

It is notable that many of the systems studied here have unknown factors. These calculations show the gravitational wave emission for a variety of cases. A measurement of the gravitational waves from these systems, compared to the calculations, could allow us to better constrain factors such as orbital period, eccentricity and stellar masses. For those systems where the nature of the compact object is unclear, such as those in 3.4.3, 6.3 and 6.3 and a new constraint on the mass might allow us to determine whether it is in fact a black hole, neutron star or white dwarf.

Measuring the signal in each polarisation and comparing the peak power in each could help to determine the angle of inclination of a system.

Measurement of gravitational waves has the potential to provide a huge amount of insight into the nature of binary systems.

Chapter 4

Many binary systems; globular cluster

4.1 Introduction

The program from chapter 2 forms the basis of a larger calculation for multiple binary systems, such as might be found in a globular cluster. In this chapter I describe how that program is extended and changed and present the results from interations of increasing complexity.

Rather than enter the parameters of hundreds or thousands of systems by hand, the variable orbital parameters are generated from statistical distributions by the monte carlo method. Various methods for generating the distributions were investigated and tested. The program is run using a batch file to input constants for that calculation and control which distribution is used to generate the variables, cycling through numerous options and outputting the results of them all, making it easy to adjust the constants and run again.

The first iteration of the program varies only eccentricity, with the stellar masses, orbital period and inclination kept constant for all systems. While not realistic, this allows study of the effect of eccentricity only on a large group of systems. Subsequent

iterations add variation of orbital period, stellar masses and inclination. Results for all of these are presented here.

4.2 Extending the program to multiple systems

The calculation remains the same as in the single system program, however the new version looks at the cumulative gravitational wave emission from numerous sources. This means running that calculation many times. Each time, the variables are generated based on a statistical distribution. These are used to run the calculation and the results added to an array. When the required number of systems is reached, the program outputs tab separated files containing a list of the results for each system and, in a separate file, the total gravitational wave output across the required frequency spectrum- all details having been specified in a batch file.

The resulting total is used to generate a graph showing power emitted in gravitational waves versus wave frequency. The orientation of the binaries would be stoichastic, so each system would emit gravitational waves at a random phase.

Using a shell script and batch file to run the program allows a set of conditions to be repeated numerous times while drawing the variables from a different statistical distribution each time (for example different mean and standard deviation of a normal distribution), and results in numerous graphs which can be compared, showing clearly the effect of changing the distribution.

The mathematics of the program, including generation of Bessel functions, is identical to that in the single system version, as detailed in chapter 2.

It should be noted that in a real globular cluster, gravitational waves would also result from three-body interactions, mergers and unbound two body interactions. These would however be one off events rather than continuous signals as would be seen from a stable or slowly evolving binary. As such, a signal from an event might be detectable in addition to the total signal from many binaries presented here, but these one off events are not included in the calculation. An estimate of the

expected gravitational radiation from the general binary population of the cluster could of course help in constructing a model signal which can be subtracted from measurements when searching for the signals of these events, as well as being used to study the cluster as a total system.

The binary systems are all assumed to be stable, as only those with a period below 500s will have a measurable change when observed for a year. (Benacquista, 2000).

4.2.1 Number of systems

Globular clusters can contain hundreds of thousands of stars. The fraction of binary systems in a globular cluster has been found to range from 10% to 50% in studied clusters (Sollima et al, 2007) and a simulation of the evolution of a star cluster starting with all stars in binary systems found that after 5Myr the binary fraction was 57% (Marks et al, 2011). So it is reasonable to simulate 100 000 systems, as in the simulation presented along with the studied clusters in Sollima et al (2007).

4.2.2 Generating statistical distributions

In order to study a variety of possible distributions of various orbital parameters, numerous different functions for generating statistical distributions are used. In all cases, a monte carlo method extracting random numbers from the distribution is used to generate the actual variables.

The even distribution is generated using a double precision version of the ran2 random number generation code from page 272 of Press (Teukolsky).

The normal distribution is generated using a modified version of the function random_normal, algorithm 712 from collected algorithms from the Association for Computing Machinery (ACM, 1992). The function is modified to work at double precision and to generate random numbers based on ran2 rather than the standard

random call. The function generates random numbers drawn from a normal (Gaussian) distribution of user defined mean and standard deviation, in this case read from the input file based on the batch file running the program.

In each case, the distributions are seeded based on the time and date, ensuring the variables generated for each run should be different.

4.2.3 Running using a batch file

Using a batch file allows the program to be run multiple times using the same values for the user defined variables, but different statistical distributions to generate the randomly set variables. The batch file is a shell script which writes the user defined variables and the parameters for the statistical distributions chosen to an input file, which is then read by the program. After the program completes, the output files are renamed according to the distributions used, and the input file is rewritten for the next distribution.

So for example, if only eccentricity is to be varied within the program, the script first fills the input file with the user defined variables for number of systems, stellar masses, radii, separation and all other parameters, then sets the choice of distribution to ‘even’. After this run completes, the output files are renamed so they can be identified, including various parameters and an indication of the distribution in the filename. The shell script then rewrites the choice of distribution in the input file to ‘normal’ and fills in the appropriate mean and standard deviation. The program is run for numerous different means and standard deviations for the normal distribution, as defined in the shell script.

The shell script also uses IDL to generate a graph of the total gravitational wave spectrum for each run and name them accordingly. When the batch is finished, the user has a set of results varying the eccentricity according to numerous different statistical distributions.

4.2.4 Frequency binning

When the orbital period is not the same for each system, the gravitational wave emission does not occur at the same frequencies. This means that for summing the emission to give an overall spectrum, the emission of each system must be added to a bin of user defined width. Since a real instrument would have a finite frequency resolution, and the gravitational wave emission lines themselves would be broadened, this is a realistic, if simplified, solution. The width of each bin, in Hz, is defined in the batch file and read into the program. Where the specified maximum and minimum frequencies do not result in an integer number of bins of this width, the maximum frequency is increased so that the final bin is of the same size as the others.

When the calculation is run, the frequency each harmonic falls at for each system is also calculated, and the power output for that system at that frequency is added to the appropriate array element for the summed output. The output file contains the bin limits as well as total gravitational wave power summed over all systems occurring within those limits (defined as greater than or equal to the bin minimum, less than the bin maximum). When plotting the results, the midpoint frequency of each bin is used. The size of the bin can obviously have some effect on the results and this is studied in subsubsection 4.3.2.

4.3 Results

4.3.1 Varying eccentricity

The eccentricity is generated from a statistical distribution as passed to the program from the batch file. It will have a value between zero and the calculated theoretical maximum eccentricity, based on the eccentricity for a system where the two stars just touch at periastron, as detailed in section 2.3 and equation 2.7. As mentioned in section 3.2, for a star which is not a compact object, the radius is calculated from

the mass as expected for a main sequence star.

The maximum possible eccentricity has a significant effect on the results. Examples of the calculation, shown in table 4.1 show a variety of possible maximum eccentricities for different types of system. The higher the maximum possible eccentricity, the more likely a result is to be skewed by this, since, as shown in previous chapters, higher eccentricity systems have far higher peak power output as gravitational waves and the peak occurs at a much higher harmonic number. For a very high eccentricity system, this can swamp the signal coming from all other systems.

Circular systems, with an eccentricity of zero, are possible, if the random number generator used for the eccentricity returns zero, and would produce emission only in the $n=2$ harmonic, as mentioned in chapter 2. It is of course unlikely that the random number generator returns a zero, but this is possible and would of course be a little more likely to occur where the maximum possible eccentricity is smaller and hence there are fewer possible values to generate.

Table 4.1: Variation of maximum possible eccentricity with period and stellar size, where m_1 is a neutron star of radius $2 \times 10^{-5} R_\odot$

period (days)	$m_2(M_\odot)$	$r_2(R_\odot)$	max eccentricity
1	1.4	2×10^{-5}	0.999993252447772
1	3.0	2.408224685	0.65057391243067
1	5.0	3.623898318	0.535922318412945
10	1.4	2×10^{-5}	0.999998546283941
10	3.0	2.408224685	0.924718431533852
10	5.0	3.623898318	0.900017494391928
100	1.4	2×10^{-5}	0.999999686806369
100	3.0	2.408224685	0.983781077737652
100	5.0	3.623898318	0.978459422152166

This is demonstrated with the two examples below.

100 000 neutron star and $3M_{\odot}$ star systems

The program was run for 100 000 binary systems, each consisting of a $1.4M_{\odot}$ neutron star with radius $2 \times 10^{-5} R_{\odot}$ and a $3M_{\odot}$ main sequence star with radius $2.408224685R_{\odot}$ and a period of 10 days. This gives a maximum eccentricity of 0.924718431533852 calculated as in equation 2.7.

The eccentricities of the 100 000 systems were allocated according to statistical distributions as in 4.2.2. The program was run for an even distribution and normal distributions with mean eccentricity varying from 0.1 to 0.9 and standard deviation varying from 0.1 to 0.9. The results were summed to give overall gravitational wave spectra for the 100 000 systems taken as a group.

Since the systems have the same orbital period, the gravitational waves from all systems in this calculation occur at the same frequencies, with the power output at any given harmonic number for a single system varying purely with orbital eccentricity.

Full results are given in the appendix.

For a small mean eccentricity, as standard deviation increases the chance of one or more very high eccentricity systems occurring in the population increases. So, as expected, as standard deviation increases, the results tend more towards those expected from a high eccentricity system, gradually swamping out the results of lower eccentricity systems. Thus for a small mean eccentricity, peak power and peak width increase with standard deviation.

This can be seen for a mean eccentricity of 0.1 in figure 4.1.

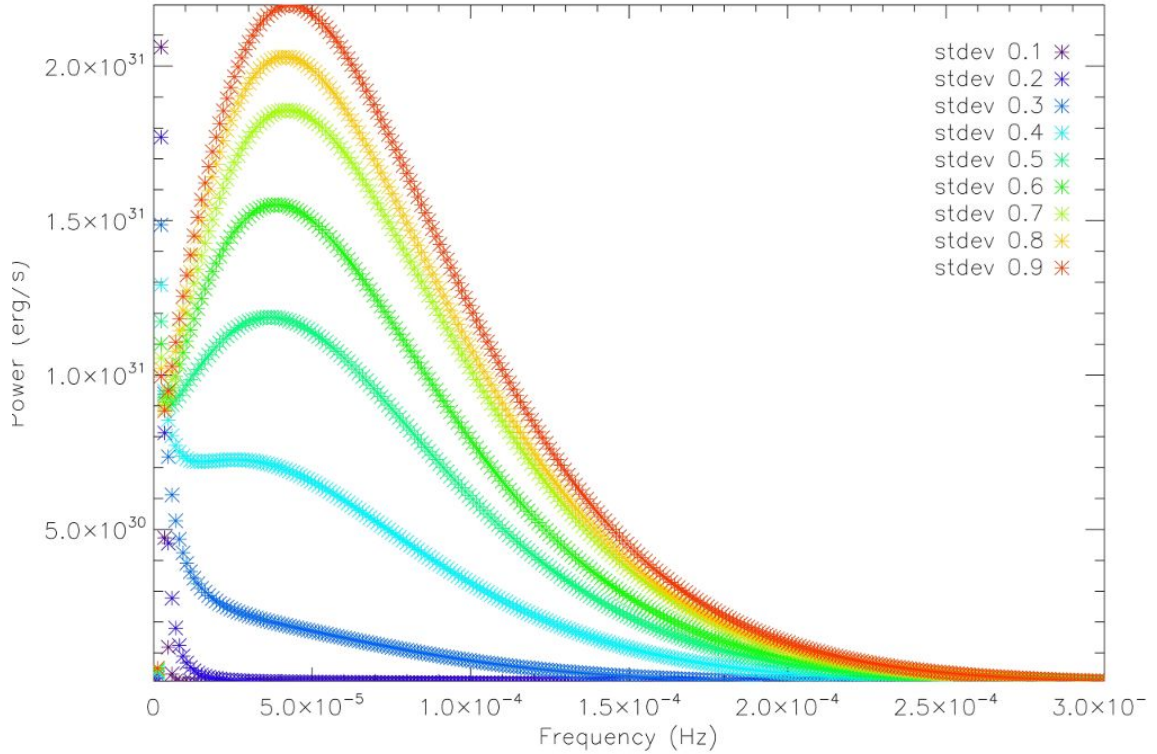


Figure 4.1: 100 000 neutron star and $3 M_{\odot}$ systems, normal distribution of eccentricities with a mean of 0.1 and range of standard deviations

However for a large mean eccentricity, as standard deviation increases the number of very high eccentricity systems in the population will decrease. This leads to the inverse of the case for a small mean eccentricity. For a large mean eccentricity, peak power and peak width increase as standard deviation decreases.

This can be seen for a mean eccentricity of 0.9 in figure 4.2.

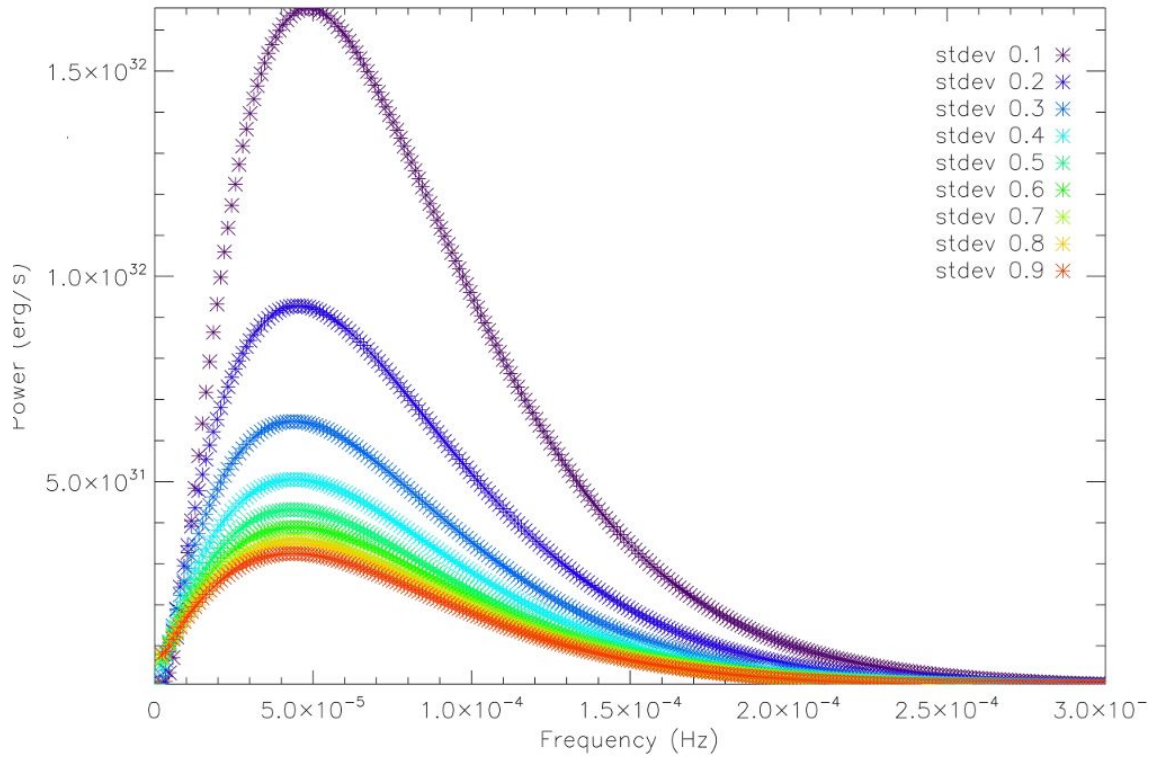


Figure 4.2: 100 000 neutron star and $3 M_{\odot}$ systems, normal distribution of eccentricities with a mean of 0.9 and range of standard deviations

For a standard deviation of 0.5, the variation of the result with mean eccentricity is shown in figure 4.3.

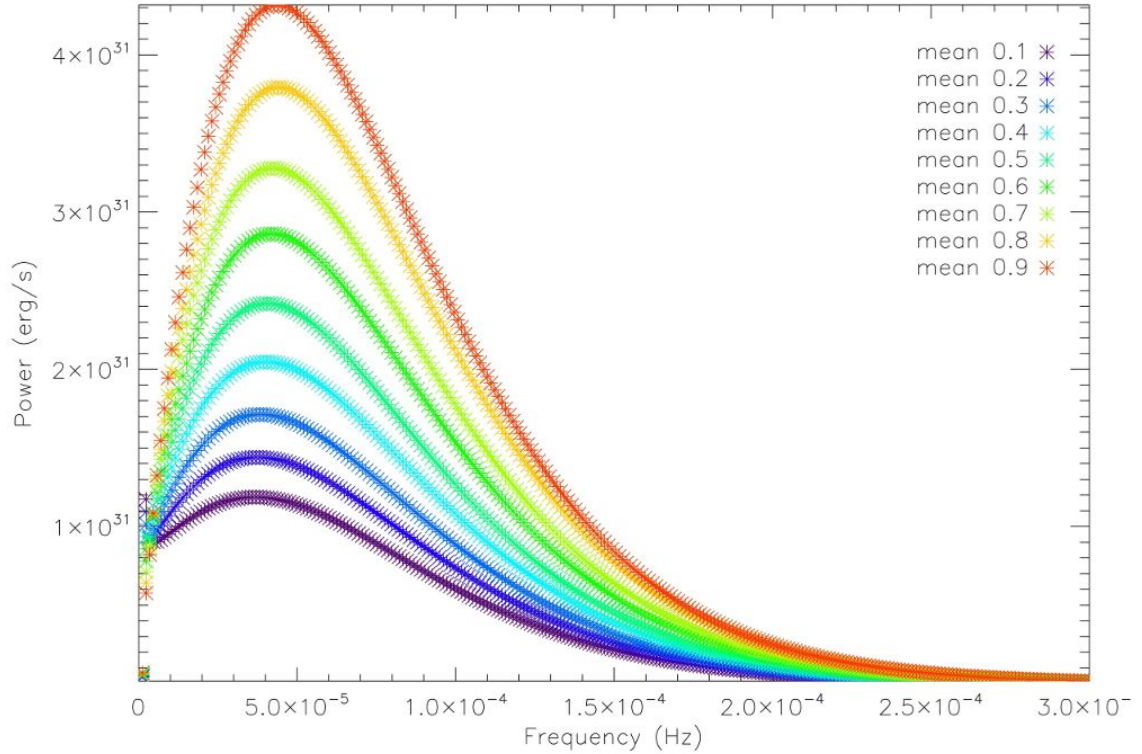


Figure 4.3: 100 000 neutron star and $3 M_{\odot}$ systems, normal distribution of eccentricities with a standard deviation of 0.5 and range of means

100 000 two neutron star systems

For this case, again run for a period of 10 days and 100 000 binary systems, the maximum eccentricity allowed by the program was 0.999998546283941

As in the previous case, since the systems all have the same period, the gravitational waves from each system occur at the same frequencies, though with differing power outputs at each harmonic number, depending on the system's eccentricity.

It can clearly be seen that higher eccentricity systems dominate the results. These were run only to a maximum frequency of 1×10^{-3} Hz- the same as the neutron star and 3 solar mass secondary model- due to the long runtime of the program for 100 000 systems. Even the results with a low mean eccentricity and small standard

deviation show a gravitational wave spectrum still rising in emitted power as the highest calculated frequency is reached. This can be seen for runs with a mean eccentricity of 0.1 in figure 4.4.

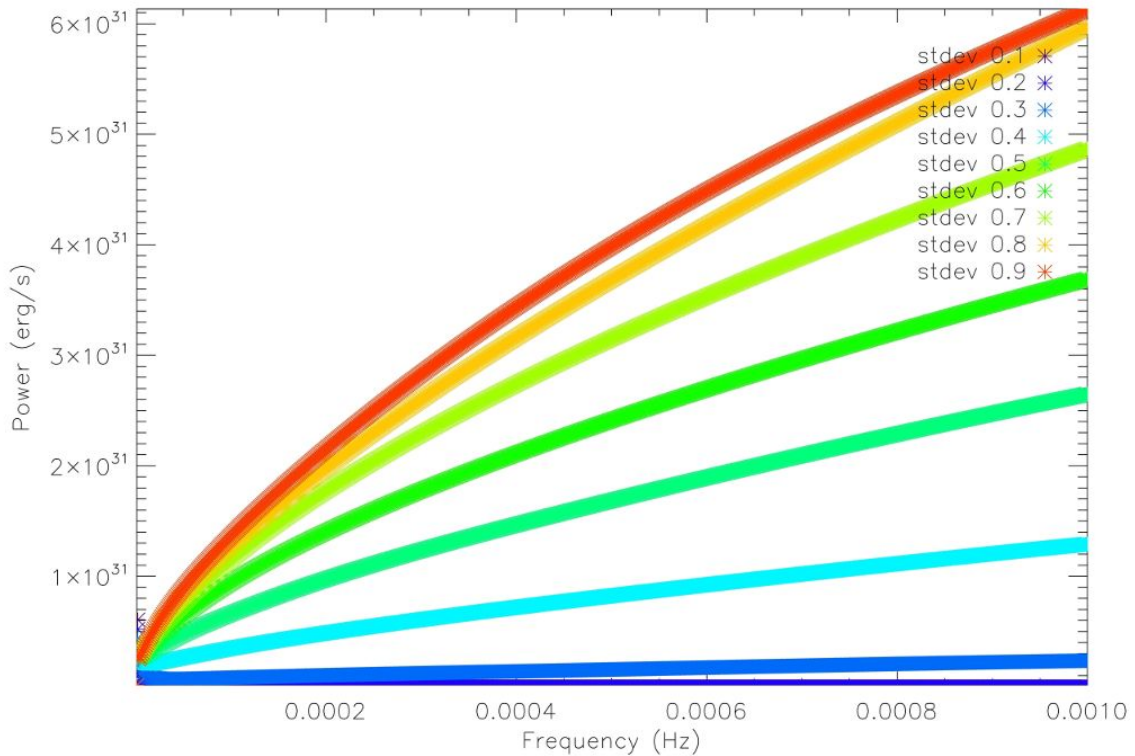


Figure 4.4: 100 000 two neutron star systems, normal distribution of eccentricities with a mean of 0.1 and range of standard deviations

Full results are given in the appendix.

4.3.2 Varying eccentricity and orbital period

Varying the orbital period means that the harmonics for each system no longer occur at the same frequencies. So the power output from each system cannot simply be summed over each harmonic to give an overall output for a cluster of systems. A real instrument would have a finite frequency resolution. So the signals are added

using frequency binning, as described in subsection 4.2.4. The width of the bin is user defined and the effect of changing the bin width on a signal needs to be shown in order to understand the final results.

Constant orbital period with frequency binning applied to summing of results

To begin with, the effect of frequency binning, as described in subsection 4.2.4 was tested for systems with the same period in order to determine the best bin size to use.

For these quick tests, the program was run for sets of 10 000 systems only, each with a 10 day orbital period, stellar masses of 1.4 and $3 M_{\odot}$ and eccentricity drawn from a statistical distribution as before. A 10 day orbital period means the system has a fundamental frequency of $1.157 \times 10^{-6} \text{ Hz}$. Tests were run with bin widths of 10^{-5} , 10^{-6} and 10^{-7} Hz . Example results, for a mean eccentricity of 0.9 and a variety of standard deviations, are shown in figures 4.5, 4.6 and 4.7 respectively. This example is chosen as the spacing between the different standard deviation results is clearest, allowing the effect of the binning on the result to be obviously seen.

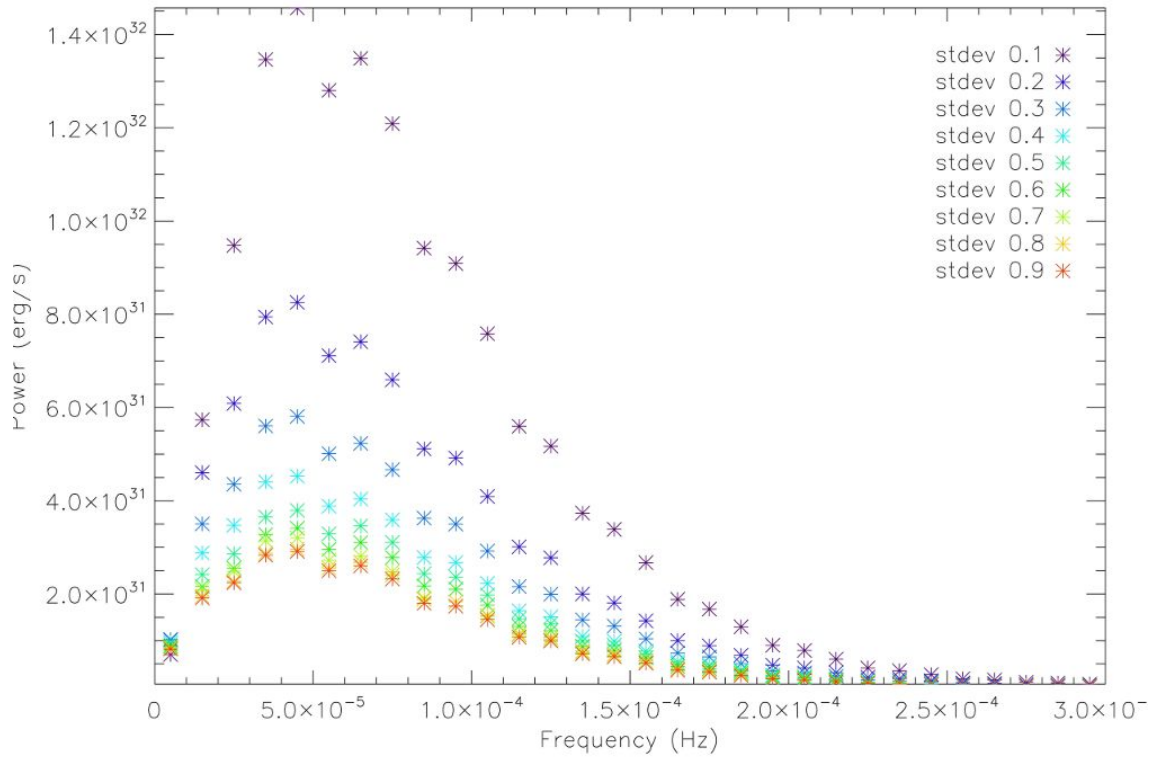


Figure 4.5: 10 000 systems with 10 day period, eccentricity distribution mean 0.9, with frequency bin width 10^{-5}Hz

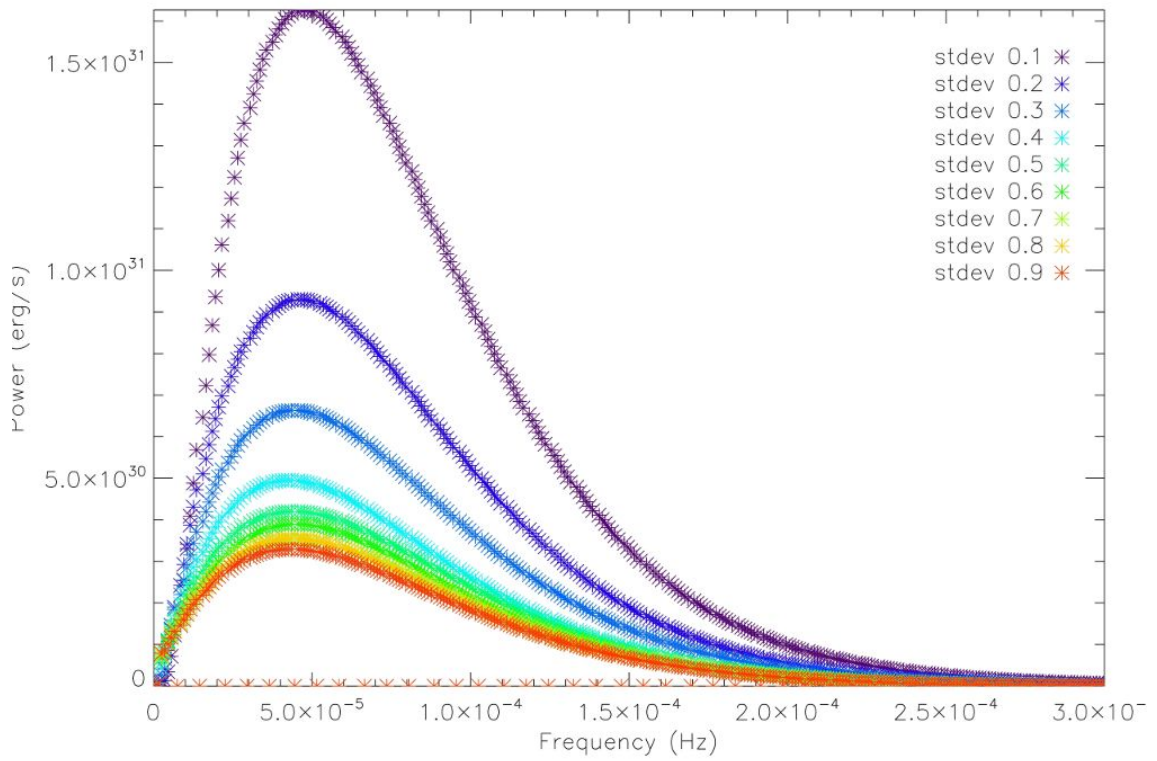


Figure 4.6: 10 000 systems with 10 day period, eccentricity distribution mean 0.9, with frequency bin width 10^{-6}Hz

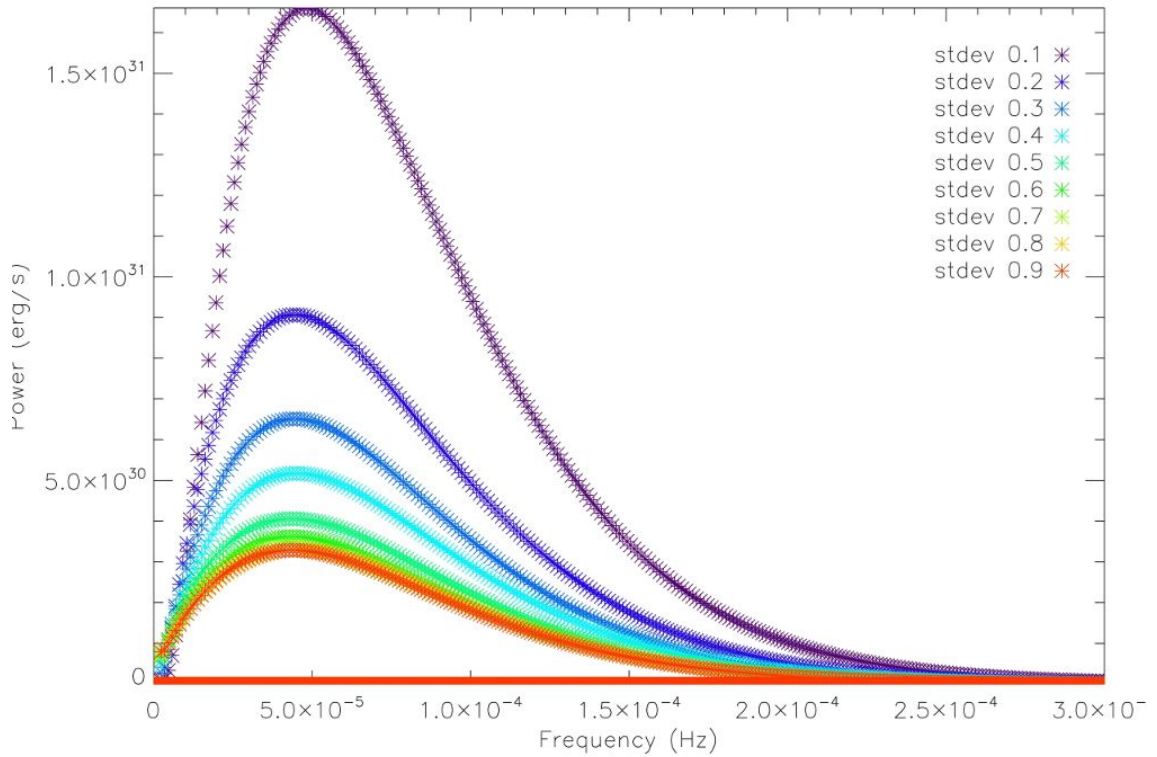


Figure 4.7: 10 000 systems with 10 day period, eccentricity distribution mean 0.9, with frequency bin width 10^7 Hz

It can be seen that with the bin width much larger than the fundamental frequency of the system, the rough shape of the spectrum is clear but detail is lost. For a bin width only slightly smaller than the fundamental frequency of the system, the detail is clear, with a few extra points at zero where no data fell in those bins. Where the bin width is much smaller than the fundamental frequency there are simply far more points at zero with no data in.

When the program is run for systems with varying orbital periods, they will no longer all have emission at the same set frequencies, which is why binning becomes important. A bin width at or near to the fundamental frequency for the system with the longest period of the set would preserve most of the data. A larger bin width may be more realistic, as signals from many systems may be difficult for an

instrument to discern. A larger bin width also makes the output graphs easier to visualise.

Period distribution

The simulation of the evolution of star cluster binaries in Marks et al (2011) includes the change in period distribution over time. As the simulation progresses the period distribution tends towards that of the galactic field, supporting the authors' suggestion that galactic field binaries may originate in clusters. The authors suggest this can be extended to globular clusters, though caution that they have simulated only much smaller clusters. So the orbital period distribution for G-dwarf binaries in the galactic field from Duquennoy & Mayor (1991) is used for the period distribution for the binaries in a globular cluster here. This is a normal distribution of $\log_{10}(\text{period})$ with a mean of 4.8 and standard deviation 2.3, as can be seen in Duquennoy & Mayor (1991). It is suggested that the period distribution does not depend on stellar type (Marks et al, 2011).

To implement this in the program, a separate program was written, using the same procedure for generating random numbers from a normal distribution as that described in 4.2.2. The period distribution program outputs a text file of 100 000 periods generated from a normal distribution with a user determined mean and standard deviation, in this case 4.8 and 2.3 respectively. The main program reads these into an array and proceeds with the calculation for all orbital periods within a user defined maximum and minimum, as set in the batch input file.

Eccentricity distribution

As for the period distribution, the Marks et al (2011) paper provides a likely eccentricity distribution. This is approximated by a normal distribution with mean of 0.65 and standard deviation of 0.33. The standard deviation was estimated by summing the fraction of the total number of systems represented by each histogram bar moving out from the peak, with half the peak included in the sum, in either

direction until 34.1%, or 1σ is reached. The mean is estimated to fall within the peak histogram bar.

The program is run for a normal distribution of eccentricities with mean of 0.65 and standard deviation 0.33. It should be borne in mind that the eccentricity for any given system is randomly drawn from these distributions and, particularly where few systems are included, a single high eccentricity value may dominate the results.

At larger orbital periods, the calculated maximum eccentricity becomes extremely large, to the point of being unrealistic. It was also necessary to consider that the calculation takes far longer to run for a very eccentric system. At higher mean eccentricities, for a large number of systems, an extremely large eccentricity might be generated. For this reason, the maximum possible eccentricity is now set to be either that calculated from the orbital period or 0.99, whichever is smaller.

Splitting into segments

The large range of possible orbital periods necessitates splitting the systems up by period. Choosing one frequency range and bin size for all systems would be difficult, a bin size small enough for the largest period systems would, if used over a frequency range large enough for the smallest period systems, result in huge array sizes and a very slow program indeed. It would also be necessary to stop calculating systems which have peaked and returned to zero as continuing to run the calculation for a large range of zeroes would again take a long time, and be wasteful. This would introduce another possible source of error.

Therefore, the systems are split up by the order of magnitude of the orbital period, with bin size and frequency range scaling accordingly. For each order of magnitude, the program performs the calculation only for systems with orbital periods within the set boundaries.

Another advantage of this is that each period block can be run simultaneously, allowing parallel processing.

The program was first run for a $1.4M_{\odot}$ neutron star and $3M_{\odot}$ main sequence

star, with the bin size set to be slightly smaller than the largest possible fundamental frequency ($n=1$) in the batch. Results can be seen in figure 4.8. Results are presented split by orbital period.

Note that the scale on each axis varies between graphs.

The effect of bin size can clearly be seen in some cases, where lines appear in triplicate due to where each data point actually falls. Bin sizes were adjusted for the next run.

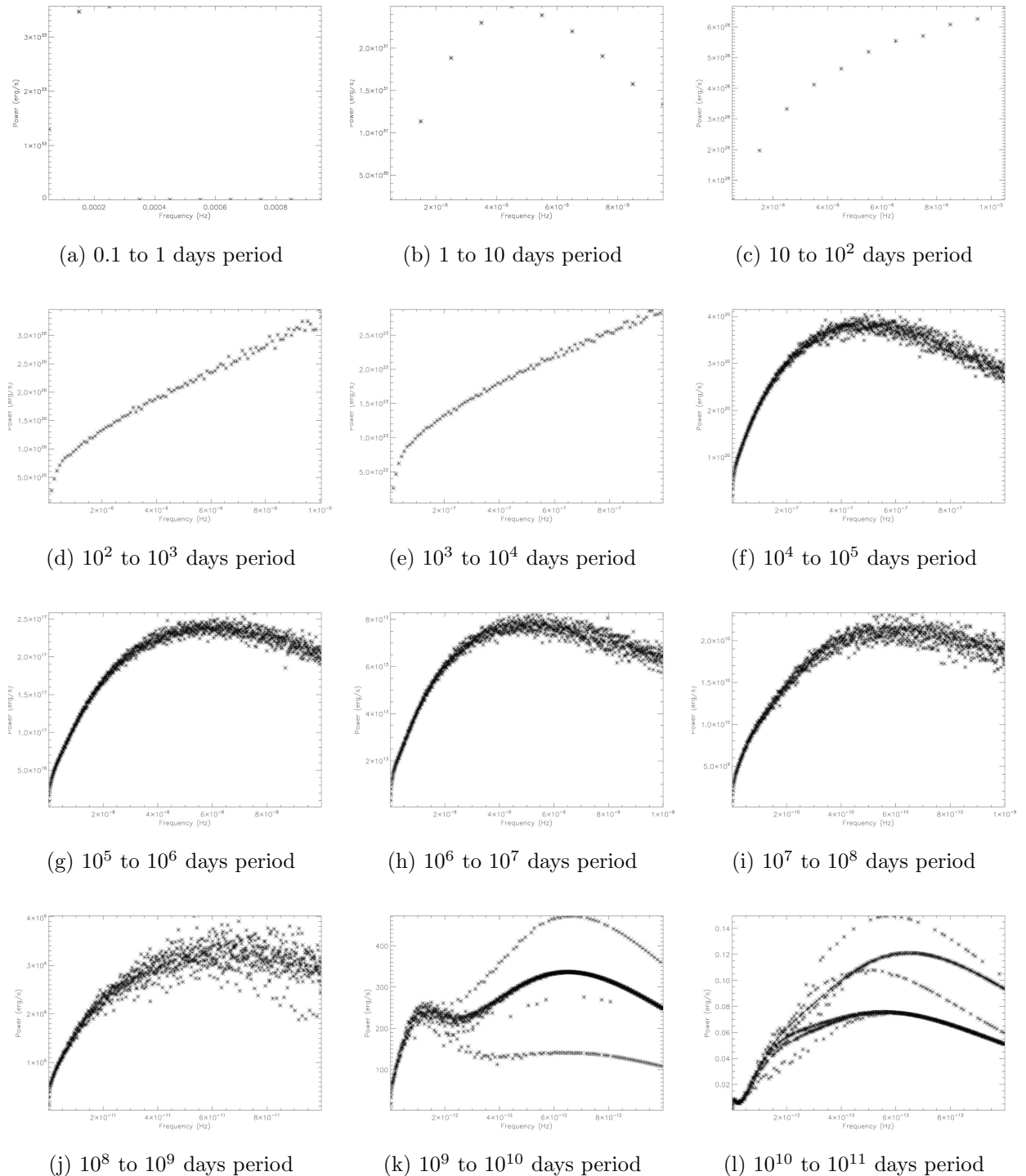


Figure 4.8: Results for 100 000 systems with masses 1.4 and $3 M_{\odot}$ split by orbital period

The program was then run for a $1.4M_{\odot}$ neutron star and $1.4M_{\odot}$ main sequence star, for better comparison with the results when also varying the mass. Since the previous results were often truncated and messy, the bin size was adjusted for each batch, though it should of course be remembered that the total power at each point does depend on bin size as explained in subsection 4.3.2.

The frequency ranges were also adjusted to allow the full curve to be seen. This means there is significant overlap between each

These results are shown in figure 4.9, again, the scale on each axis varies between the graphs.

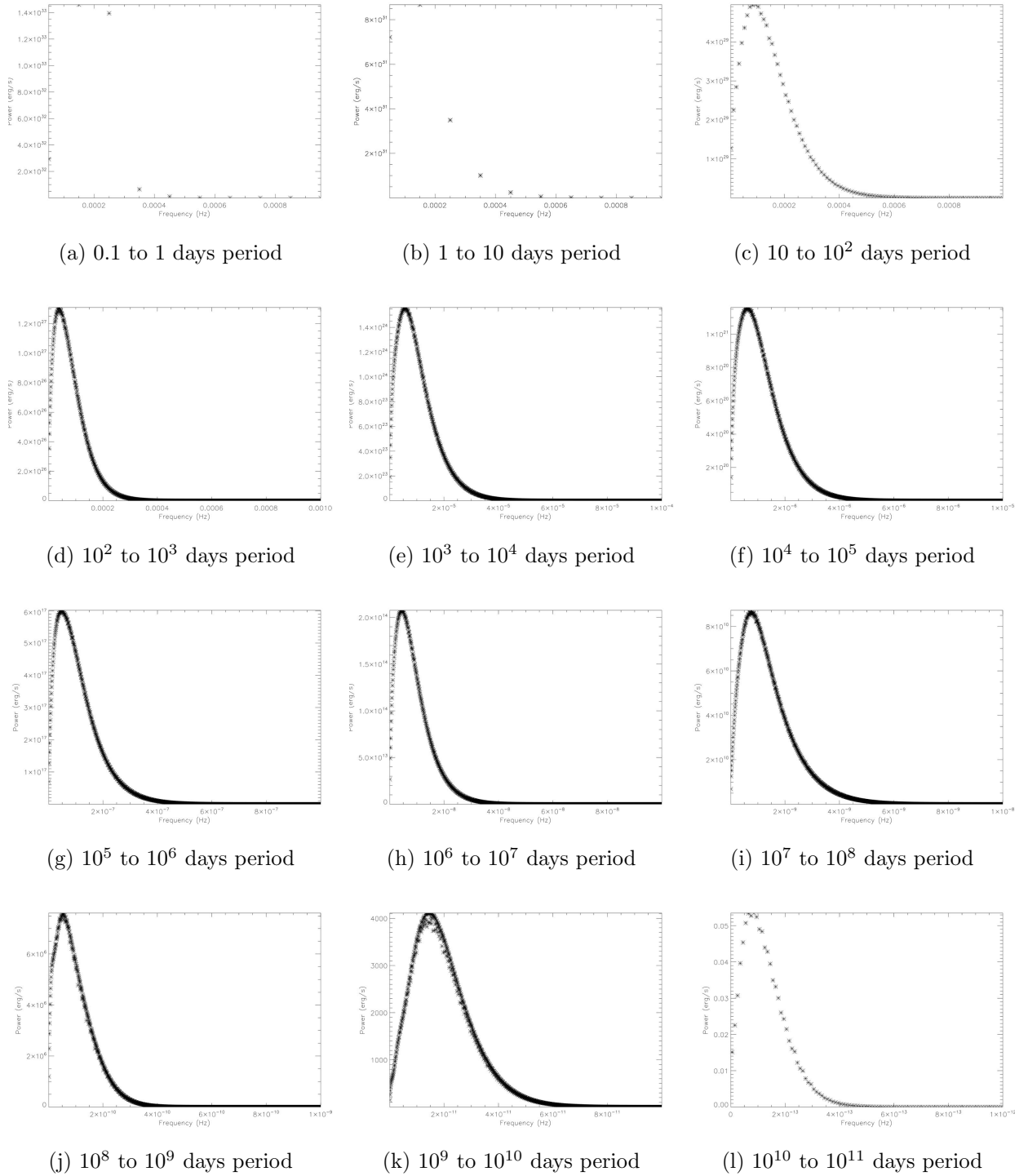


Figure 4.9: Results for 100 000 systems with masses 1.4 and 3 M_⊙ split by orbital period

4.3.3 Varying eccentricity, orbital period and stellar masses

Mass ratios

Finally, to give a realistic result, the program must also allow the stellar masses in each system to vary. Marks et al (2011) also cover this, giving results for the likely mass ratios of the binaries.

Since there are only mass ratios rather than explicit masses to work with, the program is modified to use these, by setting m_1 as a constant, in this case $1.4M_\odot$ since most of the binaries are expected to involve at least one compact object, and calculating m_2 from that, where m_2 is the larger mass. The radius of m_2 is calculated as for a main sequence star, as noted in chapter 3.

To implement this in the program, a set of 1062 mass ratios corresponding to the distribution in the graph was generated. Within each segment, the generated mass ratios are spaced evenly. The file containing the set of mass ratios is read into an array and a line chosen randomly, as for the orbital period, thus each system is assigned a stellar mass ratio randomly drawn from the distribution given.

Overall results

Results of the program for 100 000 systems, varying mass, eccentricity and orbital period, can be seen in figure 4.10. For ease of calculation and ease of viewing, these are split by period. It can be seen that in some frequency bands, results from one block of period lengths would completely overwhelm the others. As before, note the scale on each axis varies between the graphs.

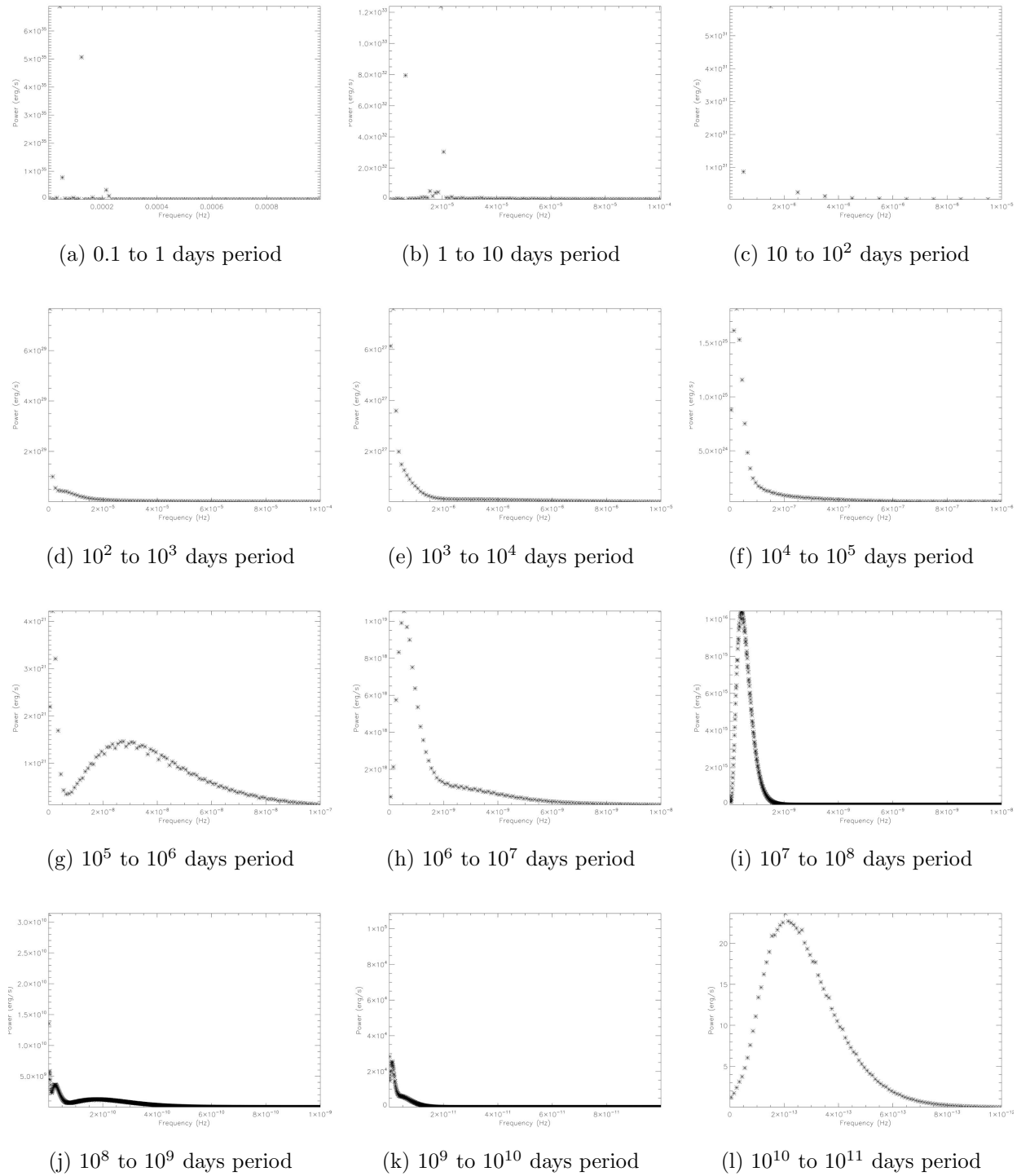


Figure 4.10: Results for 100 000 systems with varying masses split by orbital period

It should be noted that the signals for 10^6 to 10^7 and 10^7 to 10^8 day orbital periods

in this simulation have a significant overlap, meaning the lower peak power signal from the 10^7 to 10^8 day orbital periods would be swamped. In any given simulation the orbital eccentricities, randomly drawn from the distribution, can result in varied signal shapes as seen here.

It should be noted that the short period systems, as expected, emit the most power. Indeed, despite there being far fewer systems in the 0.1-1 day period range than any other, their signal is by far the most powerful. An interferometer similar to LISA, should such be built, may able to detect the signal from the shortest period systems. This is discussed further, for a range of globular clusters, in chapter 5. Pulsar timing arrays are expected to be sensitive to the 10^{-6} to 10^{-9} Hz range, which would cover many of the longer period systems, but the signal from these are less powerful, despite the expectation that there will be more of them according to the period distributionin Duquennoy & Mayor (1991).

This result could be useful in designing instruments to study globular clusters, showing how different period lengths dominate different frequency bands. Overall, a very large range of frequencies are covered.

4.4 Chapter summary

This chapter shows a monte carlo based simulation of the gravitational wave emission from a globular cluster or other large grouping of binary stars. The expected spectra of gravitational radiation, depending for each system on the mass ratio, orbital period and eccentricity, show an example of what the overall spectrum from such a cluster, split into segments, may look like.

These results could be useful when planning detectors to look at such systems, giving an idea of the power emitted in gravitational radiation at different wavebands from a globular cluster.

Actual measurements could help to determine the real distributions of orbital parameters of binary systems within globular clusters. Such measurements could

give an insight into the stellar dynamics of the cluster and may, by comparison to models, help us to understand more about how globular clusters form and evolve, the process of core collapse and the relationship of globular cluster binaries to field stars. This includes the possibility of investigating whether or not galactic field binaries do form in star clusters as has been theorised.

Chapter 5

Globular clusters in the Milky Way

5.1 Introduction

This chapter presents the results of simulating 119 galactic globular clusters using the method of chapter 4. The results are used to build up a gravitational wave globular cluster luminosity function for the galaxy.

In electromagnetic astronomy, standard candles are objects with characteristic light curves which can be used to establish the distance of their host galaxy. One variety of standard candle is the luminosity function of globular clusters over a galaxy.

For gravitational wave astronomy, the equivalent of a standard candle is a standard siren, an object with a well defined characteristic gravitational wave signal as predicted by models. Binary supermassive black holes are expected to be good standard sirens (Arun et al, 2008). However these are clearly only of use where such binaries can be found.

When the gravitational wave signal from a standard siren is found, if it is possible to identify the host galaxy in electromagnetic astronomy the combination of

measurements may be used as a cosmological probe. With a redshift measurement from electromagnetic astronomy and an independant measurement of the luminosity distance from the gravitational wave signal, the luminosity distance-redshift relationship can be investigated. This can be used to constrain cosmological parameters including the dark energy density.

This chapter models the gravitational wave emission from the binaries in the Milky Way globular clusters and discusses the possibility of using the globular cluster luminosity function in gravitational waves as such as standard siren. The waveform is modelled for the clusters in the Milky Way and this is used to construct a luminosity function for the Milky Way globular cluster peak gravitational wave emission, based on the method used in chapter 4. The possibility of using such signals as standard sirens is then discussed. The advantage of such, if possible, is that most galaxies contain globular clusters and so this could potentially be used where supermassive black hole binaries are not found. However the large and spread out nature of the signal may make this harder to measure.

It should be noted that the period, mass and ellipticity distributions used in this chapter may not necessarily be representative, but illustrate the process by which the luminosities of the globular clusters can be derived.

The gravitational wave emission from the binaries in a globular cluster can provide a useful probe of cluster evolution. The process of core collapse causes binaries to harden- and the gravitational wave signal can give a good indication of the orbital periods of the binaries, particularly the shortest period systems, in a cluster. This would enable study of the binary population in clusters at different stages of collapse and possibly recovery, perhaps helping to characterise the state of each cluster and learn more about how globular clusters evolve.

5.2 Globular Clusters and core collapse

Globular clusters were at first modelled in the 1960s by Michie, King and Hénon. Michie and King considered a cluster as a uniform gas of stars, interacting without physical collisions, leading to thermal equilibrium. Hénon's simulations however worked on the basis that whenever a star escapes from the cluster the core must shrink slightly, and the increased gravitational binding energy means the stars need to move a little faster in order to keep the cluster stable. However this leads to more stars escaping and the process accelerates under positive feedback, causing the core to shrink catastrophically. (Djorgovski, 1998)

The process of core collapse does indeed occur, but rather than leading to clusters with quasars at the core, is instead arrested by the presence of binaries. When a binary system interacts with a single star, through the 3-body interaction energy is exchanged, resulting in a more tightly bound binary system and a single star, usually the least massive of the three, moving away from each other (Benacquista, 1999). As the core shrinks, 3-body interactions become more likely to occur.

Thus the binary systems provide the necessary energy to halt core collapse. A cluster can collapse and then recover. King-Michie models, with a uniform core and gradual decrease in stellar concentration towards the tidal radius, approximate both precollapse and stabilised post core collapse clusters. Approximately a fifth of globular clusters are however thought to be post core-collapse, showing a clear density cusp near their centres (Djorgovski, 1998).

It is now thought that most globular clusters contain multiple stellar populations (Gratton et al, 2012).

5.3 Globular Clusters in the Milky Way

The Milky Way contains at least 157 globular clusters (SEDS Milky Way Globular Clusters, 2011). Of these, I have modelled the potential gravitational wave emission

from the cluster binaries for 119, all those for which a mass estimate were available at the time of writing. Data for the globular clusters in the Milky Way was taken from the catalogues Harris, 1996 (2010 edition); Gnedin & Ostriker (1997); SEDS Milky Way Globular Clusters (2011). A table of the clusters modelled, and the relevant data, is shown in 5.1. R_c is the core radius, R_t the tidal radius, both in parsecs and 'c' denotes a core-collapsed globular cluster. Cluster mass and the number of binary systems modelled (Nsys) are then listed.

Table 5.1: Globular cluster parameters

Name	R _c (pc)	R _t (pc)	Mass (M _⊙)	Nsys
NGC 5139	3.72	64.6	2.64×10^6	100000
NGC 2419	8.51	213.8	1.60×10^6	60606
NGC 6273	1.35	45.7	1.56×10^6	59091
NGC 6388	0.4	20	1.50×10^6	56818
NGC 104	0.5	54.8	1.45×10^6	54924
NGC 6715	0.66	45.7	1.45×10^6	54924
NGC 2808	0.71	41.8	1.32×10^6	50000
NGC 6441	0.35	24.8	1.30×10^6	49242
NGC 6402	2.45	97.5	1.23×10^6	46591
NGC 6401	0.45	22	1.23×10^6	46591
NGC 6316	0.62	22	1.02×10^6	38636
NGC 7078	0.21	66.4	c 9.84×10^5	37273
NGC 5824	0.52	146.6	8.98×10^5	34015
NGC 6266	0.29	14.5	c 8.98×10^5	34015
NGC 7089	1.17	73.8	8.81×10^5	33371
NGC 5904	0.89	66	8.34×10^5	31591
NGC 6356	1.12	38.8	8.19×10^5	31023
NGC 5272	1.48	104.8	7.82×10^5	29621
NGC 5024	2	120.5	7.33×10^5	27765
NGC 6205	1.82	56.2	6.27×10^5	23750
NGC 6440	0.26	13	5.72×10^5	21667
NGC 5946	0.23	72.7	c 5.66×10^5	21439
NGC 1851	0.28	48.7	5.61×10^5	21250
NGC 6656	1.23	25.1	5.36×10^5	20303
NGC 5986	1.91	31.7	4.98×10^5	18864
NGC 6218	1.07	25.7	4.93×10^5	18674
NGC 6864	0.51	38.7	4.89×10^5	18523

Table 5.2: Globular cluster parameters

Name	R _c (pc)	R _t (pc)	Mass (M _⊙)	Nsys	
NGC 5286	0.78	22.5	4.80×10^5	18182	
NGC 6541	0.58	58	c	4.67×10^5	17689
NGC 6229	1.23	50.1		4.46×10^5	16894
NGC 6626	0.42	19.6		4.42×10^5	16742
NGC 6139	0.35	22.1		4.18×10^5	15833
NGC 6569	0.95	17.7		3.85×10^5	14583
NGC 362	0.43	37.5	c	3.78×10^5	14318
NGC 6723	2.4	26.9	c	3.74×10^5	14167
NGC 5927	0.98	39		3.71×10^5	14053
NGC 6093	0.36	32.1		3.67×10^5	13902
NGC 6355	0.1	31.6	c	3.67×10^5	13902
NGC 6341	0.51	32.9		3.64×10^5	13788
NGC 6752	0.21	66.4	c	3.64×10^5	13788
NGC 1904	0.6	31.5	c	3.57×10^5	13523
NGC 6637	1	24.5		3.44×10^5	13030
NGC 6624	0.15	47.4	c	3.32×10^5	12576
NGC 1261	1.82	33.9		3.26×10^5	12348
NGC 4372	2.63	52.5		3.20×10^5	12121
NGC 4590	1.86	81.2		3.06×10^5	11591
NGC 5694	0.59	40.8		2.92×10^5	11061
NGC 6333	1.26	17.8		2.89×10^5	10947
NGC 5634	1.51	60.1		2.86×10^5	10833
NGC 7099	0.12	37.9	c	2.74×10^5	10379
NGC 6553	0.56	8.3		2.61×10^5	9886
NGC 6652	0.3	18.9		2.59×10^5	9811
NGC 7006	2.75	72.3		2.52×10^5	9545
NGC 6712	1.86	14.8		2.45×10^5	9280

Table 5.3: Globular cluster parameters

Name	R _c (pc)	R _t (pc)		Mass (M _⊙)	Nsys
NGC 6558	0.09	28.5	c	2.41×10^5	9129
NGC 6809	3.98	22.9		2.41×10^5	9129
NGC 6293	0.11	34.8	c	2.34×10^5	8864
NGC 6121	0.49	19.1		2.25×10^5	8523
NGC 6254	1.07	26.9		2.25×10^5	8523
Pal 8	3.31	18.6		2.21×10^5	8371
NGC 6584	1.66	26.3		2.19×10^5	8295
NGC 6284	0.25	79.1	c	2.17×10^5	8220
NGC 6934	1.07	36.3		2.15×10^5	8144
NGC 6171	1	32.4		2.04×10^5	7727
NGC 5897	7.24	44.6		2.00×10^5	7576
NGC 3201	2.09	42.7		1.95×10^5	7386
NGC 6342	0.16	50.6	c	1.95×10^5	7386
NGC 6304	0.36	22.7		1.93×10^5	7311
NGC 6681	0.07	22.1	c	1.89×10^5	7159
NGC 6779	1.05	24.6		1.89×10^5	7159
NGC 6517	0.11	7.3		1.82×10^5	6894
NGC 6981	2.82	47.9		1.81×10^5	6856
Pal 2	0.6	15.1		1.74×10^5	6591
NGC 6235	1	21.4		1.71×10^5	6477
NGC 5053	10.47	69.2		1.66×10^5	6288
IC 4499	5.37	69.2		1.66×10^5	6288
NGC 6539	0.63	25.1		1.60×10^5	6061
NGC 6397	0.03	9.5	c	1.59×10^5	6023
NGC 6144	2.69	53.7		1.52×10^5	5758
NGC 6760	0.59	23		1.38×10^5	5227
Pal 11	7.76	38		1.38×10^5	5227

Table 5.4: Globular cluster parameters

Name	R _c (pc)	R _t (pc)	Mass (M _⊙)	Nsys	
NGC 5466	8.91	239.8	1.33×10^5	5038	
NGC 6101	5.01	31.6	1.32×10^5	5000	
NGC 6453	0.2	63.2	c	1.32×10^5	5000
NGC 6544	0.03	9.5	c	1.30×10^5	4924
NGC 6642	0.24	23.5	c	1.26×10^5	4773
NGC 6717	0.18	21.1		1.23×10^5	4659
NGC 6352	1.48	18.6		1.22×10^5	4621
NGC 6362	2.95	37.1		1.17×10^5	4432
NGC 6638	0.65	16.3		1.12×10^5	4242
NGC 288	3.47	31.6		1.11×10^5	4205
NGC 6287	0.52	20.7		1.03×10^5	3902
NGC 6325	0.05	15.8	c	9.57×10^4	3625
NGC 4833	1.7	30.2		9.49×10^4	3595
NGC 6426	1.35	67.7		9.49×10^4	3595
NGC 6528	0.17	33.1		9.31×10^4	3527
Rup 106	5.75	28.8		8.42×10^4	3189
NGC 6256	0.07	22.1	c	7.68×10^4	2909
NGC 2298	1	19.1		7.20×10^4	2727
NGC 4147	0.55	34.7		6.69×10^4	2534
Pal 3	12.59	125.9		6.38×10^4	2417
Terzan 7	6.46	77.7		6.15×10^4	2330
NGC 6522	0.11	34.8	c	5.93×10^4	2246
NGC 6535	0.83	16.6		5.93×10^4	2246
NGC 7492	6.17	61.7		5.56×10^4	2106
Pal 4	15.85	95.5		5.41×10^4	2049
NGC 6496	1.74	8.7		4.63×10^4	1754
NGC 6366	2.14	17.8		3.92×10^4	1485

Table 5.5: Globular cluster parameters

Name	R _c (pc)	R _t (pc)	Mass (M _⊙)	Nsys
NGC 6838	0.72	10.2	3.67×10^4	1390
Arp 2	13.18	104.7	3.26×10^4	1235
Pal 5	19.5	107.2	2.84×10^4	1076
Pal 15	14.45	57.5	2.74×10^4	1038
Terzan 8	6.61	26.3	2.50×10^4	947
Eridanus	5.89	74.2	2.30×10^4	871
Pal 12	6.17	49	2.02×10^4	765
Pal 14	23.44	123	2.00×10^4	758
AM 1	4.57	77.6	1.81×10^4	686
Pal 13	2.82	28.2	5.12×10^3	194
Pal 1	0.6	19	2.54×10^3	96

The mass estimate is used to estimate the number of binaries in the globular cluster. The largest clusters have a mass of order $10^6 M_\odot$. For the largest, NGC 5139, I therefore estimate 10^5 binary systems. The number of systems for other clusters is then scaled accordingly, by cluster mass.

All binaries are modelled using the distributions from Marks et al (2011) and Duquennoy & Mayor (1991) as in chapter 4. It should be noted that Marks et al (2011) evolve their models for less time than those in Sigurdsson & Phinney (1995), however, the results of Sigurdsson & Phinney (1995) show very little change from the initial to final period distributions for evolution of up to 15Gyr. This is especially the case for the short period binaries, as noted in Sigurdsson & Phinney (1995) (Page 630) "Interestingly the short period binary population is not heavily modified showing the collisions effectively draw from the wider interacting binaries." There is some hardening of the binaries and some mergers, as indeed is the case with the shorter timescale models from Marks et al (2011), so the results should be viewed with this in mind, however, since the short period binaries can be expected to dominate the gravitational wave emission, the relative stability of their period distribution suggests applying this model to a cluster of any age is reasonable. The models of Sigurdsson & Phinney (1995) are evolved for longer, but limits placed on the maximum and minimum period for each model suggest a less complete picture than that of Marks et al (2011) and Marks et al (2011) also include results for eccentricity and mass ratio distributions.

If it however possible that post core-collapse clusters such as M15 might have a significantly different period distribution due to the hardening of binaries during the process of core-collapse. For that reason, the period distribution from model 5 of Sigurdsson & Phinney (1995), specifically aimed at modelling a core-collapsed cluster, is also used to model the 23 core-collapsed clusters. It should be noted that similar may be true of clusters that have collapsed, recovered and stabilised, but currently only post core-collapse clusters with the Hénon cusplike density profile can be identified. Note that this does not include the systems at $\log(P)=-3$, as

this is used by the authors to represent those systems which merged during their simulation, so is not part of the binary population.

Results assuming that all clusters follow the period distribution of Duquennoy & Mayor (1991), and the alternative case where post core-collapse clusters have a period distribution as shown by model 5 of Sigurdsson & Phinney (1995) but the other clusters remain as before, are both presented.

5.3.1 Simulated gravitational wave emission

The same method is used as presented in chapter 4. The eccentricity distribution and mass ratio distribution are also both as in chapter 4. However, since in a globular cluster, containing mostly old stars, main sequence stars are only expected to exist up to a mass of about $0.8M_{\odot}$ (Benacquista, 1999) and many double degenerate binaries are thought to exist, the interpretation of the mass ratio has been changed. All binaries are assumed to contain a $1.4M_{\odot}$ neutron star. This is the more massive of the pair. The mass of the second star is determined by multiplying the provided mass ratio by $1.4M_{\odot}$. Where this results in a mass of less than $0.8M_{\odot}$, the star is assumed to be a main sequence star and its radius, important for calculating the maximum possible eccentricity of the system as explained in chapter 4, is calculated as in equation 5.1. For a mass of between 0.8 and $1.35M_{\odot}$, the secondary is assumed to be a white dwarf, with radius calculated as in equation 5.2. Any secondary with a mass above $1.35M_{\odot}$ is assumed to be a neutron star with radius calculated as in equation 5.3. m_e is the mass of an electron, m_p the mass of a proton and m_n the mass of a neutron. (Benacquista, 1999). Thus double degenerate binaries are included in the model.

$$R_{ms} = M^{0.8} \quad (5.1)$$

$$R =_{wd} \frac{3\hbar^2}{5Gm_e} \left(\frac{9\pi}{4m_p^{\frac{5}{2}}} \right)^{\frac{2}{3}} M^{-\frac{1}{3}} \quad (5.2)$$

$$R =_{ns} \frac{6\hbar^2}{5Gm_n} \left(\frac{9\pi}{4m_p^{\frac{5}{2}}} \right)^{\frac{2}{3}} M^{-\frac{1}{3}} \quad (5.3)$$

The binary systems are all assumed to be stable, as only those with a period below 500s will have a measurable change when observed for a year. (Benacquista, 2000). The very smallest period binaries generated for the period distribution from Sigurdsson & Phinney (1995) may fall below this threshold. As the shortest period binaries dominate the results, for the core collapsed clusters when modelled with this distribution, the peak may change during observations of a year or more.

While it is expected that field binaries would circularise as they approach smaller periods, this is not necessarily the case for globular clusters. Binaries harden largely through three body interactions, the nature of which can lead to a range of eccentricities. (Djorgovski, 1998) Thus the eccentricity distribution of Marks et al (2011) is applied to all binaries. It is however notable that at very short periods the maximum eccentricity will be restricted due to the minimum possible stellar separation being applied, particularly in the case of a main sequence secondary star which can be expected to have a larger radius than a white dwarf or neutron star.

Results for each period distribution

Full graphs for two runs, split by orbital period as in chapter 4, are shown here to demonstrate a typical result, and show the difference between the two period distributions used for the core-collapsed clusters.

As in chapter 4, it was necessary to use different bin widths for each orbital period band. To account for this in the final results, peak emission divided by bin width is plotted.

Figure 5.1 shows the results for NGC 7099, otherwise known as M 30, where the orbital period distribution is that given in Duquennoy & Mayor (1991). However NGC 7099 is a core collapsed cluster (SEDS Milky Way Globular Clusters, 2011) so has also been modelled using the period distribution of Sigurdsson & Phinney

(1995). This is shown in figure 5.2. NGC7099 is modelled as containing 10379 binaries, as shown in table 5.2.

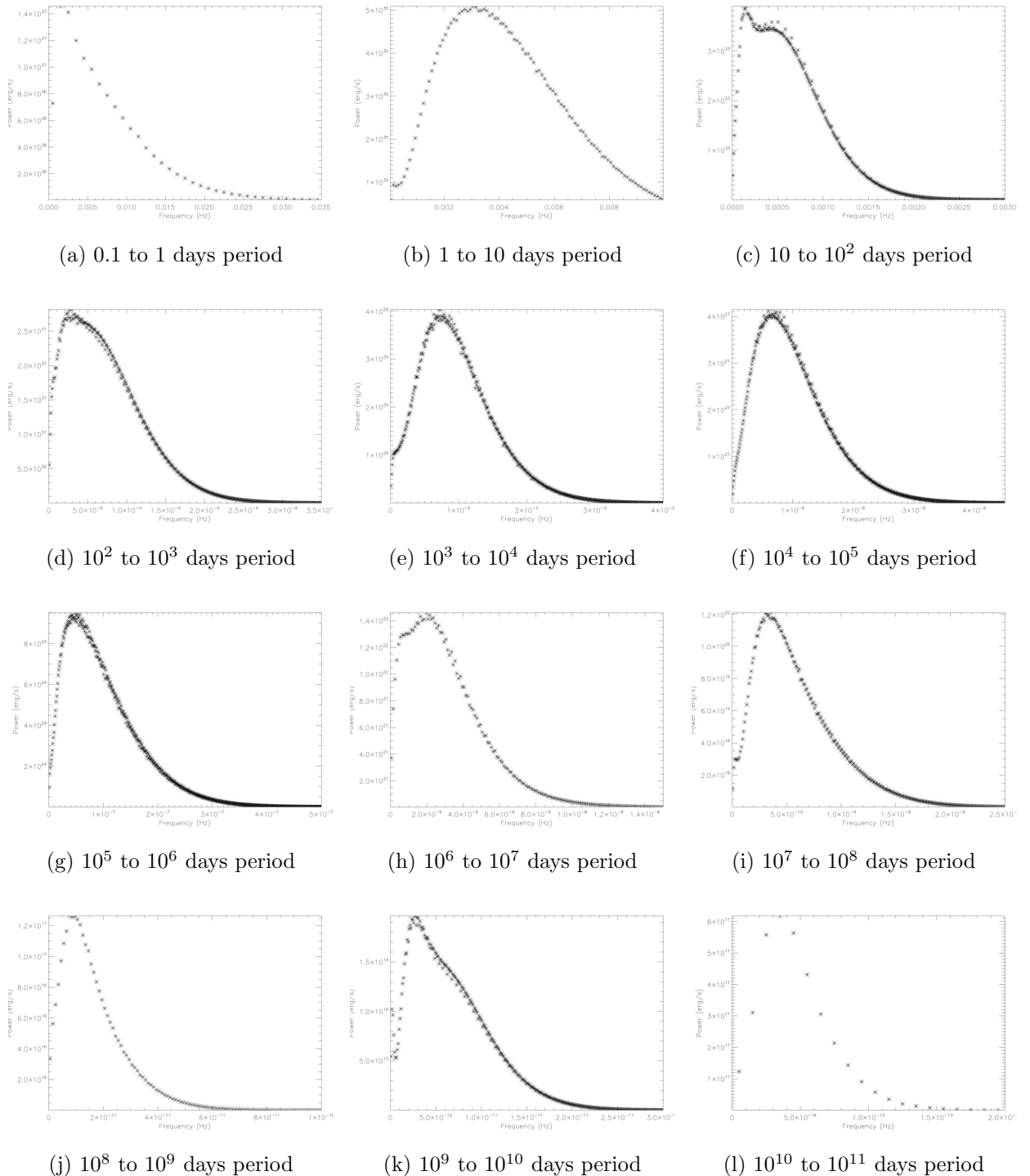


Figure 5.1: Results for NGC 7099 using the period distribution of Duquennoy & Mayor (1991)

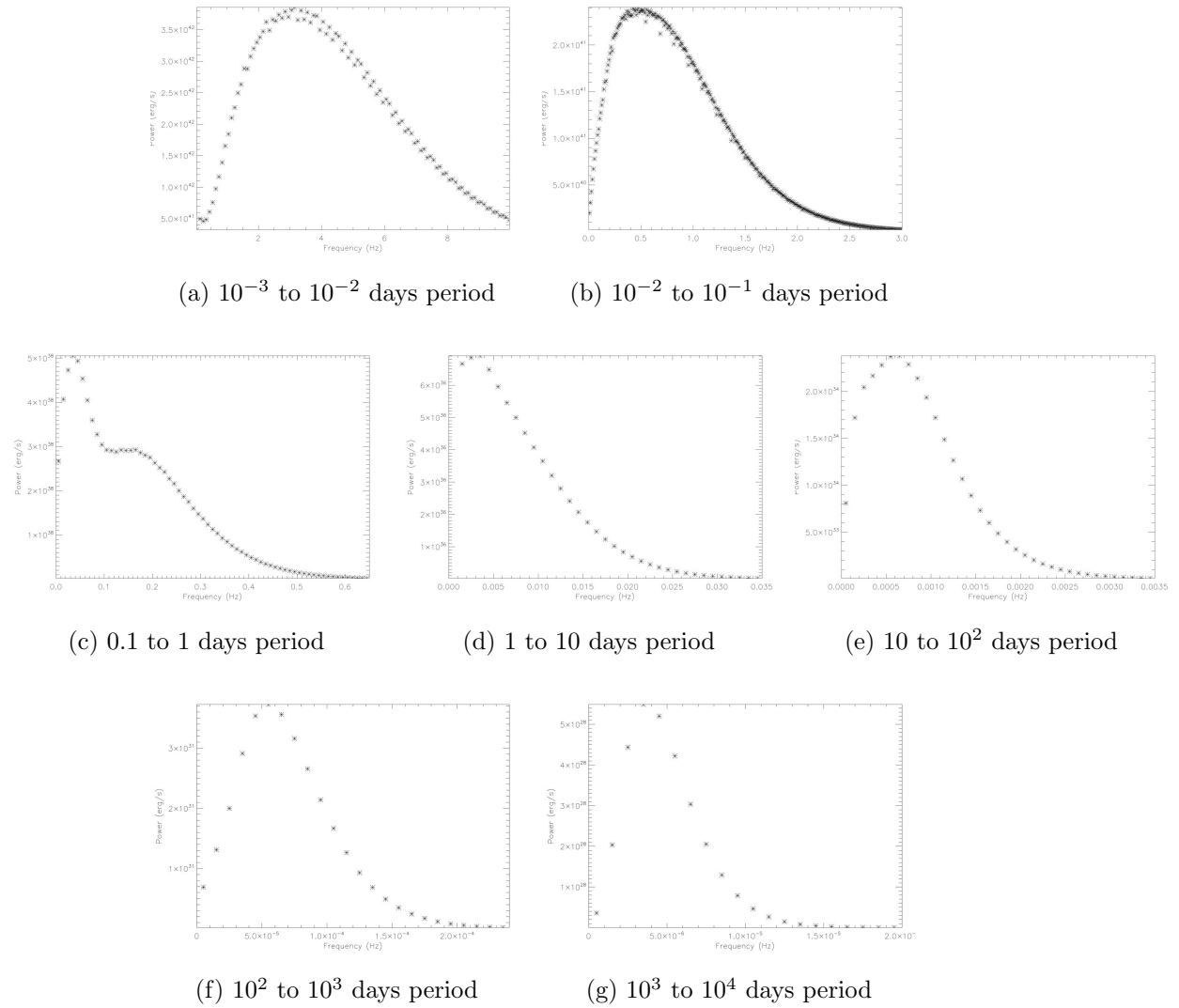


Figure 5.2: Results for NGC 7099 using the period distribution of Sigurdsson & Phinney (1995) for a core collapsed cluster

Despite the greater number of systems in longer orbital period bands, the peak emission always occurs in the shortest orbital period band, as can be seen in the examples presented above. Over all the results, the peak in the shortest period band is one or more orders of magnitude greater than the next period band (which is the next highest peak) once the difference in bin widths have been accounted for. Thus it is clear that the gravitational wave emission is always dominated by the shortest period systems.

It is worth remembering that the orbital period, mass ratio and eccentricity of each binary system is drawn randomly from the given distribution for each. Therefore it is possible that sometimes particularly extreme systems will be generated, within the bounds of the given distributions. This can lead to the double peak features seen in some of the above graphics. The dramatic effect of high eccentricity, and of short orbital period, on the gravitational wave signal from a binary system is shown in the results for individual binary systems presented in chapter 3.

Some clusters would be expected to contain binaries at the extreme limits of the distributions, but without direct measurement of the orbital parameters of all the binaries in each cluster, we cannot say which or at what orbital periods these exist. Therefore, while the results for any given cluster cannot be considered set, the aggregate results over all the clusters studied should provide a reasonable picture of the expected gravitational wave emission peaks from the stable binaries in galactic globular clusters.

Aggregate results

For the 119 clusters simulated, a plot of the peak power emitted in gravitational waves versus number of systems is shown in figure 5.3, where the core-collapse clusters are modelled with the period distribution of Duquennoy & Mayor (1991) as are the other clusters, and figure 5.4, where the core-collapse clusters are modelled with the period distribution of model 5 from Sigurdsson & Phinney (1995).

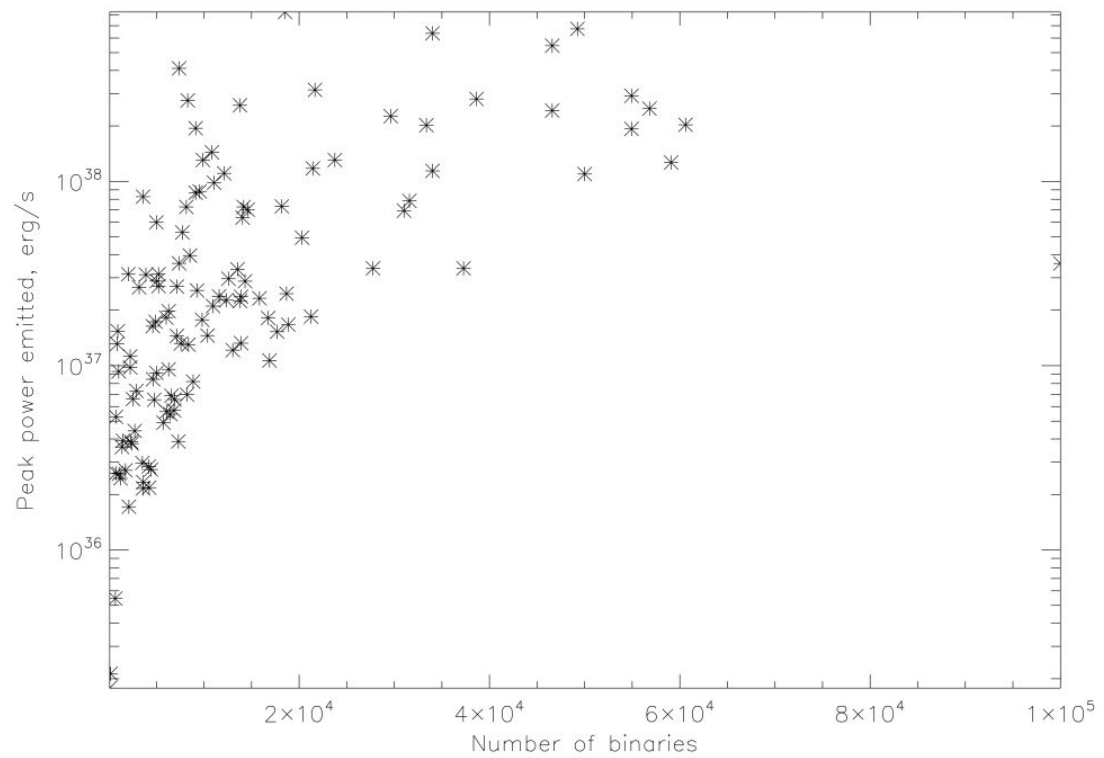


Figure 5.3: Variation of peak power with number of binaries in a cluster, all clusters take period distribution of Duquennoy & Mayor (1991)

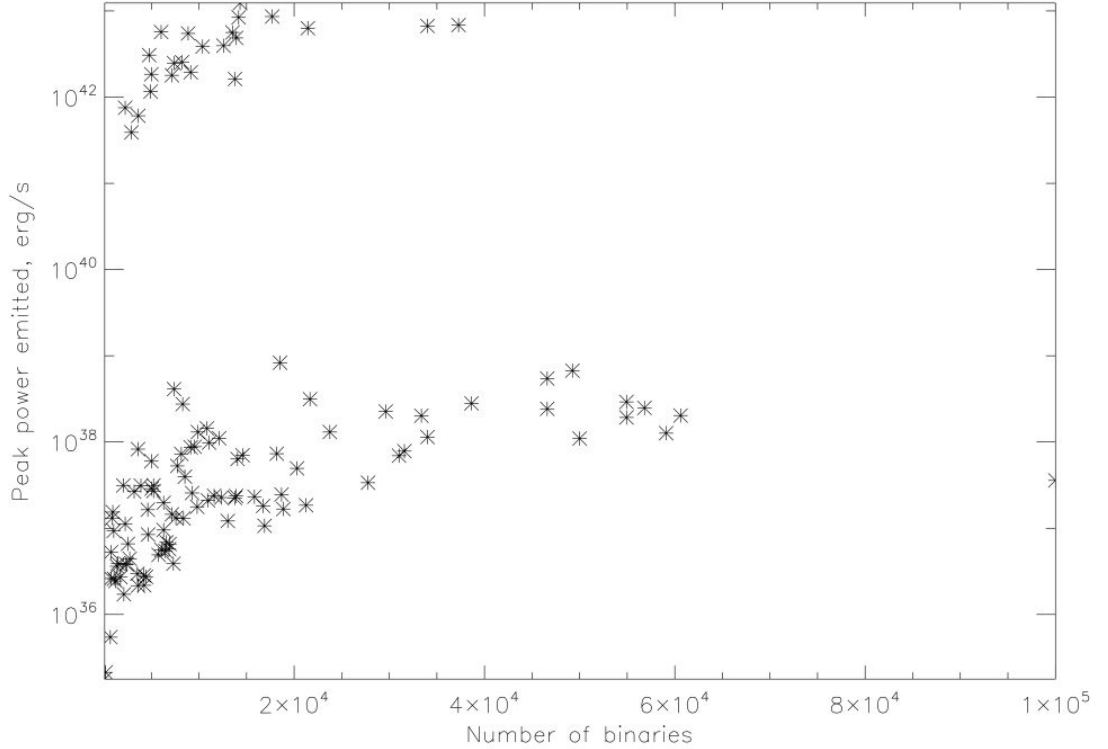


Figure 5.4: Variation of peak power with number of binaries in a cluster, core collapsed clusters take period distribution of Sigurdsson & Phinney (1995)

As for the runs shown above, the peak values used here are the output peak divided by the bin width. This ensures the two period distributions are directly comparable despite needing to be run with different bin widths due to the differing orbital period bands involved.

Despite the greater number of systems in longer orbital period bands, the peak emission always occurs in the shortest orbital period band, as can be seen in the examples presented above. Over all the results, the peak in the shortest period band is one or more orders of magnitude greater than the next period band (which is the next highest peak) once the difference in bin widths have been accounted for. Thus it is clear that the gravitational wave emission is always dominated by the shortest period systems.

There is, unsurprisingly, a correlation between number of binary systems modelled and peak power emission in gravitational waves. The greater the number of systems, the more binaries are contributing to that power output- and the greater the chance of a very eccentric system being generated, which would add a disproportionately large contribution to the output power.

The expected corellation between peak emission and the frequency at which that peak occurs is also seen, in figures 5.5 and 5.6.

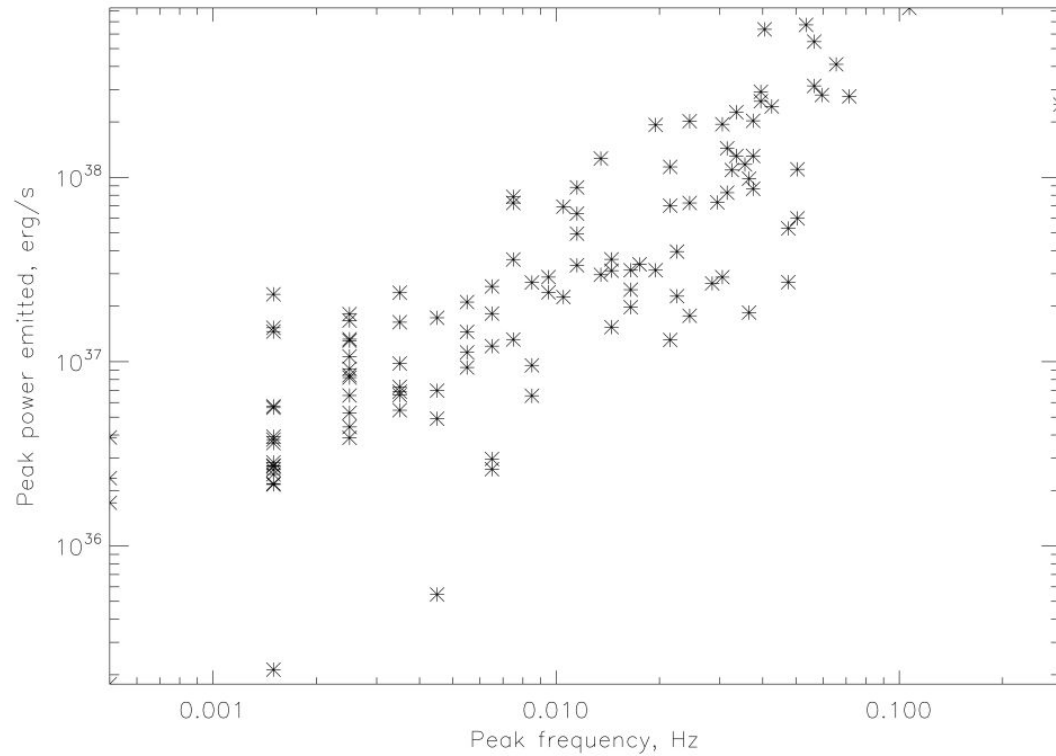


Figure 5.5: Variation of peak frequency with peak power, all clusters take period distribution of Duquennoy & Mayor (1991)

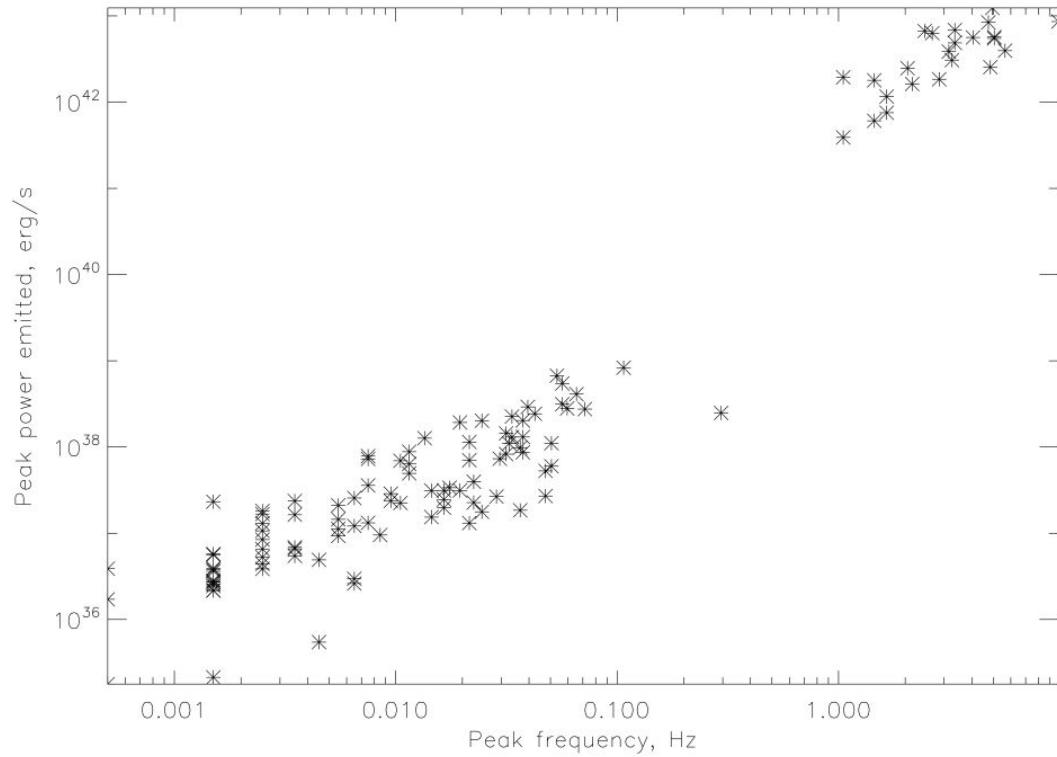


Figure 5.6: Variation of peak frequency with peak power, core collapsed clusters take period distribution of Sigurdsson & Phinney (1995)

The peaks all occur in the 10^{-4} to 10 Hz band, with most above 10^{-3} Hz, where the core collapse clusters have peaks in the 1 to 10 Hz band; or the 10^{-4} to 1 Hz band, with most between 10^{-3} and 10^{-1} , if the core collapsed clusters are modelled with the same period distribution as the non-collapsed clusters. This places the peak gravitational wave emission from globular cluster binaries largely in the LISA band. The core collapsed clusters, where modelled with the period distribution of Sigurdsson & Phinney (1995), fall between the LISA and Advanced LIGO bands. A LISA-like instrument may therefore detect the peak emission from the binaries in many, but not all of the clusters in the galaxy. For longer orbital period binaries the peaks occur at lower frequencies, so a LISA-like instrument would be expected to

detect some signal from all clusters, but would not be able to detect the peak emission from the collapsed clusters if the period distribution of Sigurdsson & Phinney (1995) is correct.

Since clusters can collapse and then rebound, and the hardening of binaries during collapse can be expected to occur gradually, it is of course likely that the real distributions fall someway between these examples. If many galactic globular clusters have collapsed and rebounded, it is possible that they might contain very tight binaries similar to those modelled for the core collapsed clusters, which would lead to higher peak emission at higher frequencies, as seen for the core collapsed clusters. This is further complicated by the possibility of multiple stellar populations, (Gratton et al, 2012), which implies that the stars may not all be of a similar age, and hence there may be binaries which have formed more recently rather than all evolving from an initial binary population combined with three body interactions.

5.4 Globular Cluster luminosity function and distance determination

The electromagnetic globular cluster luminosity function of a galaxy can be used to determine its distance. The gravitational wave luminosity function resulting from these simulations is compared to the electromagnetic and the possibility of using it for the same purpose is discussed.

5.4.1 Gravitational wave luminosity function

The peak gravitational wave emission from each cluster can be used to construct a luminosity function in gravitational radiation for the globular clusters in the Milky Way. This does not include transient sources such as mergers or three body interactions. Where all clusters are modelled using the period distribution of Duquennoy & Mayor (1991) the frequency range is 10^{-4} to 1 Hz, this luminosity function is

shown in figure 5.7 and the cumulative luminosity function in 5.9.

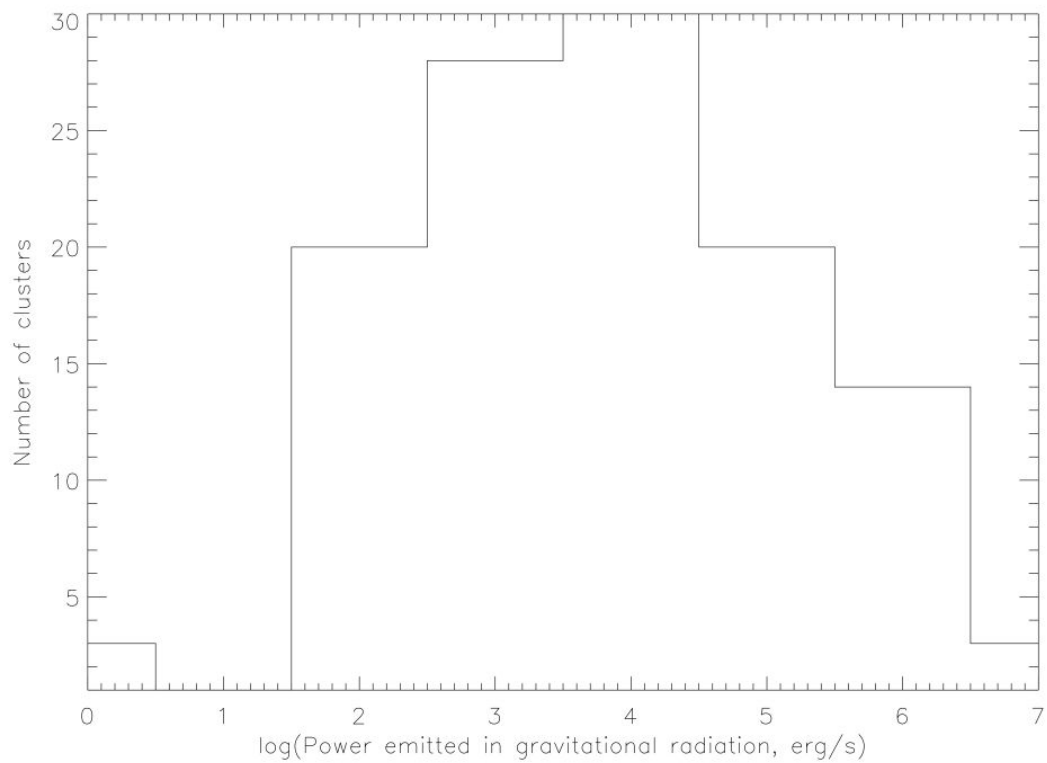


Figure 5.7: Luminosity function for peak gravitational wave emission of galactic globular clusters, all clusters take period distribution of Duquennoy & Mayor (1991)

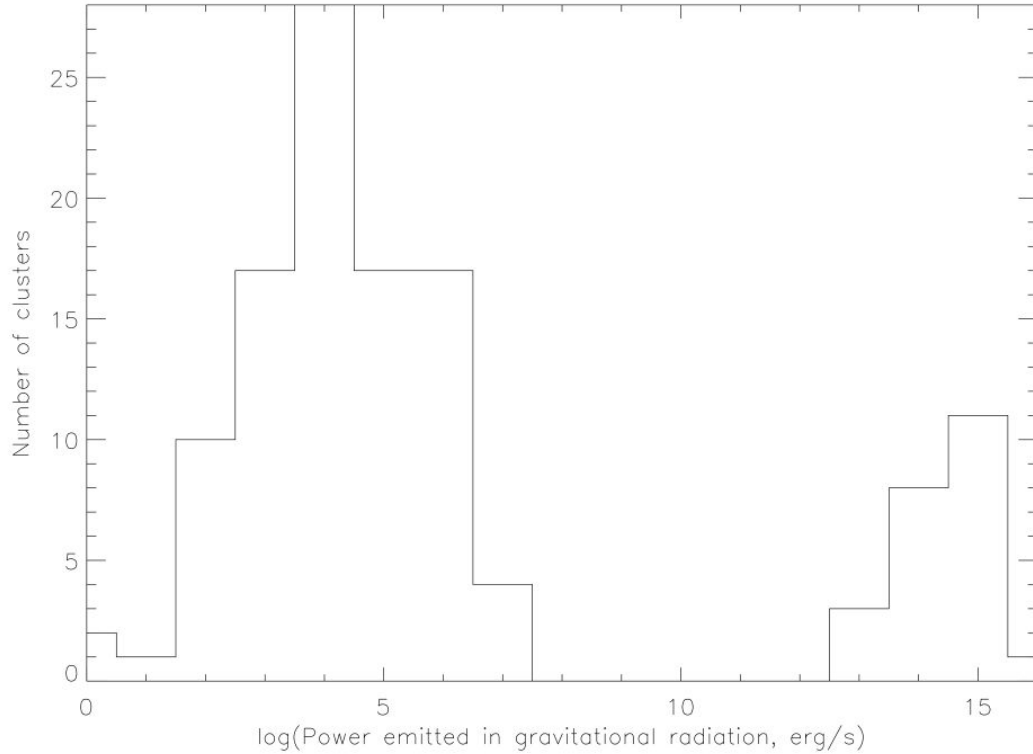


Figure 5.8: Luminosity function for peak gravitational wave emission of galactic globular clusters, core collapsed clusters take period distribution of Sigurdsson & Phinney (1995)

Where the core-collapsed clusters are modelled using the period distribution of Sigurdsson & Phinney (1995) and the others with that of Duquennoy & Mayor (1991), the frequency range is 10^{-4} to 10 Hz. This luminosity function, shown in figure 5.8, and the cumulative luminosity function in figure 5.10, clearly show two populations, the core collapsed clusters having much higher peaks due to the presence of shorter period binaries.

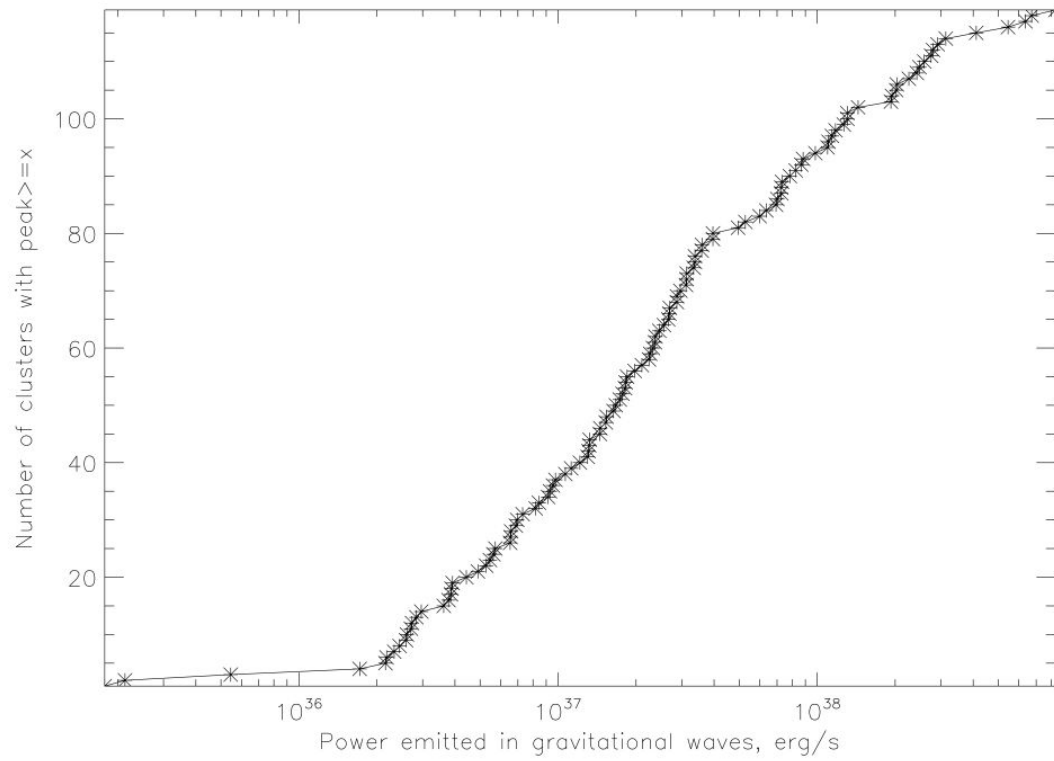


Figure 5.9: Cumulative luminosity function for peak gravitational wave emission of galactic globular clusters, all clusters take period distribution of Duquennoy & Mayor (1991)

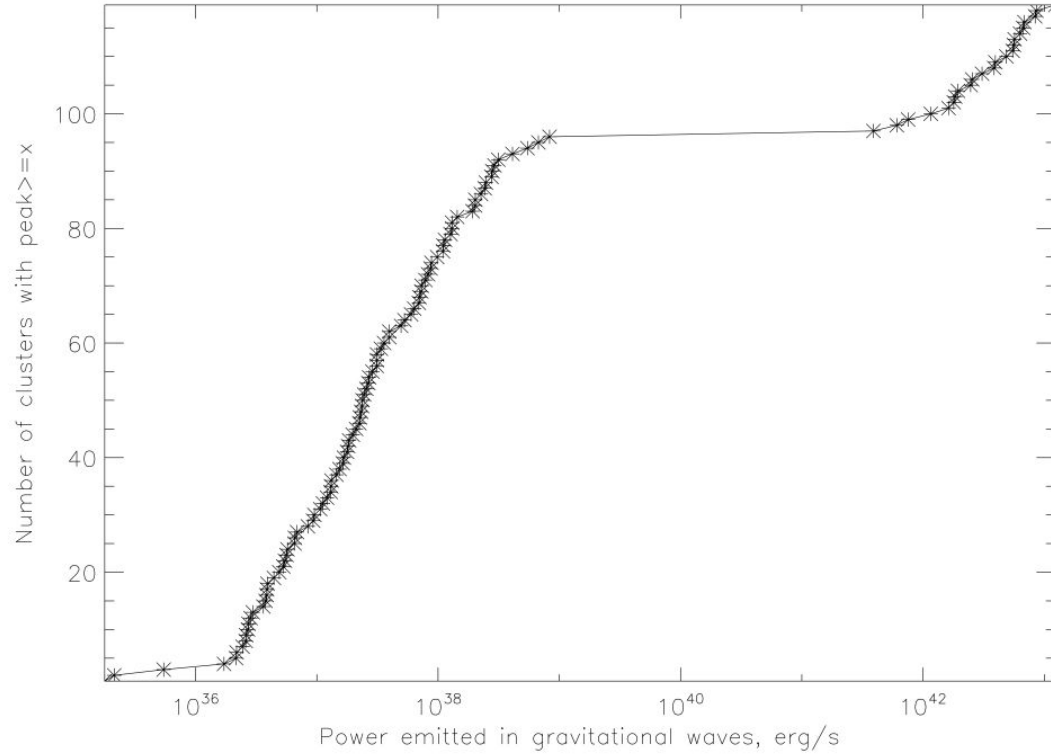


Figure 5.10: Cumulative luminosity function for peak gravitational wave emission of galactic globular clusters, core collapsed clusters take period distribution of Sigurdsson & Phinney (1995)

It is of course quite possible that rather than the extremes presented, where either all clusters have the same binary period distribution or there is a clear difference between core collapsed and non-collapsed clusters, there may be a more gradual spectrum of period distributions. Indeed, given that clusters can recover from core collapse, so some of the non-collapsed clusters may already have evolved to the point where most of the binaries have hardened significantly. A measurement of the gravitational wave emission from a globular cluster could allow the period distribution of the binary systems to be studied directly, and compared to the simulations.

5.4.2 Electromagnetic luminosity function

Figure 5.11, from Rejkuba (2012), shows the Milky Way globular cluster luminosity function, based on 129 clusters from Harris, 1996 (2010 edition). As mentioned there, the luminosity function normally used is actually a magnitude function. Being based on absolute magnitude, it is reasonable to compare this to the power emitted in gravitational waves, on a logarithmic scale.

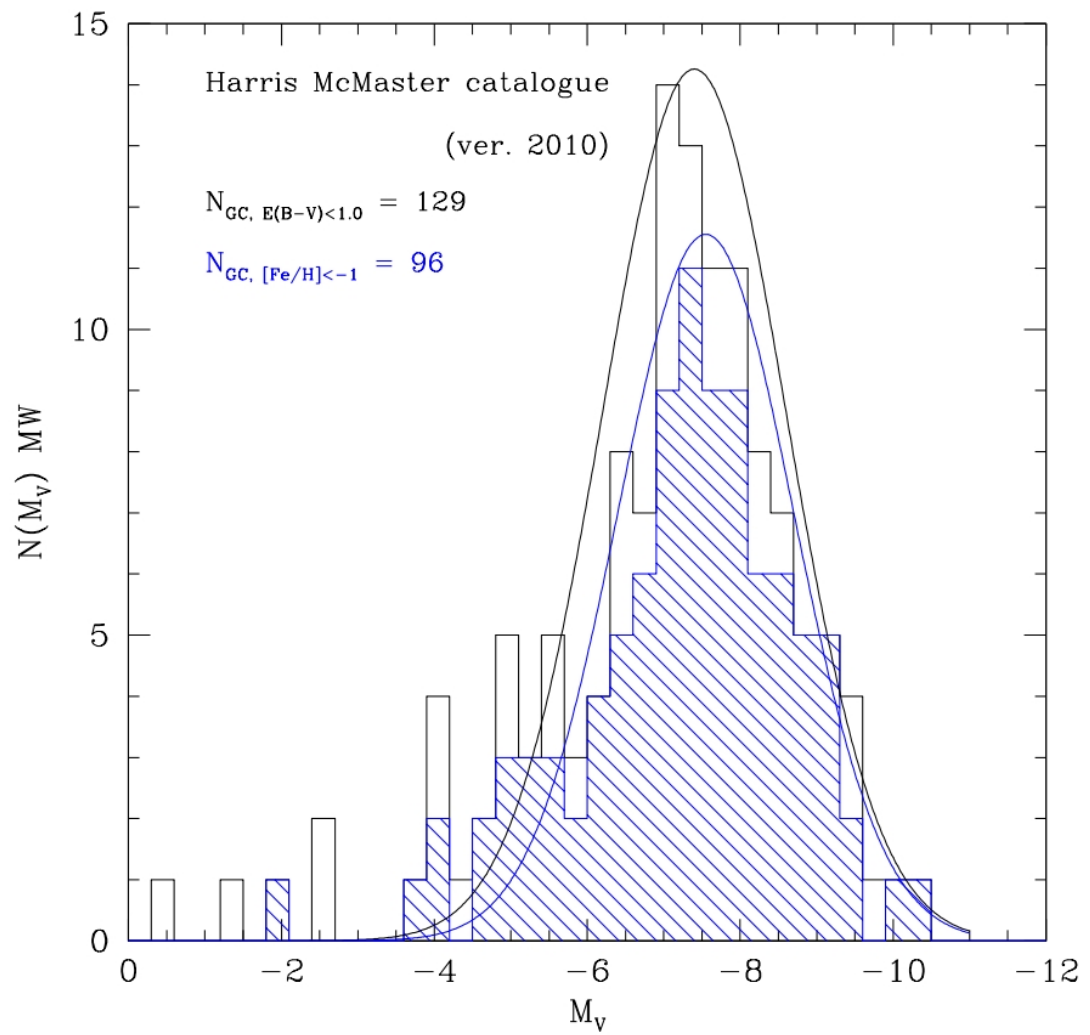


Figure 5.11: Electromagnetic luminosity function of Milky Way globular clusters, reproduced from Rejkuba (2012)

The luminosity function is fitted with a Gaussian, the parameters thereof being used to characterise the distribution. The peak, also referred to as the turnover, is a standard candle for measuring the distance to other galaxies. The peak of the globular cluster luminosity function for a galaxy is compared to that for the Milky Way or M31 and so the distance is estimated. This is of course contingent on the distance to the Milky Way or M31 clusters being known. Cepheid variables are used to estimate the distance to M31, and RR Lyrae stars for the clusters in the Milky Way. The peak is not considered to be exactly Gaussian, but the approximation is close enough to provide a good distance estimate. Other distributions which can be fitted can also be used. (Rejkuba, 2012).

For very distant galaxies, only the brightest clusters can be identified. Therefore this method only works for galaxies where the turnover point can be identified. The peak position is affected by the metallicity of the clusters, which must be taken into account Rejkuba (2012).

Rejkuba (2012) shows the cumulative globular cluster luminosity functions for the Milky Way, M31 and NGC5128 in two different spectral bands. This is included for comparison with the gravitational wave equivalent generated from the simulations. The shape of the graphs do not show any breaks for a separate population of core collapsed clusters, and hence it has more in common with figure 5.9 than figure 5.10. However, the luminosity of the electromagnetic emission from a cluster is not dependent on the period distribution of the binaries in the same way that gravitational wave emission is.

5.4.3 Distance determination with gravitational waves

Binary supermassive black holes are expected to be good standard sirens, usable for determining the distance to their host galaxies (Arun et al, 2008). However not all galaxies will contain these, so other methods of determining distance would of course be useful. A gravitational distance measurement, whatever the siren used,

could be used to constrain the redshift-distance relationship, where the host can be determined and a measurement of the redshift of the host is available. The redshift-distance relationship is given in equation 5.4, where D_L is the luminosity distance fromt the gravitational wave measurement, z the redshift, H_0 the Hubble constant and the matter energy density of the Universe is Ω_m with dark energy density Ω_d . (Arun et al, 2008)

$$D_L(z) = \frac{1+z}{H_0} \int_0^z \frac{dz'}{\sqrt{\Omega_m(1+z')^3 + \Omega_d}} \quad (5.4)$$

Therefore, a gravitational measurement of the distance to a galaxy of known redshift would provide a constraint on the dark energy density of the Universe.

For a year long observation of a monochromatic source, LISA was expected to have an angular resolution of 10^{-2} to 10^{-4} steradians (approximately 33 to 0.33 square degrees), with the resolution being better at higher gravitational wave frequencies. (Cutler, 1998; Benacquista, 1999) The core collapsed cluster NGC7099/M30 is at 26,100 light years distance, and has an angular diameter of 12 arcminutes (SEDS Milky Way Globular Clusters, 2011). The most massive globular cluster studied, Omega Centauri/NGC5139, is at 16,000 light years distance and has an angular diameter of 36.3 arcminutes (SEDS Milky Way Globular Clusters, 2011).

The work here looks at a total signal from all the binaries in a globular cluster, assuming they remain stable for the period of observation. Since these are numerous, in many cases individual signals may be difficult to distinguish. However extremely short period binaries, with period 500s or less, may evolve enough for a change in signal over a year's observation (Benacquista, 2000). If the host cluster can be identified, this signal may be used to measure the distance to the cluster.

It was expected that LISA should have been able to determine the angular position of a signal to within a globular cluster (Benacquista, 2000). It is clear that the more distant the galaxy, the greater the angular resolution needed to measure the peak signal from a globular cluster. If the culsters can be resolved it is possible

that the gravitational globular cluster luminosity function may be used to determine distance by comparison to that of the Milky Way, in analogy to the process used for the electromagnetic globular cluster luminosity function. Given the difficulty in resolving individual clusters however, barring extreme advances in gravitational wave detectors it seems this would be less useful as a standard siren for finding the distance to other galaxies than the electromagnetic version as a standard candle, except where the clusters are obscured. Comparing the two could lead to identification of obscured clusters. It should be noted, however, that if a measurement of the gravitational globular cluster luminosity function could be obtained, this would be independant of redshift as discussed above.

The overall signal from the galaxy will contain many other components, including field binaries, interactions between any central black hole and surrounding objects and any mergers that may be occurring at that time. The short period binaries expected to occur in globular clusters, particularly those which have undergone the process of core collapse, are a strong source of gravitational waves.

It seems possible, therefore, that the signal from the short period binaries in all the globular clusters, over a whole galaxy or even cluster of galaxies, summed up as done for individual clusters here, could be detectable. This also has the potential to be used as a standard siren. There is a correlation between cluster size and peak emission. If the number of globular clusters in a galaxy is known, from electromagnetic study, or can be estimated from the mass of the galaxy, the sizes of the individual clusters, and hence likely numbers of binaries in each may be estimated by comparison with the clusters in the Milky Way. Knowing the approximate number of short period binaries in all the globular clusters of a galaxy, a measurement of the peak gravitational wave emission from that galaxy could therefore lead to an estimation of the distance by comparison to the measured gravitational wave emission of globular clusters in the Milky Way, at known distances. This is a potential topic for future work.

5.5 Chapter summary

The gravitational wave emission from the binaries in a globular cluster is dominated by the shortest period binaries. The signal is expected to fall in the LISA waveband in most cases. There is a correlation between cluster size- i.e. number of binaries modelled- and peak frequency for any given set of model parameters, however where binaries at the extremes of the eccentricity or period distribution are generated they can make a significant difference to the signal.

A gravitational globular cluster luminosity function is generated, for two different models. One where all clusters have the same binary orbital period distribution, and another where the period distribution is very different, with much harder binaries, for core-collapsed clusters.

A measurement of the gravitational wave emission from a globular cluster, even where the signal from individual binaries cannot be resolved, could be used to investigate the binary period distribution, and other factors such as the mass ratio and eccentricity distributions. Studying these would provide insights into globular cluster evolution, particularly the process of core collapse, which involves hardening of binaries to slow and halt the collapse. It is possible that clusters which have collapsed and recovered might be identified by their gravitational wave emission, since the very short period binaries would remain, which would cause a much more powerful peak at higher frequency than a cluster containing only longer period binaries. The gravitational wave signal from the binaries could prove a useful tool to study globular cluster evolution.

Gravitational wave signals have the potential to act as standard sirens for distance determination, which, by studying the distance-redshift relationship, could lead to a constraint on the dark energy density of the Universe. However the difficulty in resolving gravitational wave sources suggests that using the gravitational globular cluster luminosity function for distance determination may be difficult, though it is possible that the total emission from hardened binaries in a galaxy

might be used.

Chapter 6

Conclusions

6.1 Motivation

While thus far only indirectly detected, gravitational waves have the potential to provide insight into many interesting areas of astronomy. This study into the gravitational wave emission from eccentric binaries and from globular clusters is intended not only to demonstrate some of the possible uses of gravitational wave astronomy, but also to provide theoretical predictions of the nature of the gravitational radiation from these systems, against which any future measurements may be checked. This is of course something which could validate- or not- existing theory, but perhaps more interestingly, where theory and measurement do not agree, it is possible that something new and interesting can be found.

Study of gravitational waves from binary systems could tell us a lot about their nature, both in constraining orbital parameters and in the potential insights into how such systems behave. Moreso for globular clusters, where the binary population plays a very important part in the cluster evolution.

6.2 Summary of the work

The main theme of this work gravitational wave emission from eccentric binary systems. I have studied both individual systems, calculating the gravitational wave emission from known eccentric binaries and constructing a luminosity function in gravitational waves for these; and globular clusters, containing many binaries with a range of different parameters, and considered the things we can learn from their gravitational radiation.

6.2.1 Eccentric binaries

Known binary systems with an eccentricity of greater than 0.2 were studied, including both x-ray binaries and radio pulsars in binary systems.

The systems studied demonstrate clearly the effects of orbital period, eccentricity and stellar masses on the gravitational wave output of a system. It can be seen that systems with shorter periods and higher eccentricities have relatively higher frequency peak gravitational wave emission, and so are more likely to be detectable by a LISA-like instrument.

Gravitational radiation could be used to study binaries in addition to the electromagnetic emission and may be particularly useful where the electromagnetic emission is obscured or difficult to separate from other sources. The direct link between the emission at each harmonic and the orbital parameters should help to characterise known binary systems as well as detecting unknown ones.

The gravitational luminosity function for the small sample of HMXBs studied is similar in shape to the x-ray luminosity function. However the overall gravitational luminosity function for the small sample of systems studied, including the radio pulsars in binary systems, shows a different shape. However the sample is not representative of the overall signal from the Galaxy. A measured gravitational luminosity function would in general provide insight into the overall population of binaries. It

has been suggested that field binaries may have their origin in star clusters- comparing the gravitational signal from field binaries and such clusters would allow this to be tested.

6.2.2 Globular clusters

Globular clusters contain some of the oldest stellar populations known. The binary population within a globular cluster is vital to its evolution. Binaries provide the energy that can stabilise a cluster as it collapses. Through three body interactions, the binaries lose energy to lone stars, which can then move more quickly, providing the thermal energy that stabilises the cluster. A cluster which has undergone core collapse, therefore, is expected to contain a population of very short period binaries, which would be expected to emit a strong signal in gravitational radiation.

The Milky Way contains a large number of globular clusters, of which 119 have mass estimates available. These were used to estimate the number of binaries in each globular cluster. A monte carlo simulation was then run for each, generating the orbital parameters of the binaries from statistical distributions. For clusters known to be core collapsed, two different orbital period distributions were used, one the same as that used for the other clusters, one intended to model the very hard binary population expected to be found in core collapsed clusters. These gave significantly different results, with the core collapse period distribution giving far more powerful peak gravitational wave emission at higher frequency than the results of the standard distribution. This fits with the expectations for a collection of shorter period binaries compared to longer period ones, when the mass ratio and eccentricity distributions are the same. There is a correlation between cluster size- i.e. number of binaries modelled- and peak frequency for any given set of model parameters, however where binaries at the extremes of the eccentricity or period distribution are generated they can make a significant difference to the signal. The peak emission occurs in the LISA sensitivity band for most of the globular clusters simulated. The

gravitational globular cluster luminosity function is generated for each of the two cases studied. It should however be noted that the standard distribution used may not be representative of the reality, nevertheless this provides an illustration of how the luminosities of the globular clusters may be derived.

A measurement of the gravitational wave emission from a globular cluster could tell us a great deal about the binary population. The gravitational wave signal could allow study of the binary period distribution, which could be compared to the theoretical models, and other factors such as the mass ratio and eccentricity distributions. This could provide great insights into the evolution of globular clusters, any particularly the process of core collapse.

It is possible that clusters which have collapsed and recovered might be identified by their gravitational wave emission, since at least some of the hardened binaries would remain, while some would merge. These short period binaries would cause a much more powerful peak at higher frequency than a cluster containing only longer period binaries. The gravitational wave signal from the binaries could prove a useful tool to study globular cluster evolution.

6.2.3 Distance measurement

Gravitational wave signals have the potential to act as standard sirens for distance determination, which, by studying the distance-redshift relationship, could lead to a constraint on the dark energy density of the Universe. If the gravitational globular cluster luminosity function for a distant galaxy could be measured, using gravitation rather than electromagnetism, it would be entirely independent of the redshift measurement of the host galaxy.

However the difficulty in resolving gravitational wave sources suggests that using the gravitational globular cluster luminosity function for distance determination may be difficult, as it would be necessary to measure the signal from each globular cluster in the distant galaxy- or at least a good sample of them. Given the likely angular

resolution of a LISA-like instrument, this may not be possible. The possibility of using the total signal from all the short period binaries in a distant galaxy, likely to occur mostly in globular clusters due to the core collapse process, is however worth investigating and could be an extension of this work.

6.3 Closing remarks

This thesis starts with a characterisation of the emission of gravitational waves from eccentric binary systems and applies it to both individual systems and globular clusters, ending with a discussion of the insights we may gain if- hopefully when- it becomes possible to directly measure such gravitational waves.

Calculations of the gravitational wave emission for 34 individual binary systems are presented, as are the results of monte carlo simulations of 119 globular clusters. The strong influence of eccentricity and orbital period on the gravitational wave signal from a binary system is clear throughout.

The possibility of using gravitational waves to characterise binary systems is potentially useful, even more so the chance to study globular clusters. Binaries play a huge role in the evolution of a globular cluster, studying their gravitational radiation could provide a lot of insight into this, especially the process of core collapse.

The possibility of using the gravitational globular cluster luminosity function as a standard siren is discussed. It seems likely that resolving the signal from individual globular clusters in a distant galaxy might be beyond any currently planned instruments. Of course the possibility of this improving at some point in the future cannot be ruled out, unlikely as it might seem at the moment, technology can improve in unexpected ways.

The calculations here may one day be compared to measured gravitational wave signals. This could support or disprove current theory- or reveal something entirely unexpected. Any detection of gravitational radiation would be a hugely exciting

event. Gravitational wave astronomy has huge potential and I await future discoveries with interest.

Acknowledgements

There are many people I need to thank for their help. Firstly, my family and friends, for putting up with my insane wish to do a PhD, and providing tea and sympathy on regular occasions! A special thankyou to everyone who has bought me a whisky or supplied chocolate. I have to mention my Dad in particular, who has been very supportive and always gives good advice. And Mum, who listens to me complain and always wants to help. My brother, Adam, seems to manage his PhD in a far calmer fashion- I wish him luck with his thesis and no penalty for all the equipment he broke.

In no particular order, Dave Vande Putte, Mark Cropper, Neil Cornish, Lisa Hill and Andrew Wray have all taken time to give me advice and talk over things, so thankyou very much. Curtis Saxton has also been very helpful, and Graziella Branduardi-Raymont, my secondary supervisor, whose support and suggestions I greatly appreciate. I must of course thank my primary supervisor, Kinwah Wu.

Thankyou to Alan Brown and Paul Lamb for chats, programming advice, tolerance and magically creating computing resources out of thin air when I needed them most. And thankyou to Richard Moore for an early morning dash with piles of paper!

Finally, I would like to acknowledge the funding I received for four years of my PhD from the Science and Technology Facilities Council (STFC).

Appendix

Gravitational wave speed

Gravitational waves can be modelled as a perturbation $h_{\alpha\beta}$ to the flat spacetime metric $\eta_{\alpha\beta}$

$$ds^2 = (\eta_{\alpha\beta} + h_{\alpha\beta}) dx^\alpha dx^\beta \quad (6.1)$$

Where $||h_{\alpha\beta}|| << 1$

The perturbation is related to the stress-energy tensor $T_{\alpha\beta}$

$$\left(-\frac{\partial^2}{\partial t^2} + \frac{\partial^2}{\partial x^2} + \frac{\partial^2}{\partial y^2} + \frac{\partial^2}{\partial z^2} \right) \mathbf{h}_{\alpha\beta} = -16\pi T_{\alpha\beta} \quad (6.2)$$

$$\mathbf{h}_{\alpha\beta} = h_{\alpha\beta} - \frac{1}{2} \eta_{\alpha\beta} h_\delta^\delta \quad (6.3)$$

In a vacuum, $T_{\alpha\beta} = 0$

$$\left(-\frac{\partial^2}{\partial t^2} + \frac{\partial^2}{\partial x^2} + \frac{\partial^2}{\partial y^2} + \frac{\partial^2}{\partial z^2} \right) \mathbf{h}_{\alpha\beta} = 0 \quad (6.4)$$

$\mathbf{h}_{\alpha\beta}$ is a wave

$$\mathbf{h}_{\alpha\beta} = A_{\alpha\beta} e^{-i(\omega t - \mathbf{k} \cdot \mathbf{x})} \quad (6.5)$$

Take partial derivatives

$$\frac{\partial^2}{\partial t^2} \mathbf{h}_{\alpha\beta} = -\omega^2 \mathbf{h}_{\alpha\beta} \quad (6.6)$$

$$\frac{\partial^2}{\partial x^2} \mathbf{h}_{\alpha\beta} = k_x^2 \mathbf{h}_{\alpha\beta} \quad (6.7)$$

$$\frac{\partial^2}{\partial y^2} \mathbf{h}_{\alpha\beta} = k_y^2 \mathbf{h}_{\alpha\beta} \quad (6.8)$$

$$\frac{\partial^2}{\partial z^2} \mathbf{h}_{\alpha\beta} = k_z^2 \mathbf{h}_{\alpha\beta} \quad (6.9)$$

$$(\omega^2 - k_x^2 - k_y^2 - k_z^2) \mathbf{h}_{\alpha\beta} = 0 \quad (6.10)$$

This gives the dispersion relation

$$\omega^2 = |\mathbf{k}|^2 \quad (6.11)$$

This is the same as the dispersion relation for electromagnetic waves, so it can be concluded that gravitational waves also travel at speed c.

Zero dipole component to gravitational radiation

For a charge dipole in electromagnetism

$$dipole = \sum_{\alpha} q_{\alpha} \mathbf{r}_{\alpha} \quad (6.12)$$

By analogy, replace q with m for gravitation

$$massdipole = \sum_{\alpha} m_{\alpha} \mathbf{r}_{\alpha} \quad (6.13)$$

m is constant

Take time derivatives

$$1st derivative = \sum_{\alpha} m_{\alpha} \dot{\mathbf{r}}_{\alpha} = \sum_{\alpha} m_{\alpha} \mathbf{v}_{\alpha} = \sum_{\alpha} \mathbf{p}_{\alpha} \quad (6.14)$$

$$2nd derivative = \sum_{\alpha} m_{\alpha} \ddot{\mathbf{r}}_{\alpha} = \sum_{\alpha} \dot{\mathbf{p}}_{\alpha} = 0 \quad (6.15)$$

So by conservation of momentum, the second derivative disappears and hence there is no dipole component to gravitational radiation.

Two polarisations of gravitational waves

The perturbation $h^{\alpha\beta}$ is written explicitly

$$h^{\alpha\beta} = \begin{bmatrix} 0 & 0 & 0 & 0 \\ 0 & h^{xx} & h^{xy} & h^{xz} \\ 0 & h^{yx} & h^{yy} & h^{yz} \\ 0 & h^{zx} & h^{zy} & h^{zz} \end{bmatrix} \quad (6.16)$$

Since the quadrupolar wave has only two degrees of freedom, use a transverse gauge. For a wave travelling in the z direction

$$h^{\alpha\beta} = \begin{bmatrix} 0 & 0 & 0 & 0 \\ 0 & h^{xx} & h^{xy} & 0 \\ 0 & h^{yx} & h^{yy} & 0 \\ 0 & 0 & 0 & 0 \end{bmatrix} \quad (6.17)$$

The matrix should be traceless and symmetric

$$h^{xx} + h^{yy} + h^{zz} = 0 \quad (6.18)$$

$$h_{\alpha\beta}^T = h_{\alpha\beta} \quad (6.19)$$

Set $h^{xx} = -h^{yy} = h_+$ and $h^{xy} = h^{yx} = h_{\times}$

$$h^{\alpha\beta} = \begin{bmatrix} 0 & 0 & 0 & 0 \\ 0 & h_+ & h_\times & 0 \\ 0 & h_\times & -h_+ & 0 \\ 0 & 0 & 0 & 0 \end{bmatrix} \quad (6.20)$$

So we have two polarisations, h_+ and h_\times .

Dimensional analysis for gravitational wave flux

We have, in $c=G=1$ units, from Moreno-Garrido et al (1995)

$$F_n = \frac{\pi}{8} n^2 \frac{1}{T^2} (|h_+|^2 + |h_\times|^2) \quad (6.21)$$

F_n is a flux, having units of ergs per second per cm^2 , so dimension of $\frac{\text{energy}}{\text{timedistance}^2}$.
 $|h_+|$ and $|h_\times|$ have dimensions as h_0 (2.13, of $\frac{\text{mass}^2}{\text{distance}^2}$).

T is the orbital period, having dimension *time*.

The purpose of this analysis is to convert from $c=G=1$ units back to cgs units, which will involve multiplying by an unknown number of factors of c and G .

c has dimension $\frac{\text{distance}}{\text{time}}$ and G has dimension $\frac{\text{distance}^3}{\text{masstime}^2}$

First convert the units of F_n to the standard *mass, distance, time*

$$\text{energy} = \frac{\text{massdistance}^2}{\text{time}^2} \quad (6.22)$$

Use this to set up the dimensional analysis

$$\frac{\text{massdistance}^2}{\text{time}^2} \frac{1}{\text{time}} \frac{1}{\text{distance}^2} = \frac{1}{\text{time}^2} \left(\frac{\text{mass}^2}{\text{distance}^2} \right)^2 G^\alpha c^\beta \quad (6.23)$$

$$\frac{\text{mass}}{\text{time}^3} = \frac{\text{mass}^4}{\text{time}^2 \text{distance}^4} \left(\frac{\text{distance}^3}{\text{masstime}^2} \right)^\alpha \left(\frac{\text{distance}}{\text{time}} \right)^\beta \quad (6.24)$$

$$\frac{\text{distance}^4}{\text{mass}^3 \text{time}} = \frac{\text{distance}^{3\alpha+\beta}}{\text{mass}^\alpha \text{time}^{2\alpha+\beta}} \quad (6.25)$$

Looking at *mass*, we see $\alpha = 3$.

distance and *time* both show that $\beta = -5$.

So to convert from $c=G=1$ units to cgs units, equation 6.21 must be multiplied by a factor of $\frac{G^3}{c^5}$

Meaning that, in cgs units, the flux of gravitational waves seen by the observer at R , for harmonic number n is

$$F_n = \frac{G^3}{c^5} \frac{\pi}{8} n^2 \frac{1}{T^2} (|h_+|^2 + |h_\times|^2) \quad (6.26)$$

Detailed data on HMXBs

Results for 2S 1845-024, GRO J1800-57, XTE J0421+560 and 1A 0535+262 are shown in Chapter 3. The remainder of the HMXBs studied are detailed below.

4U 1223-624

Eccentricity 0.46 (Liu et al, 2006), period 41.59 days (Liu et al, 2006). Estimated to have a supergiant star mass of $30 \pm 5 M_\odot$ (Parkes et al, 1980) and radius of $43 R_\odot$ (Parkes et al, 1980), the compact object is a pulsar (Parkes et al, 1980) and hence assumed to be a $1.4 M_\odot$ neutron star.

2S 1417-624

Eccentricity 0.45 (Finger et al, 1996), period 42.12 days (Finger et al, 1996) or 42.19 ± 0.01 days (Inam et al, 2004). Lower limit on optical star mass $5.9 M_\odot$ (Finger et al, 1996), the compact object is assumed to be a canonical $1.4 M_\odot$ neutron star. The optical star is of type B1 Ve (Liu et al, 2006), the maximum mass of a B type main sequence (V) star is about $16 M_\odot$ (Habets et al, 1981).

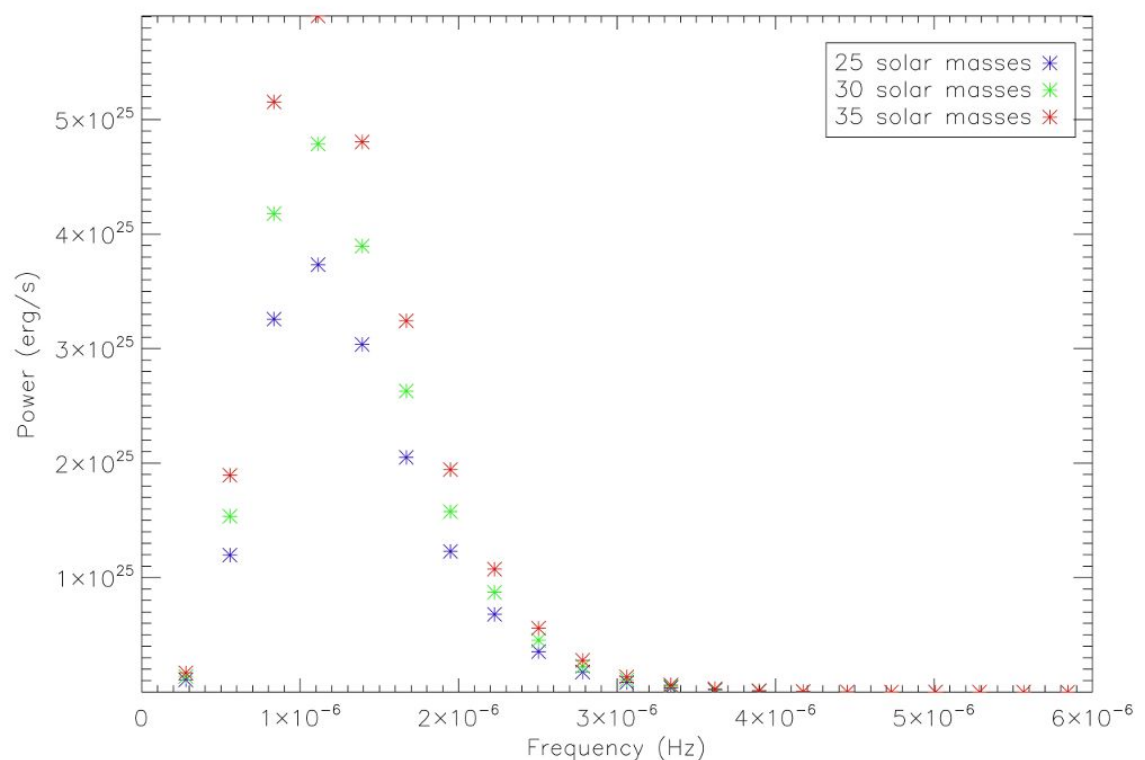


Figure 6.1: Calculated gravitational wave emission for 4U 1223-624

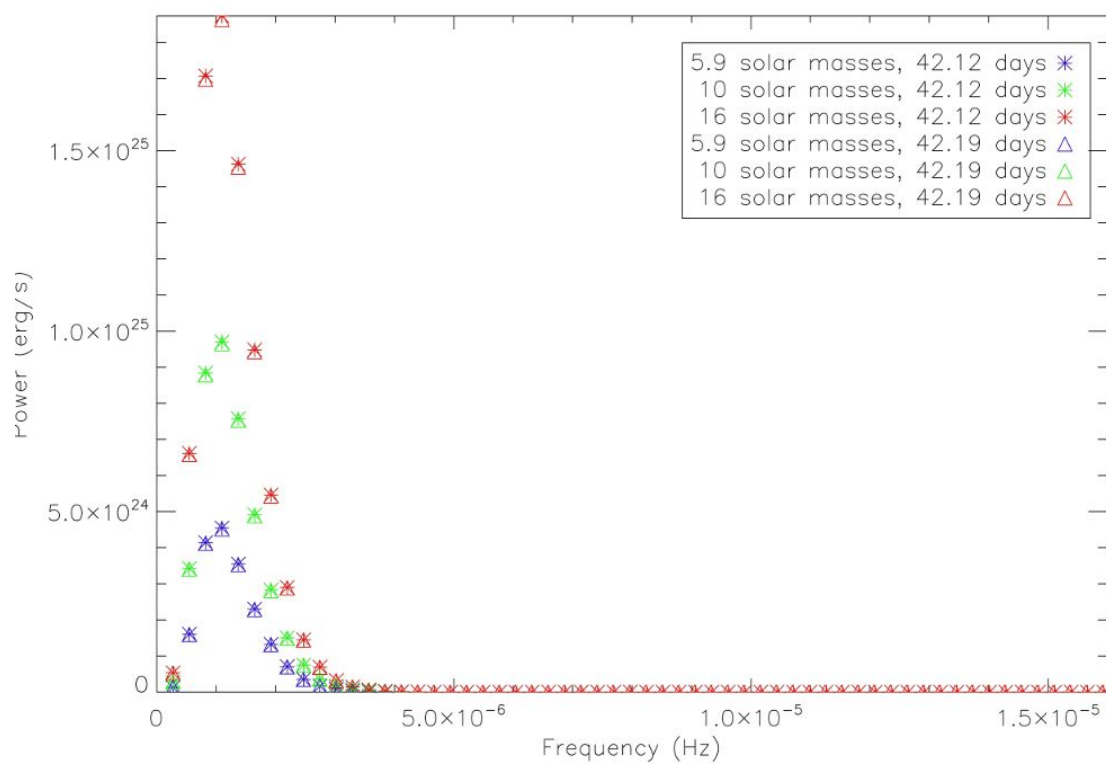


Figure 6.2: Calculated gravitational wave emission for 2S 1417-624

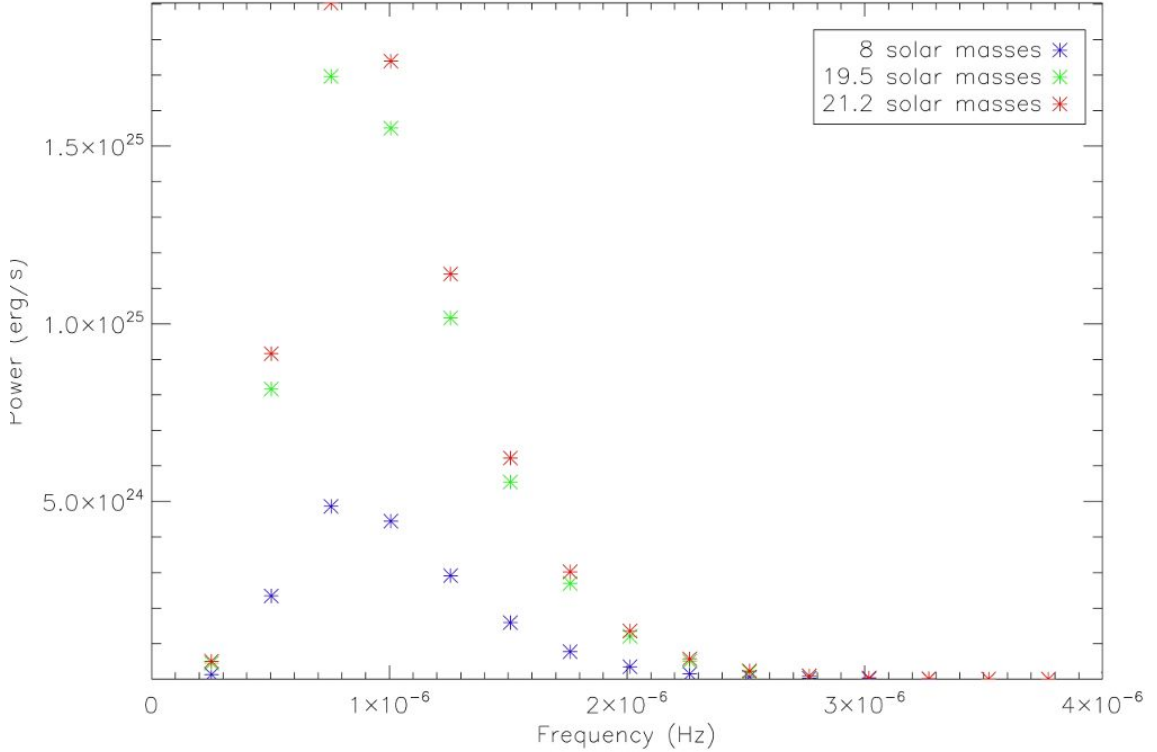


Figure 6.3: Calculated gravitational wave emission for EXO 2030+375

EXO 2030+375

Eccentricity 0.41 (Liu et al, 2006), period 46.02 (Liu et al, 2006). Mass of larger star estimated as $8M_{\odot}$ (Coe et al, 1988), or using the tables of Vacca et al (2000), estimate by spectral type (B0 Ve, (Liu et al, 2006)) is $19.5\text{-}21.2M_{\odot}$ with a radius of $8.3R_{\odot}$. The compact object is assumed to be a $1.4M_{\odot}$ neutron star.

1A 0535-668

Eccentricity >0.4 (Liu et al, 2005), period 16.7 days (Liu et al, 2005). The optical star is spectral type B0.5 IIIe, so by the tables of Vacca et al (2000), the mass is estimated as $21.5\text{-}25.1M_{\odot}$ with a radius of $14.8R_{\odot}$. The compact object is assumed to be a $1.4M_{\odot}$ neutron star. This HMXB is located in the LMC so is not included

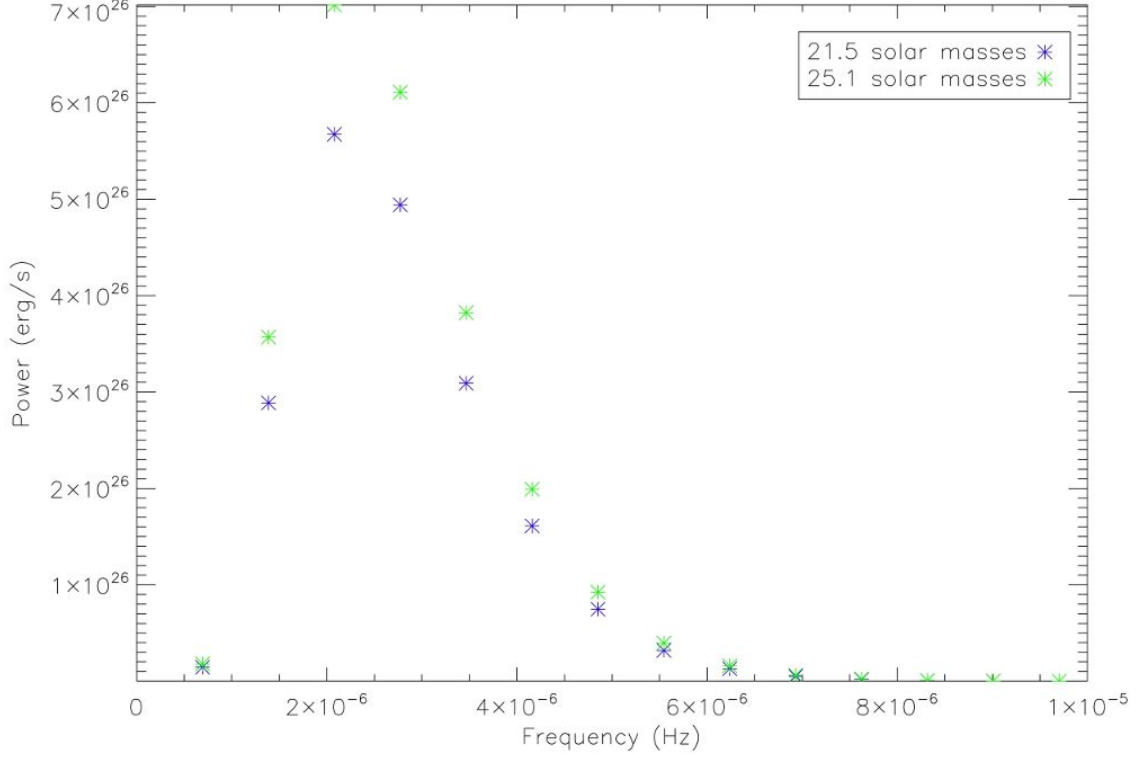


Figure 6.4: Calculated gravitational wave emission for 1A 0535-668

in aggregate data for HMXBs in our Galaxy.

Taking eccentricity as 0.4, since this is the minimum.

SAX J2103.5+4545

Eccentricity 0.4 ± 0.2 (Liu et al, 2006), period 12.68 days (Liu et al, 2006). The optical star is type B0 Ve which gives it a mass range of $19.5\text{--}21.2M_{\odot}$ with a radius of $8.3R_{\odot}$ according to Vacca et al (2000). Baykal et al (2000) suggests a mass of $7M_{\odot}$ if the system is at an inclination of 45 degrees. The compact object is a pulsar (Baykal et al, 2000) so considered to be a $1.4M_{\odot}$ neutron star.

Distance 6.5kpc (Liu et al, 2006), inclination angle of 45 degrees used in Baykal et al (2000).

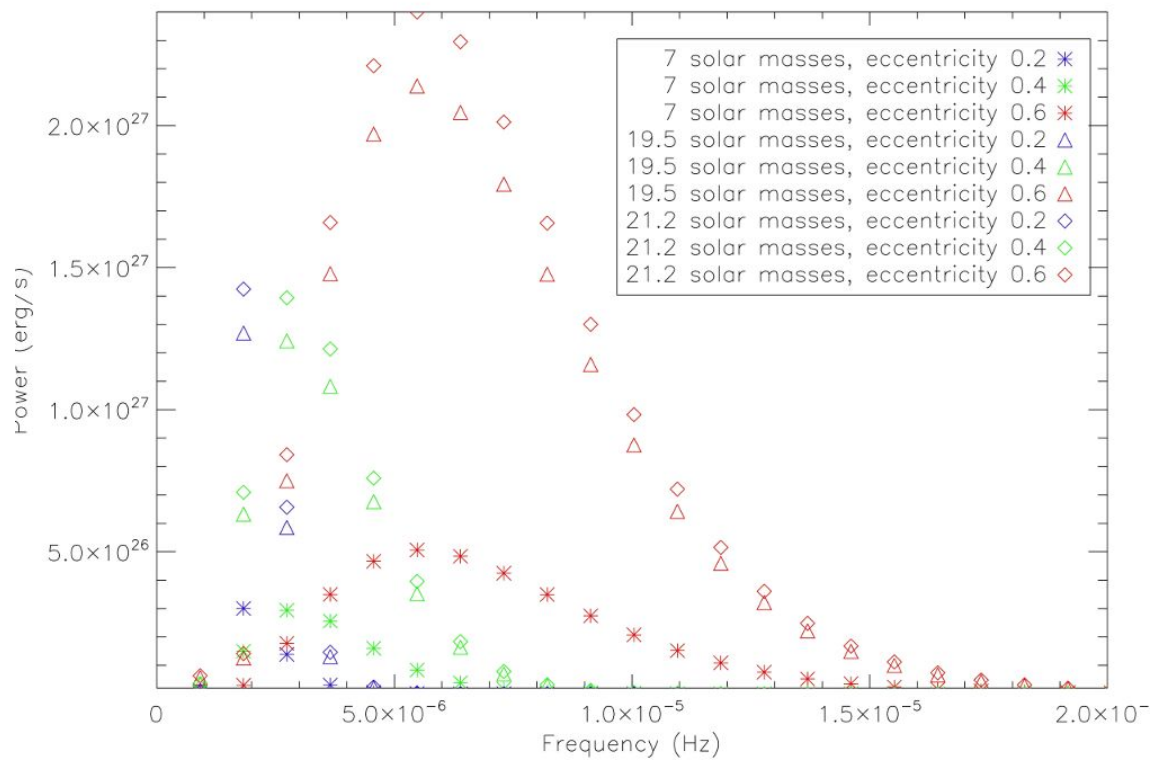


Figure 6.5: Calculated gravitational wave emission for SAX J2103.5+4545

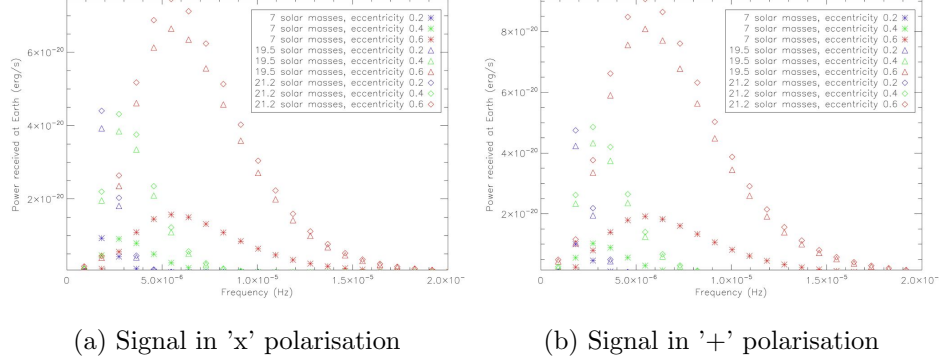


Figure 6.6: Calculated gravitational wave signal at Earth from SAXJ2103.5+4545

V 0332+53

Eccentricity 0.37 (Liu et al, 2006), period 34.25 days (Liu et al, 2006). The optical star is of type O8.5 Ve (Liu et al, 2006) which gives it a mass range of $23.6\text{--}28.0M_{\odot}$ and a radius of $9R_{\odot}$ according to Vacca et al (2000). The method of Weidner & Vink (2010) gives an estimate of $15.8\text{--}25.1M_{\odot}$. Zhang et al (2005) suggests the system consists of a $1.4M_{\odot}$ neutron star and a $\geq 20M_{\odot}$ star which fits with both of these possibilities.

GRO J1750-27

Eccentricity 0.36 (Liu et al, 2006), period 29.8 days (Liu et al, 2006). Very little data available for this, only that it is a Be X-ray binary (Liu et al, 2006). So I assume a $1.4M_{\odot}$ neutron star with an optical star that could be anywhere within the normal B spectral class mass range of $4\text{--}20M_{\odot}$.

RX J1826.2-1450

Also known as microquasar LS5039. Eccentricity is listed in the catalogue as 0.35 (Liu et al, 2006), which is also the value given in (Hoffmann et al, 2009), as 0.35 ± 0.04 . But Sarty et al (2010) suggests it could be 0.24 ± 0.08 . Period 3.9

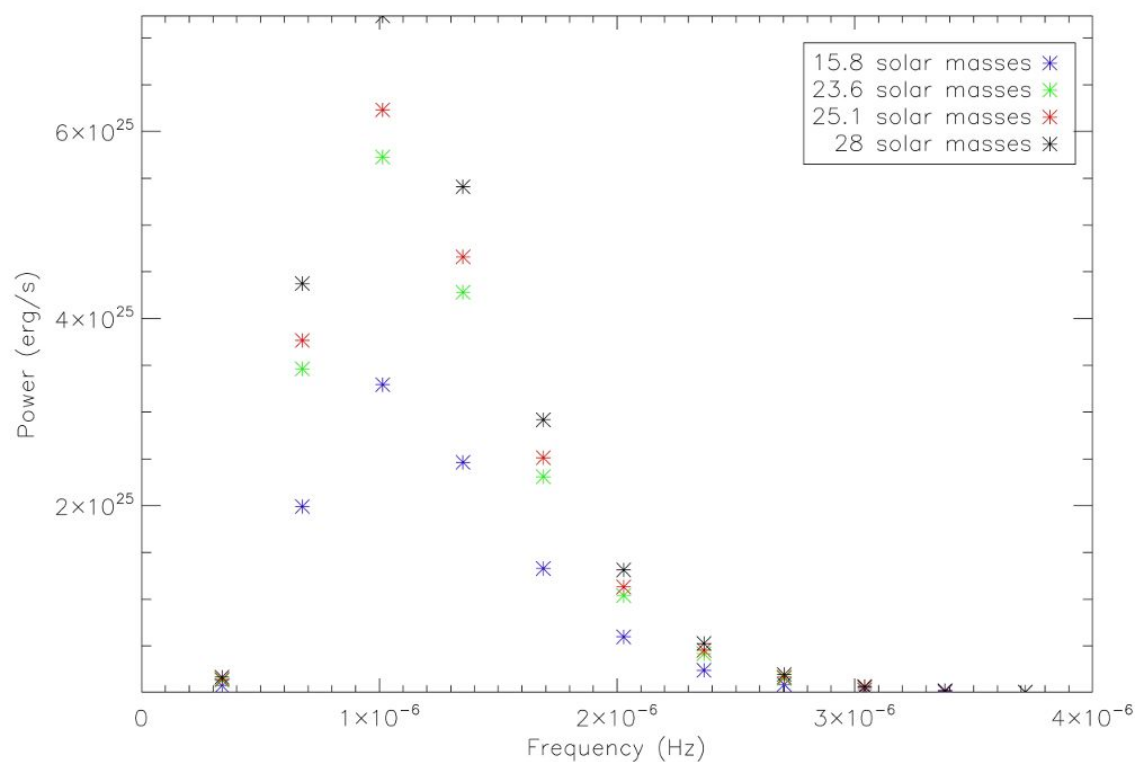


Figure 6.7: Calculated gravitational wave emission for V 0332+53

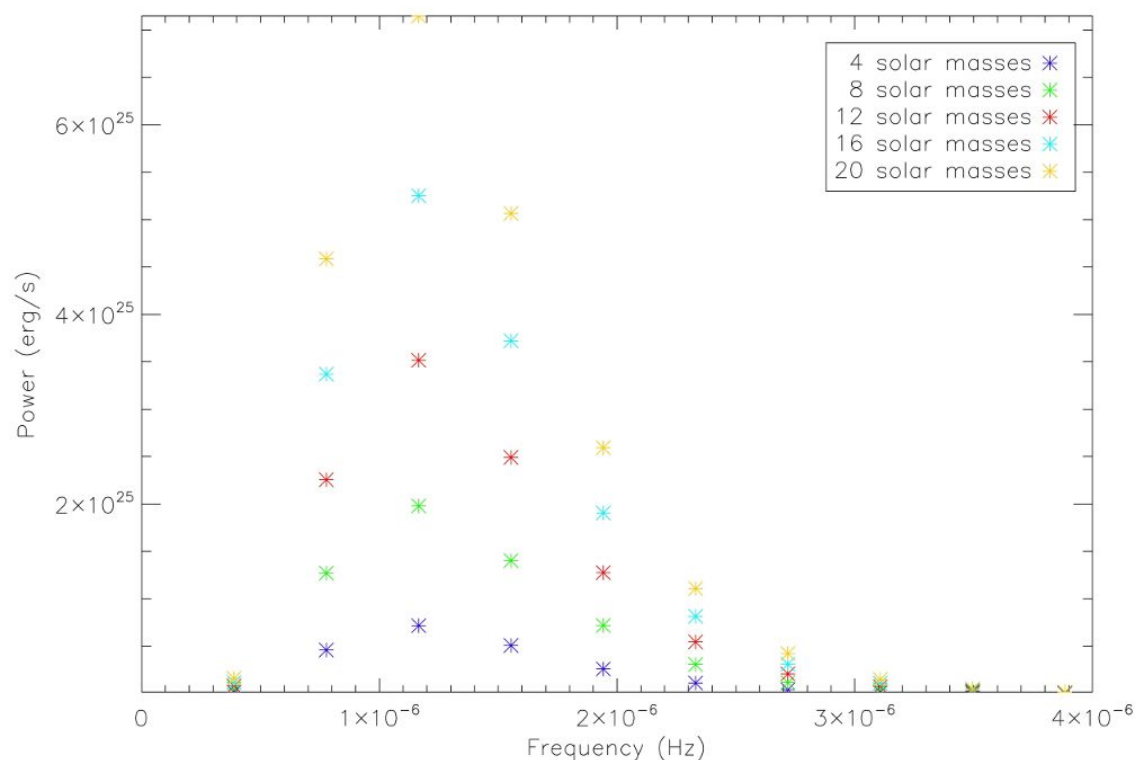


Figure 6.8: Calculated gravitational wave emission for GRO J1750-27

days (Liu et al, 2006), which Hoffmann et al (2009) agrees with. The optical star is of type ON6.5 V((f)) according to Liu et al (2006). According to Vacca et al (2000) the likely mass range for an O6.5 V star is $30.8\text{-}41.0M_{\odot}$ with a radius of $10.3R_{\odot}$. Referring to the graphs in Weidner & Vink (2010) gives an estimate of $25.1\text{-}35.5M_{\odot}$. (Sarty et al, 2010) suggest a mass of $26M_{\odot}$.

Hoffmann et al (2009) estimate, from their INTEGRAL observations, that the compact object has a mass of $3.7M_{\odot}$, noting that its nature is still under debate. At $3.7M_{\odot}$, the compact object could be a black hole. Sarty et al (2010) however suggest that a $1.8M_{\odot}$ compact object along with the $26M_{\odot}$ star mentioned above would better fit their data.

The results in figure 6.9 show the range of possible optical star masses with both an eccentricity of 0.35 and compact object of mass $3.7M_{\odot}$ and eccentricity of 0.24 with compact object of mass $1.8M_{\odot}$.

Distance 3.1kpc (Motch et al, 1997), inclination angle at least 9 degrees (McSwain et al, 2004).

4U 0115+634

Eccentricity 0.34 (Liu et al, 2006), period 24.3 days (Liu et al, 2006). The massive star has spectral type B0.2 Ve (Liu et al, 2006). Raichur & Paul (2010) suggest a mass of $19M_{\odot}$ and radius $8R_{\odot}$. Vacca et al (2000) has estimates for type B0 V and B0.5 V tabled, $19.5\text{-}21.2M_{\odot}$ with radius $8.3R_{\odot}$ and $18.4\text{-}19.3M_{\odot}$ with radius $8R_{\odot}$ respectively, compared to which the estimate in Raichur & Paul (2010) appears reasonable. The compact object is assumed to be a $1.4M_{\odot}$ neutron star.

Distance 2.5kpc (Liu et al, 2006), inclination angle 40 to 60 degrees (Negueruela & Okazaki, 2001).

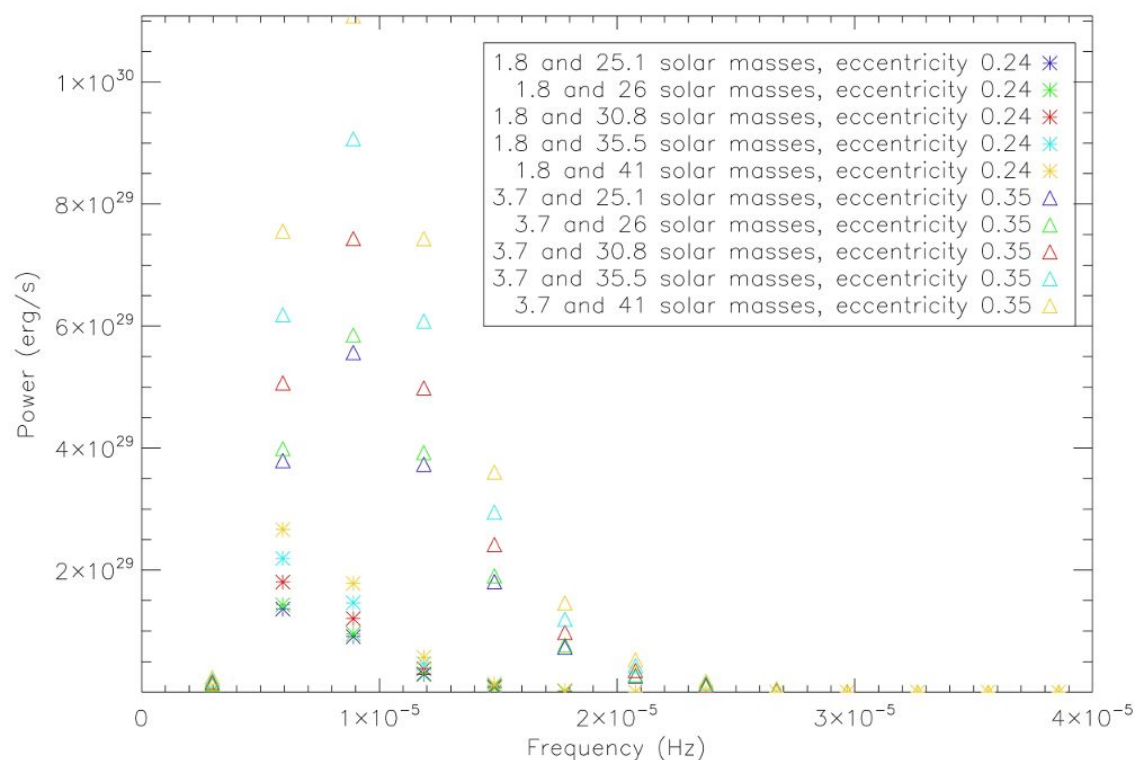


Figure 6.9: Calculated gravitational wave emission for RX J1826.2-1450

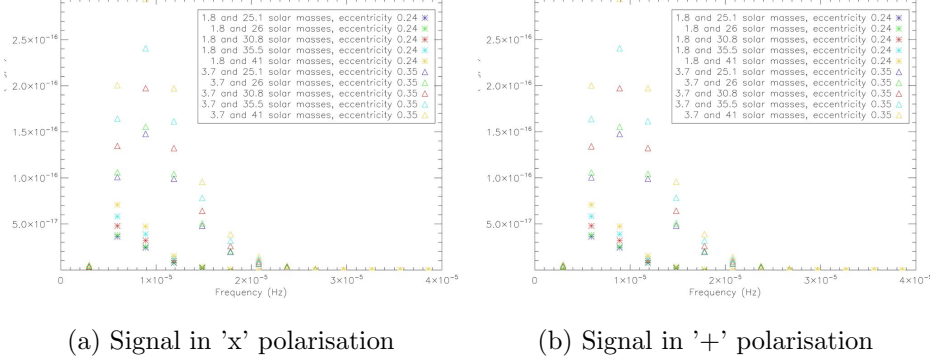


Figure 6.10: Calculated gravitational wave signal at Earth from RXJ1826.2-1450

XTE J1946+274

Eccentricity 0.33 (Liu et al, 2006), period 169.2 days (Liu et al, 2006). The spectral type is listed as B0-1 IV-Ve (Liu et al, 2006). Wilson et al (2003) suggests it has a mass of $10\text{-}16M_{\odot}$ which is a little lower than the estimates from Vacca et al (2000) for type B0V and B0.5 V, $19.5\text{-}21.2M_{\odot}$ with radius $8.3R_{\odot}$ and $18.4\text{-}19.3M_{\odot}$ with radius $8R_{\odot}$ respectively but may be reasonable since no estimates are available for type B1 V. The compact object is assumed to be a $1.4M_{\odot}$ neutron star.

Distance 9.5kpc (Liu et al, 2006), inclination angle ≥ 46 degrees (Wilson et al, 2003).

SAX J0635.2+0533

Eccentricity 0.29 (Liu et al, 2006), period 11.2 days (Liu et al, 2006). Spectral type B2 V-B1 IIIe Liu et al (2006) as stated in the discovery paper of Kaaret et al (1999). Mass of optical star estimated as $10M_{\odot}$ (Kaaret et al, 2000), compact object assumed to be a $1.4M_{\odot}$ neutron star.

Distance 2.5-5kpc (Liu et al, 2006), 3.75kpc used. Inclination angle < 25 degrees (Cusumano et al, 2000).

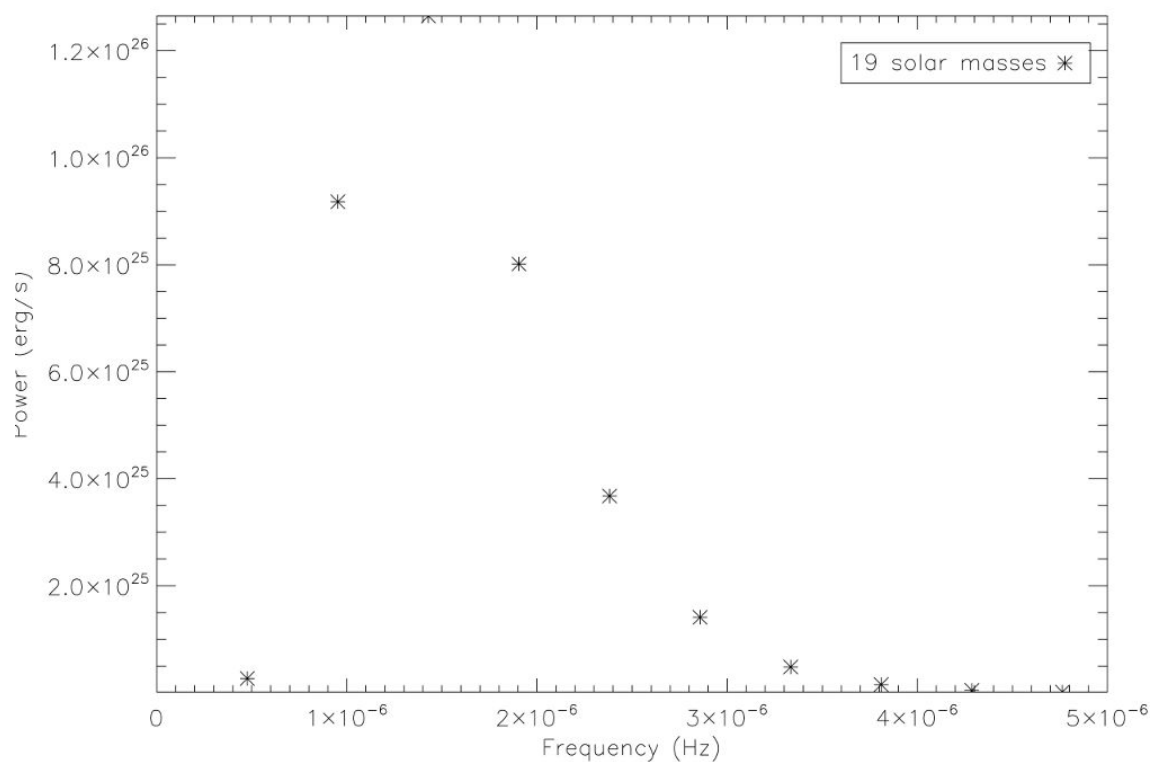


Figure 6.11: Calculated gravitational wave emission for 4U 0115+634

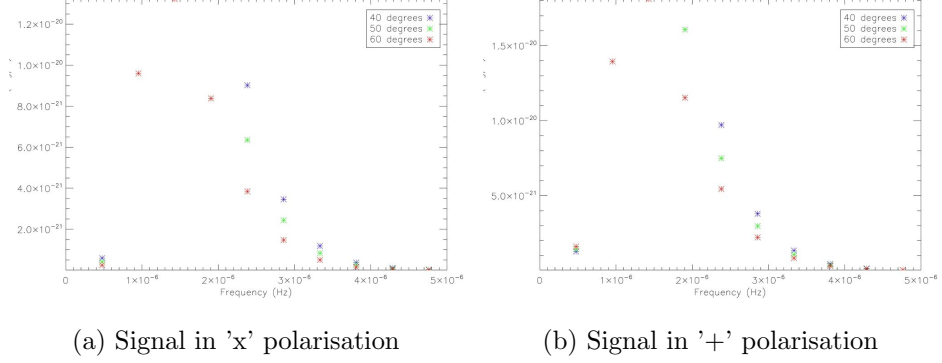


Figure 6.12: Calculated gravitational wave signal at Earth from 4U0115+634

4U 1907+09

Eccentricity 0.28 (Liu et al, 2006), period 8.38 days (Liu et al, 2006). Spectral type of the massive star was originally thought to be O8-9 Ia, but has now been narrowed down to O9.5 Iab (Gvaramadze et al, 2011), so is a supergiant. Vacca et al (2000) gives mass estimates for O9.5 Ia as $27.9\text{-}43.1M_{\odot}$ with a radius of $25.4R_{\odot}$. Reading from the graphs in Weidner & Vink (2010) the mass is estimated as either $26.3\text{-}44.7M_{\odot}$ or $29.5\text{-}52.5M_{\odot}$ depending on the model used. The compact object is assumed to be a $1.4M_{\odot}$ neutron star as in Gvaramadze et al (2011).

Distance 5kpc (Liu et al, 2006), either inclination of 47.9 degrees or almost edge on (90 degrees) (Roberts et al, 2001).

2S 0053+604

Eccentricity 0.26 (Liu et al, 2006), period 203.59 days (Liu et al, 2006). It is thought this might be a white dwarf system (Haberl, 1995). The mass of the compact object is estimated as $0.7\text{-}1.9M_{\odot}$ (Harmanec et al, 2000) and the larger star as $13\text{-}18M_{\odot}$ (Harmanec et al, 2000). The tables in Vacca et al (2000) give the mass of a B0.5 V star such as this (Liu et al, 2006) as $18.4\text{-}19.3M_{\odot}$ with a radius of $8R_{\odot}$. This system is often referred to as γ Cas.

Distance 0.19kpc (Liu et al, 2006), inclination angle 25 degrees (Hummel, 1998).

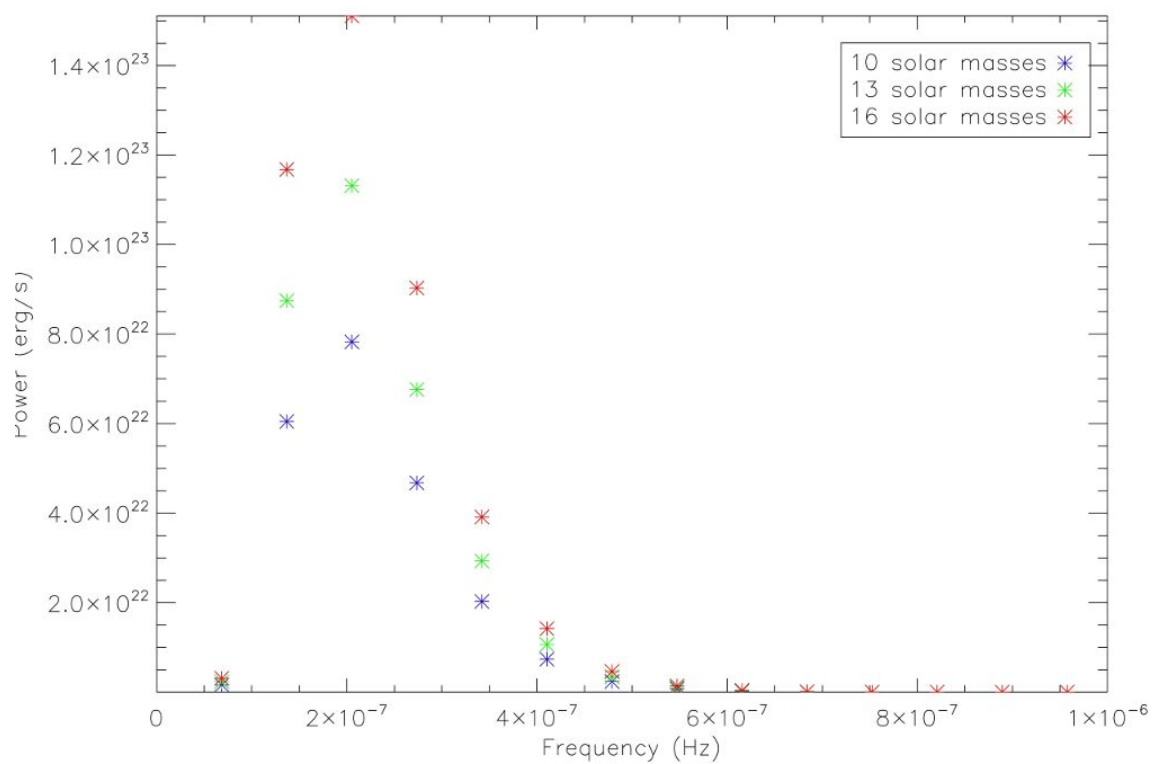


Figure 6.13: Calculated gravitational wave emission for XTE J1946+274

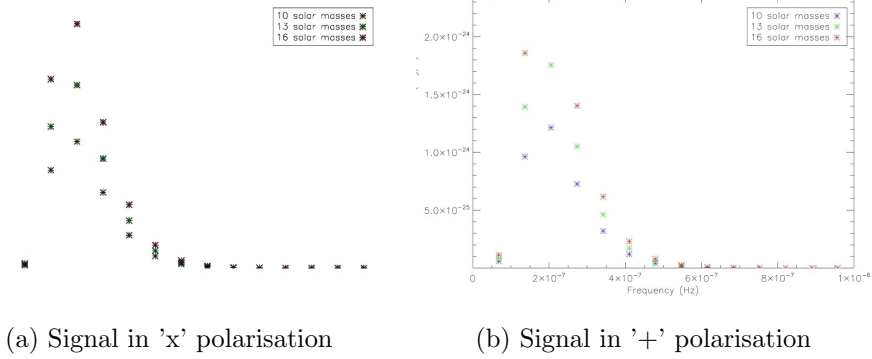


Figure 6.14: Calculated gravitational wave signal at Earth from XTEJ1946+274

4U 1700-37

Eccentricity 0.22 (Liu et al, 2006), period 3.41 days (Liu et al, 2006). The supergiant star HD1531919, of spectral type O6.5 Iaf⁺(Liu et al, 2006) is thought to be the hottest and perhaps most massive donor star in a known HMXB system (Clark et al, 2002). Clark et al (2002) suggests a mass of $58 \pm 11 M_{\odot}$ for the supergiant and a radius of $21.9^{+1.3}_{-0.5} R_{\odot}$. Heap & Corcoran (1990) suggest a mass of $50 M_{\odot}$ and radius of $18 R_{\odot}$. Both of these fit with the mass range for an O6.5 Ia in Vacca et al (2000) of $39.8\text{-}69.6 M_{\odot}$, which gives an estimated radius of $21.2 R_{\odot}$, just outside the error bound of the radius from Clark et al (2002). Reading from the graphs in Weidner & Vink (2010) gives a mass range of 39.8-63.1 for spectral type O6.5 I.

Heap & Corcoran (1990) refers to the compact object as a neutron star. Clark et al (2002) calculates its mass as $2.44 \pm 0.27 M_{\odot}$, suggesting that the compact object is either an extremely massive neutron star or a low mass black hole.

In contrast to the data above, Abubekerov (2004) suggests that, if the optical star has a mass of about $50 M_{\odot}$, depending on various factors, the compact object mass should be $2.25^{+0.23}_{-0.24} M_{\odot}$ or $2.14^{+0.50}_{-0.43} M_{\odot}$. Based on a radius of $21.9 R_{\odot}$ for the optical star, the compact object mass is estimated as $1.76^{+0.20}_{-0.21} M_{\odot}$ or $1.65^{+0.78}_{-0.56} M_{\odot}$. Finally, the paper suggests that the mass-luminosity relation for X-ray binaries gives a mass for the optical star of only $27.4 M_{\odot}$, which is stated would mean a compact

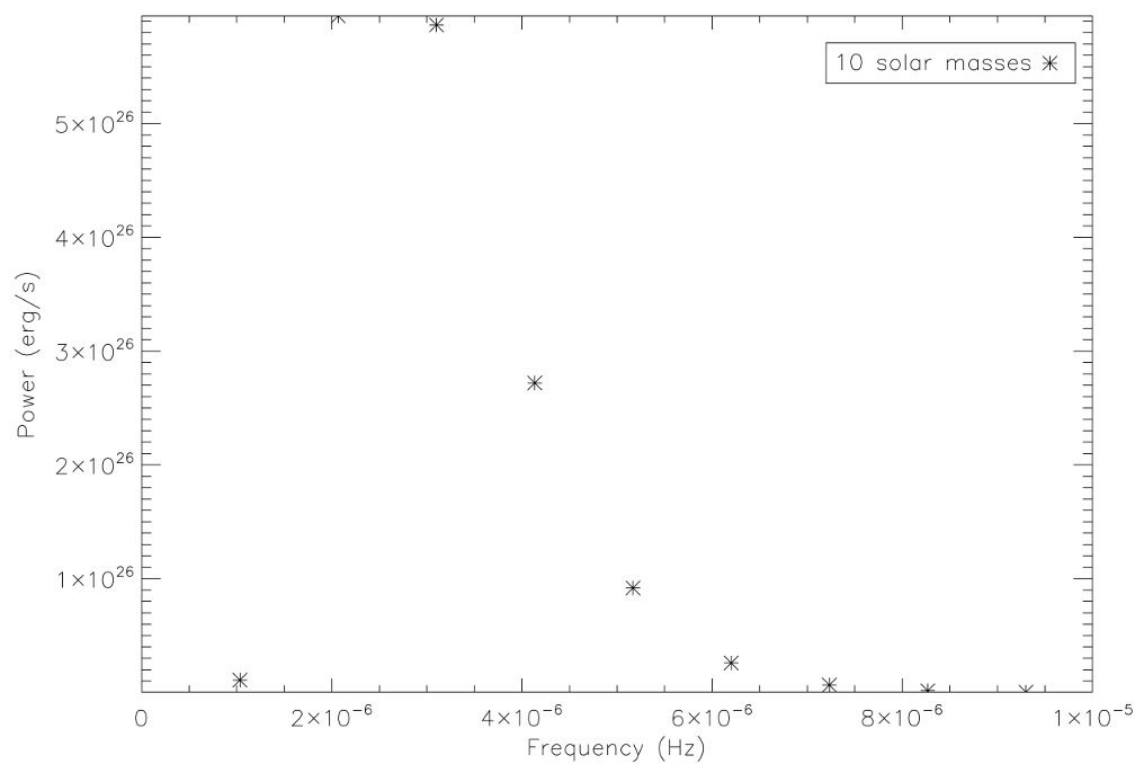


Figure 6.15: Calculated gravitational wave emission for SAX J0635.2+0533

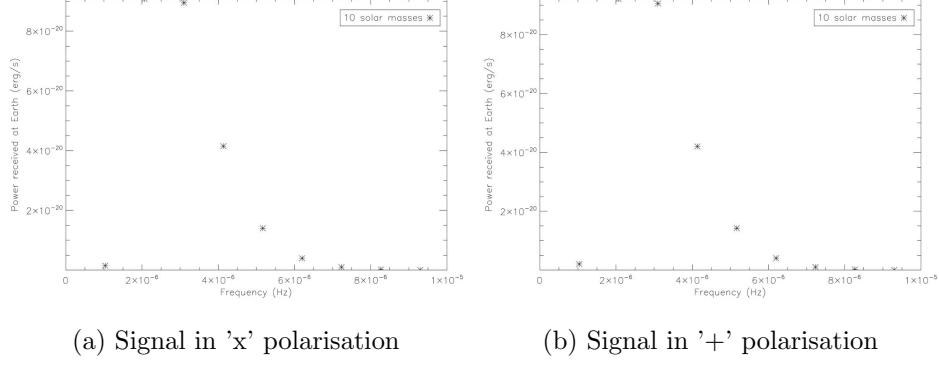


Figure 6.16: Calculated gravitational wave signal at Earth from SAXJ0635.2+0533

object of mass $1.41_{-0.08}^{+0.08} M_{\odot}$ or $1.35_{-0.18}^{+0.18} M_{\odot}$.

A measurement of the gravitational radiation from this system could perhaps help to settle this debate.

Distance 1.9 kpc (Liu et al, 2006), inclination angle >80 degrees (Heap & Corcoran, 1990).

Detailed data on radio pulsars in binary systems

Results for B1913+16 (aka J1915+1606, Hulse-Taylor binary pulsar), J0514-4002A, B1259-63 (aka J1302-6350) and J1811-1736 are shown in Chapter 3. The remainder of the radio pulsar binaries studied are detailed below.

J0045-7319

Eccentricity 0.81 (Kaspi et al, 1996), period 51.17 days (Kaspi et al, 1996). For a $1.4M_{\odot}$ neutron star, the mass of the larger star, a B star, would be $8.8 \pm 1.8 M_{\odot}$ (Kaspi et al, 1996) and has a radius of $6.4 \pm 0.7 R_{\odot}$.

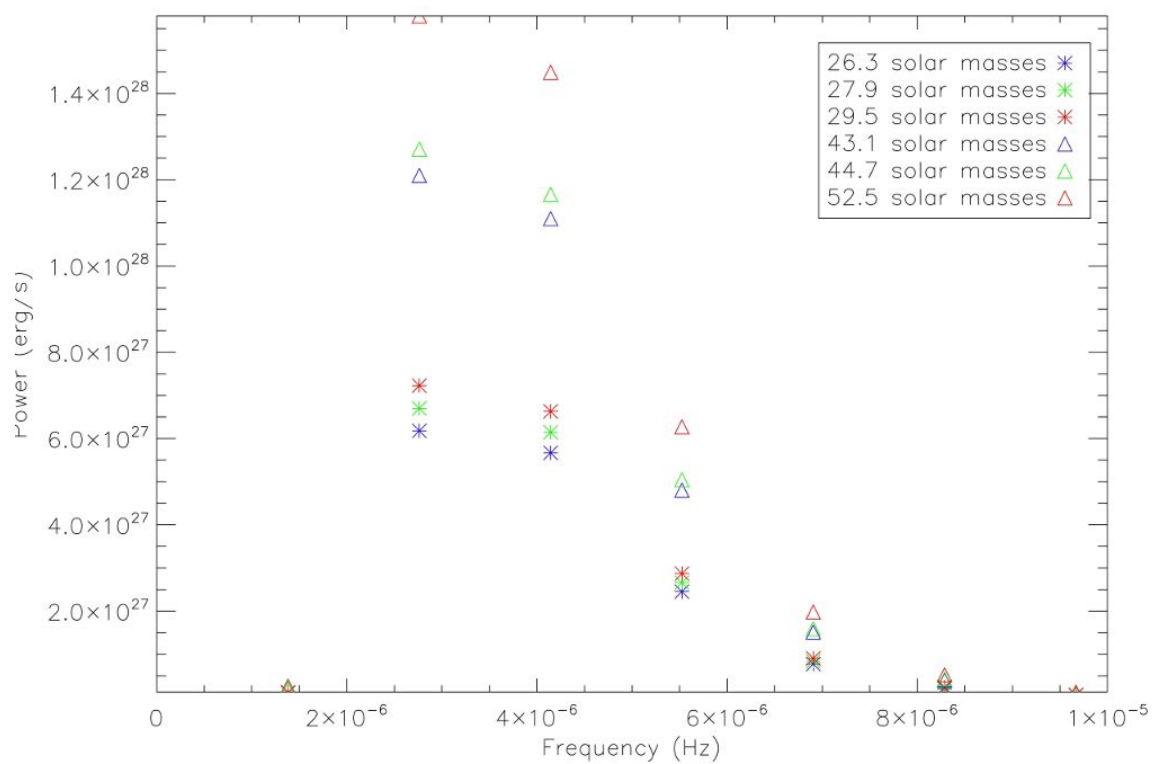


Figure 6.17: Calculated gravitational wave emission for 4U 1907+09

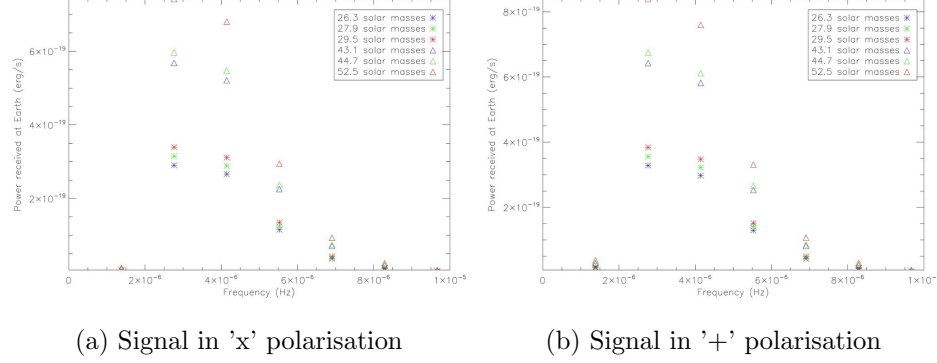


Figure 6.18: Calculated gravitational wave signal at Earth from 4U1907+09 at 47.9 degrees inclination

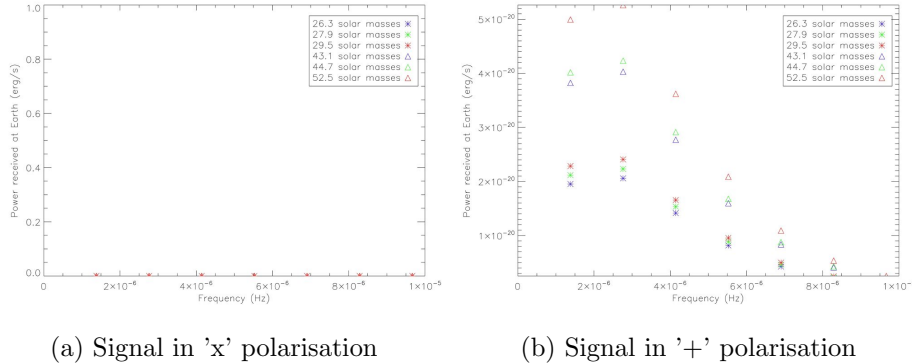


Figure 6.19: Calculated gravitational wave signal at Earth from 4U1907+09 at 90 degrees inclination

B1820-11=J1823-1115

Eccentricity 0.79 (Hobbs et al, 2004), period 357.76 days (Hobbs et al, 2004). The only mass measurement we have here is that estimated in Australia Telescope National Facility Pulsar Group (2004), which gives a minimum mass for the companion, and a 'median mass' assuming the neutron star to have a mass of $1.35M_{\odot}$, in this case giving a companion mass of $0.78M_{\odot}$, which will be used here. It should however be noted that where a mass measurement does exist in the literature, this 'median mass' often does not match it, as you can see by comparing the previous examples

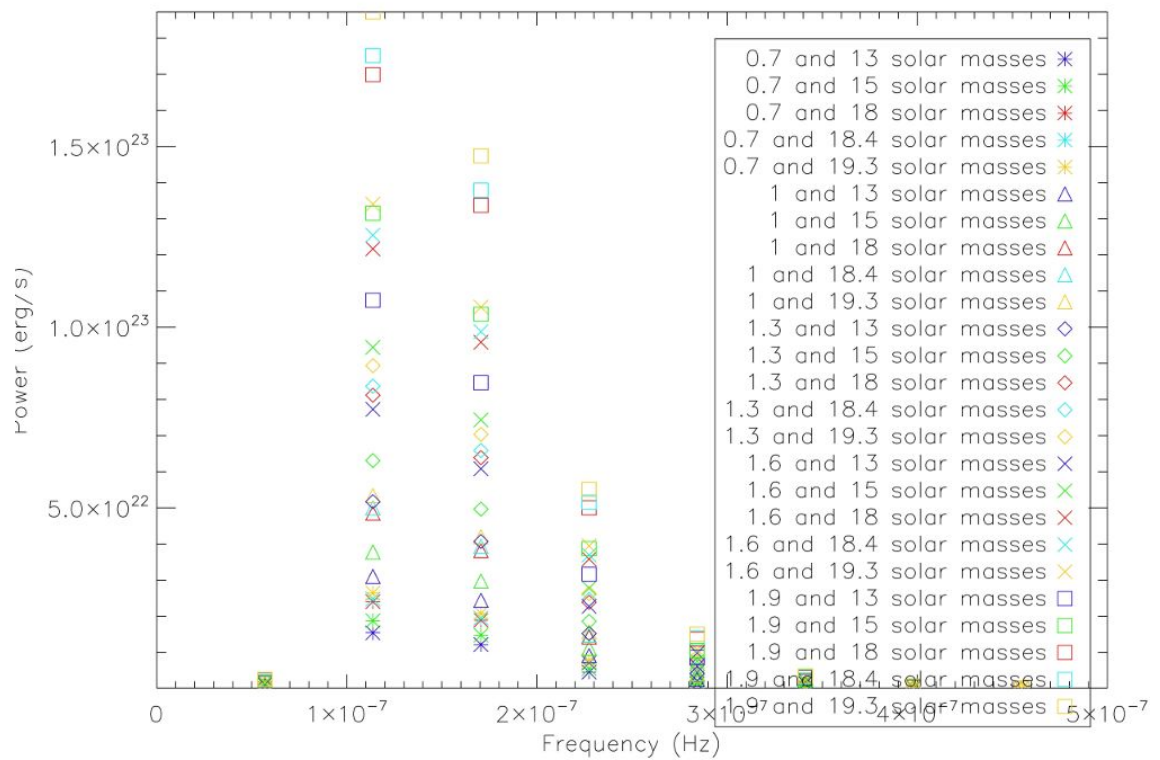


Figure 6.20: Calculated gravitational wave emission for 2S 0053+604

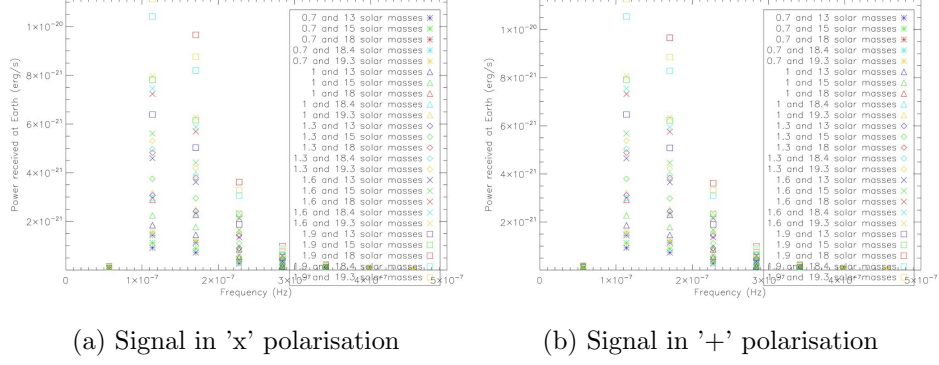


Figure 6.21: Calculated gravitational wave signal at Earth from 2S0053+604

to the 'median masses' listed at Johnston (2005).

Distance 6.29kpc (Johnston, 2005), inclination angle 60 degrees assumed in Manchester et al (2005).

J1750-37

Eccentricity 0.71 (Possenti et al, 2001), period 17.3 days (Possenti et al, 2001). Assuming a pulsar mass of $1.4M_{\odot}$, the minimum companion mass is $0.5M_{\odot}$ (Possenti et al, 2001). This pulsar is located in globular cluster NGC 6441, so is one of the few examples we have of an actual binary in a globular cluster (Possenti et al, 2001). Freire (2004) gives the mass of the companion as $0.7M_{\odot}$.

B2127+11C=J2130+1210C

Eccentricity 0.68 (Jacoby et al, 2006), period 0.34 (Jacoby et al, 2006). Pulsar mass is thought to be $1.358 \pm 0.010M_{\odot}$ and companion mass $1.354 \pm 0.010M_{\odot}$ (Jacoby et al, 2006). The very short period gives this binary a relatively high frequency peak, making it one of the best candidates for detection by LISA.

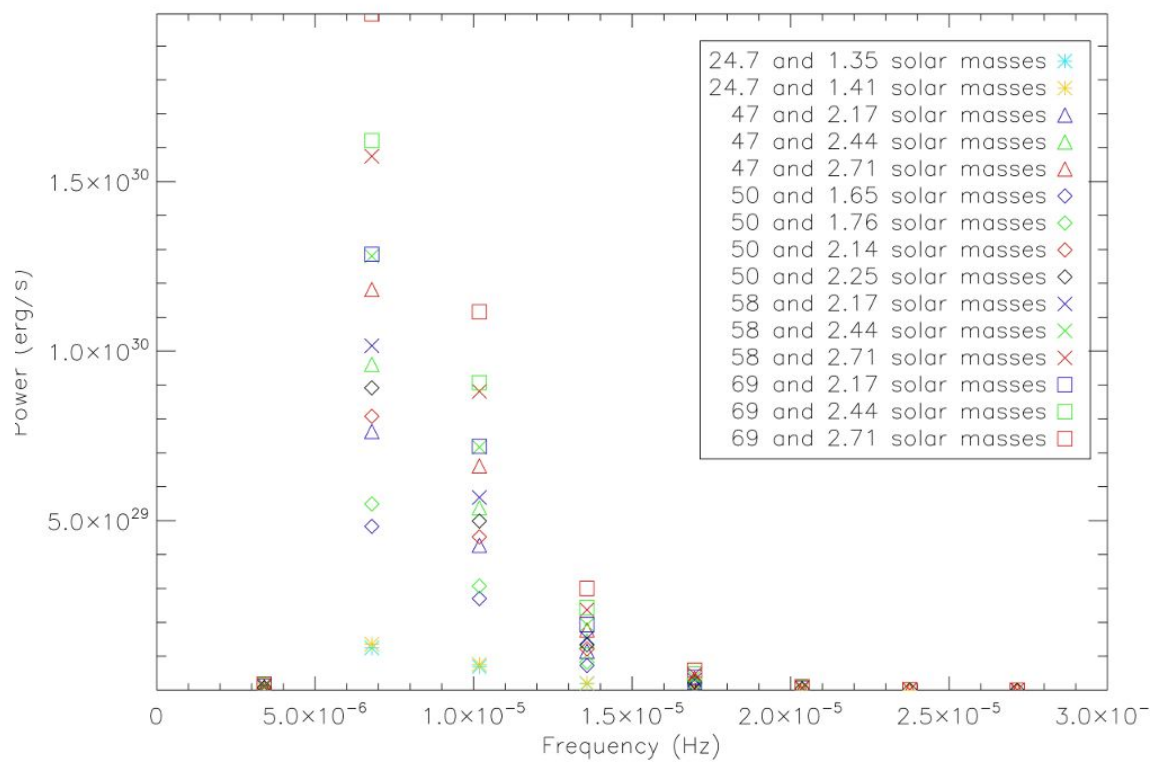


Figure 6.22: Calculated gravitational wave emission for 4U 1700-37

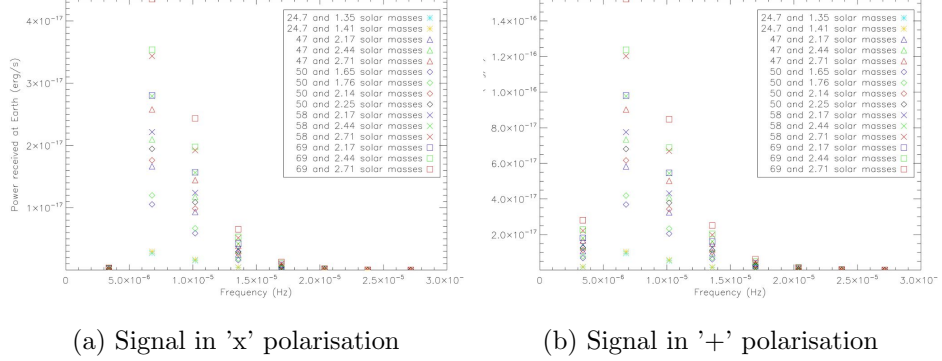


Figure 6.23: Calculated gravitational wave signal at Earth from 4U1700-37

B2303+46=J2305+4707

Eccentricity 0.66 (Thorsett et al, 1993), period 12.34 days (Thorsett et al, 1993). Thorsett et al (1993) suggest a total mass for the system of $2.53 \pm 0.08 M_{\odot}$, comprising of a pulsar of mass $1.16 \pm 0.28 M_{\odot}$ and another star of mass $1.37 \pm 0.24 M_{\odot}$. This system is likely to consist of two neutron stars.

J1740-3052

Eccentricity 0.58 (Stairs et al, 2001), period 231.03 days (Stairs et al, 2001). The mass of the more massive star is at least $11 M_{\odot}$ and it has a median mass of $15.8 M_{\odot}$ assuming a pulsar mass of $1.35 M_{\odot}$, according to Australia Telescope National Facility Pulsar Group (2004). It is thought the more massive star may be a type K5 supergiant (Johnston, 2005).

Distance 10.73kpc (Johnston, 2005), inclination angle 64 ± 8 degrees (Stairs, 2004).

J2140-2310B

Eccentricity 0.52 (Johnston, 2005), period 0.8 (Johnston, 2005). The companion has a minimum mass of $0.35 M_{\odot}$ (Ransom et al, 2004), assuming a pulsar mass of $1.4 M_{\odot}$.

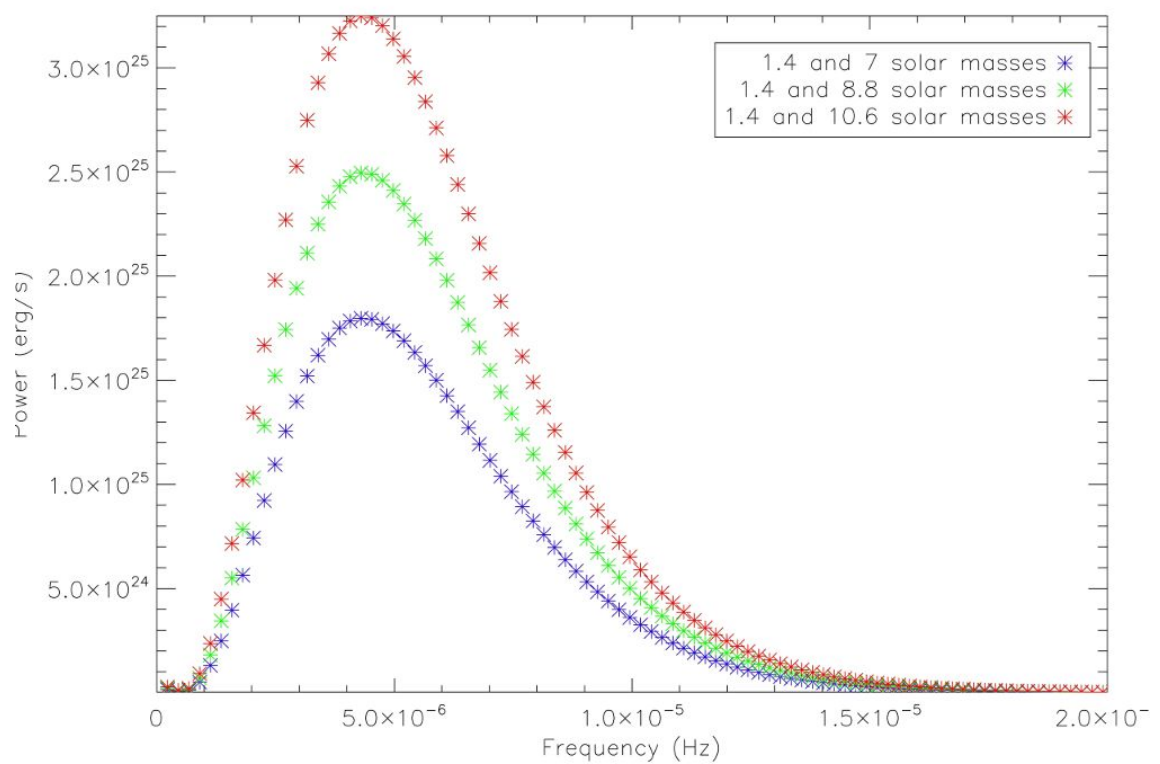


Figure 6.24: Calculated gravitational wave emission for J0045-7319

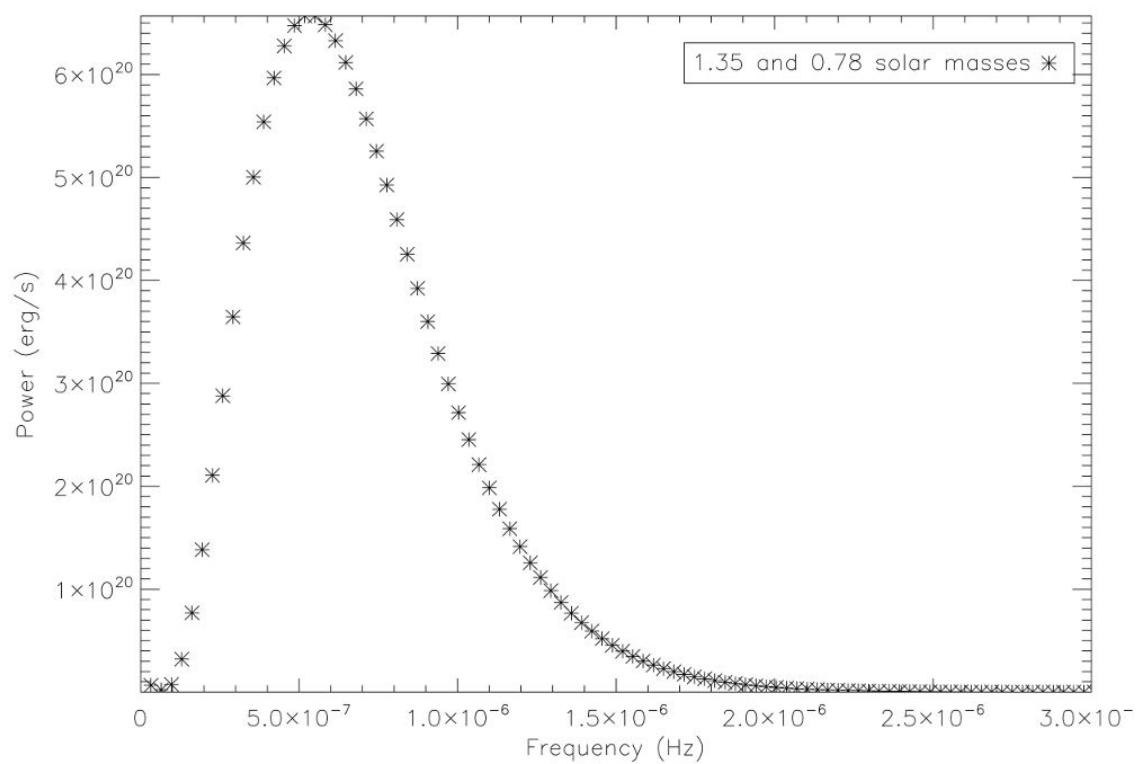


Figure 6.25: Calculated gravitational wave emission for J1823-1115

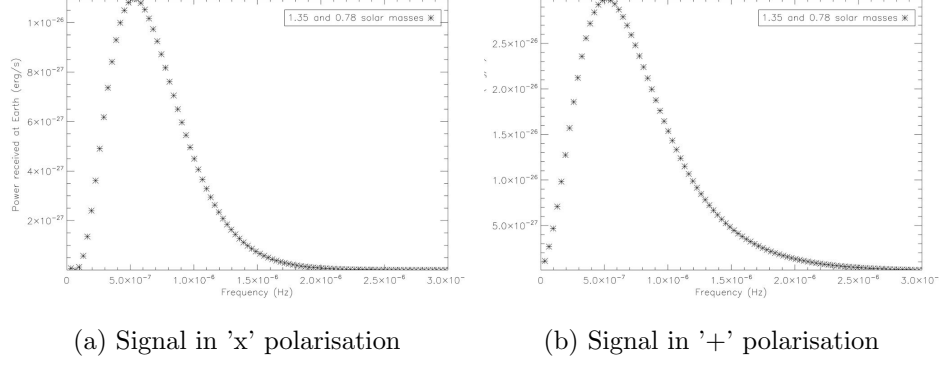


Figure 6.26: Calculated gravitational wave signal at Earth from B1820-11

This system is located in the core collapsed cluster M30 (Ransom et al, 2004).

B1534+12=J1537+1155

Eccentricity 0.27 (Konacki et al, 2003), period 0.42 (Konacki et al, 2003). The mass of the companion is thought to be $1.35M_{\odot}$ (Konacki et al, 2003). I assume a mass of $1.4M_{\odot}$ for the pulsar.

Distance 0.89kpc (Johnston, 2005), inclination angle 77.16 degrees (Thorsett et al, 2004).

J1518+4904

Eccentricity 0.25 (Janssen et al, 2008), period 8.63 days (Janssen et al, 2008). The pulsar mass is thought to be $<1.17M_{\odot}$ and the other star $>1.55M_{\odot}$ (Janssen et al, 2008).

Distance 0.71 kpc (Johnston, 2005), inclination angle <47 degrees (Janssen et al, 2008).

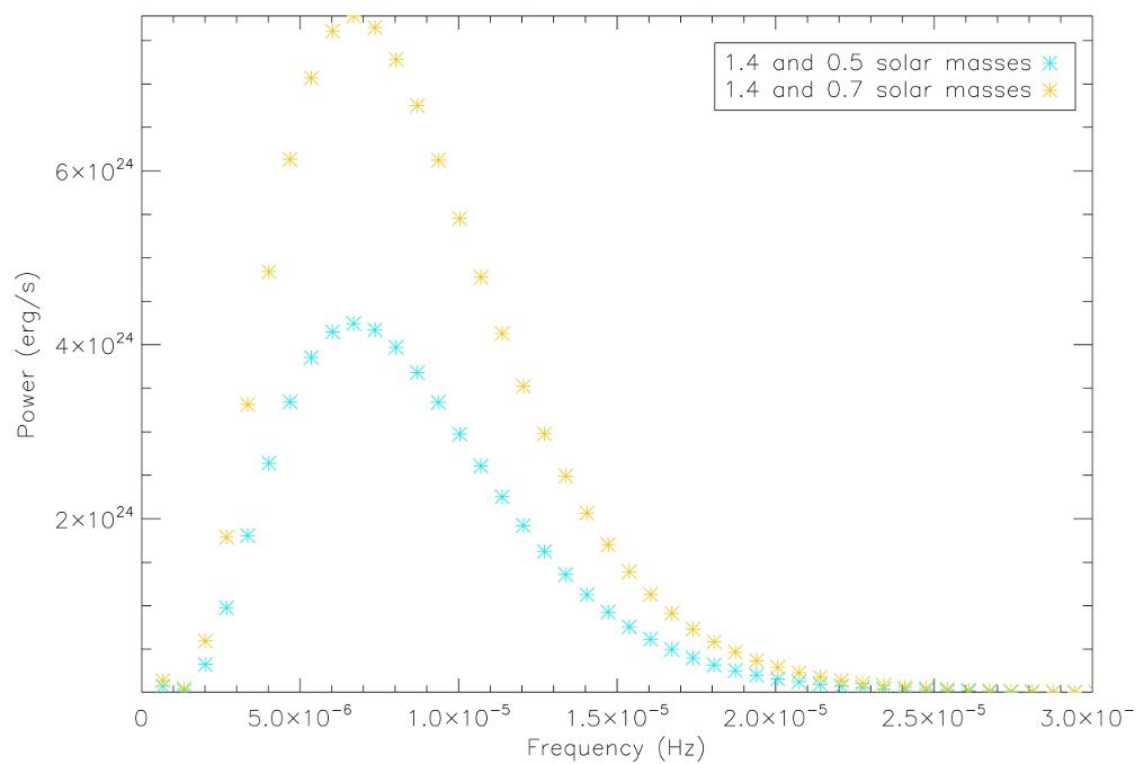


Figure 6.27: Calculated gravitational wave emission for J1750-37

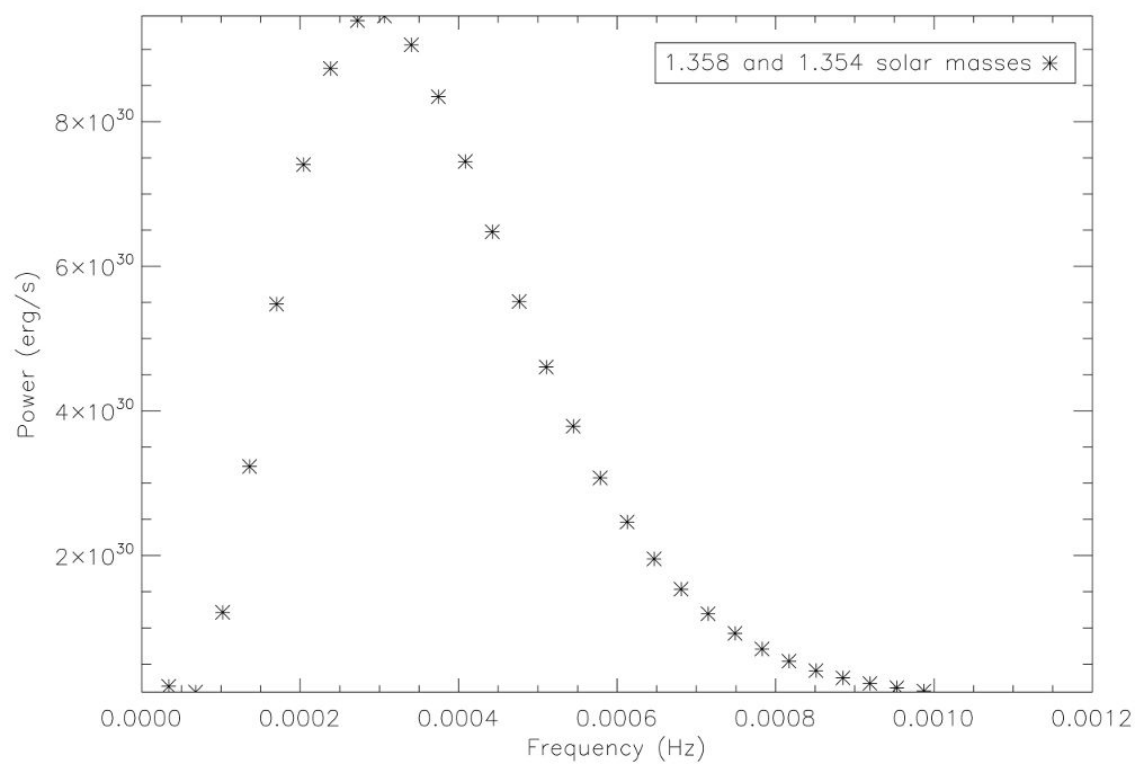


Figure 6.28: Calculated gravitational wave emission for J2130+1210C

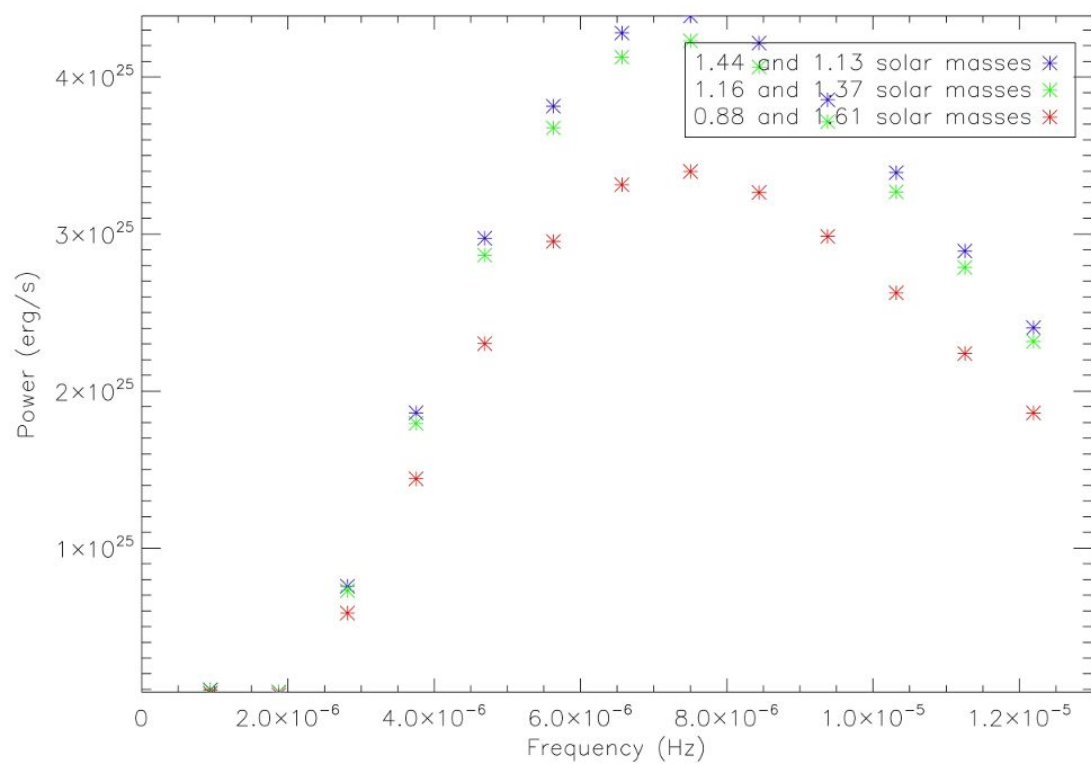


Figure 6.29: Calculated gravitational wave emission for J2305+4707

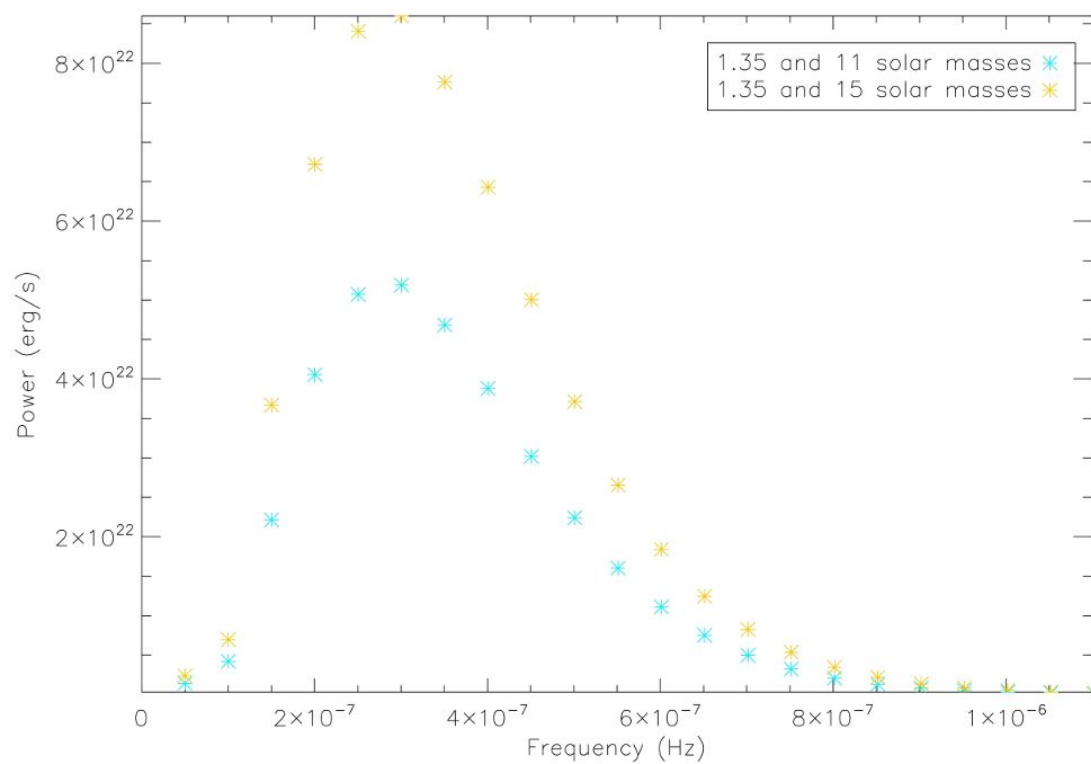


Figure 6.30: Calculated gravitational wave emission for J1740-3052

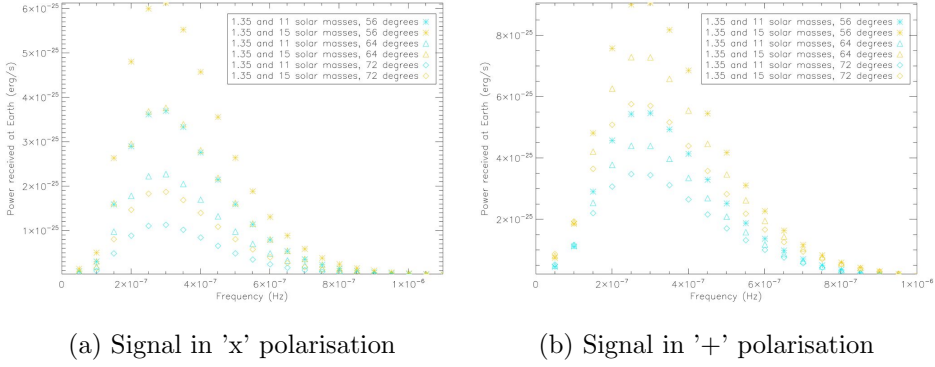


Figure 6.31: Calculated gravitational wave signal at Earth from J1740-3052

B1802-07=J1804-0735

Eccentricity 0.21 (Hobbs et al, 2004), period 2.62 days (Hobbs et al, 2004). According to Australia Telescope National Facility Pulsar Group (2004), assuming a $1.35M_{\odot}$ pulsar, the companion has a minimum mass of $0.29M_{\odot}$ and a median mass of $0.35M_{\odot}$.

Distance 3.1kpc (Johnston, 2005), inclination 10.37 to 19 degrees (Thorsett & Chakrabarty, 1999).

100 000 neutron star and $3 M_{\odot}$ systems, varying eccentricity only

Full results for the 100 000 neutron star and $3 M_{\odot}$ run, where orbital period was 10 days and only eccentricity varied.

The result for the even distribution of eccentricities is shown first, then the results for a normal distribution of eccentricities arranged by mean with varying standard deviation, followed by the same results arranged by standard deviation with varying mean.

In total this encompasses 82 runs. The even distribution was run once. For the normal distribution, the program was run for a standard deviation of 0.1, 0.2, 0.3,

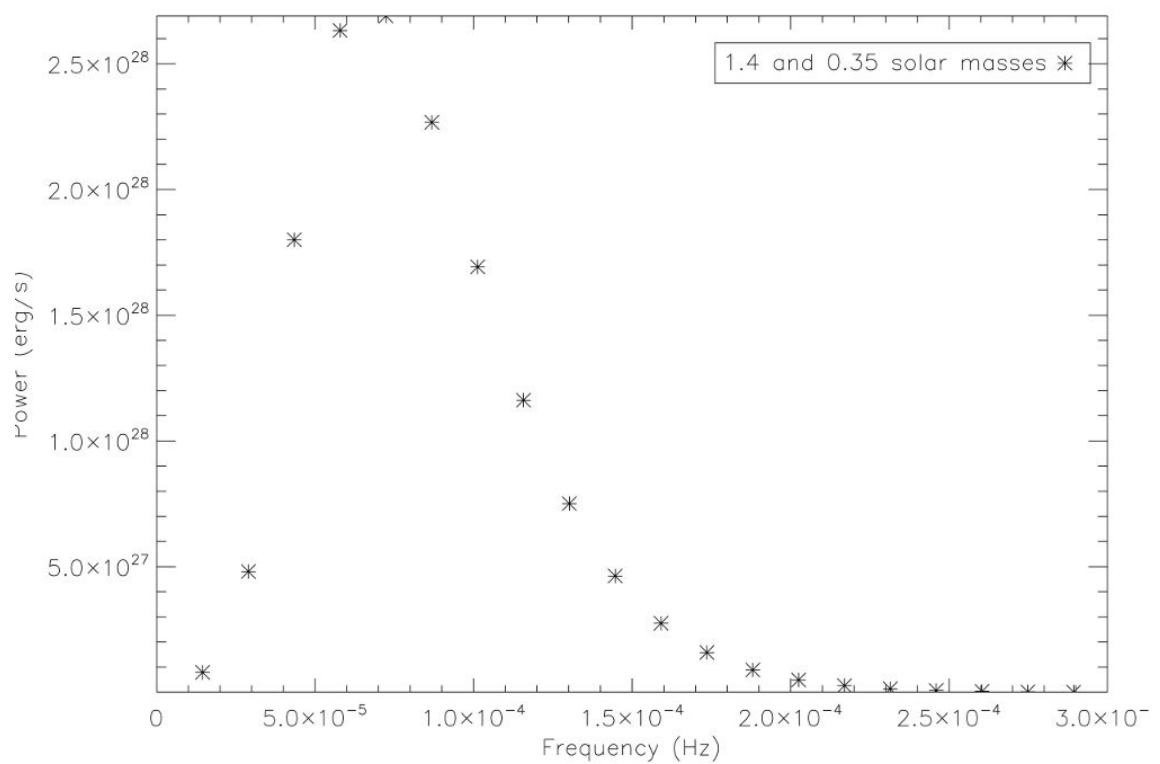


Figure 6.32: Calculated gravitational wave emission for J2140-2310B

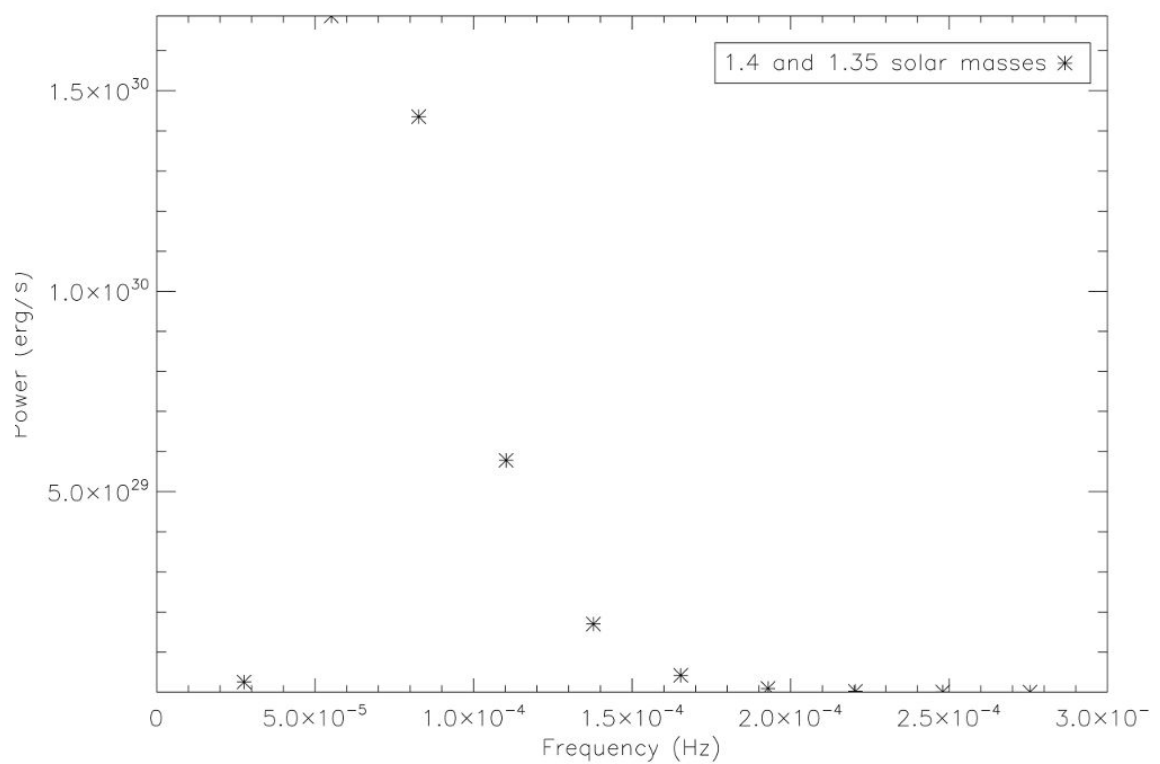


Figure 6.33: Calculated gravitational wave emission for J1537+1155

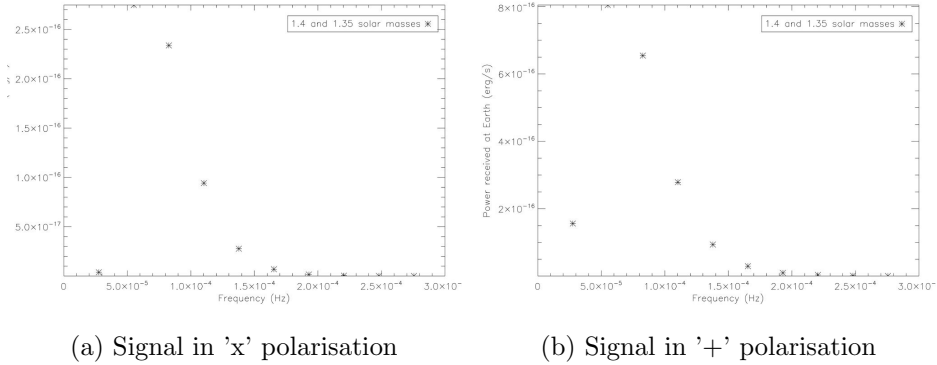


Figure 6.34: Calculated gravitational wave signal at Earth from B1534+12

0.4, 0.5, 0.6, 0.7, 0.8 and 0.9 for each of the mean eccentricities of 0.1, 0.2, 0.3, 0.4, 0.5, 0.6, 0.7, 0.8 and 0.9.

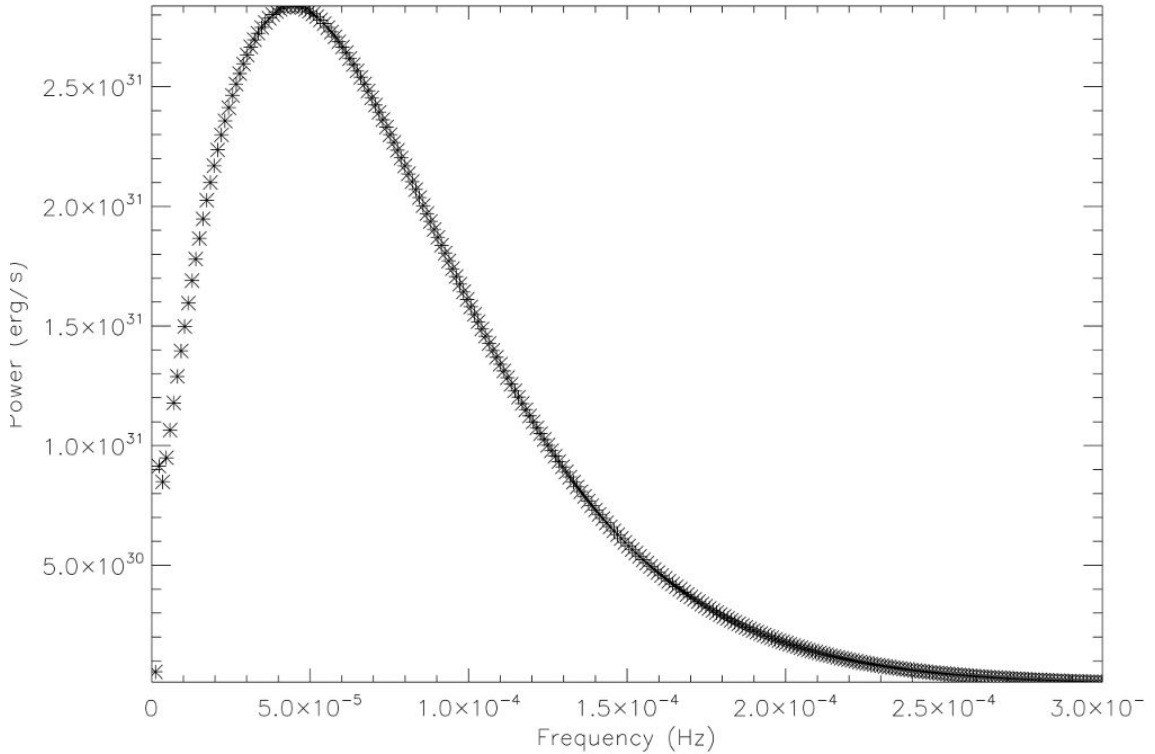


Figure 6.39: 100 000 neutron star and $3 M_{\odot}$ systems, even distribution of eccentricities

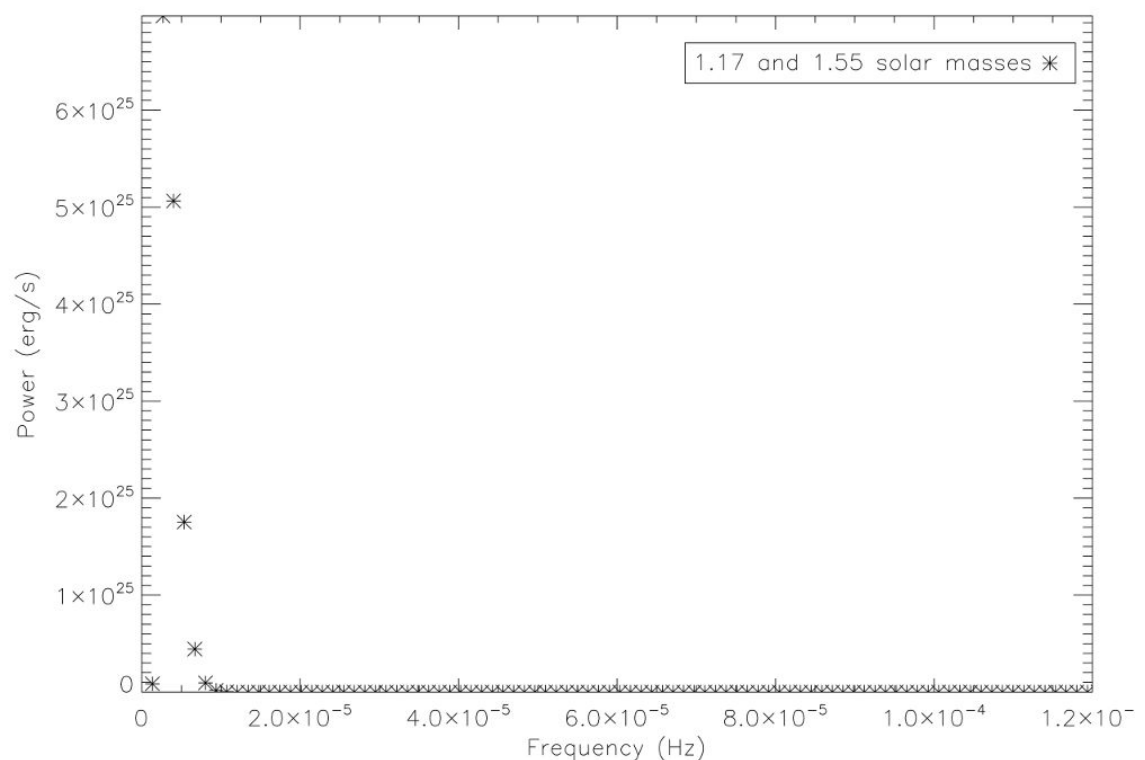


Figure 6.35: Calculated gravitational wave emission for J1518+4904

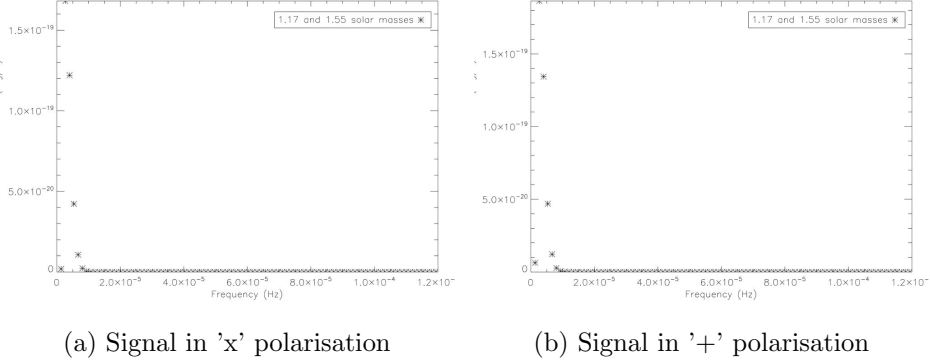
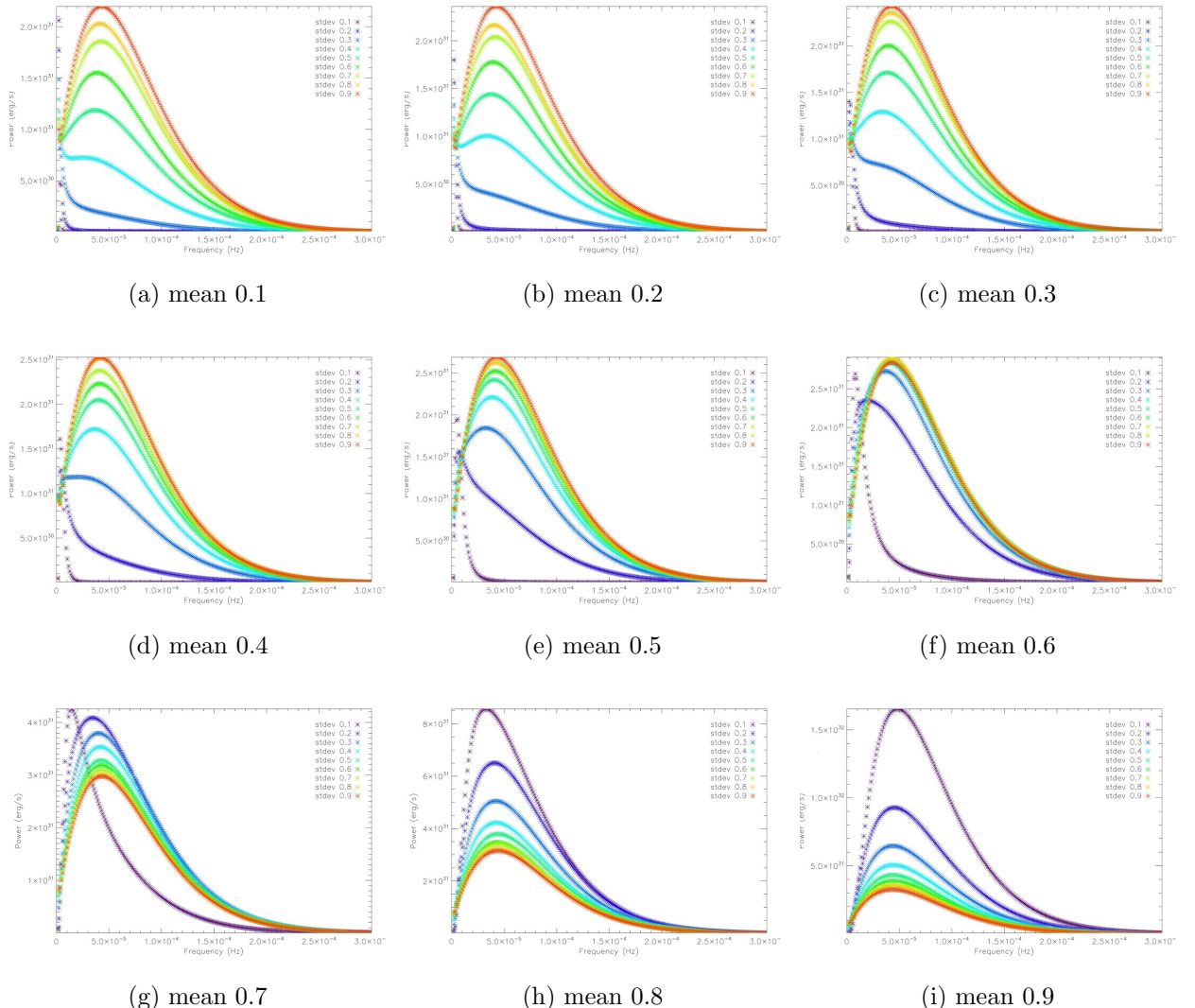


Figure 6.36: Calculated gravitational wave signal at Earth from J1518+4904

Figure 6.40: 100 000 neutron star and $3 M_{\odot}$ systems, normal distribution of eccentricities, mean 0.1-0.9, left to right top to bottom

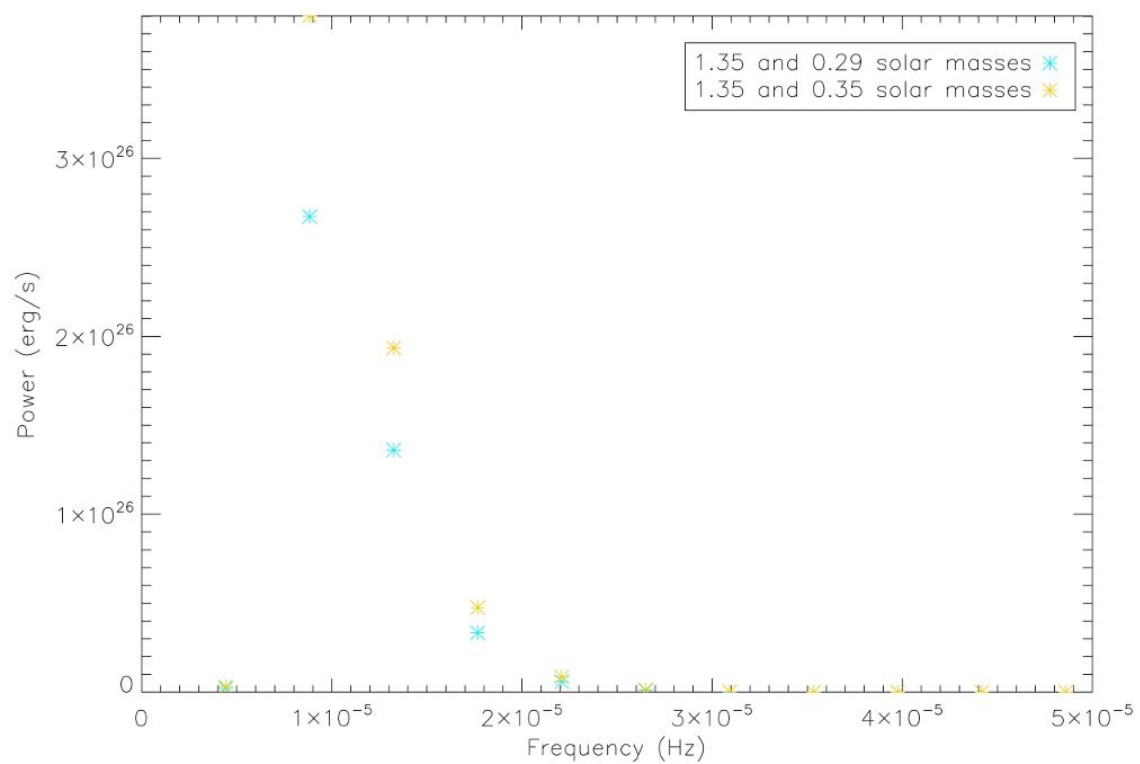


Figure 6.37: Calculated gravitational wave emission for J1804-0735

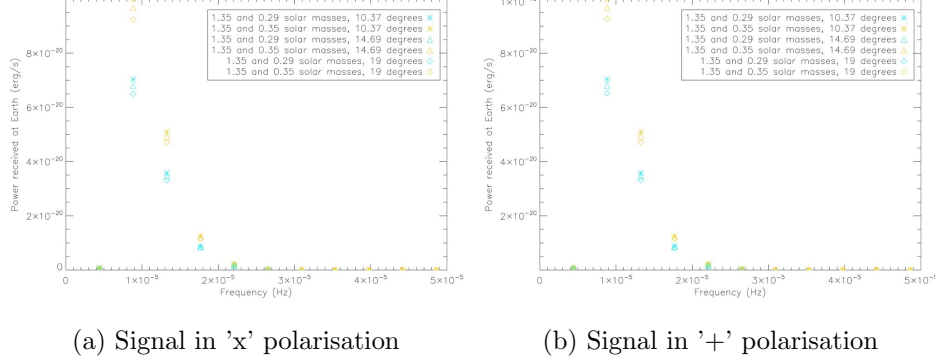
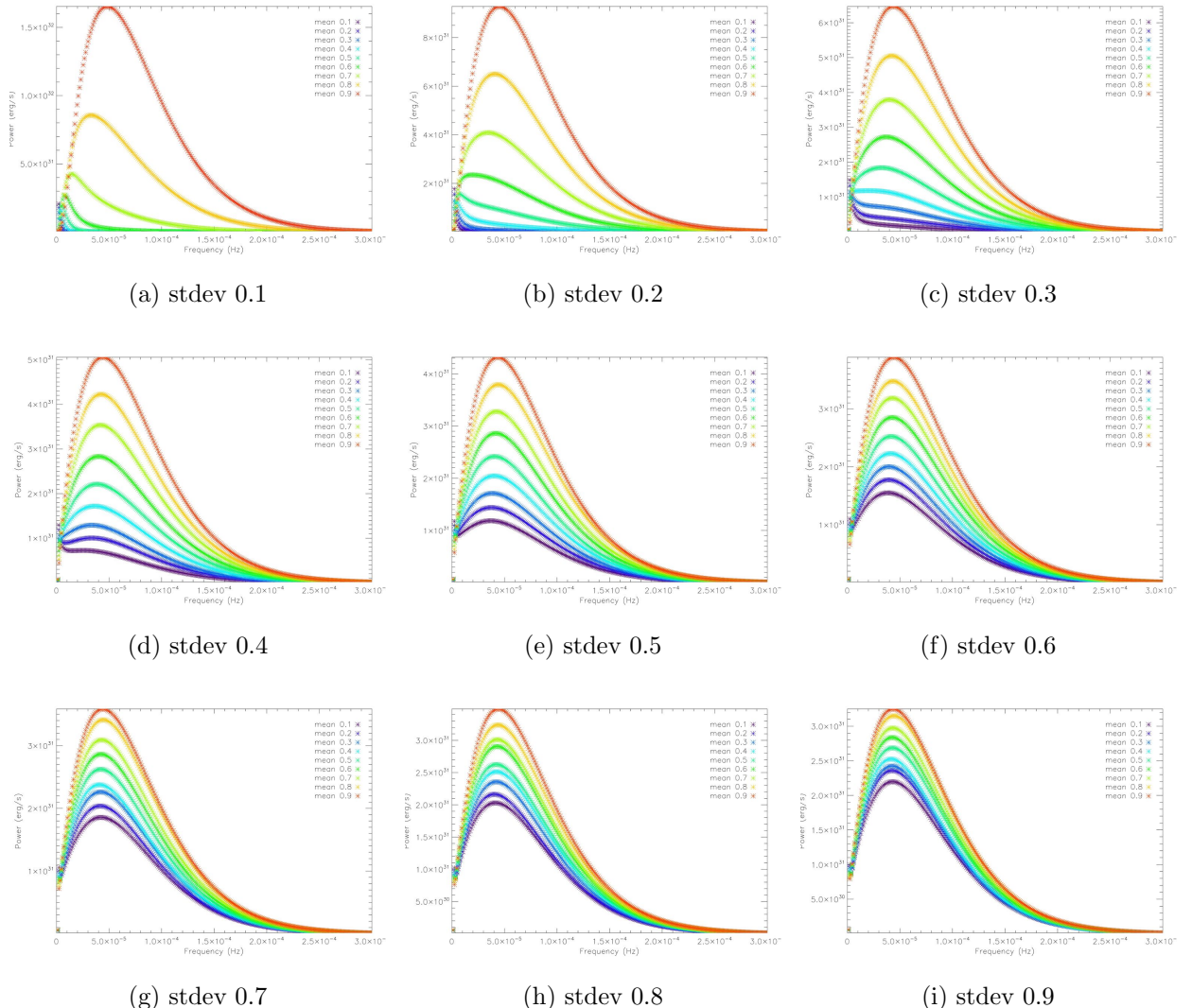


Figure 6.38: Calculated gravitational wave signal at Earth from B1802-07

Figure 6.41: 100 000 neutron star and $3 M_{\odot}$ systems, normal distribution of eccentricities, standard deviations 0.1-0.9, left to right top to bottom

100 000 two neutron star systems, varying eccentricity only

Full results for the 100 000 two neutron star run, where orbital period was 10 days and only eccentricity varied.

The result for the even distribution of eccentricities is shown first, then the results for a normal distribution of eccentricities arranged by mean with varying standard deviation, followed by the same results arranged by standard deviation with varying mean.

In total this encompasses 82 runs. The even distribution was run once. For the normal distribution, the program was run for a standard deviation of 0.1, 0.2, 0.3, 0.4, 0.5, 0.6, 0.7, 0.8 and 0.9 for each of the mean eccentricities of 0.1, 0.2, 0.3, 0.4, 0.5, 0.6, 0.7, 0.8 and 0.9.

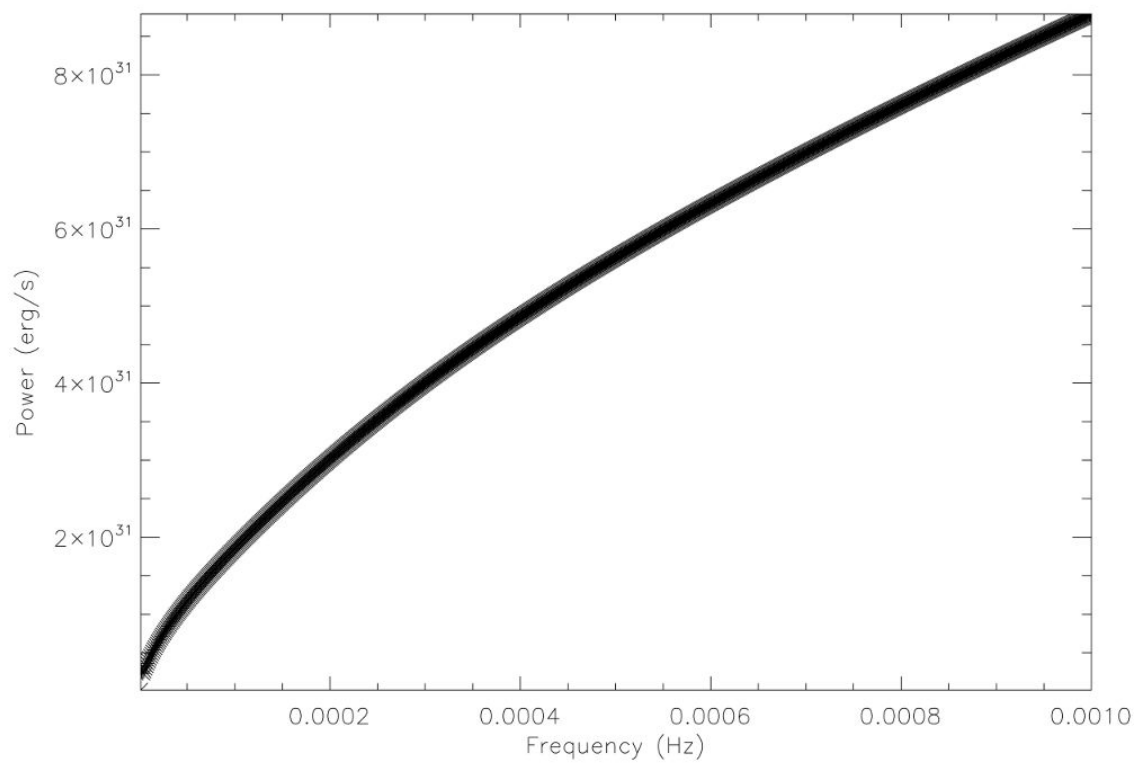


Figure 6.42: 100 000 two neutron star systems, even distribution of eccentricities

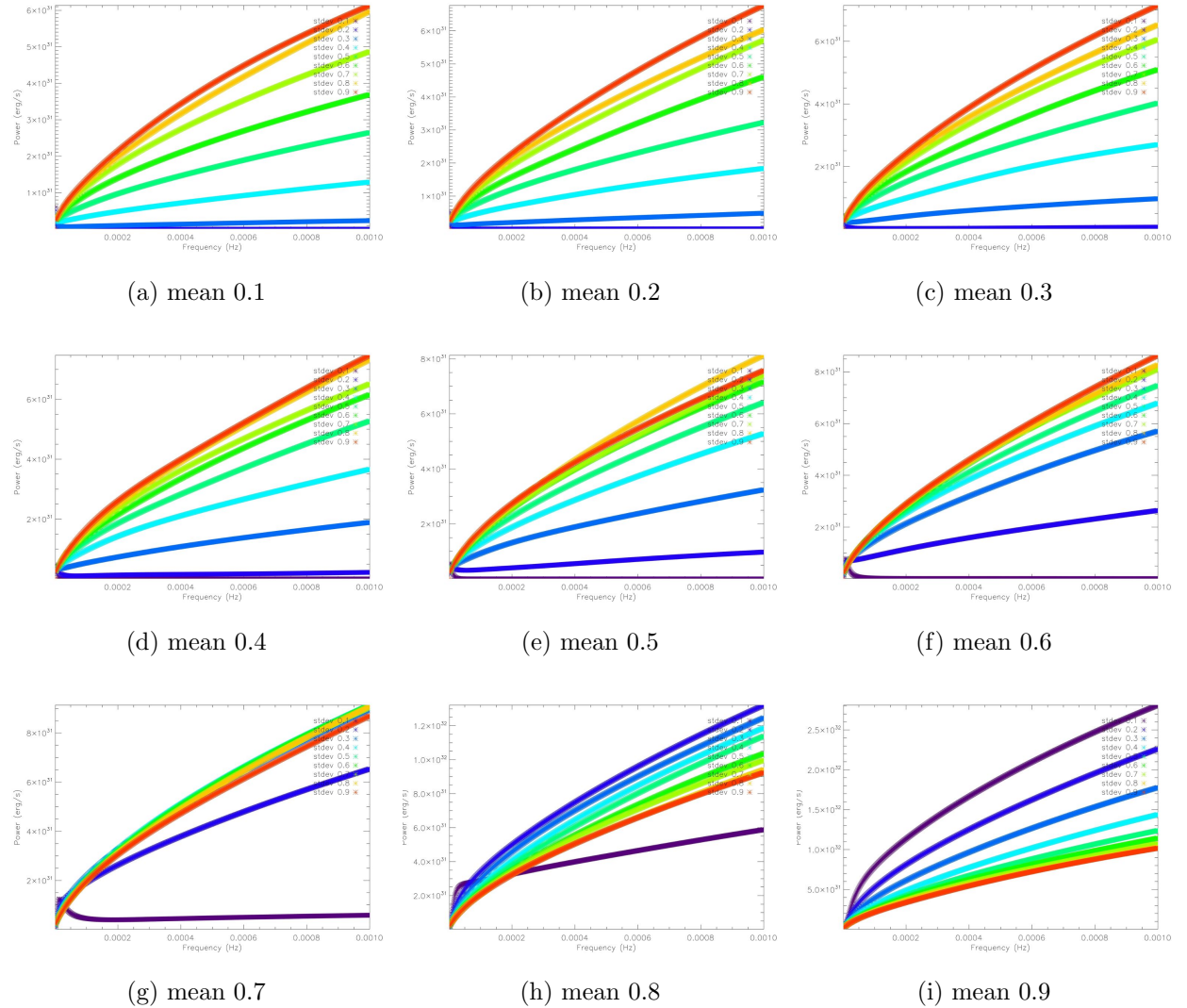


Figure 6.43: 100 000 two neutron star systems, normal distribution of eccentricities, mean 0.1-0.9, left to right top to bottom

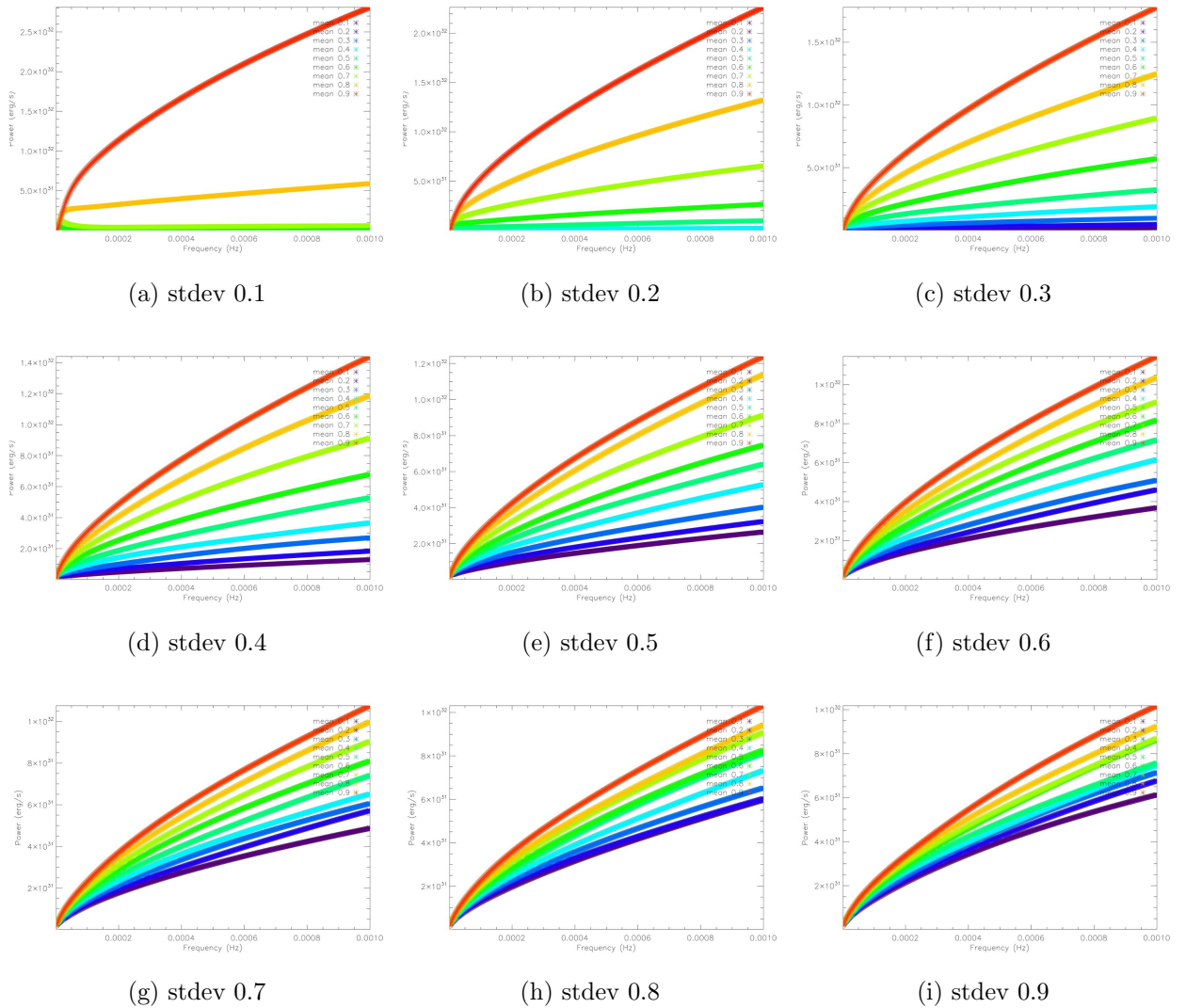


Figure 6.44: 100 000 neutron star and $3 M_{\odot}$ systems, normal distribution of eccentricities, standard deviations 0.1-0.9, left to right top to bottom

Bibliography

Bibliography

Abramowitz, M., Stegun, I. A., Handbook of Mathematical Functions 5th edition, 1968, Dover Publications Inc.

Abubekerov, M.K., Astronomy Reports, Vol. 48, No. 8, 2004, pp. 649658, Translated from Astronomicheskii Zhurnal, Vol. 81, No. 8, 2004, pp. 714725

Amaro-Seoane, P., Aoudia, S., Babak, S., Binétruy, P., Beri, E., Bohé, A., Caprini, C., Colpi, M., Cornish, N., Danzmann, K., Dufaux, J-F., Gair, J., Jennrich, O., Jetzer, P., Klein, A., Lang, R.N., Lobo, A., Littenberg, T., McWilliams, S.T., Nelemans, G., Petiteau, A., Porter, E.K., Schutz, B.F., Sesana, A., STebbins, R., Sumner, T., Vallisneri, M., Vitale, S., Volonteri, M., Ward, H., arXiv:1201.3621v1 [astro-ph.CO], 2012

Armstrong, J.W., "Low-Frequency Gravitational Wave Searches Using Spacecraft Doppler Tracking", Living Rev. Relativity 9, (2006), 1. edited 2008 (cited 2011): <http://www.livingreviews.org/lrr-2006-1>

Arun, K.G., Iyer, B.R., Sathyaprakash, B.S., Sinha, S., Van Den Broeck, C., Phys-RevD 76, 104016 (2007)

Association for Computing Machinery, Transactions on Mathematical Software, Vol. 18, No. 4, December 1992, 434-435

Australia Telescope National Facility Pulsar Group online catalogue of pulsars
<http://www.atnf.csiro.au/research/pulsar/psrcat/>

- Barsukova, E.A., Borisov, N.V., Burenkov, A.N., Klochkova, V.G., Goranskij, V.P., Metlova, N.V., Astronomer's telegram 416, 2005
- Baykal, A., Stark, M.J., Swank, J., ApJ 544:L129L132, 2000
- Belloni, T., Dieters, S., van den Ancker, M.E., Fender, R.P., Fox, D.W., Harmon, B.A., van der Klis, M., Kommers, J.M., Lewin, W.H.G., van Paradijs, J., ApJ, 527:345-352, 1999
- Benacquista, M., ApJ 520:233-238, 1999 July 20
- Benacquista, M., AIP Conf. Proc. 523, 405 (2000)
- Benacquista, M., Living Rev. Relativity, 9, (2006), 2. cited March 2013,
<http://www.livingreviews.org/lrr-2006-2>
- Brady, P., LIGO <http://www.ncsa.uiuc.edu/Cyberia/NumRel/NumRelHome.html>
- Case, G. L., Bhattacharya, D. 1998, ApJ, 504, 761
- Clark, J.S., Goodwin, S.P., Crowther, P.A., Kaper, L., Fairbairn, M., Langer, N., Brocksopp, C., A&A 392, 909920 (2002)
- Coe, M. J.; Payne, B. J.; Longmore, A.; Hanson, C. G. 1988MNRAS.232..865C
- Coe, M. J. 2000, ASPC, 214, 656
- Coe, M. J., Bird, A. J., Hill, A. B., McBride, V. A., Schurch, M., Galache, J., Wilson, C. A., Finger, M., Buckley, D. A., Romero-Colmenero, E. 2007, MNRAS, 378, 1427
- Corongiu, A., Kramer, M., Stappers, B. W., Lyne, A. G., Jessner, A., Possenti, A., D'Amico, N., Löhmer, O., 2007. The binary pulsar PSR J1811-1736: evidence of a low amplitude supernova kick. A&A, 462, 703-709

- Cusumano, G.; Maccarone, M. C.; Nicastro, L.; Sacco, B.; Kaaret, P, 2000ApJ 528L 25C
- Cutler, C., Phys.Rev. D57 (1998) 7089-7102
- Djorgovski, S.G., Sky & Telescope October 1998 38-43
- Duquennoy, A., Mayor, M., Astron. Astrophys. 248, 485-524, 1991
- E-LISA science case, ESA, arXiV:1201.3621v1
- Farmer, A.J., Phinney, E.S., Mon. Not. R. Astron. Soc, 346, 1197-1214, 2003
- Finger M.H., Wilson R. B., Scott D.M., Stollberg M., Prince T. A., IAUC 5959, 1994
- Finger, M.H., Wilson, R.B., Harmon, B.A., 1996ApJ...459..288F
- Finger, M. H., Wilson, R. B., Chakrabarty, D., 1996 A&AS..120C.209F
- Finger M.H., Bildsten L., Chakrabarty D., Prince T. A., Scott D.M., Wilson C. A., Wilson R. B., Zhang S. N., ApJ.517:449-459, 1999 May 20
- Freire, P.C., 2004, "Pulsars in globular clusters," NAIC, on line
<http://www.naic.edu/> pfreire/GCpsr.html
- Freire, P.C., Gupta, Y., Ransom, S.M., Ishwara-Chandra, C.H., ApJ, 606:L53L56, 2004
- Galloway, D.K., Sokoloski, J.L., Kenyon, S.J., ApJ, 580:10651069, 2002
- Giangrande,A., Giovanelli, F., Bartolini, C., Guarnieri, A., Piccione, A., 1980 A&AS...40..289G
- Gnedin,O.Y., Ostriker, J.P., ApJ, 474, 223, 1997
- Gratton, R.G., Carretta, E., Bragaglia, A., arXiv:1201.6526v1 [astro-ph.SR] 31 Jan 2012

- Grimm,H.-J., Gilfanov, M., Sunyaev, R., Chin. J. Astron. Astrophys. Vol. 3 (2003), Suppl., 257269
- Gvaramadze, V.V., Röser, S., Scholz, R.-D., Schilbach, E., A&A 2011, preprint arXiv:1102.2437v1 astro-ph.SR
- Haberl, F., 1995A&A...296..685H
- Habets, G. M. H. J.; Heintze, J. R. W. "Empirical bolometric corrections for the main-sequence". A&AS: 193237. Bibcode 1981A&AS...46..193H
- Harmanec, P., Habuda, P., Štefl, S., Hadrava, P., Korčáková, D., Koubský, P., Krtička, J., Kubát, J., Škoda, P., Šlechta, M., Wolf, M., A&A Letters 364, L85L88 (2000)
- Harris, W.E. 1996, AJ, 112, 1487
- Heap, S.R., Corcoran, M.F., Properties of hot luminous stars; Proceedings of the First Boulder-Munich Workshop, Boulder, CO, Aug. 6-11, 1988 (A90-36851 15-90). ASPC, 1990, p. 297-299
- Hobbs, G., Lyne, A. G., Kramer, M., Martin, C. E., Jordan, C., 2004b. Long-term timing observations of 374 pulsars. MNRAS, 353, 1311-1344.
- Hobbs, G., Archibald, A., Arzoumanian, Z., Backer, D., Bailes, M., Bhat, N.D.R., Burgay, M., Burke-Spolaor, S., Champion, D., Cognard, I., Coles, W., Cordes, J., Demorest, P., Desvignes, G., Ferdman, R.D., Finn, L., Freire, P., Gonzalez, M., Hessels, J., Hotan, A., Janssen, G., Jenet, F., Jessner, A., Jordan, C., Kaspi, V., Kramer, M., Kondratiev., V., Lazio, J., Lazaridis, K., Lee, K.J., Levin, Y., Lommen, A., Lorimer, D., Lynch, R., Lyne, A., Manchester, R., McLaughlin, M., Nice, D., Osłowski, S., Pilia, M., Possenti, A., Purver, M., Ransom, S., Reynolds, J., Sanidas, S., Sarkissian, J., Sesana, A., Shannon, R., Siemans, X., Stairs, I., Stappers, B., Stinebring, D., Theureau, G., van Haasteren, R., van Straten, W.,

- Verbiest, J.P.W., Yardley, D.R.B., You, X.P., Class. Quantum Grav. 27 084013
2010
- Hoffmann, A. D., Klochkov, D., Santangelo, A., Horns, D., Segreto, A., Staubert,
R., Phlhofer, G., A&A 494, L37L40 (2009)
- Hogan, C.J., Phys.Rev. D74 (2006) 043526
- Hough, J., 2007, Phil. Trans. R. Soc. A 2007 365, 1335-1342
- Hummel, W., 1998A&A 330 243H
- Hulse, R. A., Taylor, J. H., 1975. Discovery of a pulsar in a binary system. ApJ,
195, L51-L53
- Hughes, S.A., Thorne, K.S., Phys. Rev. D 58, 122002 (1998)
- Iaria, R., Spano, M., Di Salvo, T., Robba, N.R., Burderi, L., Fender, R., van der
Klis, M., Frontera, F., ApJ 619 (2005) 503-516
- İnam, S. Ç., Baykal, A., Swank, J., Stark, M. J., 2004 ApJ 616 463
- Jacoby, B. A., Cameron, P. B., Jenet, F. A., Anderson, S. B., Murty, R. N., Kulkarni,
S. R., 2006. Measurement of Orbital Decay in the Double Neutron Star Binary
PSR B2127+11C. ApJ, 644, L113-L116.
- Janssen, G. H., Stappers, B. W., Kramer, M., Nice, D. J., Jessner, A., Cognard,
I., Purver, M. B., 2008. Multi-telescope timing of PSR J1518+4904. A&A, 490,
753-761
- Johnston, Wm. R., Gravity gradient noise from ground waves, website
<http://www.johnstonsarchive.net/relativity/ggpresentation.html>
- Johnston, Wm. R., List of binary pulsars with references, website
<http://www.johnstonsarchive.net/relativity/binpulstable.html>

- Jones C, Tananbaum H, Giacconi R (1973) 141st Meeting Amer Astron Soc (Tucson, Arizona)
- Kaaret, P., Piraino, S., Halpern, J., Eracleous, M., ApJ, 523:197-202, 1999
- Kaaret, P., Cusumano, G., Sacco, B., ApJ, 542:L41L43, 2000
- Kaspi, V. M., Bailes, M., Manchester, R. N., Stappers, B. W., Bell, J. F., 1996a. Evidence for a neutron star birth kick from a precessing pulsar orbit. Nature, 381, 584-586
- Konacki, M., Wolszczan, A., Stairs, I. H., 2003. Geodetic Precession and Timing of the Relativistic Binary Pulsars PSR B1534+12 and PSR B1913+16. ApJ, 589, 495-502
- Kramer, M. 1998, ApJ, 509, 856
- Levine, J.L., Phys. perspect. 6 (2004) 4275
- Levine, A. M., Corbet, R. 2006, Astron. Telegram, 940
- LIGO Laboratory press and media photos http://www.ligo.caltech.edu/LIGO_web/PR/scripts/photos
- Lisa mission science office, LISA: Probing the Universe with Gravitational Waves, January 2007, LISA-LIST-RP-436
- Liu QZ, vanParadijs J, van den Heuvel EPJ, 2005 A&A, 442, 1135
- Liu QZ, vanParadijs J, van den Heuvel EPJ, 2006 A&A, 455, 1165
- Liu QZ, vanParadijs J, van den Heuvel EPJ, 2007 A&A, 469, 807
- Manchester, R. N., Hobbs, G. B., Teoh, A., Hobbs, M., ApJ, 129, 1993-2006
- Margon, B, Lampton, M, Bowyer, S, Cruddace, R (Oct 1971). "A Pulsing X-Ray Source in Circinus". Ap J. 169 (10)

- Marks, M, Kroupa, P, Oh, S, 2011, Mon. Not. R. Astron. Soc. 417, 16841701
- Masetti, N., Dal Fiume, D., Cusumano, G., Amati, L., -Bartolini, C., Del Sordo, S., Frontera, F., Guarnieri, A., Orlandini,M., Palazzi, E., Parmar, A.N., Piccioni, A., Santangelo, A., A&A 382, 104-117 (2002)
- McSwain, M. V.; Gies, D. R.; Huang, W.; Wiita, P. J.; Wingert, D. W.; Kaper, L., 2004ApJ 600 927M
- Misner, C.W., Thorne, K.S., Wheeler, J.A., 'Gravitation', Freeman 1973.
- Motch, C., Haberl, F., Dennerl, K., Pakull, M., Janot-Pacheco, E., 1997A&A 323 853M
- Moreno-Garrido, C., Mediavilla, E., Buitrago, J., Mon..Not. R. Astron. Soc. 274, 115-126 (1995)
- Murdin, P., Jauncey, D. L., Lerche, I., Nicolson, G. D., Kaluzienski, L. J., Holt, S. S. A&A, vol. 87, no. 3, July 1980, p. 292-298
- Naik S, Biswajit P, Kachhara C, Vadewale S V, Mon. Not. R. Astron. Soc, preprint
- Negueruela, I.; Okazaki, A. T., A&A 369, 108-116 (2001)
- Nelemans, G., Yungeson, L.R., Portegies Zwart, S.F., Mon. Not. R. Astron. Soc. 349, 181192 2004
- L1 Mission document, ESA.
- Numerical Algorithms Group, Oxford University, 2001, www.nag.co.uk.
- Parkes, G.E., Mason, K.O., Murdin, P.G., Culhane, J.L., 1980MNRAS.191..547P
- Peters, P. C., Mathews, J., Physical Review 131-1, 435-440, 1963.
- Pickard, L.R., jIAPS, 2008-2, 24-25, 2008

Pickard, L.R., BritGrav 12, Southampton, 2012
<http://www.southampton.ac.uk/~cjg/britgrav12/slides/Pickard.pdf>

Possenti, A., D'Amico, N., Manchester, R.N., Sarkissian, J., Lyne, A.G., Camilo, F., 2001, "Searching for millisecond pulsars in globular clusters at Parkes: Further results," on line astro-ph/0108343

Press, W.H, Teukolsky, S.A., Vertterling, W.T, Flannery, B.P., Numerical Recipes in Fortran 77 2nd edition, Cambridge University Press

Raichur, H., Paul, B., Mon. Not. R. Astron. Soc. 406, 26632670 (2010)

Ransom, S., Hessels, J., Stairs, I., Kaspi, V., Freire, P., Backer, D., 2004, "A 20-cm survey for pulsars in globular clusters using the GBT and Arecibo," Binary Radio Pulsars ASP Conference Series astro-ph/0404213

Ray, P.S., Chakrabarty, D., 2002ApJ 581 1293R

news article, http://www.theregister.co.uk/2011/09/12/gravity_wave_detector_quantum_noise/

Rejkuba, M., 2012Ap & SS.tmp...25R

Reynolds, M.T., Miller, J.M., ApJ 723:17991805, 2010

Roberts, Mallory S. E.; Michelson, Peter F.; Leahy, Denis A.; Hall, Tony A.; Finley, John P.; Cominsky, Lynn R.; Srinivasan, Radhika, 2001ApJ 555 967R

Sarty ,G.E., Matthews, J., Szalai, T., Balog, Z., Kiss, L.L., Wu, K., AIP Conf. Proc. Volume 1295, pp. 25-32, 2010

, Frommert, H., Kronberg, C., http://messier.seds.org/xtra/supp/mw_gc.html, modified 24 June 2011

Shrader, C. R., Sutaria, F. K., Singh, K. P., and Macomb, D. J.1999, ApJ, 512, 920

Sigurdsson, S., Phinney, E.S., 1995ApJS 99 609S

- Smits, R., Kramer, M., Stappers, B., Lorimer, D.R., Cordes, J., Faulkner, A., A&A 493, 1161-1170 (2009)
- Stairs, I. H., Manchester, R. N., Lyne, A. G., Kaspi, V. M., Camilo, F., Bell, J. F., D'Amico, N., Kramer, M., Crawford, F., Morris, D. J., McKay, N. P. F., Lumsden, S. L., Tacconi-Garman, L. E., Cannon, R. D., Hambly, N. C., Wood, P. R., 2001. PSR J1740-3052— a Pulsar with a Massive Companion. MNRAS, 325, 979-988
- Stairs, I.H., 2004IAUS 218 427S
- Steele, I.A., Negueruela, I., Coe, M.J., Roche, P., Mon. Not. R. Astron. Soc. 297, L5L10 (1998)
- Stewart, R.T., Nelson, J.L., Penninx, W., Kitamoto, S., Miyamoto, S., Nicolson, G.D., Mon. Not. R. Astron. Soc. 253 212 (1991)
- Sollima, A., Beccari, G., Ferraro, F.R., Fusi Pecci, F., Sarajedini, A., Mon. Not. R. Astron. Soc. 380, 781791 (2007)
- Taylor, J. H., Wolszczan, A., Damour, T., Weisberg, J. M. 1992, Nature, 355, 132
- Thorne, K.S., Winstein, C.J., Phys.Rev.D60:082001, 1999
- Thorsett, S. E., Arzoumanian, Z., McKinnon, M. M., Taylor, J. H., 1993a. The Masses of Two Binary Neutron Star Systems. ApJ, 405, L29-L32
- Thorsett, S.E., Chakrabarty, D., 1999ApJ 512 288T
- Thorsett, S.E., Dewey, R.J., Stairs, I.H., ApJ 619:1036-1045, 2005
- Turner, M., ApJ, 216, 610-619, 1977
- Vacca, W.D, Garmany, C.D., Shull,J.M. 1996, ApJ, 460, 914
- Wang, N., Johnston, S., Manchester, R. N., 2004. 13 years of timing of PSR B1259-63. MNRAS, 351, 599-606

- Weber, J., Phys. Rev. Lett. 20, 13071308 (1968)
- Weidner, C., Vink, J.S., A&A, October 2010
- Weisberg, J. M. , Taylor, J. H., 2003. The Relativistic Binary Pulsar B1913+16. Radio Pulsars, 93-98, eds Bailes, M., Nice, D. J. , Thorsett, S., Astronomical Society of the Pacific, San Francisco.
- Weisberg, J. M. , Taylor, J. H., 2004. Binary Radio Pulsars, Proc. Aspen Conference, ASP Conf. Series, eds. F.A. Rasio & I.H. Stairs.
- Wilson, C.A., Finger, M.H., Coe, M. J., Negueruela, I., ApJ, 584:9961007, 2003
- Zhang, S., Qu, J., Song, L., Torres, D.F., ApJ, 630:L65L68, 2005